Mechanics of Dented Orthogonally Stiffened Cylinders

by

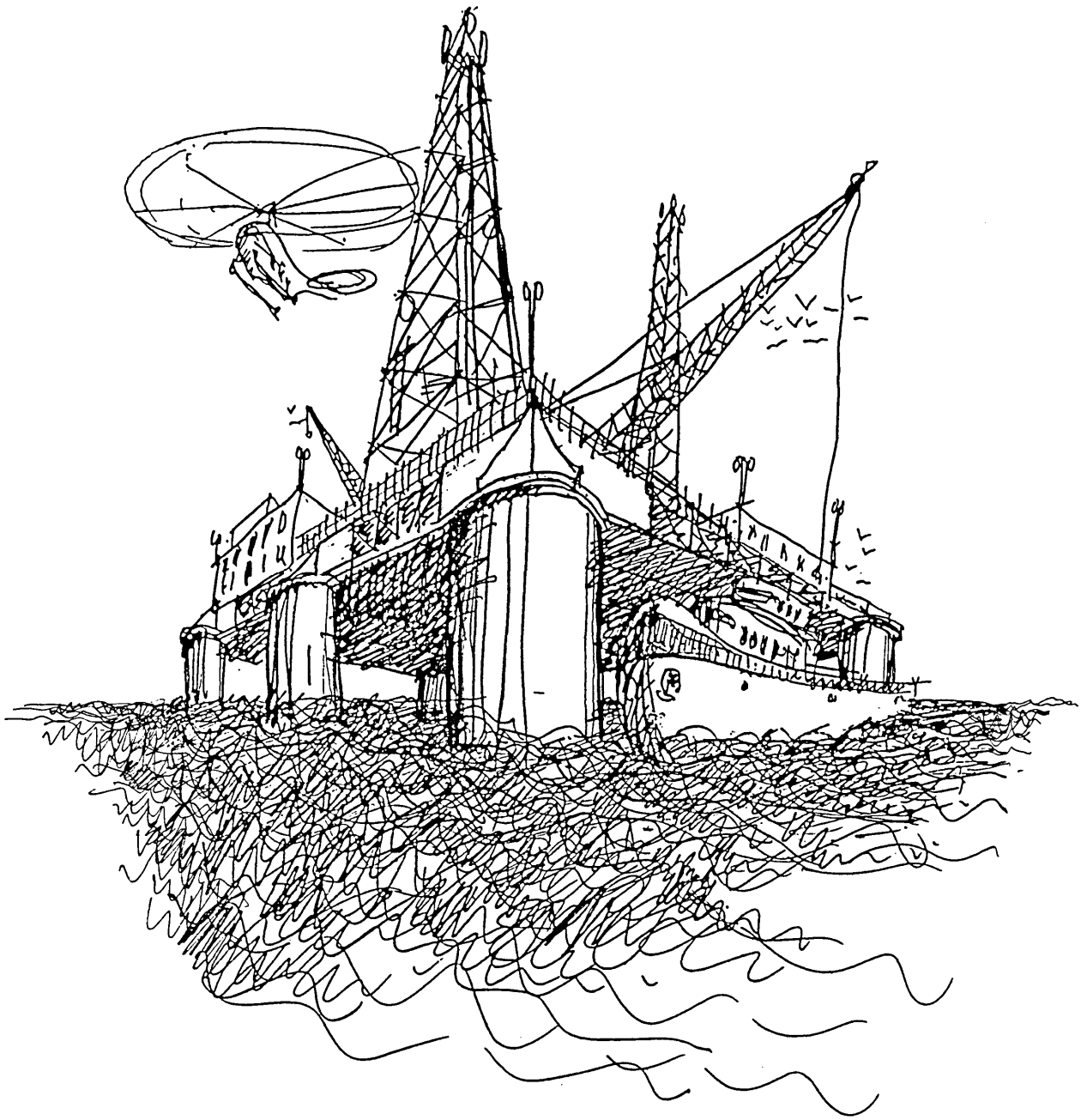
Beverley Frances Ronalds

A thesis submitted for the degree
of
Doctor of Philosophy

Faculty of Engineering
University of London

Imperial College of Science & Technology
London

June 1985



To my nephews
Geoff, Mike and Pete

(should they ever have insomnia)

ABSTRACT

Damage loading of orthogonally stiffened cylinders is considered with reference to the possible collision of a boat with the column of a tension leg platform or semi-submersible.

As a first step the plastic behaviour to large deflections of a T-section beam under central point loading is derived. Both pinned and rotationally fixed supports are considered, and in each case the axial pull-in at the supports is taken into account. By satisfying compatibility of this pull-in and the axial extensions in the plastic hinges and the elastic bars between them, the development of membrane tension with lateral deflection may be traced. The lateral load response then follows from equilibrium considerations.

The formulae compare well with the results of tests undertaken using longitudinally stiffened plates built in at both ends and subjected to central line loading.

A series of tests on orthogonally stiffened cylinders of one and three bay lengths are then described. Knife edge loading is slowly applied normal to the longitudinal axis at mid-span. The mode of deformation is similar to that of the stiffened plates and so the earlier analysis is extended to suit the cylinder geometry. Good correlation between theory and experiment is achieved. This leads to a simple means of estimating the energy absorbed during denting which may be compared with the possible impact energy involved in a ship collision.

The dented plates and cylinders are later tested under longitudinal compression to find their residual stiffness and strength. Corresponding analytical formulations are developed employing both elastic and plastic techniques, which again describe the experimental

observations well. The results give insight into whether a dented cylindrical leg remains able to support the necessary loads after collision. This allows the effects of possible damage to be taken into account in initial design, and may also help determine whether an existing damaged unit should remain in operation.

ACKNOWLEDGEMENTS

I would like to thank many people; firstly my supervisor Professor P.J. Dowling, head of the Department of Civil Engineering, who made it all possible by suggesting the project, arranging funding and allowing me the freedom to pursue it as I wished.

Experimental models of very high quality were fabricated and refurbished by Research Models and Equipment Ltd. in Reading, under the direction of Mr. N. Scott. My friends in the Steel Structures Laboratory, especially the director Mr. J. Neale and also Mr. S. Blackaller and Mr. T. Boxall, provided a steady stream of enthusiasm, new ideas and jokes during the test work, as did Mr. A. Chipling and Mr. R. Packer whilst photographing the results. Mr. C. Hargreaves developed the data logging software for the experiments. My "one day a week" colleagues on the fourth floor of the Civil Engineering building are also appreciated.

I am very grateful for my helper Cyril Sirius who executed the computations, plotted results and typed the manuscript. The entire text was proof read by Mr. A. McAlpine who provided about a zillion helpful suggestions throughout the project, and also the preface sketch.

Certainly I would not have remained in London for four and a half years without the very supportive friends I met in Mecklenburgh Square. They are all special but I shall only single out Mr. R. Dawson who introduced me to Pascal and and trotted me around the squash court each week. Those I met at Ove Arups and in the M.Sc course should also be mentioned. I am very lucky, too, that so many friends from Australia visited me in London. No one contributed more than Miss W. Skilbeck, who saw the necessity of my having a Concise Oxford.

Finally I would like to thank my parents for writing all those letters, and my nephews who sent drawings first and later letters. My sister preferred to 'phone and also accepted lengthy collect calls. Thanks Bob.

CONTENTS

Abstract 4
Acknowledgements 6
Contents 8

CHAPTER 1 16
INTRODUCTION

1.1 Background 17

1.2 Scope 18

1.3 Layout 18

CHAPTER 2 20
REVIEW OF THE LITERATURE

2.1 Introduction 21

2.2 Structures at sea 22
2.2.1 Collision risk 22
2.2.2 Impact energy 22

2.3 Structural behaviour under collision 24
2.3.1 Introduction 24
2.3.2 Vessels 25
2.3.3 Offshore structures 26

2.4 Lateral loading of beams and plates 28

2.5 Compressive strength of dented plates 31

2.6 Local buckling of stiffeners 32
2.6.1 Longitudinal stiffeners 32
2.6.2 Ring frames 33

2.7 Lateral loading of unstiffened tubes 35
2.7.1 Experimental programmes 35
2.7.1.1 Nonuniform indentation 35
2.7.1.2 Uniform indentation 39
2.7.2 Theoretical analyses 39
2.7.2.1 Introduction 39
2.7.2.2 Local denting 40
2.7.2.3 Overall bending 42

2.8 Compressive strength of damaged unstiffened tubes 46
2.8.1 Experimental programmes 46
2.8.2 Theoretical analyses 47

2.9 Moment capacity of dented tubular sections 50
2.9.1 Experimental programmes 50
2.9.2 Theoretical analyses 51

2.10 Damaged ring stiffened cylinders 52

2.11 Damaged longitudinally stiffened cylinders 54

2.12 Dynamic loading 55

2.13 Strength of undamaged stringer stiffened cylinders 56
2.13.1 Introduction 56
2.13.2 Experimental programmes 57
2.13.3 Design methods 62

2.14 Conclusions 65

CHAPTER 3 67
DENTING OF STRINGER STIFFENED PLATES

3.1 Introduction 68

3.2 Experimental programme 69
3.2.1 Introduction 69
3.2.2 Model manufacture 69
3.2.3 End conditions 70
3.2.4 Heat treatment 70
3.2.5 Material properties 71

3.3 Denting tests 71
3.3.1 Rig arrangement 71
3.3.2 Instrumentation 73
3.3.2.1 Strain gauges 73
3.3.2.2 Transducers 74
3.3.3 Final preparation 74
3.3.4 Testing procedure 75

3.4 Theoretical analysis 76
3.4.1 Introduction 76
3.4.2 Plastic capacity of stringer beam cross section 76
3.4.2.1 T-section 76
3.4.2.2 Unsymmetrical I-section 80
3.4.3 Beam analysis 83
3.4.3.1 General derivation 83
3.4.3.2 Jones' support pull-in approach 87
3.4.3.3 Hodge's support pull-in approach 88
3.4.4 Membrane yield response 90
3.4.5 Behaviour during unloading 91

3.5 Theoretical correlation 93
3.5.1 Initial elastic response 93
3.5.2 Axial force development 93
3.5.3 Strain development 96
3.5.4 Lateral load response 96
3.5.5 Energy absorption 98
3.5.6 Lateral deflection profiles 99
3.5.7 Stiffener tripping at supports 100
3.5.8 Intermediate unloading and reloading 102
3.5.9 Failure 103
3.5.10 Elasticity effects in plastic analysis 104
3.5.10.1 Postulated experimental behaviour 104
3.5.10.2 Alternative flow rule 107

3.6 Conclusions 109

Tables 3.1 - 3.5 111
Figures 3.1 - 3.17 115

CHAPTER 4 129
LONGITUDINAL LOADING OF DENTED PLATES

4.1 Introduction 130

4.2 Longitudinal compression test 130
4.2.1 Rig arrangement 130
4.2.2 Instrumentation 131
4.2.2.1 Load cells 131
4.2.2.2 Strain gauges 131
4.2.2.3 Transducers 132
4.2.3 Final preparation 132
4.2.4 Testing procedure 133

4.3 Theoretical analysis 133
4.3.1 Introduction 133
4.3.2 Initial elastic response 133
4.3.3 First yield 136
4.3.4 Plastic mechanism 137
4.3.5 Overview 140

4.4 Theoretical correlation 141
4.4.1 Simple model 141
4.4.1.1 Deflections 141
4.4.1.2 Longitudinal load response 142
4.4.1.3 Axial force development 144
4.4.2 Stiffener tripping at supports 144

4.5 Conclusions 149

Figures 4.1 - 4.8 150

CHAPTER 5 158
DENTING OF STRINGER STIFFENED CYLINDERS

5.1 Introduction 159

5.2 Experimental programme 160
5.2.1 Introduction 160
5.2.2 Model manufacture 161
5.2.3 Choice of geometry 163
5.2.4 End conditions 164
5.2.5 Material properties 166

5.3 Denting tests 167
5.3.1 Rig arrangement 167
5.3.2 Instrumentation 170
5.3.2.1 Strain gauges 170
5.3.2.2 Transducers 172
5.3.3 Final preparation 173
5.3.4 Testing procedure 174

5.4 Dent geometry 175

5.5 Theoretical analysis 178
5.5.1 Initial elastic analysis 178
5.5.2 T-section beam plastic analysis 179
5.5.2.1 Introduction 179
5.5.2.2 Stringer beam response 180
5.5.2.3 Total response of cylinder 186
5.5.2.4 Overall section behaviour 187
5.5.3 Alternative incremental plastic analysis 189

5.6 Theoretical correlation 191
5.6.1 Axial force development 191
5.6.1.1 Cylinders 1B1 and 1B2 191
5.6.1.2 Cylinders 1A1 and 1A2 195
5.6.1.3 Cylinder 3A1 199
5.6.1.4 Cylinders 3A2 and 3A3 199
5.6.2 Strain development 200
5.6.3 Lateral load response 201
5.6.3.1 Cylinder 1A1 201
5.6.3.2 Cylinder 1A2 203
5.6.3.3 Cylinders 3A2 and 3A3 204
5.6.3.4 Cylinder 3A1 204
5.6.3.5 Cylinders 1B1 and 1B2 205
5.6.4 Intermediate unloading and reloading 205
5.6.5 Failure 207
5.6.6 Energy absorption 207
5.6.7 Longitudinal pull-in 209
5.6.7.1 Pull-in during loading 209
5.6.7.2 Residual pull-in 218

5.7 Complete cylindrical column response 218

5.8 Dynamic effects 220

5.9 Conclusions 222

Tables 5.1 - 5.5 224
Figures 5.1 - 5.39 228

CHAPTER 6 257
LONGITUDINAL LOADING OF DENTED CYLINDERS

6.1 Introduction 258

6.2 Longitudinal compression tests 258
6.2.1 Rig arrangement 258
6.2.2 Instrumentation 259
6.2.2.1 Strain gauges 259
6.2.2.2 Transducers 260
6.2.3 Final preparation 261
6.2.4 Testing procedure 261

6.3 Qualitative experimental behaviour 262
6.3.1 Introduction 262
6.3.2 Cylinder 1A2 262
6.3.3 Cylinders 1B1 ad 1B2 266
6.3.4 Cylinders 3A2 and 3A3 269

6.4 Theoretical analysis 272
6.4.1 Introduction 272
6.4.2 Single bay models 273
6.4.2.1 Effective section 273
6.4.2.2 Mechanics 275
6.4.2.3 Load eccentricity 278
6.4.3 Three bay models 279
6.4.4 Modification to account for end rings 280

6.5 Theoretical correlation 282
6.5.1 Overall load and deformation characteristics 282
6.5.2 Details of local behaviour 285
6.5.2.1 Material remote from dent 285
6.5.2.2 Stringer beams adjacent to dent 287
6.5.3 Dent zone 290
6.5.3.1 Introduction 290
6.5.3.2 Cylinder 1A2 291
6.5.3.3 Cylinders 1B1 and 1B2 295
6.5.3.4 Cylinder 3A3 299
6.5.4 Summary 300

6.6 Comparison with an alternative approach 301

6.7 Complete cylindrical column response 305

6.8 Conclusions 307

Tables 6.1 - 6.2 309
Figures 6.1 - 6.44 311

CHAPTER 7 341
CONCLUSIONS OF RESEARCH

7.1 General conclusions 342
7.1.1 Collision loading 342
7.1.2 Residual strength after collision 342

7.2 Further research 344

Notation 348
Bibliography 353

CHAPTER 1

INTRODUCTION

1.1 BACKGROUND

In structural applications steel plate is frequently braced by longitudinal stiffeners called stringers. Orthogonal stiffening is a natural extension because it is usual to restrain the stringers at regular intervals with transverse frames, to enhance their effectiveness. The rectangular shapes into which the plate is divided by the stiffening are called panels. It is common practice to make the transverse members sufficiently sturdy for buckling to be confined to the longitudinally stiffened bays they delimit, and so for simplicity, many experimental and theoretical models of orthogonally stiffened components are single bay.

In the decade preceding the present one the elasto-plastic behaviour of fabricated steel plates was the object of an extensive research effort. This was fueled by several box-girder bridge failures, including one in the author's home city, Melbourne. Techniques that evolved during this work have since been applied to similarly stiffened cylindrical shells as these have recently found employment in floating offshore platforms where weight minimization is important. Studies in another area, namely accidental loading of offshore installations, have gained impetus concurrently, with emphasis laid on the response of thick-walled unstiffened tubes which are a traditional component of these structures.

The present dissertation brings together the two themes and examines the consequences of accidental loading, in particular ship collision, on orthogonally stiffened plates and shells.

1.2 SCOPE

The primary goal of the research is to enable estimation of the degree of damage to an orthogonally stiffened plate or shell component that might result from a collision, and the loss of strength it causes.

To that end a joint experimental and theoretical approach is adopted. Stringer stiffened flat plates and cylindrical shells of small scale are loaded laterally to finite deflections to simulate ship collision, and the damaged models are then tested in longitudinal compression to determine their residual strength. The majority of test pieces are single bay but several three bay cylindrical shells are also included. The value of the test work is firstly in demonstrating how a complex component actually behaves, and secondly in giving quantitative data against which a theoretical method may be validated.

Complementary theoretical work is developed to describe both loading processes. The approach chosen is analytical, based on plastic mechanism techniques which are well suited to the large deformations induced by damage. The results take the form of simple equations which have the dual advantages of allowing rapid assessment of collision damage and being readily adjustable to suit another dent shapes.

1.3 LAYOUT

The following chapter contains a statement of the collision problem for offshore installations and discusses the effect of damage on a variety of structural components by summarizing other research in the field.

Chapters 3, 4, 5 and 6 form the nucleus of the thesis. Each of the four aspects that arise from the two structural elements, namely plates and shells, and the two loading configurations, lateral and longitudinal, are treated separately. In consequence each chapter contains both experimental and theoretical work. The material is organized in a unified manner. First the relevant experimental models and the method of testing them are described. No results are presented at this stage and instead the theoretical work is developed. Experimental observations and theoretical predictions are then discussed together in considerable detail, enabling the two to be correlated directly. Lastly any additional analyses suggested by the comparison are undertaken.

The final chapter presents conclusions drawn from the work. Members stiffened orthogonally are found to be quite robust to denting which suggests their usefulness in situations where protection against accidental lateral loading is lacking.

CHAPTER 2

REVIEW OF THE LITERATURE

2.1 INTRODUCTION

The crashworthiness of ships has received rational attention for the past twenty five years. The coincident problem of the resistance of an offshore platform to ship collision became topical just over five years ago when the magnitude of the potential risk became apparent. The inclusion of accidental loading as a design limit state in several Codes heightened the need for greater understanding and prompted the development of corresponding analytical techniques.

In consequence a substantial body of knowledge has been built up pertaining to the behaviour of unstiffened tubes during collision and their residual strength afterwards, as these constitute the majority of steel jacket structures. Armed with this information it should be possible to determine how an entire framework might respond to impact. Research on these topics is surveyed in this chapter.

Relevant material on other structural elements, in particular beams and plates, is also included although this research has not, in general, been directed at the offshore collision problem. A collation of data on these components and on unstiffened tubes helps to clarify the behaviour of damaged orthogonally stiffened cylinders. The subject represents a gap in current research which this dissertation begins to fill. The work progresses from that already done on undamaged stringer and orthogonally stiffened shells with similar geometric and material properties. The review therefore concludes with a summary of information from this field.

2.2 STRUCTURES AT SEA

2.2.1 COLLISION RISK

The first point to be raised concerns the risk of offshore collisions. Numerous studies into this problem have been undertaken involving both data on actual events and numerical modelling; see, for example, Refs. [16,101,62,106]. (Numbers in square brackets tally with the alphabetically ordered bibliography at the end of the dissertation.) The accuracy of conclusions drawn from these studies is limited by the relatively short timespan from which the information comes. Nonetheless the results are important and perhaps surprising. In a report commissioned by the UK Department of Energy [117], for example, the collision risk is estimated to be of the order of 0.1 to 0.01 per year for North Sea platforms in close proximity to major shipping lanes. In fact, pilots tend to use the installations as navigational aids and approach quite closely [61]. This level of risk is far higher than normally accepted in structural design [117].

2.2.2 IMPACT ENERGY

The amount of kinetic energy that might be released in a major ship/platform collision is computed by Donegan [36] from the well-known formula

$$W = \tfrac{1}{2} C m v^2 \ .$$

In this context m represents the mass of the vessel. Currently the largest supply vessels may have 5000 tonnes displacement but the trend is increasingly towards larger boats [16,113,50]. An extreme drift velocity v may be inferred to be two metres per second for a four metre

significant wave height, which is considered to be a limiting sea-state for cargo transference. This inference follows from empirical and statistical data [61,89] and is codified [31]. The added mass term is commonly taken to be

$C = 1.4$ for sideways impact
$C = 1.1$ for forward impact.

These figures result in 14 MJ and 11 MJ of collision energy for the two collision types. As discussed in Ref. [50], however, both theoretical and experimental studies show that the quoted added mass values may significantly underestimate the actual situation for longer impact durations.

Det norske Veritas (or DnV), the Norwegian classification society, includes energy absorption capability as a design criterion. For mobile offshore units [31] the two energy values computed above are specified, and it must be possible to dissipate these without incurring overall instability [16].

Sometimes guidance is also given on a serviceability limit state which should be withstood without the need for immediate (or any) reparation. Typically a collision scenario corresponding to about 0.5 MJ is quoted [8,56,36,61].

At the opposite end of the spectrum it is clearly possible for a large merchant vessel or tanker to run into an offshore installation at full speed. It is economically impractical to impose this condition for design purposes, and instead preventive measures are recommended [16,50]: for example, sound and light signals, radar surveys, navigation restrictions and guard vessels. Fortunately the probability of such an occurrence is small [61] and the great majority of actual collisions involve authorized vessels servicing the unit [16].

It must be concluded however that quantitative guidance on design for accidental loading is lacking [50]; several Codes still give it very brief consideration [6,29,32].

In general, the momentum of both impacting bodies as well as their kinetic energy affects the collision response [21,22] but it is readily apparent that for a supply vessel hitting a large stationary platform the strain energy to be absorbed is dependent only on the kinetic energy of the boat [50].

2.3 STRUCTURAL BEHAVIOUR UNDER COLLISION

2.3.1 INTRODUCTION

Many authors, for example Donegan [36] and Furnes and Amdahl [61], have pointed out that in a ship/platform impact the collision energy may be absorbed in a number of the following processes:

: local denting
: beam deformation
: elastic deflection of framework
: global motions of floating structure and ship
: vibrations
: ship deformation
: fendering deformation (if present)

It is interesting that the approach often varies depending on the slant of the investigation. Ship researchers frequently assume the target to be rigid [94,61,129], whereas those studying rigs neglect any energy dissipation in the vessel [8,25,152,83]. Of course both schools obtain conservative results, and if they are combined a much better estimate is achieved by aportioning

the energy dissipation in proportion to the areas under the two load versus indentation curves at equal load [62]. Several approaches to the determination of the response curve pertaining to the platform are mentioned in Section 2.3.3 below, but first, brief attention is given to the boat.

2.3.2 VESSELS

Quantitative investigation of the deformation characteristics of cylindrical shell structures under accidental loading is a new discipline [66] and so guidance from the more established field of ship collision has proven useful. The first approach to damage evaluation of this latter type was made by Minorsky [100] in 1959 who related the absorbed kinetic energy to the volume of damaged steel. Due to its simplicity and its remarkable accuracy for major collisions the formulation is still used extensively today [82]. As it is less successful for low energy impacts, Rosenblatt & Son Inc. [128] developed a method based on plastic mechanism theory for this end of the range which includes supply boat collisions.

Similar techniques have been adopted by DnV in developing a computer program to perform static analyses of the uniform indentation of a ship's hull by a completely rigid object. Furnes and Amdahl [61,62] report results in the form of load versus indentation curves for various types of vessels when the rigid object is a vertical cylinder of diameter 1.5, 10 or 20m.

In the case of collisions between two ships, there have been attempts, more recently, to estimate the stiffnesses of both objects and hence their respective work contributions [174]. Due to their inherent complexity these analyses are usually carried out numerically, and in modelling the actual structures of impacting and resisting

bodies they become very case specific and the drawing of general conclusions is difficult. There are of course many different collision possibilities even for the same two boats with the same speeds, depending on the approach orientation and the locations of the contact zones [61].

2.3.3 OFFSHORE STRUCTURES

Analysis of the impact resistance of braced jacket structures is often based on the response of the impacted member only. Put another way, the energy dissipated in the first two modes listed above in Section 2.3.1 is quantified using plastic analysis and all other processes are neglected as unimportant [152,50]. Various experimental and analytical investigations of the response of tubular beams under lateral loading are discussed in some detail in Section 2.7.

Conversely, the global behaviour of a medium sized jacket in collision loading has been studied by assuming the struck member does not deform at all [61]; the exemplary contact zone quoted is a joint locally stiffened by grouting. Dynamic analyses have been undertaken using a linear-elastic frame program. It is found for this particular case that the platform absorbs a significant portion of the impact energy (the rest being taken up by the ship) but that the contribution of the vibrations to this effort is small. Comparable investigations have been undertaken by Petersen and Pedersen [112].

The overall structure is also important from another aspect. Before it may be assumed how much energy is absorbed by the struck member it must be ensured that the bending moments and axial force generated during deformation can be supported by the joints and adjacent framework.

This has been investigated by Pettersen and Johnsen [113] with the aid of a space frame program and stepwise static loading. Possible modes of member behaviour are quantified in simple formulations, namely local denting, plastic hinges, membrane tension and buckling, and the member status is updated as necessary during loading. It is possible to follow the progressive collapse of a framework with the corresponding energy absorption at all stages. Results are presented for a jack-up platform and a semi-submersible. In the second example collision with a column is considered not to be critical and so impact with a bracing member is analysed. It is concluded that a global mechanism will form only with the involvement of very high energy. In Ref. [114] the approach is applied to a cellular structure typical of ship design.

The work of Kavlie and Soreide [83] follows the principle of the above papers but with important modifications. In their semi-submersible example the model is subjected to normal gravity loads and corresponding buoyancy forces before applying the main item, which is wave loading. Next damage is introduced into the numerical model by inserting a section of tube with smaller diameter eccentrically into a bracing member. The residual strength of the modified member is meant to correspond with that resulting from a local dent, and the residual strength of the entire structure is found by reapplying the wave loading. Use is made of the Idealized Structural Unit Method [118] for the stiffness analyses. In a similar way Chyrssanthopoulos and Skjerven [18] have analysed a jack-up platform.

This type of numerical tool is very useful as several regulating authorities now state that offshore structures must have reserve strength to withstand a one year storm, for example, after being damaged [16,50,107]. Whereas typical braced jacket structures have sufficient redundancy to enable satisfactory load redistribution even after the complete removal of a member, there is much less

superfluity in floating rigs. It may therefore become necessary to take account of the capacity remaining in a damaged component to ensure overall stability [66].

For any of the above approaches to give representative predictions it is vital that the tubular joints have sufficient strength to carry the extreme forces induced by accidental loading. Numerous authors have expressed the opinion that typical tubular joints may not have this capability [61,152,58,26,186,50], especially if a collision occurs close to the junction. Thus it is their connections that largely determine the energy absorbing characteristics of tubes *in situ*.

The remainder of this chapter is devoted to the behaviour of individual members. Information has been gathered on different modes of deformation in various structural components as they might find relevance to the accidental loading of offshore installations.

2.4 LATERAL LOADING OF BEAMS AND PLATES

The body of literature on beams and plates is extensive and it is not the author's intention to review it in detail. Certain theoretical developments regarding beams are itemized below as they will put the analytical procedure of Chapter 3 in context. The principles of this type of analysis are readily applied to plates [77,94,185]. Other research into plates, considering alternative loading configurations and theoretical approaches, for example, is largely excluded.

The behaviour of a laterally loaded beam at large deflection is strongly dependent on whether axial restraint is provided by the supports. The response for full end fixity was derived in 1957 by Haythornthwaite [68] for a rigid-plastic beam with rectangular cross

section and subjected to point loading. Analysis starts with the bilinear mechanism associated with plastic collapse and assumes that the axial extension accompanying increasing lateral deflection is developed at the three hinges in accordance with incremental flow rule theory. The resulting relationship between lateral load and deflection is parabolic at first but becomes linear after the axial force reaches yield; this correlates reasonably well with his test data.

Several developments appeared in 1973, all of which continued to address rectangular sections. Jones [77] quantified the effect of partial fixity against longitudinal movement by postulating the pull-in to be proportional to the square of the lateral deflection. Solutions are given in terms of the constant of proportionality. Both simply supported and clamped beams are considered under point loading and uniformly distributed pressure, as well as an encastre square plate with lateral pressure.

An alternative solution by Hodge [72] followed soon afterwards in which proportionality between pull-in and the membrane force is assumed. His analysis covers centrally loaded, pin ended beams only. Both Hodge and Jones predict the eventual development of Haythornthwaite's linear loading equation. The effect of intermediate axial restraint, therefore, is merely to delay the attainment of membrane yield.

Almost simultaneously, elasticity was incorporated in the procedure for the first time by Campbell and Charlton [10]. Although they only consider the simple case of a centrally point loaded beam with fully fixed supports, they do include the early elastic response, and also the elastic stretch of beam segments between plastic hinges in the mechanism response. The differential equation governing this latter behaviour is solved numerically using the values of axial force and lateral deflection

existing at the change-over point as the "initial" condition.

A quite different procedure was developed several years earlier by Waszczyszyn [183]. For a point loaded, simply supported beam with complete axial restraint he assumes a sinusoidal deflected shape and monitors the progression of plasticity outwards from the centre. Both Waszczyszyn [183] and Campbell and Charlton [10] present complementary experimental results. Although correlation with the respective analyses is favourable, both show the theoretical work to overestimate the true membrane force at higher deflections.

More recently Haythornthwaite's methodology has been extended further by Low [92,94] who analyses an encastre rectangular beam loaded at mid-span through a circular indenter. As loading progresses the loaded length increases as the beam becomes wrapped around the indenter. The analysis is used to model the denting of a ship in collision with an offshore concrete platform shaft.

As discussed in more detail in Section 2.7.2.3, de Oliveira [26] adapts the approach to tubular sections. Both Low and de Oliveira employ Hodge's support pull-in criterion.

Potentially of particular relevance to this dissertation, McDermott et al [95] consider lateral loading of longitudinally stiffened plates in the context of ship collision. In their analysis plastic bending and membrane tension modes of behaviour are separated by assuming that before any axial force is induced the stiffeners trip at the supports and under the point load. They also replace the yield stress with $\frac{1}{2}(\sigma_{YT} + \sigma_{ULT})$ as a concession to material strain hardening. The symbols used here, although probably self-explanatory, are also defined at the end of this dissertation.

In discussing Ref. [95], Jones [78] points out that the linear portion of Haythornthwaite's response is also applicable to T-sections if the true plastic modulus is replaced by the parameter $At_e/4$. Here t_e is the thickness of the equivalent rectangular section.

In a quite distinct empirical investigation Wenger et al [184] have recently investigated the resistance of a stringer stiffened deck to dropped objects. Two forms of failure are observed, the predominant mode being punching shear. In several cases, though, overall deflection occurs and in rebounding the stringers buckle in a rippled pattern.

2.5 COMPRESSIVE STRENGTH OF DENTED PLATES

A discussion of the residual strength of distorted steel plating has been published by Smith and Dow [147] in the context of damage to ships. Consideration is given to various levels of deformation, namely plate dishing between stiffeners, bending of the longitudinal girders with attached plating between tranverse frames and, finally, orthotropic deflection involving all three elements. Numerical analyses have been performed in which the damage formation is first simulated in order to achieve an accurate representation of the residual stress pattern, which is thought to influence both the stiffness and strength response under subsequent in-plane loading. Torsional buckling of the stiffeners is excluded in the examples, but the present author discusses the subject briefly in the following Section 2.6.

In another paper [38] the same authors investigate the effect of a localized imperfection on the compressive strength of long plates which are simply supported along all four edges. The imperfection takes the form of a small amplitude sinsoidal dent with no associated residual

stresses, and is found to reduce the capacity more than an imperfection of the commonly assumed form that extends over the entire plate length (with the same amplitude).

2.6 LOCAL BUCKLING OF STIFFENERS

The torsional buckling of flatbar stiffeners is given some attention here as it is quite conceivable that accidental loading may induce this form of distortion in stiffened structures.

2.6.1 LONGITUDINAL STIFFENERS

A sizable volume of data exists concerning the torsional stability of metal outstands, as indicated by the literature reviews in Refs. [126,13,11]. It has been acquired experimentally, analytically and numerically.

Elastic torsional buckling brings about a sinusoidal pattern of out-of-plane deflections. With the advent of plasticity the form changes to a sharper localized mode into which the elastic curvature is engulfed. This postbuckling mode is frequently observed in tests and has been termed "tripping".

Murray [105] has analysed tripping as a plastic mechanism for the situation of simply supported stringer stiffened plates under axial compression and bending. Relatively slender stringers are employed in his tests; that is

$$h_t/t_t = 20$$

but with a small bulb for additional rigidity. Stiffener tripping occurs near mid-span when the entire plate bends

such that the stiffener experiences compression. For bending in the opposite direction with the stiffener in tension, Murray assumes a polygonal plastic mechanism in the plate panels. These analytical approaches produce unloading paths.

Most theoretical methods [124,57,91], however, are spawned from elastic buckling theory which has the advantage of enabling the peak load to be predicted. Many authors assume a sinusoidal initial out-of-straightness from which the deflection grows, and for stockier geometries failure is elasto-plastic as the maximum stresses induced by the deflection are able to reach yield.

2.6.2 RING FRAMES

Flat bar ring stiffeners may also buckle locally out-of-plane. Generally, research has been directed towards the behaviour of rings under external pressure loading [84,51], because this form of instability is not an obvious problem for cylinders in axial compression due to the rings being in tension. The strain gauge readings on the ring frames of the cylindrical shell of Tsang et al [166], subjected to compression, concur with this. However local crippling of slender rings with

$$h_r/t_r = 24$$

has been observed in compression tests on orthogonally stiffened shells [99] and is perhaps encouraged by dishing of an adjacent panel.

Two tests undertaken within the research division of DnV [172] pertain to the topic of this dissertation. Rings having T-shaped section are used to represent an internal flat stiffener with associated plating. Each is compressed

by diammetrically opposed point loads to failure, and well beyond. Being slender stiffeners,

$$h_r/t_r = 18, 30$$

for the two examples, tripping occurs at the locations ninety degrees from the points of load application.

Onoufriou and Harding [110] also observe ring frame tripping in a cylinder where the adjacent panel has been dented by lateral loading. An abrupt kink is formed corresponding to each side of the dent so that the intermediate arc of ring frame may rotate in sympathy with the deflected panel. The ring has slenderness

$$h_r/t_r = 16 .$$

Other models having rings with

$$h_r/t_r = 8 ,$$

but similar in all other respects, did not trip. Further details of the tests are given in Section 2.10 below.

This work is to be differentiated from the in-plane collapse of ring models also discussed later in Sections 2.7.2.2 and 2.10.

2.7 LATERAL LOADING OF UNSTIFFENED TUBES

2.7.1 EXPERIMENTAL PROGRAMMES

2.7.1.1 NONUNIFORM INDENTATION

Interesting empirical studies of local denting may be retrieved from the field of cylindrical vessel technology. Morris [103] has discussed the behaviour of cylinders loaded laterally through diametrically opposite rigid bosses. It is discovered that snap-through does not occur, although it is known to with spherical shells of similar section slenderness,

$$R/t = 53 ,$$

under similar loading.

More recently Tooth and Jones [162] have loaded tubes through saddles either welded in place or loose. For geometries in the range

$$48 \leq R/t \leq 84$$

the load is found to rise nonlinearly to reach a limit value.

Three papers written by Thomas et al [161] in 1976 describe a pioneering experimental investigation into the large deflection response of tubes subjected to lateral loading. This loading is applied through a wedge aligned perpendicular to the tube axis. The work has a view towards the optimization of energy absorbing devices for impact situations. Having an overall slenderness

$$L/R < 12 ,$$

where L is the member length, the tubes are therefore shorter than those generally found in offshore structures.

Two types of support conditions are considered. The tube ends are free for both and so exhibit non-planar pull-in and ovality. In one arrangement the tube rests in two V-shaped blocks, the separation of which defines the span. In some tests, however, two opposing indenters provide the only support. The papers illustrate many interesting aspects of the complex modes of behaviour exhibited by cylinders which are not accounted for in simple collapse mechanism theory.

In Norway, Furnes and Amdahl [61] have applied lateral load to slightly longer tubes which are bolted at their ends into a stiff frame. They observe that local denting of the surface of the tube under the indenter is generated initially, accompanied by steeply increasing load. Eventually overall bending occurs simultaneously with the denting and is indicated by deflection of the surface diametrically opposite the wedge. At this point the lateral stiffness starts to decrease and quite soon the model collapses. The mode change occurs at

$$\delta_0/R = 0.7 .$$

Similar observations are made by Thomas et al but at a lower deflection. This is presumably due to the larger flexural restraint present in the Norwegian models.

Tubes comprising the braced jacket structures found offshore usually fall within these ranges of geometry [25,50]

$$10 \leq R/t \leq 30$$

$$20 \leq L/R \leq 60 .$$

Several authors have indented tubes typifying these

section and column slendernesses.

In point loading simply supported tubes without axial restraint, Foss and Edvardsen [58] note three phases of behaviour. Firstly elastic bending occurs and this is later accompanied by local denting. Finally, at the point of peak load the dent becomes fully plastic and starts to propagate.

Soreide and Amdahl [152,154] have tested tubes with end conditions that give complete flexural fixity but allow axial movement to be either free or fully prevented. The latter restrained case exhibits greater ovalization and, of course, much greater load capacity. However the results are much less sensitive to another factor, namely the speed of loading, as demonstrated by undertaking both quasi-static and dynamic tests. Further discussion of these impact tests is included in Section 2.12.

In a series of publications Smith and his colleagues [145,146,148,149] have considered several damage processes. They note that local denting will be the predominant mode of deformation in short and/or thin-walled members when loading is applied through a rigid structure, especially when contact occurs close to the member ends. Conversely, for long tubes of small diameter to thickness ratio subjected to slower loading by a deformable structure near mid-span, overall bending will prevail.

To produce deflections in the form of overall bending in their test pieces, lateral load is applied through a rubber lined semi-circular cradle. To obtain mainly local denting a wedge is used which is reacted by the cradle. Without this support bending would accompany the denting, induced by longitudinal pull-in of the fibres. Many intermediate cases which combine both local and overall damage are also included.

Rashed, collaborating with Taby and Moan [120] and later with Ueda [169], has undertaken lateral loading experiments resembling the local denting tests of Smith et al.

INDENTER SHAPE

The major indenter shape employed by Smith et al is a sixty degree knife edge. The apex is rounded to a 10mm radius for full sized testing [146] and scaled proportionally for smaller models [145]. Other forms are experimented with as well [149], for example a square nose and a round one having a relatively large radius. Other investigators also employ blunter indenters. For similar small scale tests Rashed, Taby and Moan [120] have a 5mm radius, and Ueda and Rashed [169] a 25mm one. Thomas et al [161] use a 6mm flat flanked by radii. Reseachers in Norway chose a square indenter which is implied to model the impact of a boat with vertical sides [61]. It is apparent [61] that wider indenters give stronger load versus dent depth responses, although the variation is quite small. Further confirmation of this result is given by Smith [149].

DENT GEOMETRY

In the opposing indenter set-up of Thomas et al [161] an exponential decay of deflection is found along the longitudinal centre line, given by

$$\omega/\delta_0 = \exp(-0.65x/R) \qquad (2.1)$$

for a section slenderness of

$$R/t = 16 .$$

Here ω is the lateral deflection at a longitudinal distance x from the dent centre. These symbols, illustrated in Fig. 5.8, are consistent with those adopted

elsewhere in this dissertation. Eqn. (2.1) implies a practical total dent length of

$$L_D = 14R$$

(Ref. [25]). Photographs in Ref. [161] show the dent to be approximately diamond shaped in plan with the edges slightly concave rather than straight.

Smith et al present several lateral deflection diagrams [146,149]. The dent profile appears to be sharper than predicted by Eqn. (2.1) when the knife edge is used, but the application of a round indenter produces a more gradual profile near the dent centre. As the primary concern of Rashed et al is with the residual strength of dented tubes they do not include information on the lateral deflection profiles.

2.7.1.2 UNIFORM INDENTATION

In the quest for improved impact attenuation systems Reid [123] and his co-workers have subjected tubes with various support arrangements to uniform deformation by loading through either a longitudinal line or a rigid platten. Complementary analytical work is noted in Section 2.7.2.2 below.

2.7.2 THEORETICAL ANALYSES

2.7.2.1 INTRODUCTION

Early analyses of the behaviour of cylinders under radial loading were usually elastic. Morley [102], for example, in 1960 used governing differential equations of cylindrical shell theory to study an infinitely long cylinder subjected to opposing radial point loads.

More pertinent to damage, however, are larger deflections with plasticity, and various analytical procedures that have emerged in the past are now reviewed in several catagories.

2.7.2.2 LOCAL DENTING

INDENTATION MODELS

It was mentioned earlier, in Section 2.7.1.1, that an exponential dent profile produces an almost diamond shaped dent in plan, except that the edges are a little concave. On the other hand, if a bilinear profile is assumed the diamond becomes convex, as demonstrated in Fig. 5.8. It is easy to see why several authors have simplified the plan shape to a diamond in their mechanism analyses of denting.

Thomas et al [161] have derived an expression for the amount of energy dissipated in forming a "bow-tie" mechanism. This deformation pattern occurs when the two wedge indenters meet at the mid-depth of the tube and eight triangular shaped planes incline outwards to the ends of the model. The work done in flattening the curved surfaces and rotating the hinge lines is quantified in terms of the final deflection.

A similar approach is used by de Oliveira [25,26] to compute the work necessary to produce a diamond shaped dent on the top of the tube only, which is applicable when there is only one indenter. The mechanism contains four angled hinge lines and one hinge line normal to the tube axis, such as would occur with a knife edged wedge. The principles are readily extended to consider the pattern formed by a square nosed indenter, where the two triangular faces are separated by a flat rectangle.

Furnes and Amdahl [61] have analysed the same mechanism shape with two important modifications. Firstly they incorporate the energy absorbed by the tensile forces

in elongating the generators. They also consider the mechanism at various consecutive stages of deflection in order to take account of the deformation history. In this way a relationship between lateral load and deflection may be defined. At small deflections, when overall bending does not take place, it is found to agree fairly well with the experimental results. The formulation has been included in several computer programs which aim to predict the collision resistance of offshore structures [113,83].

In contrast, Ellinas and Walker [48] simplify the approach by assuming that energy is dissipated only at the central hinge under the indenter. This is based on an observation that elsewhere the hinges are not well defined. The exponential dent profile Eqn. (2.1) is used to quantify the rotation of the central plastic hinge. They find also that the lateral load increases in proportion with the square root of the dent depth and this agrees very well with experimental results for tubes with no axial or rotational restraint at their ends [50].

Plastic methods have also been applied to other dent shapes. Tooth and Jones [162] give detailed derivations of the collapse load for the rectangular shaped mechanism observed to form around a saddle as it supports a cylinder.

Another rather different method is proposed by Morris and Calladine [104] for correlation with Morris's tests, which were mentioned earlier [103]. The mechanism consists of a series of polygons which fan out to form a ring around the loaded boss. An incremental analysis is performed. In each step the shapes of the polygons are optimized and after computing the load capacity small compatible rotations are imposed to give a new configuration. The method compares well with the test data and has been simplified a little by de Oliveira [25].

RING MODELS

Whereas indentation models incorporate varying dent depth along the tube, ring models treat a slice in which the lateral deflection is assumed to be constant. They are useful, therefore, in analysing situations where lateral load is applied over a length comparable to the length of the tube. Because their models were quite short, Thomas et al [161] chose ring models to correlate with their opposing indenter tests. De Oliveira [26] has suggested their application to non-uniform dents by dividing the deformed zone into a series of rings and summing each contribution to the energy absorption.

Several ring collapse mechanisms have been formulated to describe the lateral loading of a tube between rigid flat platens [30,121,122]. The formulae predict increasing load capacity after plastic collapse. This is enhanced by strain hardening which is incorporated into the second and third of the above three references. Reid [123] has summarized the work and also includes the result for a ring compressed by diametrically opposed point loads. In this case the load diminishes after collapse. These methods find application in the analysis of layered tube systems for use in energy absorbing devices.

Numerous analyses of the behaviour of rings under external pressure, including buckling and collapse, have also been developed but these are not sufficiently relevant to the topic under consideration to be discussed here.

2.7.2.3 OVERALL BENDING

The overall bending behaviour of tubular members under accidental lateral loading has been discussed in several papers. Commonly the authors adopt relatively simple analytical approaches based on the plastic mechanism of a beam. This is only valid, of course, if the

member is able to develop its full plastic moment capacity and most of the papers give guidance on the geometries that may be considered sufficiently compact. Commonly the work of Sherman [142] is quoted which demonstrates that the plastic moment is achievable for

$$R/t \leq 18 .$$

To survive the very large rotations indicative of damage without strength erosion, though, a more realistic limitation may be [50]

$$R/t \leq 10 .$$

The majority of members on offshore jackets fall outside this range but Ellinas and Walker [48] have suggested, in these cases, replacing the yield stress with an effective limit stress equal to that which induces local buckling.

If the supports provide axial restraint, lateral deflection induces membrane tension forces which increase the load carrying capacity markedly. This phenomenon has already been discussed in Section 2.4 for beams of rectangular section. However de Oliveira's derivation for a tubular member is described here. In Ref. [25] he presents a load versus deflection relationship for central point loading which assumes full axial and flexural fixity at the supports. This is extended in Ref. [27] to consider the dynamic effects that ensue when the load is produced by a falling mass.

In Ref. [26] de Oliveira adopts different end conditions by providing axial and rotational springs there. The mechanism therefore has only one plastic hinge and all of the axial extension forced upon the member is assumed to be generated in this hinge. To facilitate computation of the extension a linear approximation of the yield condition is made. The static lateral load is applied at an arbitrary point along the span to maintain

generality.

In this paper de Oliveira includes an interesting sample calculation chosen to typify a supply boat collision with an offshore structure. It is found that only ten to fifteen per cent of the kinetic energy is absorbed in local denting. The remaining impact energy is able to be dissipated in beam bending with relatively little build up of membrane tension; in fact

$$n < 0.18$$

where n is the axial force as a proportion of the yield force. It is shown however that this mode might well be curtailed by failure of the tubular joints.

Ellinas and Walker [48] base their approach on yet another set of support conditions. Full flexural restraint combined with complete freedom to pull in longitudinally is assumed. Also in contrast to the above methods, they consider the reduction in the plastic moment capacity at the central hinge due to denting there. How the effective capacity is evaluated follows in Section 2.9.2.

So, whereas de Oliveira [26] treats local and overall deformation modes distinctly and sums their contributions to energy absorption, Ellinas and Walker [48] assume a behaviour sequence. Local denting occurs first which gradually erodes the stiffness to bending deformations. At a certain point the beam is made weak enough to be able to bend in an overall mode and thereafter the dent depth is assumed to remain unchanged. The change-over point may be evaluated by equating the lateral load versus deflection responses for the two modes.

More recently the ideas of Ellinas and Walker have been generalized by Richards and Andronicou [125] to incorporate either pinned or encastre supports, with or without full axial restraint. In situations where pull-in

is prevented it is found that the lateral load remains almost constant in the beam mechanism phase as the loss in load carrying capacity of the plastic hinge is compensated by membrane action. Failure is deemed to occur when the membrane force reaches yield.

The predicted work done in forming plastic hinges and generating tensile yield forces in laterally loaded tubes has been compared with actual experimental observations by Foss and Edvardsen [58]. This determines the degree of optimism inherent in simple plastic methods, which for some geometries and loading configurations is quite significant. One example is the tubes with no flexural or axial end restraint discussed in Section 2.7.1.1. Here the energy absorbed during testing is about fifty percent of that predicted by considering the rotation of a perfect plastic hinge at mid-span, and is attributable to a combination of deleterious effects which may include local buckling and ovalization as well as denting.

Smith et al [146] have studied lateral bending of tubes, without denting, using another tool - finite element analysis. The four support combinations of flexural and axial fixity and freedom are all considered. Using the program, information may be obtained on the residual stresses remaining after the load is removed, and a saw-tooth pattern of alternating tensile and compressive stress is found. Importantly, the stress under the point of load application is tensile which retards the development there of compressive yield under subsequent longitudinal loading. The inclusion of residual stresses in the numerical analysis therefore has little effect on the computed compressive strength of bent tubes [148].

Another finite element program developed by Soreide and Amdahl [152] includes the effect of the dent on overall bending.

2.8 COMPRESSIVE STRENGTH OF DAMAGED UNSTIFFENED TUBES

2.8.1 EXPERIMENTAL PROGRAMMES

In 1979 Smith and his co-workers [145] published experimental results concerning the effect of damage on the buckling strength of tubular members, and in doing so expressed the interest of the UK Admiralty Marine Technology Establishment, now the Admiralty Research Establishment, in the damage problem. Different methods of lateral load application were employed, as discussed earlier in Section 2.7.1.1, with the aim of producing local denting and overall bending deformations both together and in isolation. The initial deflections present in all real columns, however, are amplified by the longitudinal pull-in of dented fibres which means that all models contain some deflection in the overall mode. The residual stiffness and strength of the damaged models and their postbuckling responses are found by loading them to and beyond failure in axial compression.

More data have come from further testing [149] which includes several at full scale [146]. Rashed, Taby and Moan [120] have undertaken a similar series of compression tests on models damaged predominantly in the local mode.

In Ref. [173] Valsgard and Foss summarize a series of compression tests on dented tubular stub columns with pinned ends. It may be inferred from the presented graph of results that the strength reduction is comparable to the loss of cross sectional area in the dent. Put another way, additional deleterious effects including bending which might be introduced by the eccentricity of the remaining effective area do not seem to come into play.

2.8.2 THEORETICAL ANALYSES

Smith et al [145] have studied the behaviour of many tubular columns with a large-displacement elasto-plastic plane frame analysis based on the finite element method. Initial deflections in the overall mode are built into the geometric formulation of the mesh and residual stresses are also readily included.

The program cannot treat local buckling and so is restricted to tubes having relatively stocky sections. For the same reason it is unable to form a rigorous analysis of dented tubes. By representing the dent zone in an approximate manner, however, the program gives a relatively simple and quick solution which is ideal for parametric studies [148]. It is assumed that the dented fibres behave as though they are in the advanced postbucking regime, which may be represented by a bilinear response of reduced stiffness and strength [146]. Thus

$$E_D/E = k_D = \sigma_{yc\,D}/\sigma_{yc} \ .$$

Because the reduction factor k_D must also allow for the presence of residual stresses and other complexities, it is evaluated not from theoretical considerations but by correlation of the predictions of the program with empirical data. This is done with the aid of a regression analysis [149] which incorporates all the relevant test results of Smith et al and Rashed et al. The outcome is

$$k_D = 0.3 \ .$$

The final numerical procedure gives quite good estimates of the experimentally observed load-shortening curves. It further demonstrates that for either local or overall damage the residual strength is insensitive to the location along the member length of the lateral loading that induced the damage [148].

Richards and Andronicou [125] adopt the reduction factor k_0 in their development of the stress/strain characteristics of dented sections under the action of applied bending moment and axial force. These are incorporated into a strength analysis of damaged tubular columns which treats the dented zone as one element and divides the intact regions into other elements. Pinned ends are assumed so the geometry is given an initial overall deflection in the form of a half sine wave. Account is taken of plasticity and large displacements, and the results attained agree well with those of Smith [149].

A quite different analytical approach is pursued by Rashed et al [120] to complement their experimental programme. A model of behaviour under longitudinal compression is built up based on the following postulates:

(a) The column is initially straight and any early elastic bending deformations are neglected. The compressive stresses are uniform even in the damaged region because the tendency for the dent to bend inward is restrained by the surrounding undamaged tube.

(b) Uniform stressing continues until the dent centre line forms a plastic hinge. This is calculated by considering the plastic capacity under combined bending and compression of the centre of a bilinear mechanism, assuming the outer ends support no moment. The load causing dent plastification is thus given by

$$\sigma_{DP}/\sigma_{YC} = \sqrt{\xi^2 + 1} - \xi \qquad (2.2)$$

where

$$\xi = 2\tilde{\delta}_{DD}/t \qquad (2.3)$$

and $\tilde{\delta}_{DD}$ is the mean depth for the arc of dented

fibres. The notation adopted here is not entirely consistent with that used in Ref. [120], but is explained in greater detail in Section 6.6.

(c) In further loading the dent deflects freely, carrying no more load. Thus the axial load acts on a reduced cross section and at an eccentricity to the centroid of the effective area, causing bending. The intact portions of the column remain straight but are angled so as to meet the curved segment tangentially. The resulting deflected shape is magnified by the axial load according to Euler effects, which of course increases the moment acting at the dent.

(d) Ultimate load is deemed to be reached when the fibres adjacent to the dent start to yield. It may be calculated by iterative solution of a formula in which the lateral deflection and longitudinal load are interrelated.

(e) The load remains constant at this ultimate value during increasing deflection to form a plastic hinge throughout the effective cross section at the dent location.

(f) Unloading then occurs governed by plastic mechanism theory and is followed numerically.

Ellinas [49] has developed a modified version of the ultimate strength equation of Rashed et al which caters for combined overall bending and local denting damage. The overall bending damage is treated as a large initial imperfection. It is increased by adding a component which accounts for other structural defects, such as residual stresses, and magnified further by the Euler effect. The eccentricity of loading on the effective section in the dented region is similarly magnified. Rearrangement produces a quadratic equation for the load capacity.

Richards and Andronicou [125] compare Ellinas's predictions with those obtained numerically and find that the correlation is excellent for undented tubes. When denting is present, however, the analytical results are significantly lower than the others. In Ref. [125] this is attributed to the dented material being assumed ineffective by Ellinas. In fact, the analyses of Rashed et al [120] and Ellinas consider the dent to have full stiffness, and the strength is reduced by factor

$$k_D = \sigma_{DP}/\sigma_Y \ .$$

2.9 MOMENT CAPACITY OF DENTED TUBULAR SECTIONS

2.9.1 EXPERIMENTAL PROGRAMMES

A series of bending tests on dented tubes have been described by Ueda and Rashed [169]. The experimental arrangement ensures that the tubes are subjected to pure bending moment with the dent located in one of three places: compression side, tension side or neutral axis. Results are presented in the form of moment-curvature plots and the observed capacities are compared with analytical predictions discussed in Section 2.9.2 below.

It is possible also to deduce effective moment capacities from the collapse loads of simply supported tubes under lateral point loading in Ref. [161].

2.9.2 THEORETICAL ANALYSES

Although relatively little experimental data concerning the response of dented sections to bending is known to this author, many reseachers have considered the problem theoretically. The results usually form an intermediate step in their analyses of how the overall member behaves under some loading situation. All methods are based on plastic distributions of stress.

Only the shape of the dented section is assumed by Soreide and Amdahl [152] to affect the moment capacity and so they consider that the flattened material in the dent is able to carry the full compressive force induced by bending. This approach supersedes an even more optimistic result by Kjeoy and Amdahl [88] in which dents of

$$\delta_0/R \leq 0.4$$

are taken to cause no reduction in bending strength whatsoever.

In contrast, Rashed et al [120] give the dented fibres a maximum stress of σ_{0p} which parallels their approach in quantifying the compressive strength of dented sections. Ellinas and Walker [48] simplify their solution and in Ref. [50] Ellinas demonstrates his method to give close but conservative estimates of the test data in Ref. [161]. The same cannot be said for the two formulations mentioned in the paragraph above.

Ueda and Rashed [169] have derived a general ultimate strength interaction relationship for axial load and bending moments in two perpendicular directions. The dent plastification stress is again utilized when the dent experiences compression; in tension however, dented fibres are assumed able to support stresses up to yield. The predictions agree well with their experimental work and

are also similar to the theoretical predictions of Richards and Andronicou [125]. These last authors designate a reduced strength factor of

$$k_D = 0.5$$

to the dented fibres, following Smith's methodolgy [149].

2.10 DAMAGED RING STIFFENED CYLINDERS

In comparison with unstiffened tubes relatively little effort has been afforded to stiffened cylinders in the realm of damage. This scarcity of information allows its presentation without the system of sub-headings adopted in Sections 2.7 to 2.9.

Smith and Dow [147] have discussed the consequences of damage on the residual strength of ring stiffened cylindrical shells under external pressure. Because interframe buckling may be either axisymmetric or lobular they consider damage consistent with each of these forms. It is concluded that a local indentation is unlikely to cause serious loss in strength but that scope exists for parametric investigation of the axisymmetric deformation. The latter may be caused by accidental overload or by an underwater explosion.

The other possible mode of failure is general instability. Damage sympathetic to this involves ring frame bending and is conservatively investigated by Smith and Dow with a two dimensional ring model of a single frame and its associated shell plating. The damage process is represented by a radial point load acting on the ring and is reacted by a force distributed uniformly around the circumference. A plastic mechanism analysis is derived for comparison with finite element runs. The latter also enables residual stress distributions in the ring frame to

be determined as well as the residual strength under subsequent external pressure loading.

Researchers at two centres, at least, have investigated how local denting affects the axial strength of ring stiffened cylinders.

A preliminary study using the method of finite differences is described by Frieze and his colleagues at the University of Glasgow [59,60]. Local damage is simulated by applying a point load at mid-bay whilst allowing the cylinder ends to pull in longitudinally. The subsequent responses under axial compression show that for the relatively stocky geometries under investigation the stiffness is unaffected and strength loss is not marked.

At Imperial College Onoufriou and Harding are currently undertaking a comprehensive experimental and numerical study into the problem. In the tests cylinders are dented through a knife edge with 1mm radius aligned normal to the longitudinal axis. They are then crushed axially. In both procedures the rigs used are the same as those described in Chapters 5 and 6 of this dissertation. Numerically, the axial loading response is modelled by finite element analysis of a mesh that duplicates the shape of the dented cylinder. By comparison with a similar analysis of a nearly perfect cylinder the strength loss due to damage may be ascertained.

Results are presented in Ref. [110] pertaining to the first test, where the indenter is located at mid-bay and damage is confined to that bay alone. Empirical data relating to the lateral load build up during denting and the ensuing dent shape and residual stresses are given. This third item is not included in the strength analysis. By investigating two different mesh configurations and two methods of axial load application the numerical work yields responses covering a quite broad range. However it is again concluded that the dent has only a relatively

small weakening effect in this rather closely stiffened model where

$$L/R = 0.15$$

$$R/t = 167 .$$

A similar project of research is underway at the University of Surrey under the auspices of the same cohesive buckling programme. This time the dented cylinders are subjected to external pressure together with axial loading. Results, however, are not yet available.

2.11 DAMAGED LONGITUDINALLY STIFFENED CYLINDERS

Walker and Davies [177] have described an axial compression test on a cylindrical model with eight stringers in which one of the panels was given an initial imperfection at mid-span of twice the thickness of the skin. The result is a ten per cent strength loss in comparison with similar nearly perfect models, combined with reduced stiffness. Further discussion of the entire experimental programme of Ref. [177] is given in Section 2.13 below.

Concerning another type of stiffening Carney and Veillette [17] have carried out an experimental programme with short tubes braced internally by two tension straps which cross to form an X-shape. The energy absorption characteristics of these tubes are determined by impacting them radially between two platens.

2.12 DYNAMIC LOADING

Passing references to dynamic loading have been made already in this chapter. It is not the purpose of this Section to review developments in the field in any detail but only to highlight some of the structural components relevant to offshore engineering that have received attention.

Concerning the denting of tubes Reid [123] has described impact tests undertaken to study the effects of material strain rate sensitivity and system inertia on the deformation process. The second issue, only, is considered by Davies [21,22] when addressing patch loading of a concrete caisson as part of a ship collision problem.

As mentioned in Section 2.7.1.1, Soreide and Amdahl [152] have investigated the effects of loading rate on longer tubular beams. The lateral loading was chosen to correspond to a speed of one or two metres per second for a full sized structure. For beams where axial fixity against pull-in is provided, the enhanced straining rate has negligible influence on the overall bending response, although about a ten per cent reduction in local dent deformation is noted. This might be expected as rapid localized straining in the dent zone elevates the yield stress there.

Based on rigid-plastic methods, theoretical consideration has also been given to lateral impact loading of both beams and plates; see for example Refs. [159,75,80,27]. An application of this work is in quantifying the extent of slamming damage in ships [76].

The plastic crumpling under axial impact of unstiffened [116], ring stiffened [4] and stringer stiffened [81] cylindrical shells has been addressed as well.

Comments on how inertia forces and strain rate might influence the response of stringer stiffened cylinders to lateral impact of the form investigated in this dissertation will be found in Section 5.8.

2.13 STRENGTH OF UNDAMAGED STRINGER STIFFENED CYLINDERS

2.13.1 INTRODUCTION

To ascertain the effect of a dent it is clearly essential to have, as a yardstick, knowledge of how a nominally perfect model with the same geometry behaves. In this dissertation, therefore, the compressive strength of stringer stiffened cylindrical shells is important. Over the years a wealth of experimental data has built up involving various methods of fabrication, geometries and loadings and with it comes a complementary body of theoretical understanding.

It may seem surprising to the reader that this material will not be summarized in detail here. This is firstly because several comprehensive reviews of cylindrical shell literature have been published at Imperial College alone in the past year [1,54,52,168]. Second, the behavioural complexity of cylinders means that when geometric and material properties are changed markedly, the new response cannot be confidently inferred from prior knowledge. Such variation has fueled a vast number of papers, as the reviewers have emphasized. It also results in much of the information being of limited value to the present work for other than background reading.

By way of example attention will be turned briefly to stringer stiffened cylinders subjected to axial compression. An important motivator of previous studies in

this field was the development of aeroplanes and later aerospace vehicles. The shells employed in these structures differ from those under consideration in the present research in several aspects [180]. Being thin and composed of high strength aluminium alloys ensures that buckling is elastic whereas yielding inevitably accompanies failure of the stockier steel members found offshore [108,63,67]. The behaviour of the latter thus nestles somewhere between that of light elastic cylinders and the ductility of the thicker unstiffened tubes traditionally used in braced jacket construction. Also, models representing airborne components usually contain more stiffeners, with lower cross sectional aspect ratio h_t/t_t , than their counterparts in the ocean and are shaped integrally by machining down thicker material. For offshore installations stiffeners are welded onto the shell and thus produce different types of geometric imperfection and residual stresses.

2.13.2 EXPERIMENTAL PROGRAMMES

Of all the axial compression tests undertaken on stringer stiffened cylinders, only a very small proportion are of direct relevance to the offshore industry. An inventory follows, starting with the work of Walker and his colleagues at University College. Most of the models designed in the United Kingdom were chosen to typify the range of geometries found in practice [63]. However the Imperial College tests [43] exhibited such stocky behaviour that later tests there by Agelidis [1] involved lighter sections to clarify their suitability for possible future construction.

In 1976 Walker and Davies [177] published results of a preliminary series of compression tests on stringer stiffened cylinders, and these were augmented by further testing [180,181]. Models at about one-twentieth scale

were built up segmentally from thin steel sheet by rolling curved panels and fusion welding them two at a time to an intermediate stringer. Each end of the completed cylinder was bolted between concentric rings to provide a clamped end condition.

Two general geometries are contained in the programme. Four of the cylinders are relatively stocky,

$$R/t = 90$$

$$L/R = 1.3 ,$$

with eight stringers. With the exception of the damaged model mentioned earlier in Section 2.11, these attain loads slightly above "squash" although their stiffnesses are lower than the simple elastic prediction.

The remaining shells have mostly either twenty or forty stiffeners (one contains thirty, however) and geometry within the ranges

$$200 \leq R/t \leq 360$$

$$0.4 \leq L/R \leq 1.6 .$$

Although a few of the models reach yield load, most do not, the range being

$$0.65 \leq p_{Am} \leq 1.04$$

for the forty stringer models and

$$0.52 \leq p_{Am} \leq 0.82$$

when the number of stiffeners is halved. Here p_{Am} represents the peak load as a proportion of squash load. Analytical methods are developed in tandem which correlate reasonably well with the observations.

Three of the above geometries were also fabricated at larger scale

$$k = 1/8,\ 3/16$$

where k is the scale factor, at the University of Glasgow. The researchers, Green and Nelson [63], note that even fabricating at these sizes it is difficult to keep the residual strains and imperfections induced by welding within the limits expected for prototype structures. They therefore only stitch welded the stringers intermittently to the can.

The initial stiffnesses exhibited by the Glaswegian models are close to the elastic predictions, and two of them fail at similar nondimensionalized load to their counterparts tested by Walker and his team. The third reaches only two thirds of the peak load observed in the smaller model and is attributed to premature weld failure [63].

This third larger scale model, having three bays, was the first orthogonally stiffened cylinder to be tested as part of the recent offshore related research in the United Kingdom [44]. Soon afterwards a second three bay test was undertaken at Imperial College using a similar size and geometry,

$$R/t = 170$$

$$L/R = 1.1\ ,$$

but with twenty rather than thirty stringers [42]. Here collapse occurred at

$$p_{fm} = 0.87\ .$$

Five years after the original tests of Walker and Davies [177], Imperial College reported a similar small

scale experimental programme [42]. Similiar, but with several important differences. First, these new models were fabricated by welding the stringers to a flat plate which was later made cylindrical, and second, they were then heat treated to remove the residual stresses. Such modifications serve to reduce the level of imperfections. Heat treatment has the additional advantage of producing a material characteristic with a distinct yield plateau to replace the gradual nonlinearity demonstrated by the original steel.

Many details of Fahy's tests [42] and those that followed, undertaken by Agelidis [1], are given later (see Chapters 5 and 6) due to their considerable value in the work to be presented. To round off the current discussion it may be stated that the Imperial College small-scale models load with the expected elastic stiffness and, with one exception, exhibit capacities very close to yield.

A comparison is of interest between Fahy's three cylinders and their counterparts of nominally identical size and geometry in the University College test series [181]. For the forty stringer models similar peak loads are observed at the two centres, but for the pertinent twenty stringer geometry failure occurred at fifteen per cent lower load at University College. A sharper contrast is found with deflections, however, with the unit end shortening being several times larger than the yield strain at the attainment of peak load in the Ref. [181] results. This is encouraged by panel buckling at low load. The variation in response has been attributed [44,54] to the presence in the earlier tests of residual stresses and higher local imperfections, as well as a degree of rotational flexibility inherent in the end ring detail. Insensitivity to geometric imperfections allows the forty stringer models to attain loads approximating squash [54], notwithstanding, but the broader panels of the twenty stringer shells must be more susceptible to imperfection.

In the United States of America a compression test on a long fabricated shell has been reported [87]. The model includes 25 bays, each having 24 stringers, and represents at one-fifth scale the pontoon legs of a braced jacket with

$$R/t = 250$$

$$L/R = 0.21 .$$

The peak load recorded is

$$p_{A_m} = 0.80$$

but it should be noted that the same model had previously been tested to failure under hydrostatic pressure. Between the two loadings the large number of buckled shell panels were "popped back close to their original cylindrical shape" [87] but no attempt to stress relieve the model was made.

A more extensive testing programme has been completed recently at Chicago Bridge and Iron Industries in Illinois. Large scale three bay models were fabricated to give the centre bay a slenderness within the confines

$$190 \leq R/t \leq 500$$

$$0.4 \leq L/R \leq 1.0 ,$$

with the end bays always thirty per cent shorter. Despite this prudence failure is initiated in an end bay in the majority of compressive tests, and is always aided by torsional instability of the slender stringers

$$h_t/t_t = 16 .$$

The observed capacities [55] fall within the range

$$0.43 \leq p_{Am} \leq 0.94 ,$$

the strongest model being very similar in geometry to one of Agelidis's tests [1] that failed at

$$p_{Am} = 1.07 .$$

Two of the American geometries are duplicated and the second model tested without prior heat treatment. Comparison of the results show residual stresses to reduce the peak load by about ten per cent.

2.13.3 DESIGN METHODS

Depending on their geometric and material properties, orthogonally stiffened cylindrical shells subjected to uniaxial compression may buckle in a variety of modes [86,34], as follows:

: local buckling of the stringers
: local shell buckling between stringers
: interframe buckling of one or more stringers together with the shell
: general instability including both stringers and rings
: overall buckling of the cylindrical column

A frequently applied tenet in the design philosophy of stiffened structures is to ensure that general instability is preceded by either shell or interframe buckling [108], because the first mentioned collapse mode may be catastrophic as there is no strength reserve afterwards. This is achieved by specifying ring frame sizes that make the general buckling stress higher than the stresses that precipitate other modes. For similar reasons stringer slenderness limits are also stipulated to prevent torsional buckling [171] as this mode would shed load rapidly to the shell panels, causing them to fail

very suddenly.

In general, more design freedom is allowed for the remaining modes of collapse. Consideration is given firstly to local shell buckling.

Koiter [90], in 1956, wrote on the elastic critical stress of a perfect, axially loaded curved panel with simply supported edges. He presented the result in terms of a total curvature parameter

$$\bar{\varphi} = \frac{1}{2\pi}.[12(1-\nu^2)]^{1/4}.\frac{b}{\sqrt{Rt}}$$

to be

$$\sigma_{cr} = \frac{\pi^2 E}{3(1-\nu^2)}.\left[\frac{t}{b}\right]^2.(1+\bar{\varphi}^4) \quad . \qquad (2.4)$$

It is clear that as $\bar{\varphi}$ approaches zero, Eqn. (2.4) is asymptotic to the result for a flat plate, that is

$$\sigma_{cr} = \frac{\pi^2 E}{3(1-\nu^2)}.\left[\frac{t}{b}\right]^2 \quad .$$

Conversely, for large $\bar{\varphi}$ the equation converges on the solution for an long unstiffened cylinder [140], thus

$$\sigma_{cr} = \frac{E}{\sqrt{3(1-\nu^2)}}.\frac{t}{R} \quad .$$

It is well known that the elastic postbuckling response of a flat plate is stable, so that loading is able to continue after buckling but with a reduced stiffness. Koiter [90] shows this to be valid for all

$$\bar{\varphi} \leq 0.64$$

whereas for higher $\bar{\varphi}$ the slope of the postbuckling curve

becomes negative. This signals the advent of imperfection sensitivity.

The panels of orthogonally stiffened shells are bounded by stiffeners which provide flexural restraint to the edges and are thereby likely to increase the limit of positive postbuckling [54]. Syngellakis and Walker [160] have shown, though, that in this case there exists a cluster of critical loads in the immediate vicinity of the lowest so that mode coupling gives the potential for higher imperfection sensitivity.

Even when buckling is unstable the panels will unload into the stiffeners and collapse will only occur after the stringers reach capacity. Of course this bonus is precluded if the stiffeners are so flexible that they buckle laterally at a faster rate than the shell [65,54].

The DnV buckling notes [34] incorporate a slightly modifed version of Eqn. (2.4) for use with knock-down factors covering imperfections, residual stresses and material yield. Harding and Dowling [65] have demonstrated that this design method compares reasonably well with the curved panel strength predictions of a large-deflection elasto-plastic numerical approach which includes critical mode imperfections of the magnitude typically assumed in bridge design.

Interframe buckling of the stringers and associated shell is another possibly critical mode of failure. For narrow panelled cylinders orthotropic elastic buckling theory may be employed to obtain a equation for the critical stress of a perfect stringer stiffened model which has the same form as that for a column on an elastic foundation. Equating the two formulae determines the stiffness of the foundation, which represents the effect of shell curvature on the behaviour of the stringers. Consequently, several authors [180,171,67,54] have suggested, for this buckling mode, the analysis of a

single stringer together with its attached plating as a beam-column. Thus in elasto-plastic situations the cylinder capacity may be estimated by adapting the Perry-Robertson approach for column design. The stringer beam-column is given an initial sinusoidal imperfection which is amplified under compressive loading until first yield occurs. Local shell buckling effects are taken into account by using an effective width of associated panel.

Various versions of the method [180,171,67,54] are found to produce conservative predictions of the available experimental strengths, for several reasons. Simple supports are often assumed for the stringer column. A stringer with maximum imperfection is analysed and failure is equated with initial yielding. These two assumptions exclude the spread of plasticity through the section of the stringer under consideration, as well as any stress redistribution to other stringers that lie elsewhere in the circumferential wave pattern and thus have smaller deflection. Residual stresses are also accounted for cautiously.

Existing Code recommendations do not include this approach, preferring instead to either treat the cylindrical shell as a stiffened plate [34] which is even more conservative [86], or to apply the traditional knock-down factors to the perfect elastic buckling stress [53].

2.14 CONCLUSIONS

The principles of plastic collapse theory are well known. Recently they have been utilized to gain an understanding of the energy absorbing capability of tubes, which are found to provide an efficient cushion against impact. Offshore oil and gas rigs were constructed of tubes before their crashworthiness became an issue, which is fortuitous as ship collision is now realized to be a

prominent hazard to the safety of these structures.

A survey of information concerning the behaviour of unstiffened tubes, both during accidental loading and afterwards when they are subjected to functional loads, has been presented in this chapter. The quantity of data is considerable, in stark contrast to that for orthogonally stiffened cylindrical shells which are the primary topic of this dissertation. However a knowledge of tubes is relevant to the present work and useful information is also available from investigations of other structural units, especially beams and plates. The research presented later in this dissertation draws on material given about both types of element within this chapter, despite these latter studies being frequently born of other engineering requirements, quite separate from offshore impact design.

Given the collision risk, and the increasing use of light orthogonally stiffened shells in buoyant structures, it appears imperative that some specific consideration should be given to their collision resistance. It is hoped that the following chapters will go some distance towards achieving an understanding of the potential problem.

CHAPTER 3

DENTING OF STRINGER STIFFENED PLATES

3.1 INTRODUCTION

As part of a study into the effects of accidental loads it is fruitful to investigate the behaviour of stiffened plates loaded well beyond the elastic limit. This has relevance in its own right; to evaluate, for example, the possible consequences of a dropped object hitting the deck of an offshore structure or the pontoon of a semi-submersible. However the investigation also enables a basic understanding to be built up which facilitates the study of other structural units, such as stiffened cylinders. Plate models afford the advantages of simplicity and economy over cylinders in both fabrication and testing. Similarly, for analysis, plates do not have the additional complexities of curvature and transverse restraint.

This chapter is specifically concerned with devising an analytical model of dent development in stiffened plates. The experimental programme explained below provides a source of data against which the theory is checked. In both this and the next chapter emphasis is placed on experimental technique as well as theory because knowledge gleaned in both areas will be applied to cylinders later in the dissertation.

3.2 EXPERIMENTAL PROGRAMME

3.2.1 INTRODUCTION

Of primary interest throughout this dissertation are individual "stringer beams", by which is meant the T-shaped sections comprising a stiffener and its associated plating. The preliminary test programme consisted of two longitudinally stiffened plate samples. The first included four stringer beams and the second had three. Geometric details of these elements are given in Table 3.1 at the end of the chapter.

The first test specimen was laterally loaded to failure to assess its ultimate deflection capability. This was required to help plan the degree of damage to be applied to future tests before loading in longitudinal compression. It was necessary to ensure that the very thin steel used in the models was able to undergo large bending strains before rupture, that when scaled were comparable to what a full sized component might withstand. In particular, the welding process should not have impaired the ductility. Whether the end connection detail affected the mode of failure was also important.

With the knowledge that the first test proved satisfactory, Plate P2 was unloaded prior to rupture to allow a subsequent compression test, details of which are presented in Chapter 4.

3.2.2 MODEL MANUFACTURE

Section 5.2.2 includes a description of the method used to fabricate longitudinally stiffened cylinders. It will be seen there that the stiffeners were TIG welded to

a plate which was later wrapped around a mandrel to give it circularity. The present test pieces were off-cuts from this early stage of the fabrication process and so, by definition, had very similar properties to their cylindrical counterparts.

3.2.3 END CONDITIONS

There were two end plates at each end of the test pieces. One lay above the plate and the other below, the latter being slotted to accommodate the stringers. They were welded together and to the stiffened plate on the outer side of the support to minimize any resulting distortion within the clear span. The end plates were bevelled in preparation for the welding and afterwards were ground flat to remove excess weld metal. Clearance holes for M8 bolts were then drilled into both top and bottom end plates. They were located midway between the stringers to enable bolt placement to be as close as possible to the plate. Fig. 3.1 is a drawing of Plate P1 showing its support conditions.

3.2.4 HEAT TREATMENT

For heat treatment the samples were securely braced by threading tension rods through the bolt holes in the end plates, and then packing with sand. Details of temperature and duration are as given in Section 5.2.2. Heat treatment stress relieved the weld zone and produced a material response with an extensive yield plateau.

3.2.5 MATERIAL PROPERTIES

No coupons could be made for tensile testing as the original steel plate was no longer available. However, as both the heat-treatment process and the material were the same as those of Fahy's cylinders [42], his material properties are assumed here, namely:

$$\sigma_{YT} = 335 \quad N/mm^2$$

$$E = 200 \times 10^3 \quad N/mm^2 \ .$$

Also

$$\sigma_{YC} = \sigma_{YT} + 10 \quad N/mm^2$$

where

σ_{YC} = compressive yield stress
σ_{YT} = tensile yield stress averaged from the coupon tests.

3.3 DENTING TESTS

3.3.1 RIG ARRANGEMENT

The end plates were bolted to a stiff test frame, photographed in Fig. 3.2. Grade 8.8 bolts were used in Test P1 and in torquing up to nominally 85 per cent of proof load (3.1m.kgf) thread stripping failure occurred several times. Hence the bolts on one end connection were only torqued to 2.7m.kgf. High strength socket head cap screws with 3.1m.kgf torque were used for Plate P2 with no visible thread distortion.

The end connection was designed to prevent rotation and excessive pull-in under the action of the membrane tension induced at large deflections. It is seen from Fig. 3.2 that the vertical members of the test frame were extremely stocky and so were essentially unable to bow inward. Most of the support flexibility was attributable to the bolted connection. The bolts were torqued up to ensure that stretching of the connection in the longitudinal direction, caused by the tension force, was resisted by the through-thickness stiffness of the entire vertical member and not just the bolts. Even when the stiffened plate samples had attained uniform tensile yield ample precompression remained in the connection.

Another foreseeable source of pull-in was that of the tension forcing the end plates to bend inwards between the bolts, whilst pivotting at the weld and inducing prying forces at the outer edges of the end plates. The extent of this behaviour was dependent on the flexural stiffness of the end plates as well as the weld strength.

The success of the end connection in supporting the applied loads was one of the major questions concerning experimental technique to be answered by the preliminary testing programme. Ascertaining the ease of fabrication of the end plates to give a close fit to the stiffened plate, even allowing for the presence of unavoidable geometrical imperfections, was also important. Such difficulties would be heightened by the curvature of the later cylindrical models.

The test frame rested on the loading platen of a denting rig similar to that used for the cylindrical tests, and is described in Section 5.3.1. Above was another platen from which a knife edge indenter was supported via a rod which passed through a hole in the top of the frame. The wedge formed an angle of $\pi/3$, softened by a 3mm tip radius, which followed the indenter geometry of Smith et al [145]. The bottom platen was raised slowly

using a screw jack wound by hand so that the model reacted against the knife edge. Lateral loading was applied centrally across the entire plate width as the longitudinal edges were free, and was monitored with a Bytrex five tonne capacity load cell.

3.3.2 INSTRUMENTATION

3.3.2.1 STRAIN GAUGES

Post-yield linear gauges supplied by Tokyo Measurement Laboratories were aligned axially along one stringer beam, both on the top of the plate and on the stiffener, so that some indication of the distribution of strain through the T-section could be obtained. Strain differences in gauges placed on each side of a stiffener at a section showed out-of-plane deformations. On Plate P1, YL-5 gauges were placed at quarter-span, as illustrated in Fig. 3.1, to monitor membrane tension where bending effects are minimal. Locations near the end connection and under the indenter were also gauged to show plastic hinge behaviour, although the large gauge base size, relative to the stringer, limited the expected accuracy of these readings. In Plate P2, smaller YL-3 gauges were positioned at quarter-points only.

Although post-yield gauges are theoretically able to measure tensile strains up to 0.2, in Test P1 most peeled off well before this, presumably due to the glue being insufficiently ductile and the wiring becoming taut. By testing soon after the gauges were placed while the glue was fresh, and leaving loops of wire near the gauge connections to provide some slack, no gauges failed during Test P2.

3.3.2.2 TRANSDUCERS

For vertical deflection measurement, four Sangama linear transducers with 50mm travel were spaced at sixth-points along one stiffener. A fifth was used to measure the relative movement of the loading platens and hence the central deflection.

Holes were drilled through each end of the test frame in line with the stiffener/plate junction of the two outermost stringers. Sangama linear transducers mounted longitudinally measured any tendency for the stringer beams to pull in relative to the frame, which was regarded as being rigid.

Four banks of three 10mm travel, small linear transducers were positioned near each end of the two outermost stringers to measure out-of-plane deformations. Flats on the end of the transducer rods were in contact with 1.5mm and 3mm diameter steel balls glued near the outstand tip. The angle to the horizontal of the transducer mount was increased several times during the test to remain in line with the stiffened plate, and the resulting adjustments to the readings noted.

All of the aforementioned transducers are visible in Fig. 3.2 which was photographed at the completion of Test P1. Much wiring is also seen which connected the transducers and gauges to a data logger.

3.3.3 FINAL PREPARATION

By monitoring strains it was seen that sliding the stiffened plate with attached end plates into the test frame caused a small compressive stress and sagging bending moment, both being relatively uniform across the span. The compression indicates the close tolerances to

which the rig was constructed. It was sized to just fit the first test piece, and for Plate P2 accurately machined spacers were sandwiched between the end plates and the vertical frame members to accommodate its shorter length. In both tests the bending was due to the sides of the supporting frame being vertical whereas the end plates seemed to slope just slightly inwards towards the stringers.

Next the bolts were inserted and torqued up, which produced a slightly reduced bending moment and membrane pretension. Magnitudes of these forces, both before and after bolting, are given in Table 3.2. The indenter was set up and the platen separation adjusted until the knife edge just touched the model. Testing then proceeded.

3.3.4 TESTING PRECEDURE

Lateral deformation was applied in very small increments to ensure that the elastic response and the ensuing nonlinearity to fully plastic behaviour were all followed accurately. Once shape hardening had become prominent the deflection steps were increased in size, as exemplified by the spacing of test points in Fig. 3.9(a). The loading rate was effectively very slow because the instrumentation was read after each increment and logged both on floppy disk and at the printer.

3.4 THEORETICAL ANALYSIS

3.4.1 INTRODUCTION

In this Section a theoretical model of the behaviour of stiffened plates under lateral loading is developed. A discussion of the experimentally observed behaviour is postponed until later in the chapter (Section 3.5) when it is compared with the predictions.

Because the plates are supported at both ends only and subjected to line loading across their entire width, they may be treated as a series of point loaded T-section beams. The response involves several phases. The initial elasic behaviour is relatively unimportant for the geometries under consideration due to early yield at the stiffener tip. With the development of plastic hinges additional load is carried by a build up of membrane tension, due to stretching resisted at the supports. The plastic capacity of a T-section under combined bending moment and axial force is required for this stage of the analysis and is derived immediately below. Eventually the span yields uniformly in tension. The plastic hinges now have no moment capacity and additional load is carried by string action until rupture occurs.

3.4.2 PLASTIC CAPACITY OF STRINGER BEAM CROSS SECTION

3.4.2.1 T-SECTION

Consider the section in Fig. 3.3(a) where the equal area axis is assumed to lie in the panel and the centroidal axis within the stiffener, as occurs with typical stiffened plate geometries. It may be shown that

$$y_{cen} = h_t - (h_t A_t - tA_p)/2A$$

$$y_{eqa} = h_t + (A_p - A_t)/2b \ .$$

These dimensions represent the distance from the outstand tip to the centroidal and equal area axes respectively. The latter equation is valid for

$$h_t \leq y_{eqa} \leq h_t + t \ .$$

Also

$$Z_p = A^2/4b + A_t^2(1/t_t - 1/b)/2 \ . \qquad (3.1)$$

In these equations

$A_p = bt$

$A_t = h_t t_t$

$A = A_p + A_t$ = total cross sectional area of stringer beam.

The plastic interaction capacity is given using the sign convention that tensile force N and hogging bending moment M causing tension in the top of the panel are both positive. A typical stress distribution is drawn in Fig. 3.3(a) in which the material response is assumed to be rigid/perfectly plastic. Of course steel exhibits elasticity but it is generally recognized that this alters the plastic capacity only slightly.

Firstly moments are taken about the equal area axis. Hence if the neutral axis lies within the panel, that is, for

$$-1 \leq n \leq C_0 \ ,$$

then

$$m_{eqa} + fn^2 = 1 \ . \qquad (3.2)$$

Alternatively, if the neutral axis lies in the stiffener, then

$$C_0 \leq n \leq 1$$

and

$$m_{eqa} + \frac{bf}{t_l} n^2 - ((A_p/A_l)^2 - 1)(1-f)n = \frac{bf}{t_l} - (A_p/A_l)^2(1-f) \ .$$

Here

$$f = A^2/4bZ_p = bt_e^2/4Z_p$$

and therefore

$$1-f = A_l^2(1/t_l - 1/b)/2Z_p$$

from Eqn. (3.1). Thus f is the proportion of the T-section plastic modulus provided by a uniform plate with the same cross sectional area

$$A = bt_e \ ,$$

t_e being the thickness of the equivalent plate. Also

$$C_0 = (A_p - A_l)/A \ ,$$

and n and m are nondimensionalized equivalents of axial force and bending moment respectively; that is

$$n = N/\sigma_y A$$

$$m = M/\sigma_y Z_p \ .$$

When bending is considered about the centroid an extra component $(1-f)n$ must be added to the bending moment

ratios given above due to the net axial force acting through the lever arm

$$y_{eqa} - y_{cen} = (1-f)Z_p/A \ .$$

Hence for

$$-1 \leq n \leq C_0 :$$

$$m_{cen} + fn^2 - (1-f)n = 1 \qquad (3.3)$$

and for

$$C_0 \leq n \leq 1 :$$

$$m_{cen} + \frac{bf}{t_l}n^2 - (A_p/A_l)^2(1-f)n = \frac{bf}{t_l} - (A_p/A_l)^2(1-f)$$

$$= 1 - \frac{(C_0A)^2}{4Z_p}\left[\frac{1}{t_l} - \frac{1}{b}\right] \ .$$

Fig. 3.4 is the interaction curve for a typical longitudinally stiffened plate geometry. The approximate formulae given by Carlsen [13] give results reasonably similar to this derivation.

Normality is readily verified. With the neutral axis within the panel, for example

$$\frac{de_{eqa}}{d\theta} = z_{eqa} = \frac{A.n}{2b} = -\frac{Z_p}{A}\frac{dm_{eqa}}{dn} = -\frac{dM_{eqa}}{dN}$$

where z_{eqa} is the distance between the equal area and neutral axes. The second and third terms in this series of equations are derived from the geometry of Fig. 3.3(a), and the fourth from Eqn. (3.2). Similarly

$$\frac{de_{cen}}{d\theta} = z_{cen} = z_{eqa} - (1-f)\frac{Z_p}{A} = -\frac{Z_p}{A}\frac{dm_{cen}}{dn} = -\frac{dM_{cen}}{dN} \ . \qquad (3.4)$$

This time Eqn. (3.3) is utilized. Thus it is shown that each vector of deformation rates is perpendicular to its corresponding interaction curve.

All of the above formulae remain valid when the equal area axis lies in the stiffener if all panel and stiffener parameters are interchanged; for example:

$$b \leftrightarrow t_l$$

$$t \leftrightarrow h_l \ .$$

A new sign convention that gives consideration to bending moment causing compression at the top of the panel is also required. This is apparent from Fig. 3.3(b). An alternative approach which retains moment in the hogging sense is to change the sign of the axial force where it appears in the equations. Fig. 3.4 demonstrates the validity of this adjustment.

3.4.2.2 UNSYMMETRICAL I-SECTION

Although not directly applicable to the models under consideration, similar formulae are also presented for an I-section with unequal flanges. Their use would be for T-bar rather than flat bar stiffening, when the associated panel is again included.

Three situations are possible. First, it is assumed that the equal axis lies within the web. It follows that

$$Z_{pl} = \frac{A^2}{4t_l} - \frac{A_f^2}{2}\left[\frac{1}{t_l} - \frac{1}{b_f}\right] - \frac{A_p^2}{2}\left[\frac{1}{t_l} - \frac{1}{b}\right]$$

where

$A_p = bt$ = panel cross sectional area

$A_l = h_l t_l$ = web cross sectional area

$A_f = b_f t_f$ = flange cross sectional area

$A = A_p + A_l + A_f$ = total cross sectional area.

Again tensile force and hogging bending moment are considered to be positive in presenting the plastic interaction formulae and moments are taken about the centroid. For

$$-1 \leq n \leq -C_{0p} :$$

$$m_{cen} = \frac{t_l}{b} f_l (1-n^2) + \frac{Z_{Pp}}{Z_{Pl}} (1-f_p)(1+n) . \qquad (3.5)$$

$$-C_{0p} \leq n \leq C_{0f} :$$

$$m_{cen} = 1 - f_l n^2 + \left[(1-f_l) + \frac{A_p^2}{Z_{Pl}} \left[\frac{1}{t_l} - \frac{1}{b} \right] \right] . n .$$

$$C_{0f} \leq n \leq 1 :$$

$$m_{cen} = \frac{t_l}{b_f} f_l (1-n^2) + \frac{Z_{Pf}}{Z_{Pl}} (1-f_f)(1-n) . \qquad (3.6)$$

In these equations

$$f_p = A^2 / 4bZ_{Pp}$$

$$f_l = A^2 / 4t_l Z_{Pl}$$

$$f_f = A^2 / 4b_f Z_{Pf}$$

$$C_{0p} = (A_l + A_f - A_p)/A$$

$$C_{0f} = (A_l + A_p - A_f)/A$$

As expected Eqns. (3.5) and (3.6) are similar in form, with all panel and flange parameters interchanged. The small anomaly in signs is a consequence of retaining hogging bending as positive.

The second situation occurs when the equal area axis is in the panel. Different formulae apply now, as follows

$$Z_{pp} = \frac{A^2}{4b} + \frac{(A_l + A_f)^2}{2}\left[\frac{1}{t_l} - \frac{1}{b}\right] - \frac{A_f^2}{2}\left[\frac{1}{t_l} - \frac{1}{b_f}\right]$$

$$-1 \leq n \leq -C_{0p} :$$

$$m_{cen} = 1 - f_p n^2 + (1-f_p)n \ .$$

$$-C_{0p} \leq n \leq C_{0f} :$$

$$m_{cen} = 1 - \frac{(C_{0p}A)^2}{4Z_{pp}}\left[\frac{1}{t_l} - \frac{1}{b}\right] - \frac{bf_p}{t_l}n^2 + \left[\frac{Z_{pl}}{Z_{pp}}(1-f_l) + \frac{A_p^2}{Z_{pp}}\left[\frac{1}{t_l} - \frac{1}{b}\right]\right].n \ .$$

$$C_{0f} \leq n \leq 1 :$$

$$m_{cen} = \frac{bf_p}{b_f}(1-n^2) + \frac{Z_{pf}}{Z_{pp}}(1-f_f)(1-n) \ .$$

Third, if the equal area axis lies in the flange, the second suite of formulae are still valid if all panel and flange symbols are swapped. For example, the plastic modulus becomes

$$Z_{pf} = \frac{A^2}{4b_f} + \frac{(A_l + A_p)^2}{2}\left[\frac{1}{t_l} - \frac{1}{b_f}\right] - \frac{A_p^2}{2}\left[\frac{1}{t_l} - \frac{1}{b}\right] \ .$$

In accordance with the concluding paragraph in Section

3.4.2.1 this alteration causes the bending moment specified to be in the sagging sense.

It is apparent that the interaction equation for bending moment capacity in the presence of axial force is always parabolic for both T-sections and I-sections. A check on the correctness of the second series of formulae for unequal I-sections is available from Low [93]. He quotes numerical values of the coefficients defining the parabolas for a particular cross section where the equal area axis lies within the panel.

Tsang and Harding [167,168] give a step-by-step computation procedure for the plastic moment capacity of an asymmetrical I-section in the presence of axial force. They consider the applied axial force to be resisted in a middle portion of the section such that the two parts of the stress block above and below the central zone carry equal and opposite force. The bending moment is computed by multiplying this force by the lever arm separating the centroids of the two equal areas. The moment must therefore act about the centroid of the central area if the force in this third area is not to contribute. In the approach the location of the centroid varies with the value of applied axial force. Hence the results differ from those derived above and would be less suitable for use in the beam analysis of this chapter.

3.4.3 BEAM ANALYSIS

3.4.3.1 GENERAL DERIVATION

The plastic behaviour of a centrally point loaded T-section beam with either rotationally fixed or pinned supports is developed. The beam is modelled by two elastic bars meeting at the central plastic hinge and with axially flexible connections to the supports (see Fig. 3.5).

Vertical deflection stretches the elastic bars which causes the membrane tension force to increase from its initial value. However axial extension also occurs at the end connections and the plastic hinges, the latter being governed by flow rules. The analysis is made tractable by using small deflection approximations and neglecting the effect of the small shear force on plastic hinge capacity.

Equilibrium of the force system in Fig. 3.5 gives:

$$N = F\cos\theta_j + \tfrac{1}{2}P_D\sin\theta_j \approx F$$

$$V = \tfrac{1}{2}P_D\cos\theta_j - F\sin\theta_j \approx 0 .$$

The alternative approximate equations are valid for small θ_j. The subscript j used in Fig. 3.5 identifies the stringer beam number, which will be useful in the later cylinder work. However, as all stringer beams in the stiffened plates behave identically, such nomenclature is unnecessary and so the subscript is dropped in this and the following chapter. From Fig. 3.5 also:

$$\tfrac{1}{2}P_D(a_I - \tfrac{1}{2}\Delta) = F\delta + M_s + M_c .$$

Assuming

$$\tfrac{1}{2}\Delta/a_I \ll 1$$

and non-dimensionalising leads to

$$p_D = \tfrac{1}{2}(m_s + m_c + n\delta A/Z_p) \qquad (3.7)$$

where

$$p_D = P_D/P_P$$

and

$$P_P = 8M_P/L ,$$

the latter clearly being the plastic collapse load of an encastre beam.

Moments are defined as follows:

$$-1 \leq n \leq -C_0 :$$

$$m_c = \frac{bf}{t_l}(1-n^2) - (A_p/A_l)^2(1-f)(1+n) .$$

$$-C_0 \leq n \leq 1 :$$

$$m_c = 1 - (1-f)n - fn^2 .$$

With encastre supports:

$$-1 \leq n \leq C_0 :$$

$$m_s = 1 + (1-f)n - fn^2 .$$

$$C_0 \leq n \leq 1 :$$

$$m_s = \frac{bf}{t_l}(1-n^2) - (A_p/A_l)^2(1-f)(1-n) .$$

With simple supports:

$$m_s = 0 .$$

Here moments are taken about the section centroid. Both moments and axial force are considered positive when acting as shown in Fig. 3.5, which explains the variations in sign.

The task remaining is to determine the relationship between axial force and lateral deflection. The unit membrane extension of each half-span caused by the applied lateral load is found from the deformation geometry to be

$$e/a_I = \sqrt{(\delta/a_I)^2 + (1 - \tfrac{1}{2}\Delta/a_I)^2} - 1$$

$$\approx \tfrac{1}{2}(\delta/a_I)^2 - \tfrac{1}{2}\Delta/a_I \qquad (3.8)$$

$$= (e_a + e_s + e_c)/a_I \ .$$

This last equality satisfies compatibility. In it e_c represents the centroidal extension in each half of the central hinge, which is defined by

$$\frac{de_c}{d\theta} = z_c = -\frac{Z_p}{A}\frac{dm_c}{dn}$$

after Eqn. (3.4). For each support hinge, if they exist, e_s is similarly defined. All hinges have the same rotation θ .

The elastic bar extension e_a is given by

$$e_a/a_I = \frac{\sigma_Y}{E}(n - n_I) \qquad (3.9)$$

where n_I is the initial pretension existing before application of the lateral load. It may seem inconsistent to include elasticity here when it has been neglected in formulating the response of the plastic hinges. This, however, preserves the accuracy of the analysis. Elastic stretch is the dominant behavioural mode of the bars whereas it is a secondary effect in the highly plastic hinge zones.

Two different approaches towards quantifying the pull-in of the supports will be investigated. The first is given here, and the second in Section 3.4.3.3.

3.4.3.2 JONES' SUPPORT PULL-IN APPROACH

Following a concept initiated by Jones [77], but adopting somewhat different notation, the unit axial displacement at the supports may be defined to be

$$\tfrac{1}{2}\Delta/a_I = \Delta/L = \tfrac{1}{2}(1-\gamma_*)(\delta/a_I)^2 \qquad (3.10)$$

where γ_* is a support stiffness parameter. This equation derives from the condition associated with the limit load (or plastic collapse) solution that

$$de/a_I = 0 \ .$$

Substituting Eqn. (3.10) into Eqn. (3.8) results in the following governing differential equation

$$C_{1*}\frac{dn}{d\delta/L} + (z_s + z_c)/L - \gamma_*\delta/L = 0 \ , \qquad (3.11)$$

when use is made of the small deflection approximation

$$\theta \approx 2\delta/L \ .$$

Here

$$C_{1*} = \tfrac{1}{4}\sigma_{YT}/E \ .$$

The parameter $(z_s + z_c)/L$ is found by taking derivatives of the relevant bending moment relationships and so assumes a variety of values depending on the type of flexural restraint at the supports and how much axial force is present. The results for all permutations are listed in Table 3.3.

Integration of the governing equation gives sequential formulae for the build-up of membrane tension from various initial values n_I. The first integration constant is evaluated using the boundary condition that

$$n = n_I \quad \text{at} \quad \delta/L = 0 \, .$$

This assumes that the elastic bending deformation is small. Subsequent constants C_i are found in each axial force range by equating with the previous response at the change-over point

$$n = \pm C_0 \, .$$

The formulae are presented in Table 3.4(a).

Two of the equations have particular interest as they are relevant to the conditions existing in the stiffened plate tests, and so they are numbered (3.12) and (3.13). These two equations are also drawn in Fig. 3.6(a) for a range of γ_* values. It is seen that they meet tangentially at

$$n = C_0 \, .$$

The geometry and initial pretension present in Test P1 is utilized for the example and the actual experimental points are also included for comparison.

3.4.3.3 HODGE'S SUPPORT PULL-IN APPROACH

A second, and rather more obvious, treatment of support pull-in is attributable to Hodge [72] but has been adopted by several other authors, [92,26]. The supports are assumed to incorporate linear springs, representing their attachment to an elastic structure. This gives

$$\tfrac{1}{2}\Delta/a_I = \Delta/L = \frac{\sigma_Y}{E}(n-n_I)/\mu \, .$$

Here

$$\mu = k_1 L/2AE \qquad (3.14)$$

relates the support stiffness to the half-span axial stiffness and k_1 is the spring stiffness, (see Fig. 3.5).

Using the alternative definition the differential equation now becomes:

$$C_1 \frac{dn}{d\delta/L} + (z_s + z_c)/L - \delta/L = 0 \qquad (3.15)$$

where

$$C_1 = \frac{\frac{1}{4}\sigma_{YT}/E}{\gamma}$$

$$\gamma = 1/(1 + 1/\mu) \ .$$

Thus γ combines the similar elastic responses of the supports and the beam segments between hinges. It is apparent from the above and also Eqn. (3.10) that in both formulations the support axial stiffness parameter lies within the range

$\gamma_*, \gamma \approx 0$ for supports free to pull in
$\gamma_*, \gamma = 1$ for complete axial restraint.

The term $(z_s + z_c)/L$ again takes on relevant values from Table 3.3. For example, with encastre supports and within the range

$$C_0 \leq n \leq 1 \ ,$$

Eqn. (3.15) becomes

$$C_1 \frac{dn}{d\delta/L} + n/C_3 - C_4 - \delta/L = 0 \qquad (3.16)$$

where the constants C_3 and C_4 are defined below Table 3.3. This equation is singled out as it will find special relevance later in Section 3.5.10.1.

The solution of Eqn. (3.15) leads to the formulae in Table 3.4(b). Those pertinent to the plate tests are again labelled: this time Eqns. (3.17) and (3.18). They are plotted in Fig. 3.6(b) for Plate P1 and various values of γ. Comparison of Figs. 3.6(a) and (b) verifies that both Jones' and Hodge's formulations give identical predictions when

$$\gamma_* = 1 = \gamma$$

as there is no pull-in at the supports. Elsewhere they differ. For the experimental correlation of Section 3.5, Hodge's approach will be used exclusively because of its clear physical meaning.

If pinned rather than fixed ends are assumed but all other conditions remain as for Fig. 3.6(b), Fig. 3.6(c) is generated. The degree of flexural restraint at the supports clearly has a marked effect on the form of the membrane tension build up.

The applied load versus deflection response is found by substituting formulae from Table 3.4 into Eqn. (3.7) and the bending moment relationships.

3.4.4 MEMBRANE YIELD RESPONSE

Figs. 3.6 demonstrate that the membrane tension force eventually reaches uniform yield, that is

$$n = 1 .$$

The hinge moments about the centroid become zero at this time and the structure acts as a pinned truss with members carrying constant force. Further increase in applied load is resisted by geometry change only. Thus

$$p_D = \frac{L\Delta}{4Z_p} \sin\theta \ . \qquad (3.19)$$

If small deflections are assumed as with the above analysis a linear approximation is attained:

$$p_D = \delta\Delta/2Z_p \ . \qquad (3.20)$$

This is entirely consistent with Eqn. (3.7).

3.4.5 BEHAVIOUR DURING UNLOADING

Studying the response of the stiffened plates during unloading gives valuable insight into the residual stresses resulting from denting. The relaxation of membrane tension during rebound of the dented stringer beams may be predicted simply, as follows.

When small deflection approximations are made, the total axial extension of a stringer beam is given in terms of lateral deflection by Eqn. (3.8). Differentiation leads to

$$\frac{2de}{L} = \frac{4\delta}{L}.\frac{d\delta}{L} - \frac{d\Delta}{L} \ . \qquad (3.21)$$

If unloading is predominantly elastic little axial deformation will occur at the plastic hinge locations. The major component is due to membrane force reduction. Therefore

$$\frac{2de}{L} = \frac{2de_s}{L} = \frac{\sigma_y}{E}.dn$$

after Eqn. (3.9).

If Jones' pull-in criterion is assumed the incremental axial displacement of the supports is

$$\frac{d\Delta}{L} = 4(1-\gamma_*)\frac{\delta}{L}.\frac{d\delta}{L} \qquad (3.22)$$

from Eqn. (3.10). Alternatively, the use of Hodge's approach leads to

$$\frac{d\Delta}{L} = (1/\gamma - 1)\frac{\sigma_Y}{E}.dn \ . \qquad (3.23)$$

Substitution of Eqn. (3.23) into (3.21) gives

$$\frac{dn}{d\delta/L} = 4\gamma\frac{E.\delta}{\sigma_Y L} \ . \qquad (3.24)$$

The same formula results if Eqn. (3.22) is used instead of Eqn. (3.21) except that γ_* replaces γ.

Because the behaviour is basically elastic the membrane tension unloading curve is linear, with the slope specified by Eqn. (3.24). The parameters dn and $d\delta/L$ are taken to be negative increments of nondimensionalized membrane force and lateral deflection, respectively.

3.5 THEORETICAL CORRELATION

Comparison between the theoretical predictions and the actual test behaviour is now possible.

3.5.1 INITIAL ELASTIC RESPONSE

As a first step, the early lateral deflection response under knife edge loading was compared with a derivation of the theoretical elastic behaviour of a centrally loaded beam. A variable degree of flexural end restraint was incorporated into the analysis, as were the effects of axial pretension. Details of the development are not given here as it is relatively straight forward and the principles are well known. However the major conclusion drawn from the analysis is cited, which is one concerning experimental technique; specifically, that the devised end connection provides a good approximation to true flexural fixity. This holds even though the beam length is considered to be the clear span rather than the length between welds, and gives an indication of how accurately the end plates fit the stiffened plate samples.

3.5.2 AXIAL FORCE DEVELOPMENT

Further loading of the stiffened plates produces a three hinged mechanism, followed by increasing membrane tension. Figs 3.7(a) and (b) show the build up of membrane tension in Plates P1 and P2 respectively. To find the experimental points a linear strain block is drawn through each pair of strain gauge measurements at quarter-span, one of which is located on the top of the plate and the other being the average of the two stiffener readings. Linearity is a very common assumption and is frequently

expressed in terms of plane sections remaining plane. Strain changes in each load step are converted into stress changes by

$$d\sigma/\sigma_Y = d\epsilon/\epsilon_Y$$

with the proviso

$$|\sigma/\sigma_Y| \leq 1 .$$

The resulting stress block acting on the stringer beam cross section implies a net axial force which is plotted in nondimensional form. The three unload/reload paths in Fig. 3.7(b) will be elaborated upon in Section 3.5.8.

Also included in Figs. 3.7(a) and (b) are the predictions of Eqns. (3.17) and (3.18). In both diagrams these define the upper curve which is drawn in a solid line. Each value of the support axial stiffness parameter γ is chosen to give the best overall fit to the test data. The values are of the same order as those estimated by considering the through-thickness stiffness of the bolted end connections, but somewhat smaller. There are two reasons for this. Firstly, other sources of pull-in at the supports contribute a little to their flexibility; the end plates bend inwards and there may also be slight overall bending of the vertical columns of the test frame. Secondly, the tests exhibit an initial elastic-plastic bending response where lateral deflection occurs without development of membrane tension. For rigid-plastic theory to follow this softer behaviour the true γ value must be modified.

There are also two reasons why the γ value is lower in Test P2 than Test P1. The geometry of the stiffened plate in Test P2 has a higher axial stiffness, and also the insertion of packing plates into its end connections reduces their through-thickness stiffness. Both of these factors affect Eqn. (3.14).

The theoretical membrane tension might increase only very slowly early in the response, and it is possible for it to even decrease slightly if the induced hinge extensions are greater than the total geometric extension. Such behaviour is amplified in the experimental response due to the existence of hogging moments at the quarter-point gauge locations which tend to give the centroidal strain a compressive component. Knife edge loading introduces a hogging shape between the centre and each support which has been quantified as an exponential curve [161], as mentioned in Section 2.7.1.1. In the present tests the curvature is swamped by the bilinear plastic mechanism and so is not visible, but some elastic bending strains are still present. In addition membrane tension causes the plastic moment to be larger at the support hinges than the centre, which is apparent from the interaction diagram in Fig. 3.3. This increases the hogging at quarter-span.

Further into the responses of Figs. 2.7(a) and (b), test and theory lie closer together, that is, until

$$n = C_0 \ .$$

Thereafter they diverge. Waszczyszyn [183] and Campbell and Charlton [10] quote experimental axial tension results for rectangular sections and both cases show the same trend for theory to significantly overestimate the tension value at higher loads. An explanation for this is developed in Section 3.5.10 and includes a derivation of expressions on which the broken lines in Figs. 2.7(a) and (b) are based.

3.5.3 STRAIN DEVELOPMENT

It is of interest to compare the theoretical magnitudes of the several components of centroidal extension which combine to produce the total geometric stretching. This is done in Fig. 3.8 for the conditions existing in Test P1, hinge extensions being derived by integrating the flow rules. Nondimensionalizing the extensions by dividing by the original half-span length means that the curve representing each elastic bar describes a true strain. Not so for the plastic hinges where the extension actually occurs over a much shorter length. It is apparent that at higher dent depths, that is

$$\delta/L > 0.03 ,$$

only a relatively small part of the total strain is provided by the elastic bars. It this component of strain, of course, that reflects the axial force increase.

3.5.4 LATERAL LOAD RESPONSE

The lateral load response during denting of the two stiffened plates is plotted in Figs. 3.9(a) and (b). The broken line included in Fig. 3.9(b) will be discussed in Section 3.5.7. There is excellent correlation between experiment and the theoretical predictions utilizing Hodge's pull-in approach, despite the inaccuracy mentioned earlier in reproducing the membrane tension. This is because the damage load is fairly insensitive to the exact form of the axial force build-up, as exemplified by Fig. 3.11 using the geometry of Plate P1. The figure shows that for higher γ values, when a reasonable degree of tension development occurs (Fig. 3.6(b)), the lateral load behaviour is quite insensitive to the actual γ value. Thus, as a corollary, an accurate estimate of the support

axial stiffness is not essential in determining the load capacity when reasonably stiff supports are present. Quantitative guidance on the level of stiffness required for this to hold is given in Section 3.5.5 below.

Further demonstration of this property is provided by Figs. 3.12 and 3.13 in which the axial force and lateral load build-up, respectively, are plotted for a range of initial pretension values. The curves utilize the geometry of Plate P1 and Jones' pull-in criterion is adopted. The membrane tension responses cover a broad range but eventually converge onto a single line. The predictions for the corresponding lateral load in Fig. 3.13 are, however, closely spaced throughout.

It is apparent that the response curves become linear at higher deflections when the membrane tension force attains yield. Only part of the lateral loading response of Plate P1 is presented in Fig. 3.9(a), but Fig. 3.10 shows the complete behaviour until rupture. Alongside is plotted Eqn. (3.19) in a broken line. The full line is its linear approximation, Eqn. (3.20), for which deflections are limited to being finite by making mathematical simplifications based on small rotations. The two curves are essentially coincident until

$$\delta/L = 0.10$$

which gives an indication of the validity of the small deflection simplification in the flow rule analysis. Thereafter they begin to diverge with the experimental points following the slope given by the "exact" theory until strain hardening effects become apparent at

$$\delta/L = 0.12 .$$

Strain hardening is neglected in the simple mathematical model.

It is seen, however, that the linear membrane yield equation describes behaviour throughout the loading process reasonably well. This holds whenever the supports have significant stiffness against axial pull-in.

3.5.5 ENERGY ABSORPTION

Nearly linear behaviour enables the energy absorbed during denting to be easily estimated. Hence

$$W = \tfrac{1}{2}P_D\delta = N_p.(2e')$$

that is:

$$\frac{W}{N_pL} = 2(\delta/L)^2 \qquad (3.25)$$

where

$$(2e')/L = 2(\delta/L)^2$$

and $2e'$ is the total apparent membrane extension assuming axially fixed supports.

The ratio of experimental to theoretical work done, the latter being given by Eqn. (3.25), is plotted against lateral deflection in Fig. 3.14. The diagram shows that the simple energy estimate is very close for larger dent depths. At small deflections the true energy absorption capability is underestimated as work expended at the plastic hinges is neglected. Somewhat similar calculations are undertaken by Foss and Edvardsen [58] for stocky tubes.

Energy absorption provides a convenient means of quantifying the effect of partial axial fixity at the supports. This is done with the aid of Fig. 3.11 which

depicts loading responses for Plate P1. The curve in that Figure labelled

$$\gamma = 0.1$$

represents the response when the stiffness of the supports is just over ten per cent of the axial stiffness of the plate. It is apparent that this curve dips below the linear membrane yield approximation. It may be computed that the dip corresponds to a thirteen per cent reduction in energy dissipation (in comparison with the linear equation) in the region before the true response reaches membrane yield. With additional loading the two curves are coincident and so the percentage loss is diminished. For the curve with

$$\gamma = 0.5 ,$$

where the support stiffness equals that of the plate, the energy loss is only 1.6 per cent.

The corresponding figures for Plate P2 are even lower because its geometry has a higher ratio of Z_p/A. For γ values of 0.1 and 0.5, the energy losses are 4.4 and 0.1 per cent respectively. It may be concluded, therefore, that the requirement of "significant" axial stiffness at the supports for the linear approximation to be valid, may be satisfied by a stiffness of at least ten percent of the span axial stiffness.

3.5.6 LATERAL DEFLECTION PROFILES

Although there are few monitoring points, the vertical transducer readings show that during loading the early double curvature in the stiffened plates, due to elastic bending, gradually straightens into a V-shape with sharp fold-lines at centre and supports. This dent profile

is also apparent in Fig. 3.2.

3.5.7 STIFFENER TRIPPING AT SUPPORTS

Near the supports the stiffeners deflect out-of-plane as seen in Fig. 2.15, a photograph of the underside of Plate P2. Murray [105] has analysed a similar stiffener buckling mode at the centre of a simply supported longitudinally stiffened plate. In Section 4.4.2 his "tripping" mechanism is adapted to suit the test work of the present dissertation. However the geometry of the stiffener deformation, illustrated in Fig. 4.6, is of interest here.

The amplitude of the trip is defined theoretically by assuming that the axial shortening of the stiffener free edge within the mechanism equals that near the support due to overall bending. Hence:

$$h_t\theta = 2a_{tr}(1 - \sqrt{1 - (\hat{w}/a_{tr})^2}) \ .$$

For small $\hat{w}/a_{tr}$, this becomes

$$(\hat{w}/h_t)^2 = \theta\tan\beta \ , \qquad (3.26)$$

using

$$a_{tr}/h_t = \tan\beta \ .$$

The rotation θ required to satisfy the compatibility equation (3.26) has twice the value derived by Murray as each half span now has a tripping mechanism.

Eqn. (3.26) is plotted in Fig. 3.16 using

$$\beta = 0.3 \quad \text{radian}$$

as observed for Plate P2. The peak experimental out-of-plane deflections at the stiffener tip are also shown. These are found by interpolating the readings of three transducers oriented perpendicular to the stiffeners. The Plate P2 results follow the theoretical form although the actual values are significantly smaller. Tripping deformation appears to occur for $n > C_0$, which is presumably because the stiffener tip compressive strain at the support hinge begins to increase rapidly here. This is made apparent by looking jointly at Figs. 3.8 and 3.17. The former shows that the centroidal extension rises very sharply after $n = C_0$, and the second diagram illustrates that this induces comparable compressive strains at the outstand tip.

In contrast, the stocky stiffeners in Plate P1 deflect very gradually, and in fact form a sinusoidal shape extending for a horizontally projected length of about 0.16 times the span rather than distinct kinks. Hence the inaccuracy of Murray's mechanism approach in this case is understandable.

Due to the presence of membrane tension which tends to oppose trip growth it may be concluded that for lateral loading of encastre plates with stiffener slenderness

$$h_t/t_t \leq 0.65\sqrt{E/\sigma_y}$$

(at least), the support hinge moment may be calculated from plastic interaction formulae ignoring tripping. This is borne out by the good correlation between theory and experiment achieved earlier in Figs. 3.9. For comparison the damage load response for Plate P2 assuming pinned ends is also shown in Fig. 3.9(b) with a broken line, and this differs markedly.

3.5.8 INTERMEDIATE UNLOADING AND RELOADING

Plate P2 was unloaded at

$$\delta/L = 0.100$$

to allow a subsequent longitudinal loading test to be carried out. It was also unloaded and reloaded at two intermediate deflections. One of the purposes behind this was to ascertain whether it altered the loading path, as such periodic unloading would be necessary in the later cylinder tests in order to determine the dent shape. Other purposes were to investigate the residual stresses and the modified stiffness.

The experimental relaxation in membrane tension during rebound is plotted in Fig. 3.7(b). The points fall reasonably close to the linear predictions of Eqn. (3.24) although the latter are not included to preserve clarity.

The fall off in lateral load produced by the relaxing membrane tension defined by Eqn. (3.24) is

$$\frac{dp_0}{d\delta/L} = 2\gamma \frac{E.AL}{\sigma_Y Z_p} (\delta/L)^2 \ .$$

However this mode of rebound implies rotation at the plastic hinges in the opposite sense to the prior dent growth. Initially this cannot occur and so elastic bending is generated in the form of double curvature in each half span.

The unloading path is steeper, therefore, due to the additional component of lateral load required to produce flexure. However as unloading continues some yielding develops at the hinge locations in this new sense, making rotation possible. At this stage the slope of the lateral load versus dent depth unloading curve decreases a little.

Such nonlinearity is apparent in the unload/reload paths of Fig. 3.9(b).

When finally unloaded Fig. 3.7(b) shows that the mean residual membrane tension stress is about 0.12 of yield. Unbolting the end connections allows a little additional relaxation. This is not only demonstrated by the strain gauge readings, but also by the fact that the stiffened plates slide out of the test frame easily.

Under the action of bending as a plastic mechanism without membrane stretching, followed by unloading, the residual stresses in the extreme fibres at hinge locations would be expected to be opposite in sign to those existing there during loading. This is caused by the hinges rotating in the opposite direction during unload. However the large membrane tension force existent in the present tests, and its subsequent relaxation, modifies the residual stress blocks. This point will be raised again in Section 4.4.1.2 in explaining the response of the dented plate under longitudinal compressive loading.

After rebound the permanent set of Plate P2 is

$$\delta_D/L = 0.095 ,$$

indicating a recovery of five per cent.

3.5.9 FAILURE

At a central deflection of

$$\delta/L = 0.175$$

Plate P1 ruptured at the end of the clear span, which of course marks the limit of validity of the plastic analysis. This dent depth implies a total apparent strain

of

$$(2e_m')/L = 0.06 ,$$

which is somewhat smaller than the ultimate apparent strain of

$$(2e_m')/L = 0.10$$

suggested by McDermott et al [95] after several stiffened plate tests, and also Pettersen and Johnsen [113]. The latter authors base their choice on a literature survey. Further discussion of fracture strain magnitude is included in Section 5.8.

Maximum straining would be expected to be at the mid-span stiffener tip and significant necking is apparent at that point. That rupture does not commence there means that some curtailment of ductility occurs near the support. However large displacements are attained, and there is no obvious yield or pull-in at the support, so it may be concluded that the method of end connection is adequate.

3.5.10 ELASTICITY EFFECTS IN PLASTIC ANALYSIS

3.5.10.1 POSTULATED EXPERIMENTAL BEHAVIOUR

In the range

$$C_0 \leq n \leq 1$$

the theoretical membrane tension response is approximately a linear function of lateral deflection, especially for the geometry of Plate P2 (Fig. 3.7(b)). Referring to the differential equation (3.16) this approximate relation is

$$n = C_3(\delta/L + C_4 - C_1C_3)$$

when Hodge's support pull-in approach is employed. Similarly the test plots are linear:

$$n' = C_3'(\delta'/L + C_4' - C_1C_3') \ . \qquad (3.27)$$

In Eqn. (3.27) the primes refer to experimental values. The constants C_3' and C_4' are found, respectively, from the slope followed by the test points and the implied axial force axis intercept. Values are given in Table 3.5 in terms of a ratio

$$r_3 = C_3'/C_3 \approx C_4/C_4' \ .$$

From this an experimental instantaneous centre of rotation may be inferred:

$$(z_s' + z_c')/L = n'/C_3' - C_4'$$

$$= \delta'/L - C_1C_3'$$

from Eqn. (3.27). Because C_1 is very small for axially stiff plate material and supports, this approximates to

$$(z_s' + z_c')/L \approx \theta'/2 \ . \qquad (3.28)$$

Now, when the theoretical and experimental axial forces are equal, that is

$$n = n' \ ,$$

then

$$(z_s' + z_c')/L = \frac{(z_s + z_c)/L}{r_3} \ . \qquad (3.29)$$

The physical reasoning for this is as follows. At a particular membrane tension and hence elastic bar stretch,

the experimental lateral deflection is larger than predicted. For compatibility the hinge extensions must be larger and this is caused by higher $z_s' + z_c'$ from the flow rule.

To aid further explanation, the upper part of Fig. 3.17 illustrates the behaviour of a rigid-plastic support hinge under increasing axial load as it moves around the interaction curve. A small change dz_s in the distance between the centroid and the instantaneous centre of rotation produces a stress change

$$d\sigma/\sigma_y = 2$$

within this strip dz_s only, and hence a bending moment change

$$dM = -z_s dN ,$$

as given by normality.

However for an elastic-plastic material, as depicted at the bottom of Fig. 3.17, the behaviour differs. The extension increment $\frac{1}{2}d\theta.dz_s'$ at the midpoint of strip dz_s' due to rotation $d\theta$ about the instantaneous centre of rotation, causes an average stress change over the strip of

$$d\sigma/\sigma_y = \frac{E}{\sigma_y}\frac{d\theta.dz_s'}{2l_h} .$$

Here l_h is some measure of the hinge length. Summing the stress changes over a series of increments dz_s' leads to a parabolic stress distribution within the elastic region. To produce the same membrane tension therefore, z_s' must be larger than z_s. In contrast, the actual bending moment supported by the elastic-plastic section is only slightly smaller than the rigid plastic prediction for the capacity in the presence of this membrane tension.

3.5.10.2 ALTERNATIVE FLOW RULE

The traditional flow rule gives:

$$\frac{de_s'}{d\theta'}/L + \frac{de_c'}{d\theta'}/L = (z_s' + z_c')/L$$

$$\approx \theta'/2$$

from Eqn. (3.28). This relationship is also parabolic. Integrating up from the initial condition of zero hinge extension and rotation leads to:

$$(e_s' + e_c')/\theta' = \tfrac{1}{2}(z_s' + z_c') \ .$$

The geometric distance represented here is marked in Fig. 3.17. The equation is not truly valid as Eqn. (3.28) does not apply in the early stages of the response. However the deformations are small here and alter the subsequent behaviour very little.

For $r_3 \approx \frac{1}{2}$ it follows from Eqn. (3.29) that the experimental membrane tension will be modelled by a modified flow rule

$$z_s + z_c = (e_s' + e_c')/\theta' \ ,$$

using total rather than incremental deformations. This formulation is considerably simpler as integration is not necessary.

Compatibility requires:

$$C_1\frac{(n-n_I)}{\delta/L} + (z_s + z_c)/L - 2\delta/L = 0$$

replacing Eqn. (3.15), and gives, for

$$-C_0 \leq n \leq C_0 :$$

$$n = \frac{C_1 n_I + \frac{1}{2}(\delta/L)^2}{C_1 + \frac{\delta/L}{C_2}}$$

and for

$$C_0 \leq n \leq 1 :$$

$$n = \frac{C_1 n_I + C_4 \delta/L + \frac{1}{2}(\delta/L)^2}{C_1 + \frac{\delta/L}{C_3}} .$$

Unlike their rigid-plastic counterparts Eqns. (3.17) and (3.18), the present curves do not meet tangentially. The two formulations may be compared in Figs. 3.7(a) and (b) and it is seen that they bound the experimental results. For

$$n \leq C_0$$

the curves are very similar; that is

$$z_s + z_c = (de_s + de_c)/d\theta \approx (e_s + e_c)/\theta .$$

This implies that $z_s + z_c$ must be nearly constant, and also that the total hinge extension is approximately linearly dependent on lateral deflection, which is apparent in Fig. 3.8 as well. The divergence of the curves for

$$n \geq C_0$$

is due to dz_s needing to increase by a factor of about b/t_t to produce the same axial force increment dN. This factor has a value of thirty for the geometries of the tests and so causes a causes a rapid change in $z_s + z_c$. In this latter region the correlation between the actual

deformation flow rule and the results of Plate P1 with the smaller Γ_3 value is especially close.

New lateral load responses predicted using the above equations for axial force are very similar to those drawn earlier and so they are not included in Figs. 3.9(a) and (b). This is because the precise way in which the membrane tension develops has little effect on load capacity, as discovered in Section 3.5.4. Such behaviour diminishes the importance of deciding which flow rule should be adopted.

Generalizing, for many years the relative merits of total and incremental flow rules (traditionally referred to as deformation and flow theories, respectively [70]) have been debated. In essence incremental flow theory is more correct. However, particularly in the realm of plastic buckling, total strain theories have frequently been shown to give better correlation with experimental results [73]. Several authors, for example, Budjanski [9] and de Donato and Maier [23] have proved also that these total theories are valid in a broad range of loading situations. In the present work the predictions of the two rules differ, with the experimental data falling between them. The total deformation flow rule has the advantage of providing a much simpler, as well as the more accurate, description of the observed response.

3.6 CONCLUSIONS

Consistent with the dual themes of testwork and theory within this chapter, conclusions are drawn in two distinct areas.

Concerning experimental method, the test set up is seen to perform well. In particular the end connection is able to provide the required restraint without modifying the stiffened plate response which is very ductile. Thus a

similar connection detail with the same dimensions will be adopted for the later cylinder tests.

Secondly, although only two tests have been undertaken, it may be tentatively concluded that the mechanism analysis derived herein accurately predicts the lateral loading response of longitudinally stiffened plates to large deflections. For stiffeners with slenderness

$$h_s/t_s \leq 0.65\sqrt{E/\sigma_y},$$

at least, tripping at the supports does not reduce this load-carrying capacity. The development of membrane tension seems to be better described using a simplified flow rule which is suggested to allow for elastic unload. However the damage load is fairly insensitive to the exact form of the membrane tension build up; in fact, for axially stiff supports a linear equation defining the membrane yield response reasonably describes the behaviour throughout loading. This enables the energy absorbed during damage to be easily estimated. The supports may be regarded as having sufficient stiffness for this simplification if they exert about ten per cent of the plate axial stiffness.

TABLE 3.1 Stiffened plate properties

PLATE NO.	GEOMETRY				MATERIAL
	$t = t_l$	b/t	h_l/t_l	L/t	E/σ_{YT}
P1	0.84mm	30	8	240	600
P2	0.86	30	16	220	600

TABLE 3.2 Initial forces

	PLATE P1		PLATE P2	
	UNBOLTED	BOLTED	UNBOLTED	BOLTED
MOMENT M_I/M_Y	0.40	0.40	0.07	0.04
TENSION n_I	-0.03	0.36	-0.01	0.24

TABLE 3.3 Parameter governing extension at hinges

AXIAL FORCE n	PARAMETER $(z_s + z_c)/L$
Encastre supports:	
$-1 \leq n \leq -C_0$	$n/C_3 + C_4$
$-C_0 \leq n \leq C_0$	n/C_2
$C_0 \leq n \leq 1$	$n/C_3 - C_4$
Simple supports:	
$-1 \leq n \leq -C_0$	$n/C_5 + C_6$
$-C_0 \leq n \leq 1$	$n/2C_2 + C_7$

$$C_0 = (A_p - A_t)/A$$

$$C_2 = Lb/A$$

$$C_3 = \frac{2L/A}{1/t_t + 1/b}$$

$$C_4 = (A_p - A_t)(1/t_t - 1/b)/2L$$

$$C_5 = 2Lt_t/A$$

$$C_6 = A_p^2(1/t_t - 1/b)/2LA$$

$$C_7 = (A_t/A_p)^2 C_6$$

TABLE 3.4 Formulae for membrane tension development

(a) JONES FORMULATION $\Delta/L = 2(1-\gamma_*)(\delta/L)^2$	
Encastre supports:	
$-1 \leq n_1 \leq -C_0$	
$-1 \leq n \leq -C_0$	$n = C_3(\gamma_*\delta/L + (n_1/C_3 + \gamma_* C_{1*} C_3 + C_4)\exp(-1/(C_{1*} C_3)\delta/L) - (\gamma_* C_{1*} C_3 + C_4))$
$-C_0 \leq n \leq C_0$	$n = C_2(\gamma_*\delta/L - C_{1*} C_2[\gamma_* + C_i \exp(-1/(C_{1*} C_2)\delta/L)])$
$C_0 \leq n \leq 1$	$n = C_3(\gamma_*\delta/L - C_{1*} C_3[\gamma_* + C_i \exp(-1/(C_{1*} C_3)\delta/L)] + C_4)$
$-C_0 \leq n_1 \leq C_0$	
$-C_0 \leq n \leq C_0$	$n = C_2(\gamma_*\delta/L + (n_1/C_2 + \gamma_* C_{1*} C_2)\exp(-1/(C_{1*} C_2)\delta/L) - \gamma_* C_{1*} C_2)$ (3.12)
$C_0 \leq n \leq 1$	$n = C_3(\gamma_*\delta/L - C_{1*} C_3[\gamma_* + C_i \exp(-1/(C_{1*} C_3)\delta/L)] + C_4)$ (3.13)
$C_0 \leq n_1 \leq 1$	
$C_0 \leq n \leq 1$	$n = C_3(\gamma_*\delta/L + (n_1/C_3 + \gamma_* C_{1*} C_3 - C_4)\exp(-1/(C_{1*} C_3)\delta/L) - (\gamma_* C_{1*} C_3 - C_4))$
Simple supports:	
$-1 \leq n_1 \leq -C_0$	
$-1 \leq n \leq -C_0$	$n = C_5(\gamma_*\delta/L + (n_1/C_5 + \gamma_* C_{1*} C_5 + C_6)\exp(-1/(C_{1*} C_5)\delta/L) - (\gamma_* C_{1*} C_5 + C_6))$
$-C_0 \leq n \leq 1$	$n = 2C_2(\gamma_*\delta/L - 2C_{1*} C_2[\gamma_* + C_1 \exp(-1/(2C_{1*} C_2)\delta/L)] - C_7)$
$-C_0 \leq n_1 \leq 1$	
$-C_0 \leq n \leq 1$	$n = 2C_2(\gamma_*\delta/L + (n_1/2C_2 + 2\gamma_* C_{1*} C_2 + C_7)\exp(-1/(2C_{1*} C_2)\delta/L)] - (2\gamma_* C_{1*} C_2 + C_7))$

TABLE 3.4 (continued)

(b) HODGE FORMULATION		
$\Delta/L = (1/\gamma - 1)\frac{\sigma_{YI}}{E}(n - n_I)$		
where $\gamma = 1/\left[1 + \frac{2AE}{k_1 L}\right]$		
Encastre supports:		
$-1 \leq n_I \leq -C_0$		
$-1 \leq n \leq -C_0$	$n = C_3(\delta/L + (n_I/C_3 + C_1C_3 + C_4)\exp(-1/(C_1C_3)\delta/L) - (C_1C_3 + C_4))$	
$-C_0 \leq n \leq C_0$	$n = C_2(\delta/L - C_1C_2[1 + C_i\exp(-1/(C_1C_2)\delta/L)])$	
$C_0 \leq n \leq 1$	$n = C_3(\delta/L - C_1C_3[1 + C_i\exp(-1/(C_1C_3)\delta/L)] + C_4)$	
$-C_0 \leq n_I \leq C_0$		
$-C_0 \leq n \leq C_0$	$n = C_2(\delta/L + (n_I/C_2 + C_1C_2)\exp(-1/(C_1C_2)\delta/L) - C_1C_2)$	(3.17)
$C_0 \leq n \leq 1$	$n = C_3(\delta/L - C_1C_3[1 + C_i\exp(-1/(C_1C_3)\delta/L)] + C_4)$	(3.18)
$C_0 \leq n_I \leq 1$		
$C_0 \leq n \leq 1$	$n = C_3(\delta/L + (n_I/C_3 + C_1C_3 - C_4)\exp(-1/(C_1C_3)\delta/L) - (C_1C_3 - C_4))$	
Simple supports:		
$-1 \leq n_I \leq -C_0$		
$-1 \leq n \leq -C_0$	$n = C_5(\delta/L + (n_I/C_5 + C_1C_5 + C_6)\exp(-1/(C_1C_5)\delta/L) - (C_1C_5 + C_6))$	
$-C_0 \leq n \leq 1$	$n = 2C_2(\delta/L - 2C_1C_2[1 + C_i\exp(-1/(2C_1C_2)\delta/L)] - C_7)$	
$-C_0 \leq n_I \leq 1$		
$-C_0 \leq n \leq 1$	$n = 2C_2(\delta/L + (n_I/2C_2 + 2C_1C_2 + C_7)\exp(-1/(2C_1C_2)\delta/L) - (2C_1C_2 + C_7))$	

TABLE 3.5 Values of experimental constant

PLATE NO.	$r_3 = C_3'/C_3 = C_4/C_4'$
P1	0.60
P2	0.67

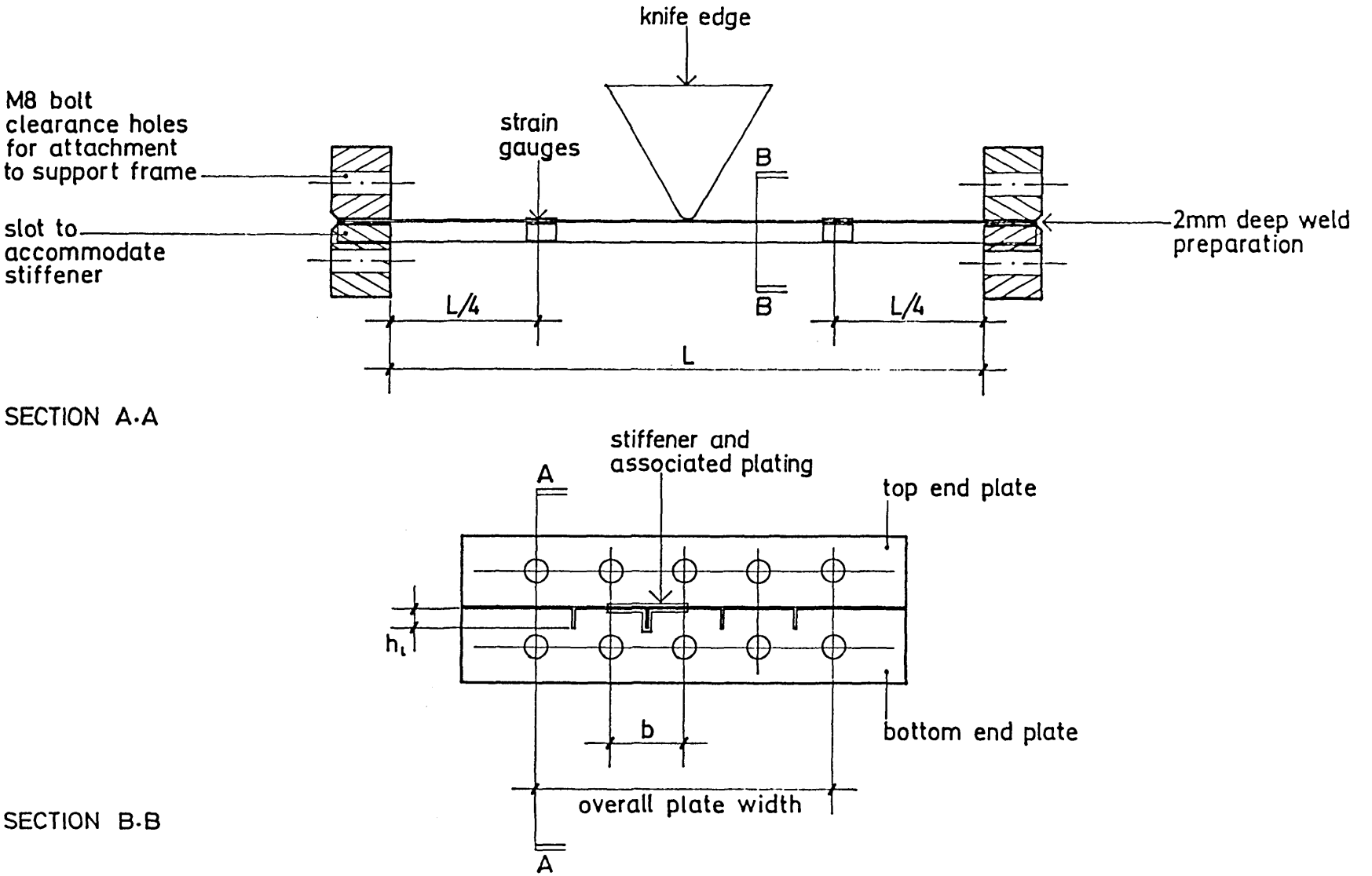


fig. 3.1
Stiffened plate test pieces

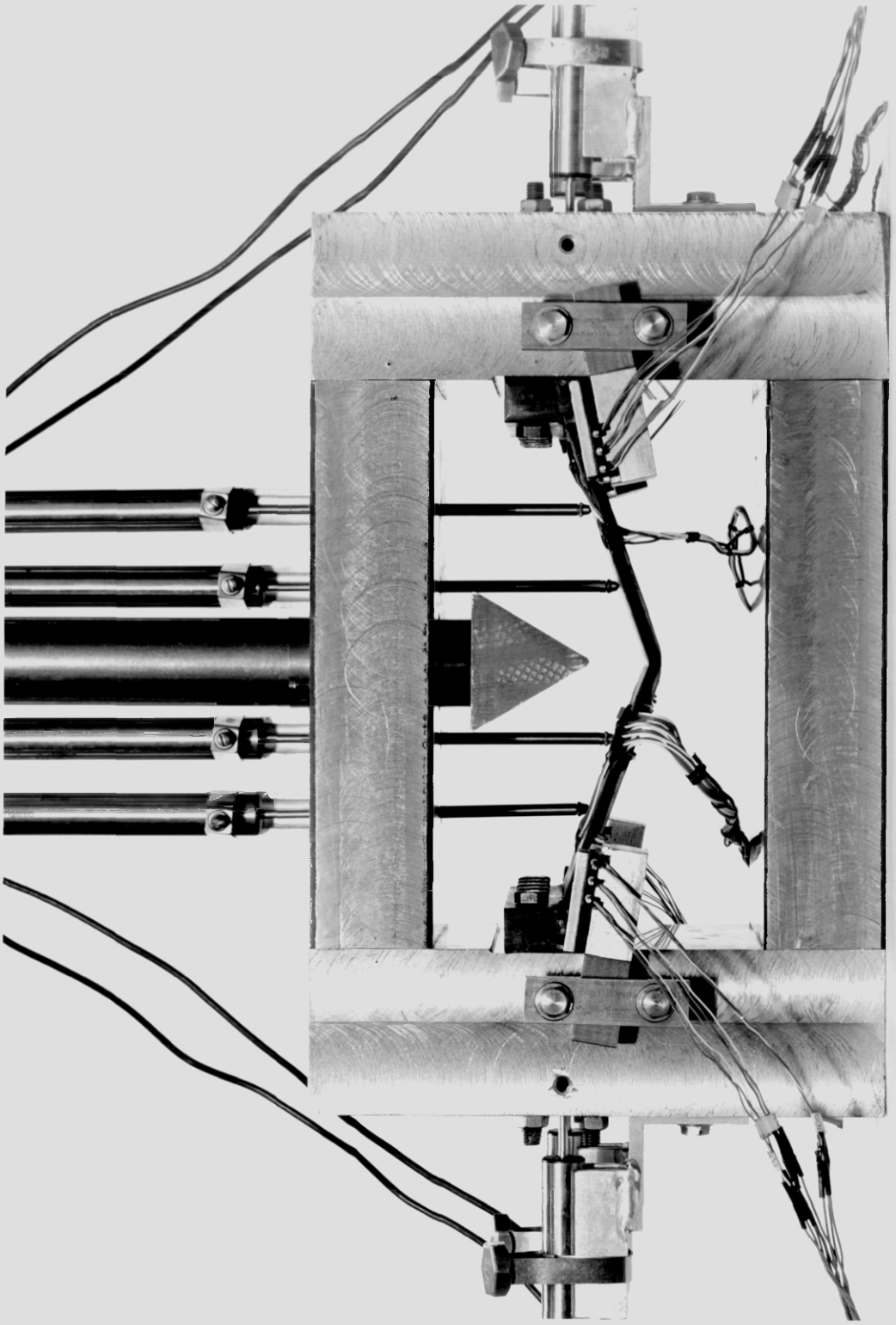
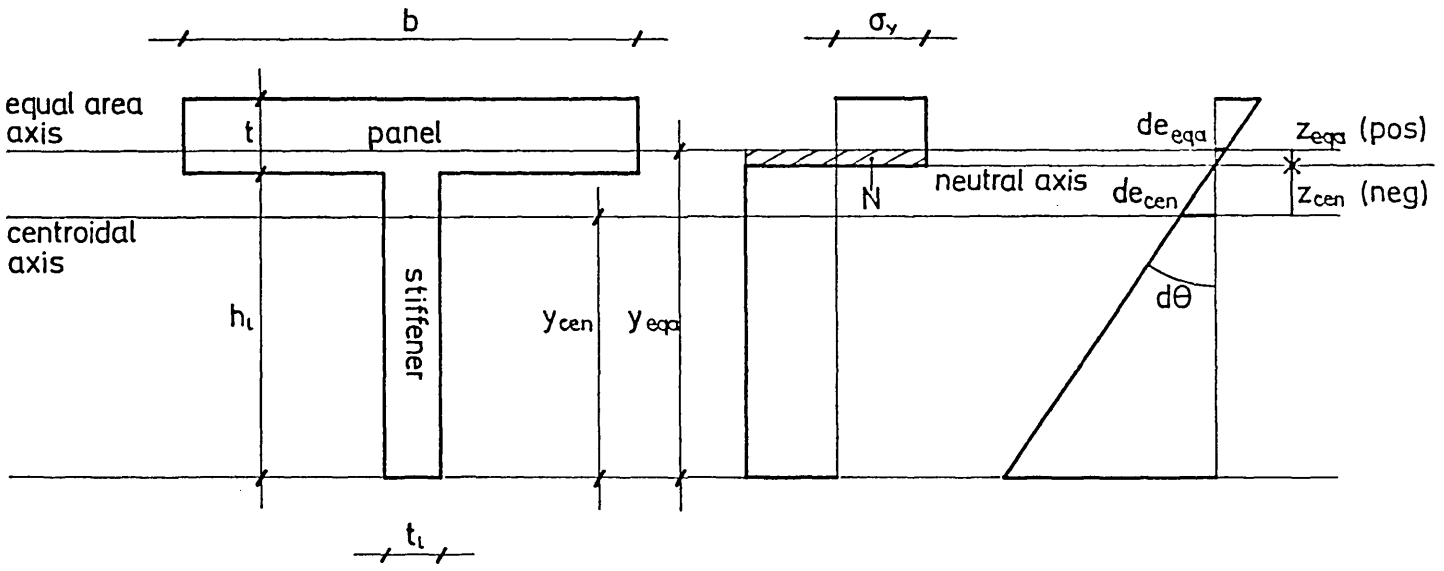
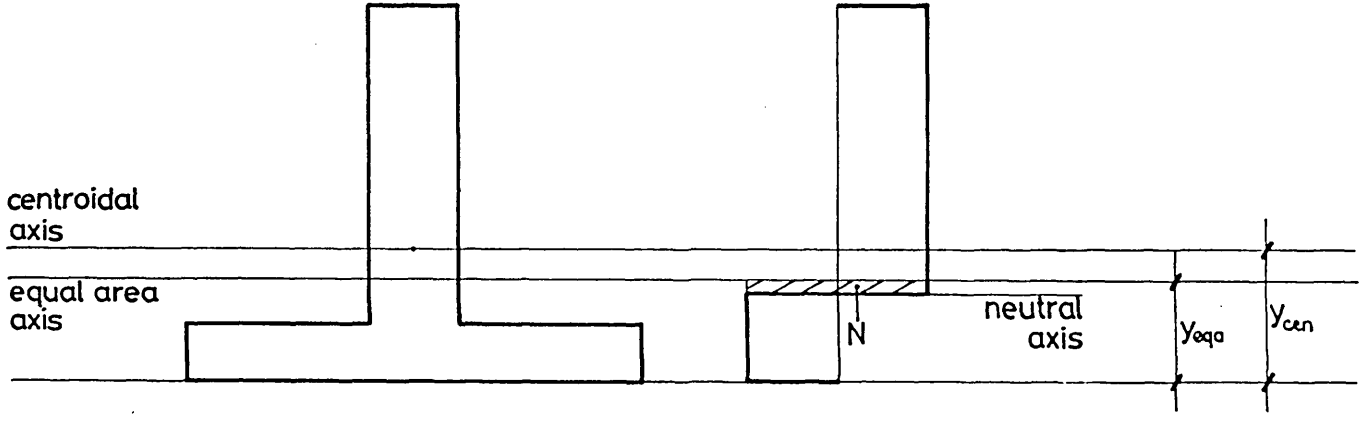


fig. 3.2
Test rig for denting stiffened plates



(a) Equal area axis in panel



(b) Equal area axis in stiffener

fig. 3.3
T-section plastic capacity

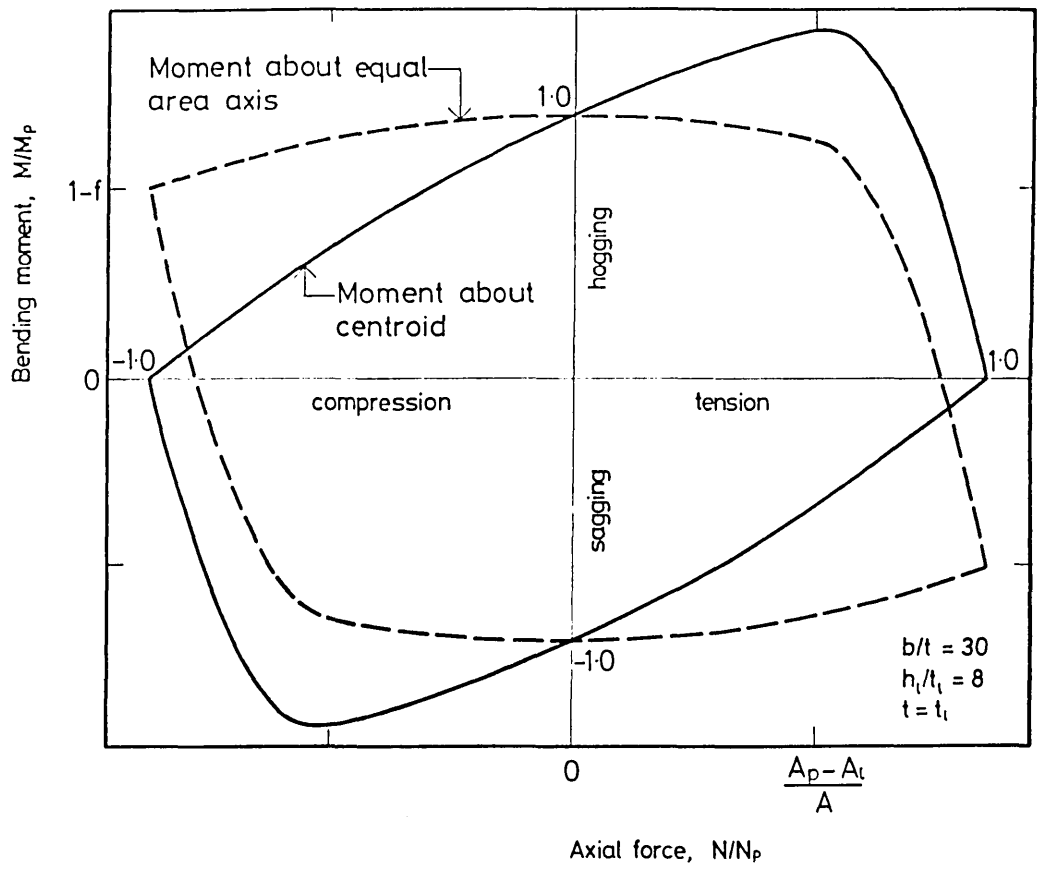


fig. 3.4
Plastic interaction curve under bending moment and axial force
T-section geometry as for Plate P1

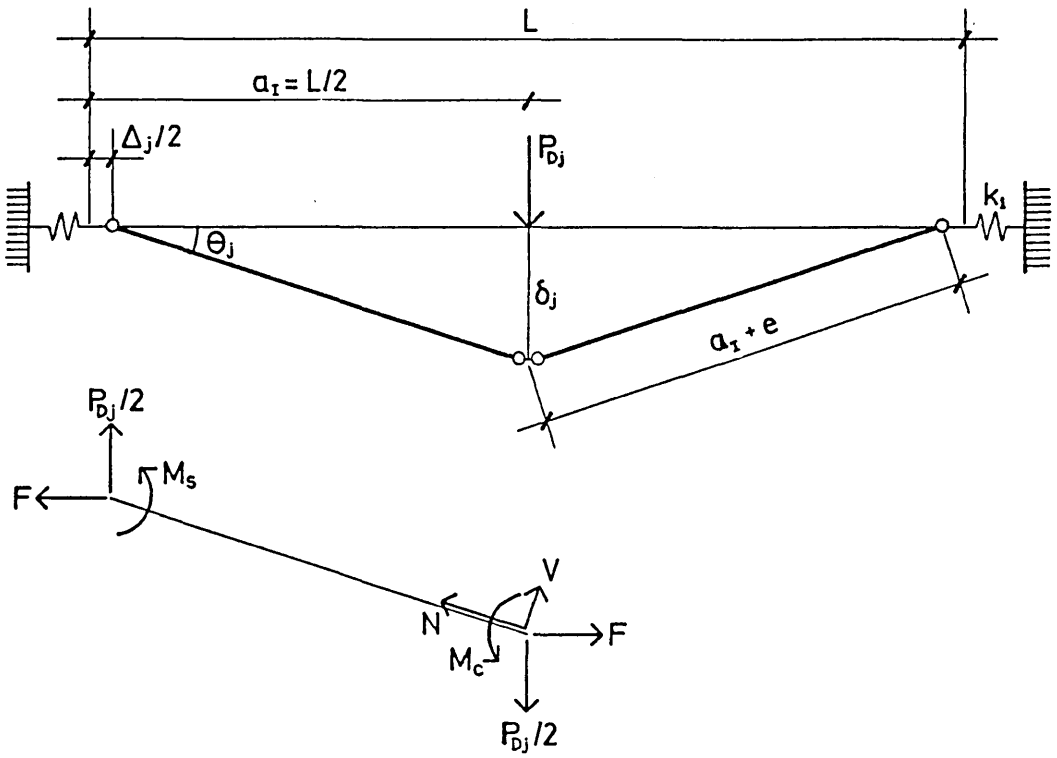


fig. 3.5
Plastic beam analysis
Forces and deformations

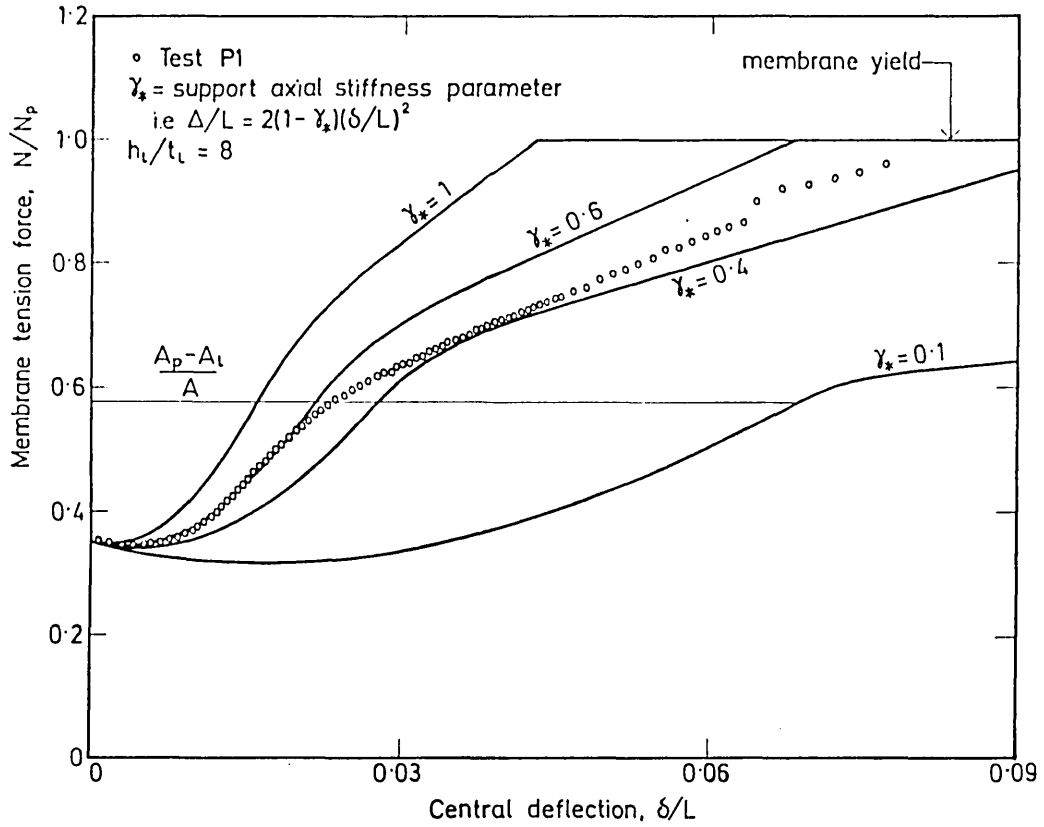


fig. 3·6 (a)
Theoretical and experimental membrane tension development with deflection
Test P1

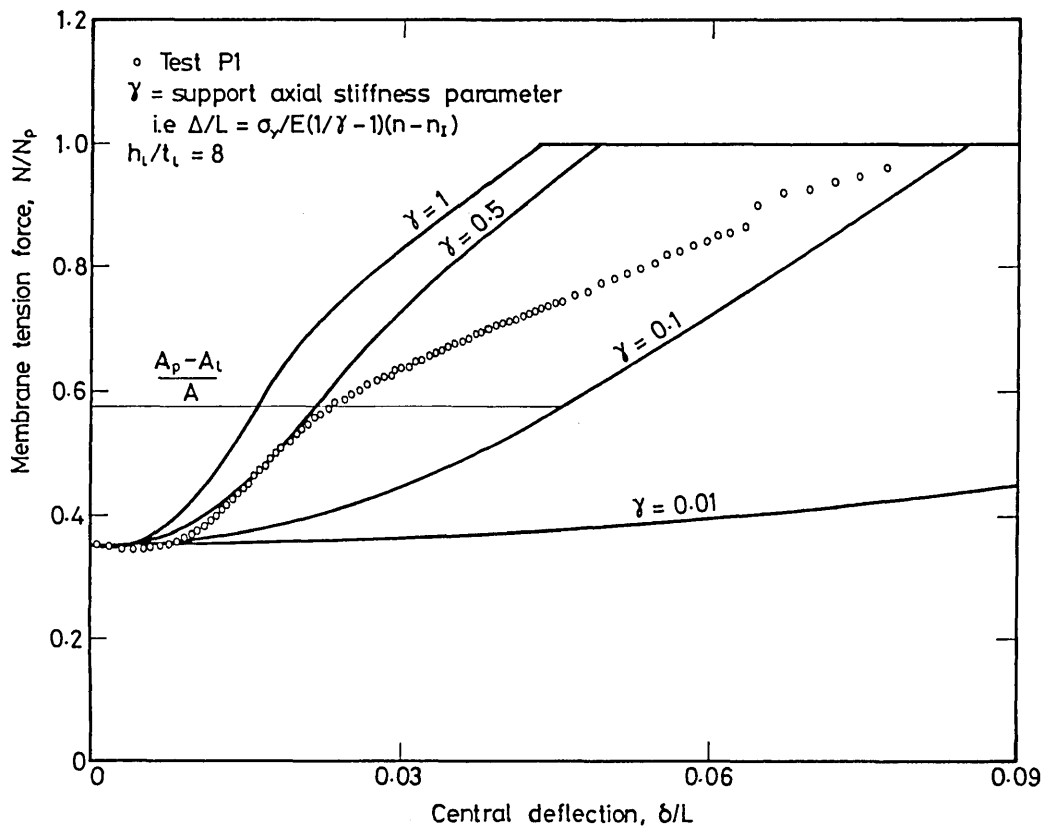


fig. 3·6 (b)
Theoretical and experimental membrane tension development with deflection
Test P1

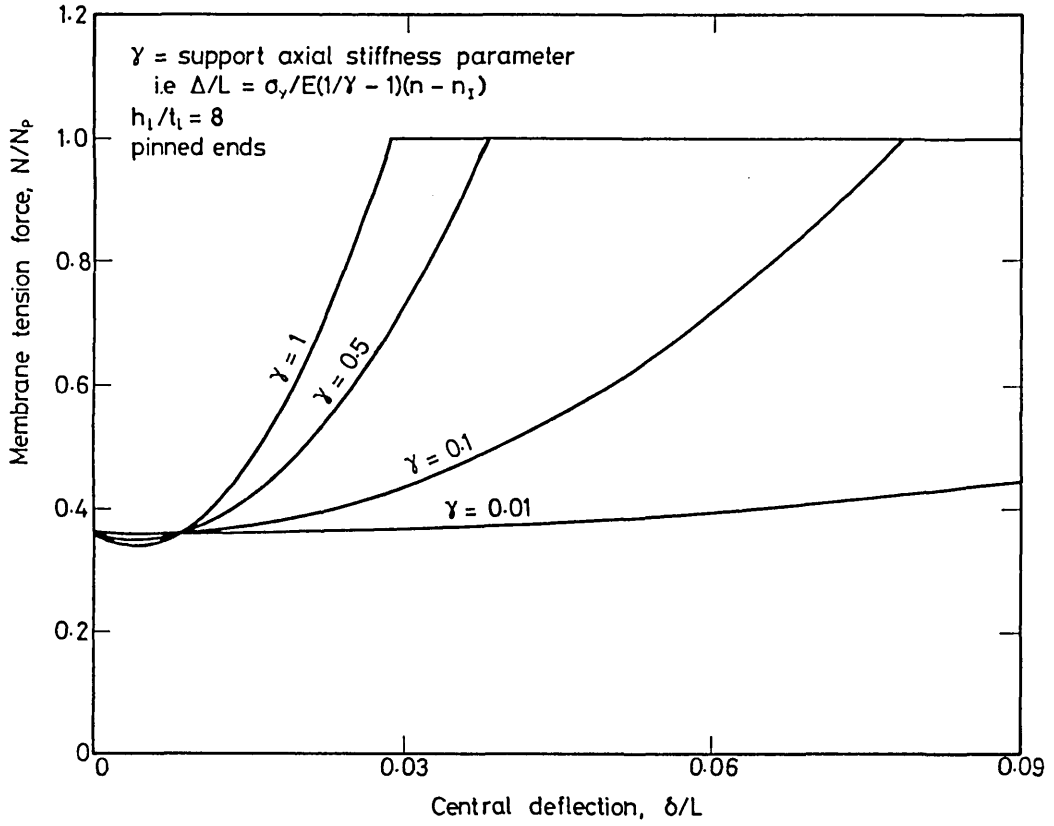


fig. 3.6 (c)
Membrane tension development
Test P1 geometry with simple supports

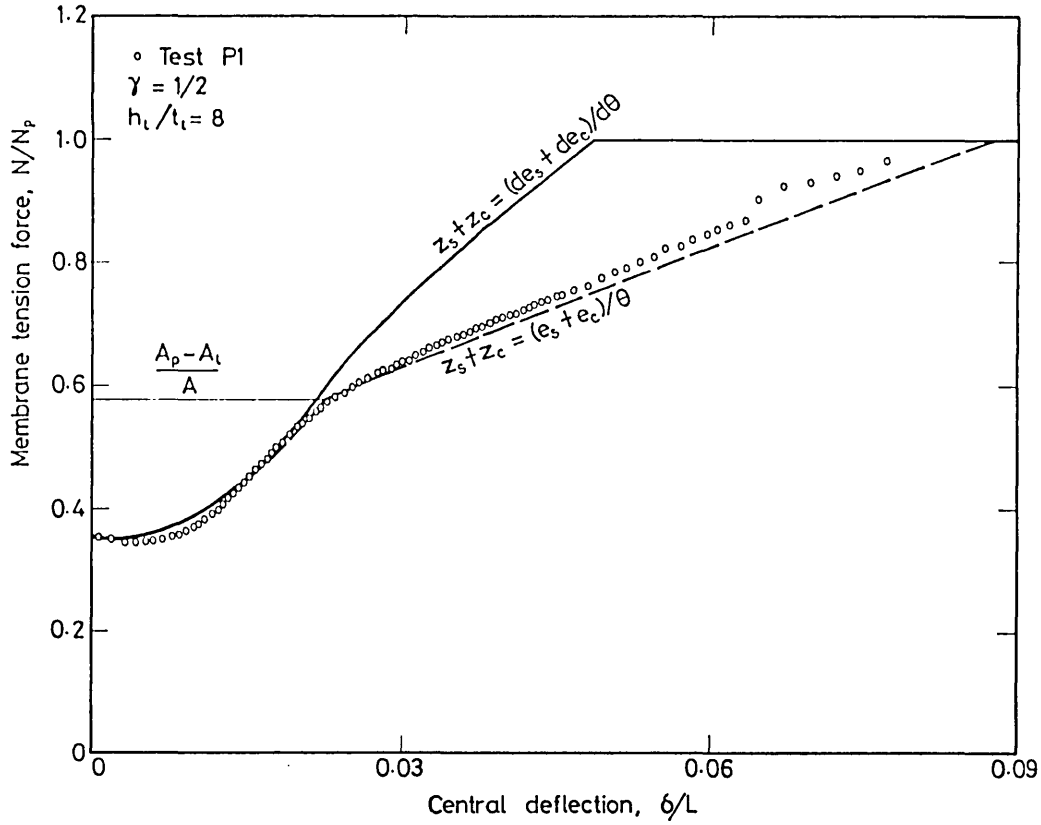


fig. 3.7(a)
Theoretical and experimental membrane tension development with deflection
Test P1

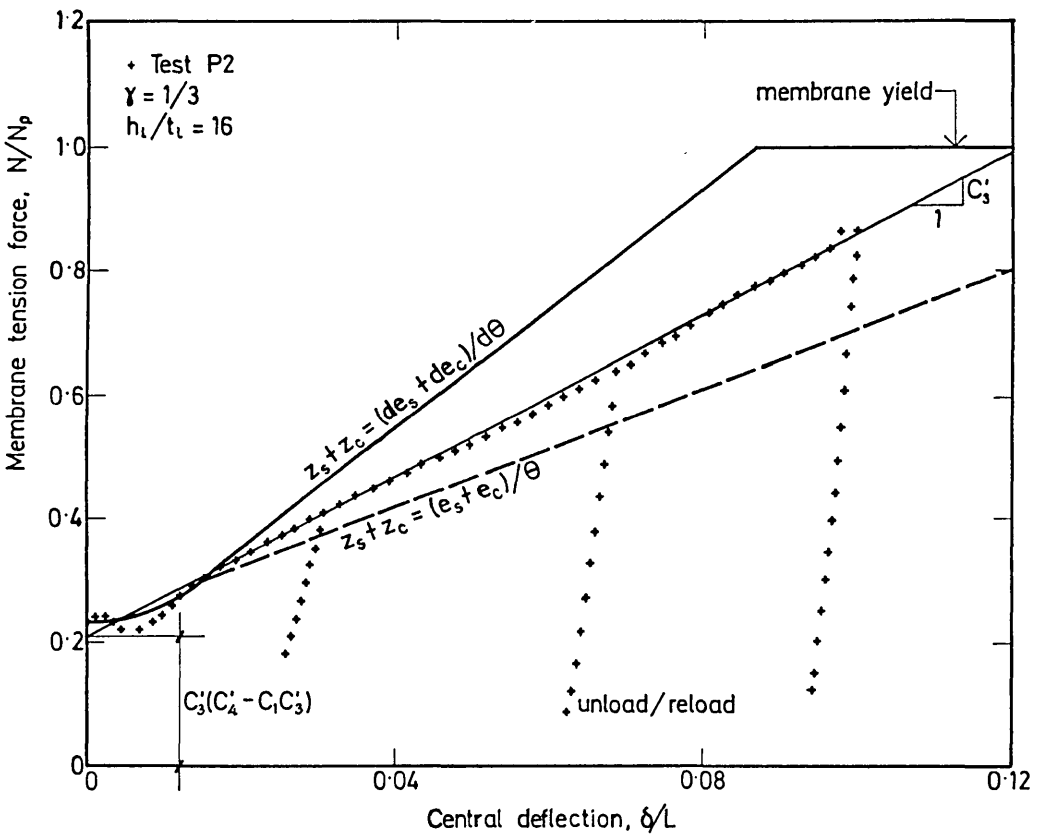


fig. 3.7(b)
Theoretical and experimental membrane tension development with deflection
Test P2

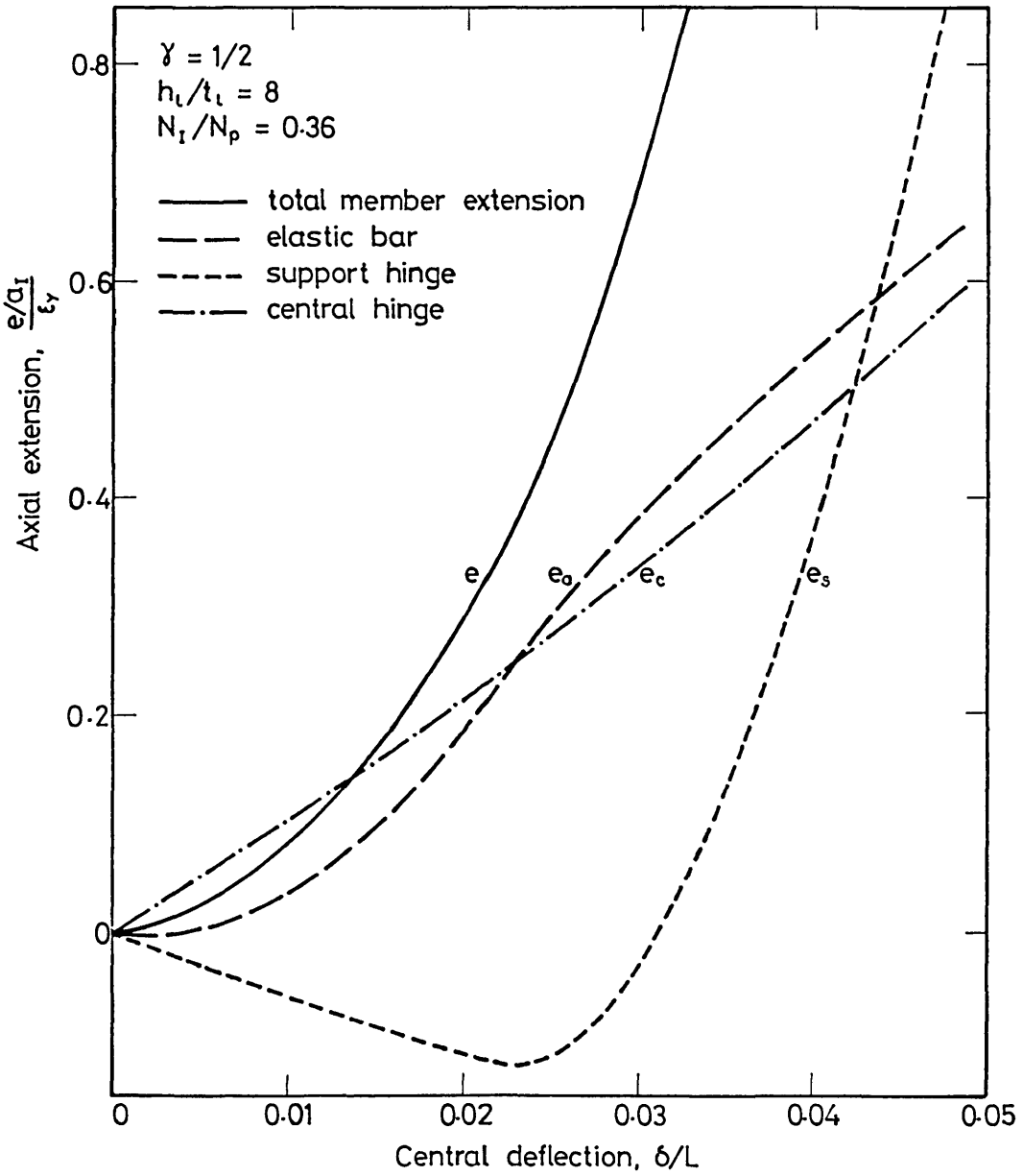


fig. 3·8
Development of membrane extension components with lateral deflection
Test P1 geometry

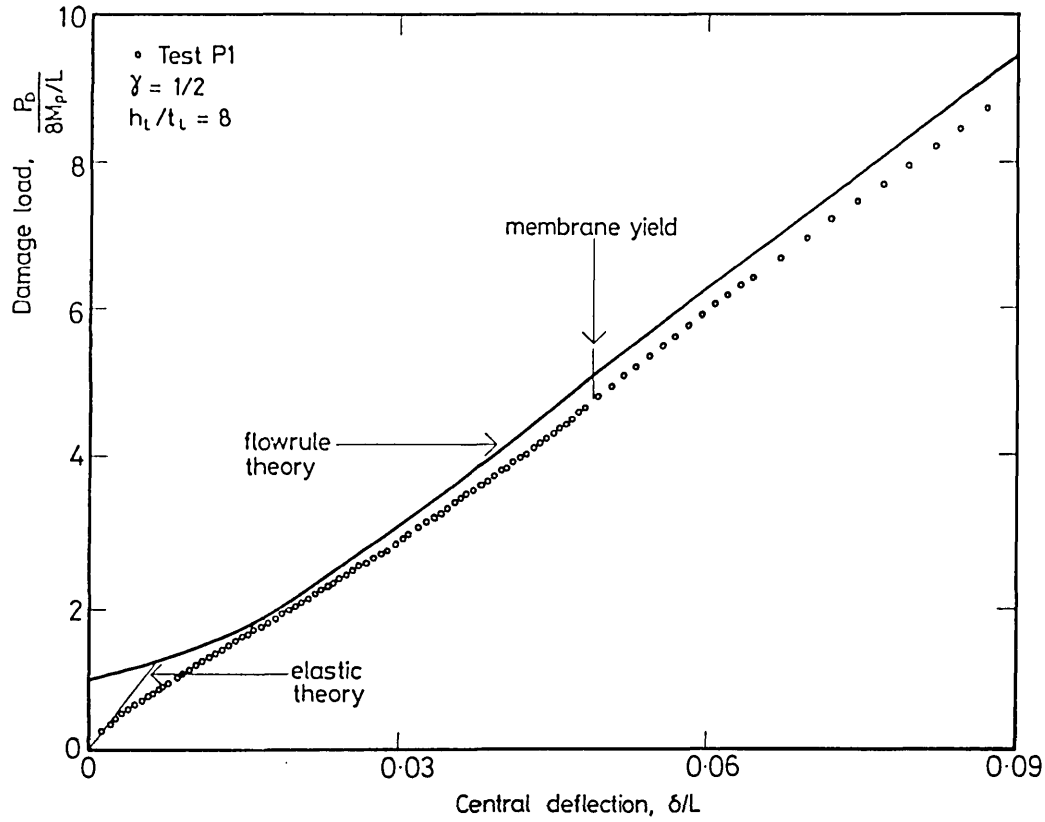


fig. 3·9(a)
Theoretical and experimental lateral load - deflection relationship
Test P1

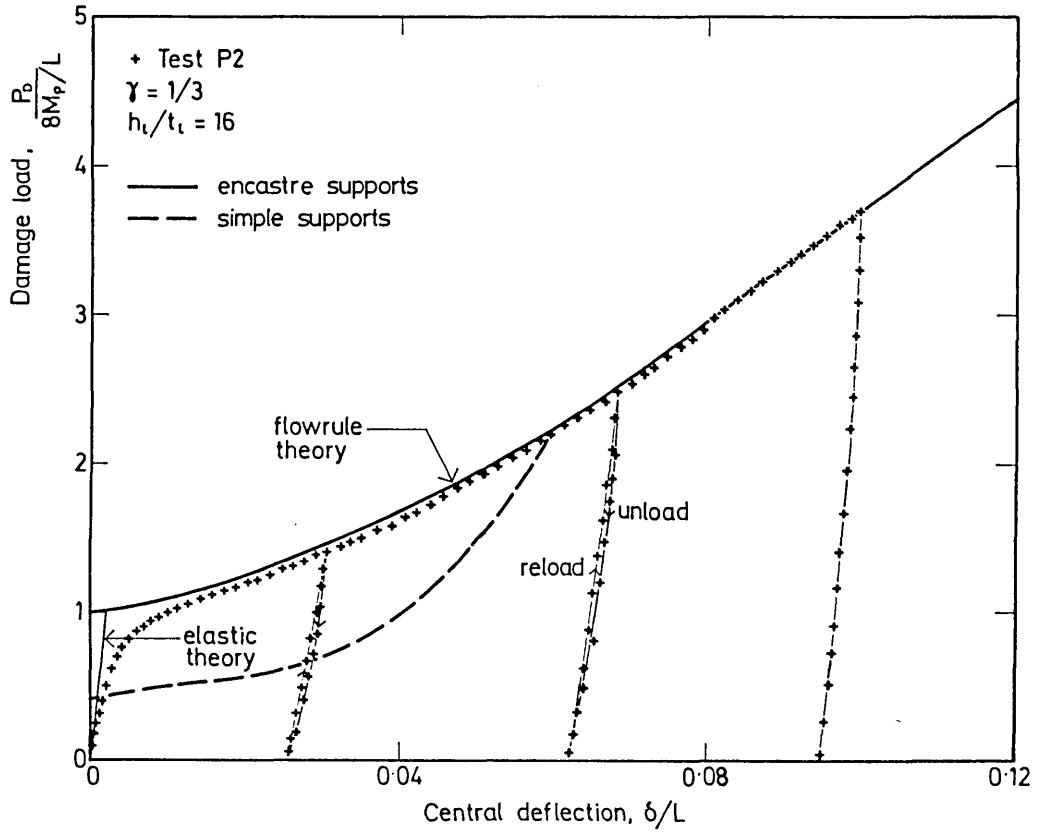


fig. 3·9(b)
Theoretical and experimental lateral load - deflection relationship
Test P2

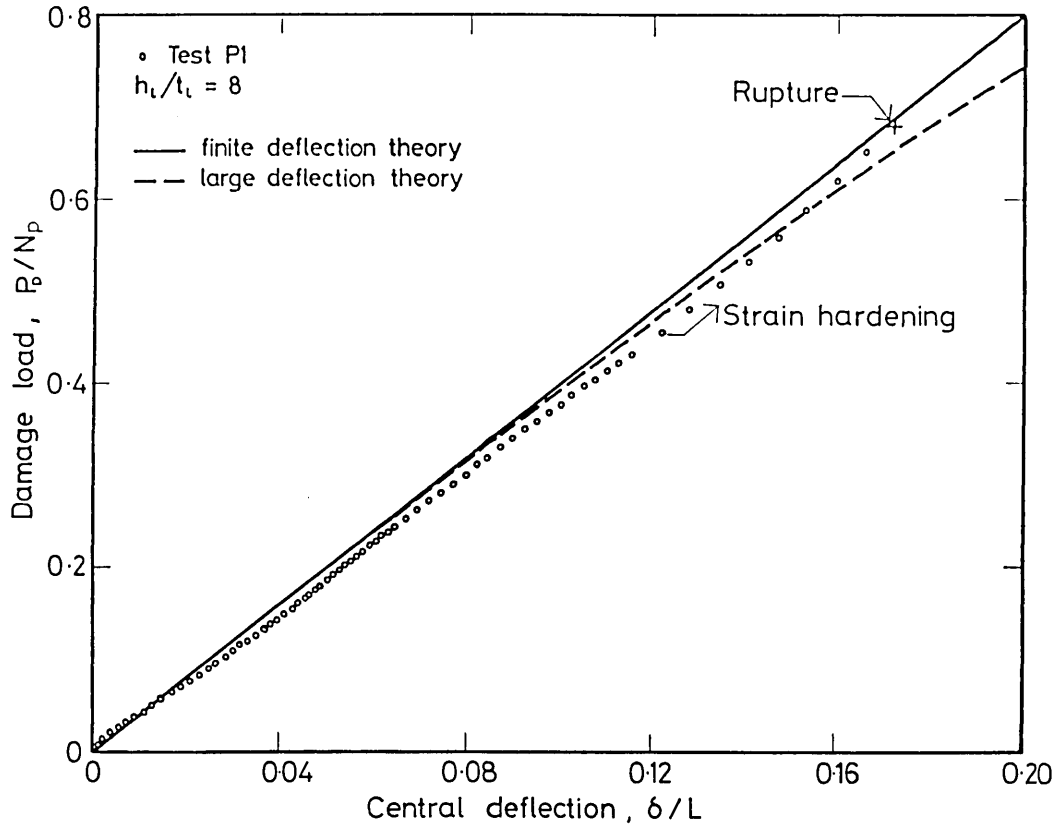


fig. 3.10
Theoretical and experimental lateral load with membrane yield
Test P1

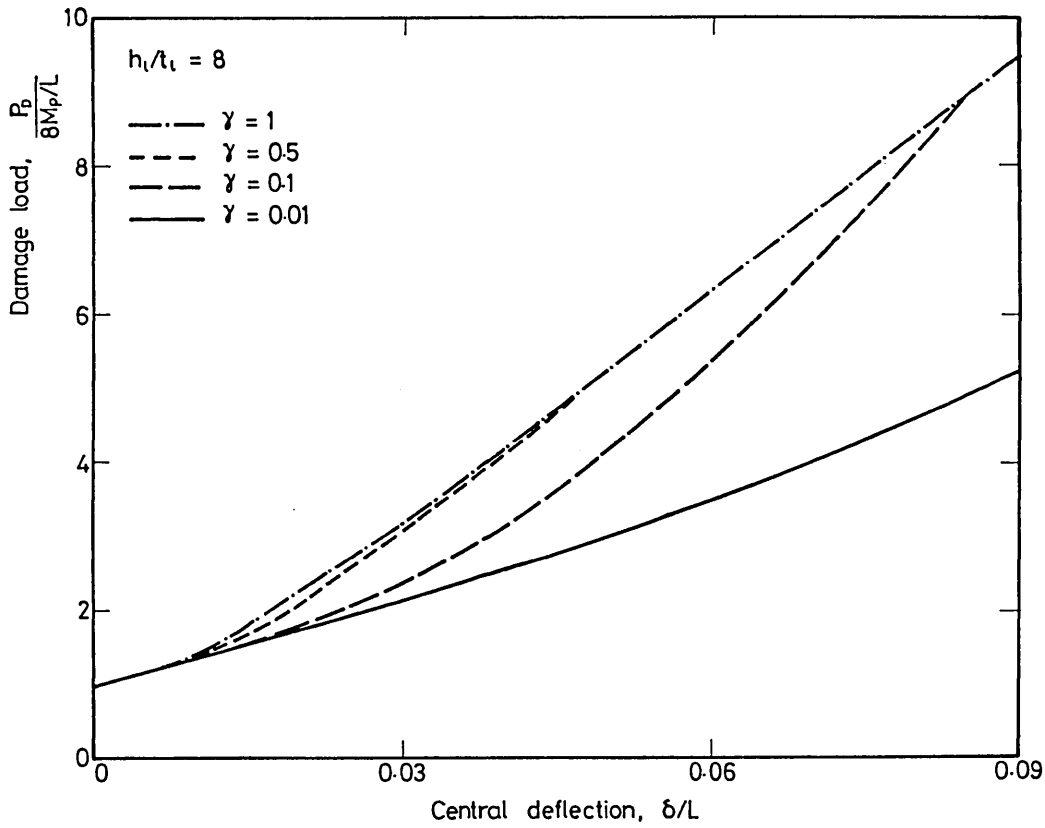


fig. 3.11
Variation of lateral load - deflection response with support axial stiffness
Test P1 geometry

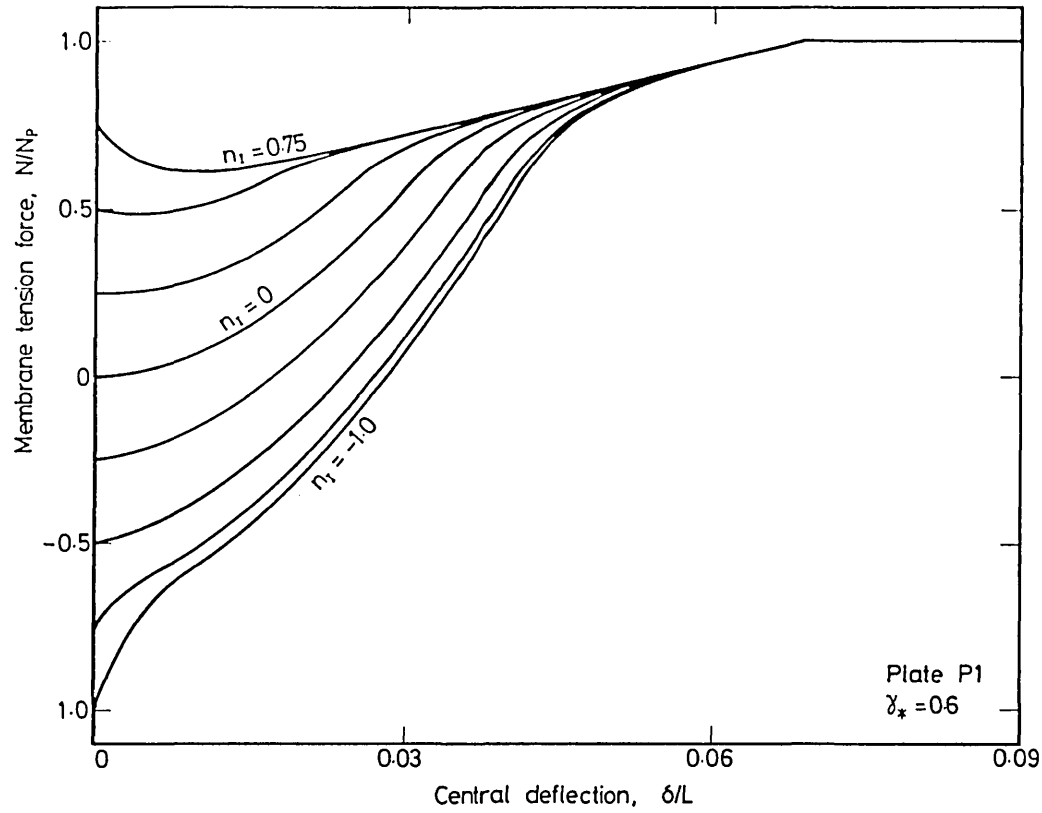


fig. 3·12
Membrane tension development from various initial values
Plate P1

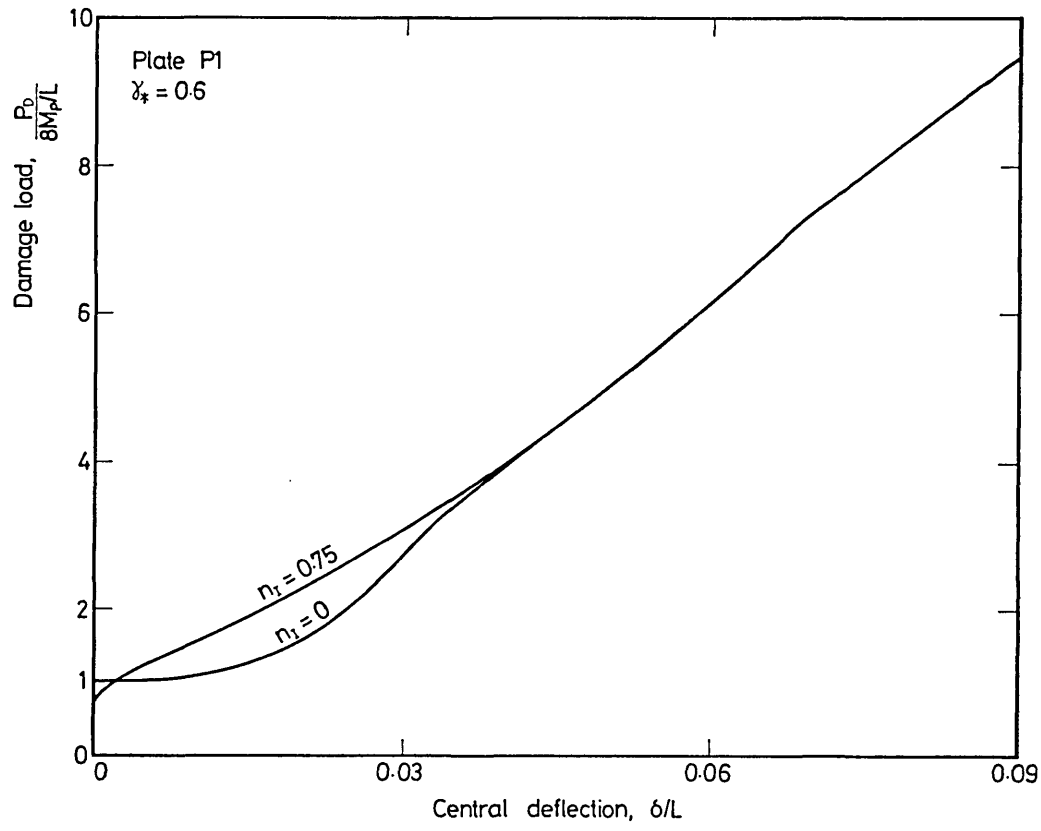


fig. 3·13
Lateral load - deflection relationship for various initial pretension values
Plate P1

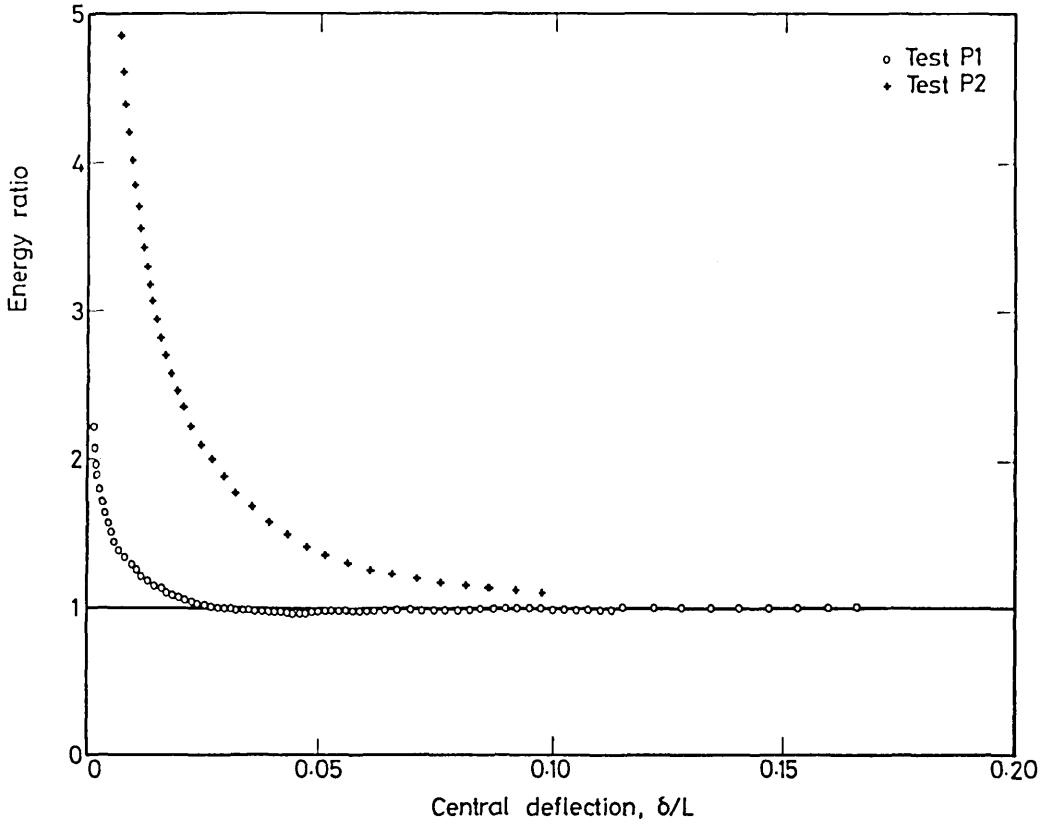


fig. 3·14
Ratio of experimental work done to area under linear response approximation

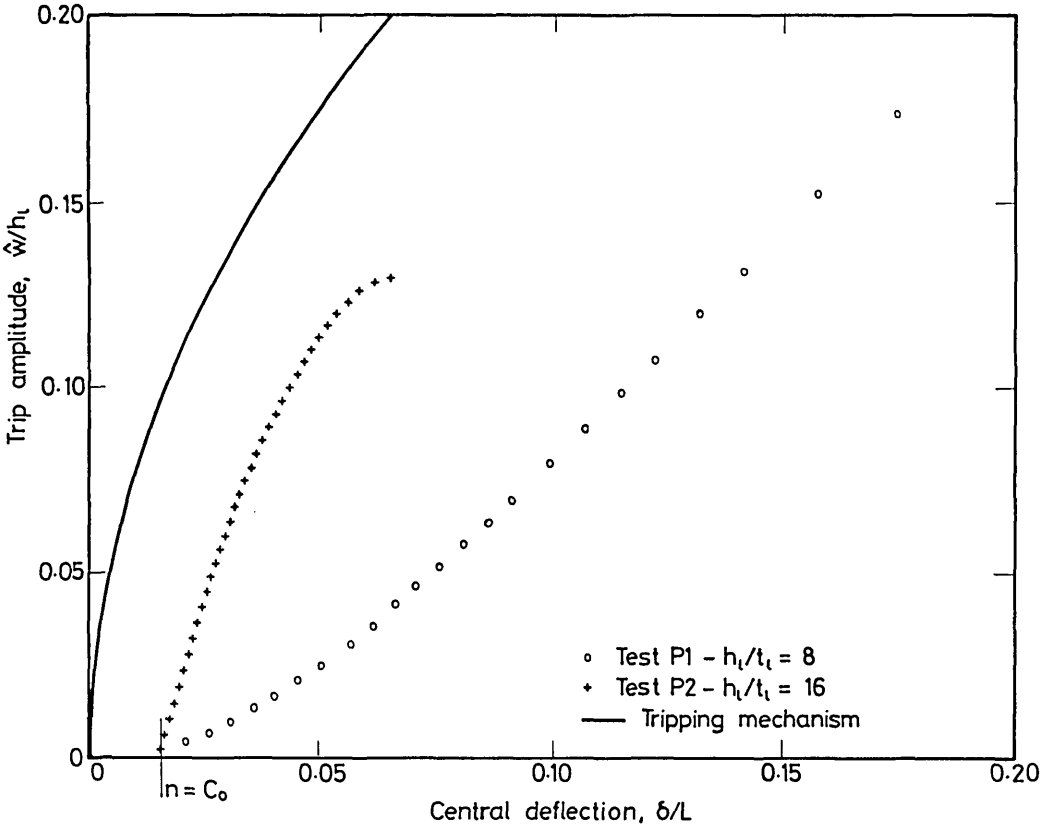


fig. 3·16
Growth of stiffener trip at support with lateral deflection

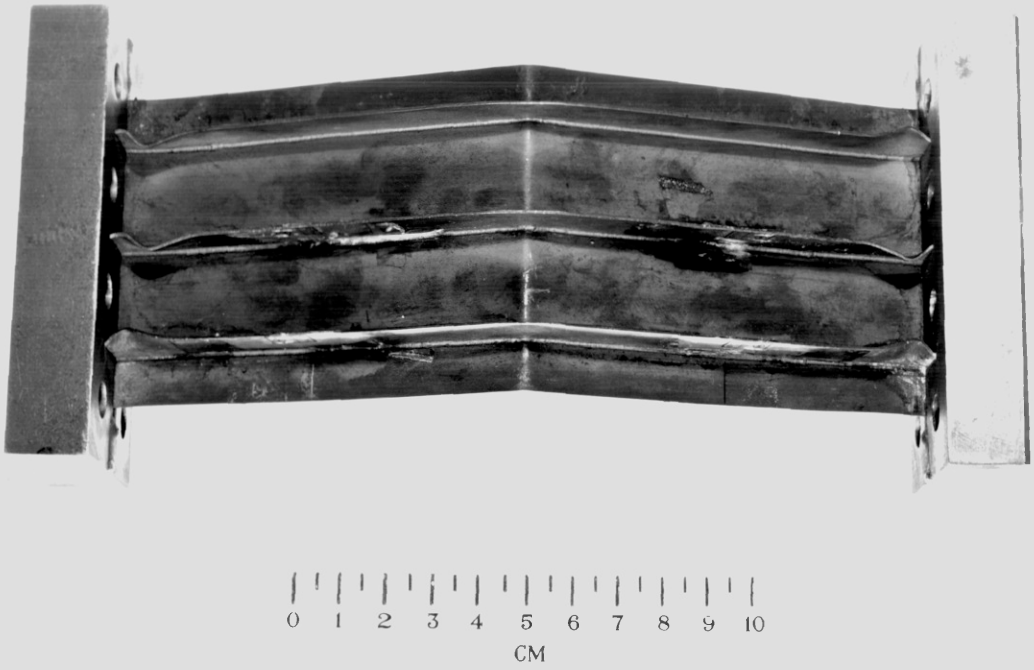


fig. 3.15
Underside of stiffened plate showing tripping mechanism
Plate P2

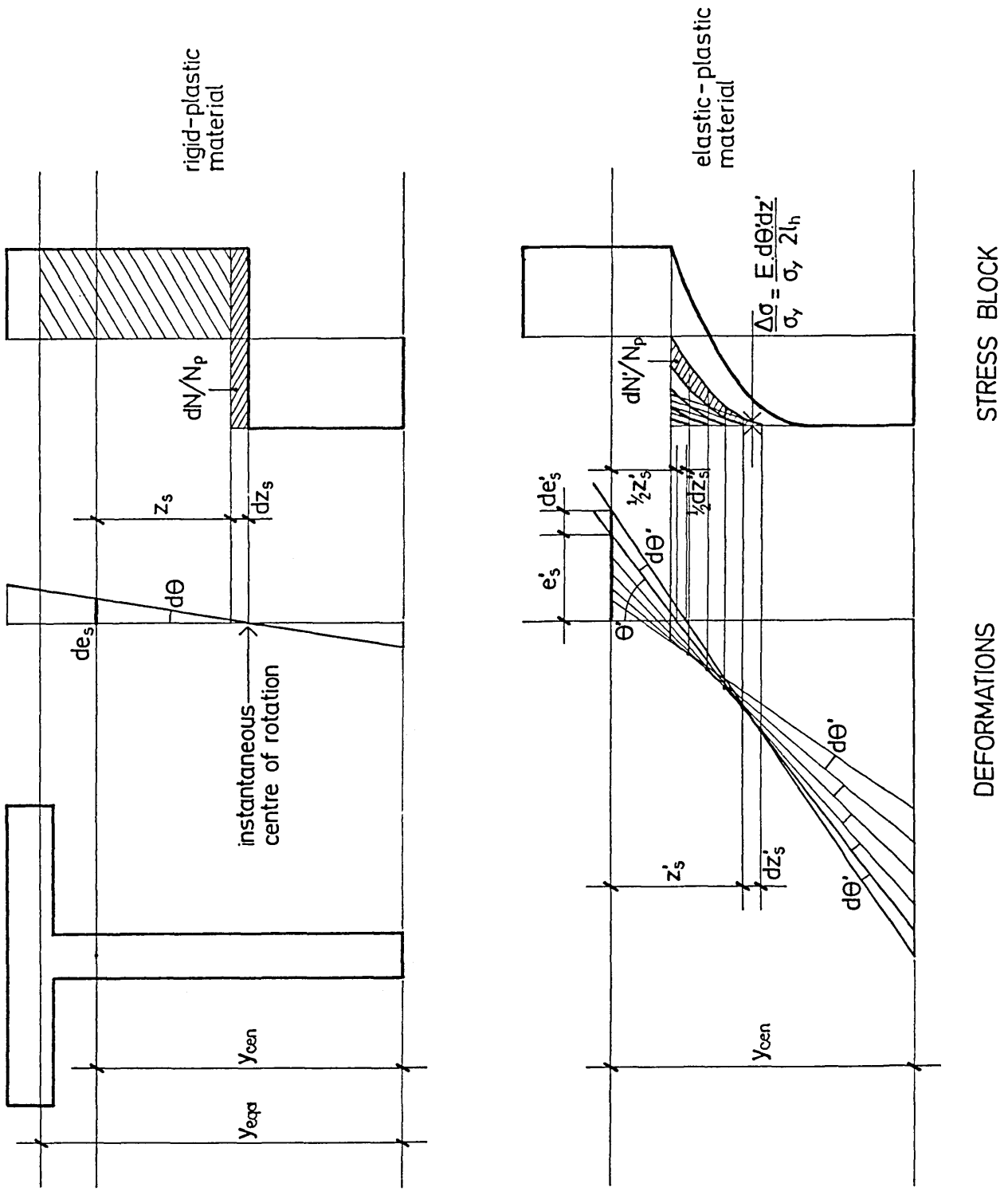


fig. 3.17
Support plastic hinge
Behaviour under increasing axial tension

CHAPTER 4

LONGITUDINAL LOADING OF DENTED PLATES

4.1 INTRODUCTION

Plate P2, which retained significant lateral deflection after denting, was later loaded in longitudinal compression to determine its residual stiffness and strength. By contrasting the observed response with that expected of a perfect beam-column with a V-shape, it is possible to ascertain the effect of imperfections such as residual stresses and local distortions caused by the damage. A more refined analysis that takes account of imperfections is developed near the end of the chapter and agrees well with the experimental results.

4.2 LONGITUDINAL COMPRESSION TEST

4.2.1 RIG ARRANGEMENT

The test rig is pictured in Fig. 4.1. With its longitudinal axis oriented vertically, Plate P2 was positioned within the rig and attached by its end plates. Both end connections were designed to provide high flexural fixity and were symmetrical about the centroidal axes of the stiffened plate where it joined the connections.

Four aluminium load cells arranged in a square were sandwiched between two platens at the top of the testing frame. The upper platen was bolted to the roof of the rig. Two different screw attachments were used for the load cells. A grub screw on the longitudinal axis of each load cell fastened it to the lower platen. On the top two screws were used for each load cell, the line joining them lying parallel to the panels of the stiffened plate

sample. This arrangement minimised the generation of bending moments within the load cells. Calibration runs were undertaken with another load cell occupying the position of the test piece, and these showed the set up to reliably measure the applied load.

The uppermost end plate of Plate P2 was bolted to the lower platen, which was stiff enough to have negligible flexural deformation during loading. The bottom end plate was attached to a stocky plunger via a connection piece with a recess on one side into which the end plate fitted closely, and a shear key below. This prevented lateral movement. The other end of the plunger rested on a spherical bearing, and the plunger was able to slide smoothly but with close fit through a relatively deep block. Longitudinal shortening was slowly applied by raising the plunger and its bearing with the aid of a hand operated wheel.

4.2.2 INSTRUMENTATION

4.2.2.1 LOAD CELLS

Linear strain gauges were glued onto each side of the thin neck of the load cells, in the same line as the screws to the upper platen. The dimensions were carefully designed to satisfy two conflicting criteria. The neck size gave the sensitivity required for accurate measurement of the expected load whilst exhibiting relatively little axial flexibility.

4.2.2.2 STRAIN GAUGES

Tokyo Measurement Laboratories' YL-3 strain gauges were positioned at the quarter-points of a second stringer beam on both panel and stiffener, matching those placed before denting. As the first set of gauges had previously

been stretched to large elongations, the new gauges allowed a check to be made on their ability to subsequently read small compressive strains during longitudinal loading.

4.2.2.3 TRANSDUCERS

End shortening within the clear span was measured using 50mm travel Sangama linear transducers, aligned vertically. Two transducers were positioned, one near each longitudinal edge of the test piece. Contact was made on the inner side of the end plates, at the centroidal axis of the stiffened plate lying parallel to the panels. For clarity the transducers are not present in Fig. 4.1.

A similar horizontally mounted transducer, visible in the photograph of Fig. 4.1, monitored the additional lateral deflection. Two small flats, forming a right angle, were incorporated to ensure that the maximum deflection was always measured, even though the location of this deflection moved upwards a little during compression. One flat was screwed onto the transducer rod and the other touched the apex of the ridge in the panel.

4.2.3 FINAL PREPARATION

Strains and load cell readings were monitored as Plate P2 was put into the rig and the bolts tightened up lightly. All readings were very small, which showed that no significant distortion of the test piece occurred due to incorrect support separation or local lack of fit. After the transducers were set in place the test was ready to begin.

4.2.4 TESTING PRECEDURE

Longitudinal compression was applied in extremely small steps by carefully turning the wheel. The increment was chosen to ensure that the initial elastic loading path was accurately portrayed, as well as the subsequent increasing nonlinearity to peak load. Continued end shortening enabled the post buckling path to be determined also.

4.3 THEORETICAL ANALYSIS

4.3.1 INTRODUCTION

As a first step, standard principles of structural analysis are employed to develop an idealized model of the response of the dented plate under compression. The accuracy of the simple model is tested in Section 4.4.1 where it is compared with the behaviour actually observed.

4.3.2 INITIAL ELASTIC RESPONSE

The "initial" shape of the stiffened plate and its early elastic deformation are sketched in Fig. 4.2(a). In this diagram the subscript "D" marks the magnitudes of various deflection quantities existing at the beginning of longitudinal loading and produced by the denting process.

In deforming further the ends of each half span are assumed to be fixed against rotation, but sway is permitted where the half spans meet at the centre. The applied longitudinal load is divided into axial and transverse components; that is

$$N/P_A = \cos\theta_D \qquad (4.1)$$

$$V/P_A = \sin\theta_D \ .$$

For simplicity the deflections caused by these forces are considered separately and then summed. Thus it is assumed that superposition holds.

The compressive strain caused by the axial force is given by

$$n\sigma_{YC}/E = 1 - a/a_0 = \Delta_H/L \ .$$

It is implied here that the actual length of the curved member is very similar to its projected length a. This is readily verified. The compression produces a small decrease in the lateral deflection:

$$\frac{\Delta\delta_N}{L} = \frac{\Delta_H}{L}\frac{\tan\theta_D}{2} = \frac{n\sigma_{YC}}{E}\frac{\delta_D}{L}$$

where

$$\tan\theta_D = 2\delta_D/L \ .$$

The transverse force V produces a peak transverse deflection given by

$$\hat{g} = \frac{Va^3}{12EI}$$

according to simple bending theory. Its vertical component is thus

$$\frac{\Delta\delta_V}{L} = \frac{n\sigma_{YC}}{E}\frac{\delta_D}{L}C_{10}.(1 - n\sigma_{YC}/E)^3$$

$$\approx \frac{n\sigma_{YC}}{E}\frac{\delta_D}{L}C_{10}$$

when it assumed that

$$a/a_0 \approx 1 .$$

Here

$$C_{10} = \frac{AL^2/I}{48\cos^2\theta_0}$$

and use is also made of the geometric relationship

$$L/2a_0 = \cos\theta_0 .$$

The component of the transverse deflection in the longitudinal direction is

$$\frac{\Delta_V}{L} = 4\delta_0 \frac{\Delta\delta_V}{L}\frac{}{L} .$$

By summing the two components in each direction the total deflections are found to be

$$\frac{\Delta\delta}{L} = \frac{\Delta\delta_V}{L} - \frac{\Delta\delta_N}{L} = n\sigma_{YC}\frac{\delta_0}{E}\frac{}{L}(C_{10} - 1) \qquad (4.2)$$

and

$$\frac{\Delta}{L} = \frac{\Delta_V}{L} + \frac{\Delta_N}{L} = n\frac{\sigma_{YC}}{E}((2\delta_0/L)^2 C_{10} + 1) . \qquad (4.3)$$

If, as an opposite extreme, the supports are assumed to be pinned the same formulae apply with C_{10} given four times the above value.

Interaction between the axial and transverse forces, and in particular, amplification of the transverse deflection by Euler effects, is readily included. Now:

$$\frac{\hat{g}}{a_0} = \frac{2\delta_0}{L}(C_{11} - 1)$$

and so

$$\frac{\Delta\delta_v}{L} = \frac{\delta_0}{L}(C_{11} - 1)$$

where

$$C_{11} = \frac{2(1-\cos C_{12})}{C_{12}\sin C_{12}}$$

$$C_{12}^2 = \pi^2 N/N_E$$

$$= 12C_{10}n\sigma_{yc}/E \ .$$

Here

$$N_E = \pi^2 EI/a_0^2$$

is the Euler buckling force. For the geometry and material properties under consideration

$$N_E/N_P = 10 \ .$$

This results in the modified transverse deflection being negligibly larger than that given earlier.

4.3.3 FIRST YIELD

Compressive yield first occurs in the stiffener tip near the support under the combined action of axial force and bending moment. The magnitude of the bending moment is

$$M_s = \tfrac{1}{2}Va_0 \ .$$

Using first order theory, the longitudinal load at which yield is initiated is

$$P_{AY}/N_P = p_{AY} = 1/(\cos\theta_0 + \tfrac{1}{2}(\delta_0/L)(LA/Z_{min})) \ .$$

If the Euler refinement is incorporated this becomes

$$p_{AY} = 1/(\cos\theta_0 + \tfrac{1}{2}(\delta_0/L)(LA/Z_{min})C_{11}) \ .$$

4.3.4 PLASTIC MECHANISM

The ideas behind the analysis that follows were instigated by Paris [111]. In determining the postbuckling behaviour of struts he set aside the Euler criterion. Instead he assumed a plastic hinge at mid-length and evaluated its capacity under combined axial compressive force and bending moment. The moment is induced by lateral deflection of the strut, which gives the applied load an eccentricity at the hinge location. This flexure causes longitudinal shortening which is added to that due to axial compressive strains.

The method is clearly demonstrated by Supple and Collins [158] who apply it to initially straight tubes. Examples of both pinned and fixed ends are developed with suitable sinusoidal deflection modes.

Carlsen et al [15] have applied the approach to simply supported T-section struts. Again the struts are initially straight but this time they are considered to deform into a bilinear shape. The end shortening induced by lateral deflection is computed assuming the legs of the mechanism are incompressible. To this is added a component due to direct stress and also the inward movement of the load application point caused by rotation at the supports. The strut is assumed to bend such that the top of the panel is in tension at the central plastic hinge. (The

stiffened plate tested in this chapter is of course predisposed to bend in the opposite direction.) The direction of bending adopted by Carlsen et al means that the plastic capacity of the section is given by one interaction equation throughout the loading process.

The method adopted in this dissertation is illustrated in Fig. 4.2(b). Equilibrium of the forces drawn in the diagram gives

$$P_A\delta = M_s + M_c \qquad (4.4)$$

and

$$N/P_A = \cos\theta \ . \qquad (4.5)$$

Comparison of Eqns. (4.1) and (4.5) shows that the extra deformation caused by longitudinal loading is now assumed to be finite.

Fully plastic hinges are assumed at the centre and supports and their capacities may be determined from the interaction formulae given in Section 3.4.2.1. Thus, for

$$0 \le n \le 1 :$$

$$m_s = 1 - (1-f)n - fn^2 \ .$$

Also

$$0 \le n \le C_0 :$$

$$m_c = 1 + (1-f)n - fn^2 \ .$$

$$C_0 \le n \le 1 :$$

$$m_c = \frac{bf}{t_l} - (A_p/A_l)^2(1-f) + (A_p/A_l)^2(1-f)n - \frac{bfn^2}{t_l} \ .$$

Here moments and axial force are considered positive when acting as shown in Fig. 4.2(b). Hence compressive force is positive, which is convenient for column work, whereas the opposite sign convention is adopted in the work of Chapter 3.

The mechanism is assumed to deform such that its initial V-shape is amplified. Hence:

$$\frac{\delta}{L} = \frac{a.\sin\theta}{a_0 2\cos\theta_0} \tag{4.6}$$

$$\frac{\Delta}{L} = 1 - \frac{a.\cos\theta}{a_0\cos\theta_0} \ . \tag{4.7}$$

Here δ is the total lateral deflection, including that caused by the denting test. The major difference between these equations and the approach used by Carlsen et al is that axial shortening of the legs is included in the deformation geometry.

In concurrence with the ideas of Section 3.4.3 this axial strain does, in general, have several sources; that is

$$1 - a/a_0 = (e_a + e_s + e_c)/a_0 \ .$$

The nondimensionalized elastic bar compression to be inserted into this equation is

$$e_a/a_0 = n\sigma_{yc}/E \ .$$

The centroidal compression at the support and central plastic hinges are represented by e_s and e_c respectively and are defined by flow rules. However it may be shown that for the geometry under consideration the total hinge compression is even smaller than the bar compression and so may be neglected. The resulting lone axial shortening component is the same as that assumed by Supple and

Collins [158] and Carlsen et al [15].

Substituting this axial shortening into Eqns. (4.6) and (4.7) gives

$$\Delta\delta/L = \tfrac{1}{2}(1 - n\sigma_{yc}/E)\sin\theta/\cos\theta_0 - \delta_0/L$$

$$\Delta/L = 1 - (1 - n\sigma_{yc}/E)\cos\theta/\cos\theta_0$$

and thus Eqn. (4.4) becomes

$$\tan\theta = \frac{2\cos\theta_0}{C_{13}}\frac{(m_s + m_c)}{n(1 - n\sigma_{yc}/E)} \qquad (4.8)$$

where

$$C_{13} = LA/Z_p \ .$$

4.3.5 OVERVIEW

Before undertaking a detailed experimental correlation an overview is made of the various stages of the response. Fig. 4.3(a) shows typical relationships between longitudinal load and end shortening using the geometry of Plate P2. As might be expected the unloading curve predicted by Eqn. (4.8) is much more gradual when the "initial imperfection" is larger. For a dent depth of

$$\delta_0/L = 0.095 \ ,$$

which corresponds with the test case, the elastic flexural response given by Eqn. (4.3) is also drawn. For completeness the experimental points are included as well.

During plastic collapse the variation of longitudinal load with lateral deflection is almost independent of the initial dent depth, as long as this depth is reasonably

small. Put another way, plotting Eqn. (4.8) in Fig. 4.3(b) yields only one line. However there are two other theoretical curves in Fig. 4.3(b). The uppermost curve depicts a simplified mechanism which ignores plastic interaction capacities; that is

$$P_A \delta = 2M_p \ .$$

At smaller loads the predictions of this equation are virtually identical to the more rigorous analysis developed above. Pettersen and Johnsen [113] find this occurs also for simply supported tubular struts typical of bracings used in offshore construction. The third, solid line shows the load causing first yield for all initial lateral deflections.

4.4 THEORETICAL CORRELATION

4.4.1 SIMPLE MODEL

4.4.1.1 DEFLECTIONS

Fig. 4.4 shows the development of end shortening and lateral deflection. The experimental points follow the form predicted by plastic mechanism theory although the end shortening values are higher. This extra compressibility is probably caused by local yield within the span due to residual stresses and geometrical imperfections present after damage loading and also the additional compressive flexibility at trip locations. A third contribution source may be centroidal compression in the plastic hinges which is neglected in the derivation.

There is no indication of panel buckling during the test. This is to be expected as the panels are relatively stocky. Also, they carry significant compressive stresses

only near the plastic hinge at mid-span and here the sharp angle change acts as reinforcement.

4.4.1.2 LONGITUDINAL LOAD RESPONSE

The experimental load versus deflection response is plotted in Figs. 4.5(a) and (b). Early deviation is seen from the theoretical elastic behaviour developed above by assuming encastre supports. This is probably due to yielding at the centre and supports, in the presence of residual stresses.

Smith et al [146,147,148,149] have developed an understanding of the effect of residual stresses. In the context of damaged steel ships Smith and Dow [147] consider that the compressive stiffness and strength of orthogonally stiffened plating, which has been damaged such that the stringer beams are bent laterally between transverse frames, will be influenced by the residual stresses.

Consideration has also been given to the longitudinal load response of stocky, simply supported tubes after bending damage. In earlier work Smith et al [146] simulated the damage process numerically so that the resulting residual stress distribution might be included in their subsequent analysis of axial loading. It was found however [148] that the inclusion of these stresses had negligible effect and so they were ignored in later work [149]. This is because rebound during lateral unloading produces stresses in the outer fibres that oppose those caused by subsequent longitudinal compression. It is noted in Section 3.5.8, however, that the significant membrane tension in the present stiffened plate test modifies the residual stresses. Thus regions of stress which are sympathetic with subsequent action under longitudinal load are induced. This softens the response.

Any rotation of the supports will also increase the flexibility, but a study of the strains in the four load cells indicates that the end plate rotation is several orders of magnitude smaller than that produced by a pin ended response. For comparison the elastic prediction for a simply supported plate is also drawn in Fig. 4.5(b) and it markedly underestimates the early experimental stiffness.

The longitudinal load levels out to a maximum lying thirteen per cent above the first yield prediction (see Fig. 4.5(a)). This reserve of capacity is much smaller than expected for the high T-section shape factor

$$Z_p/Z_{min} = 1.75 .$$

However it is larger than that found by Carlsen [13] for simply supported T-section struts with relatively small initial imperfections because the bending mode is much more important in the present work. Carlsen determines first yield by two different approaches, the Perry-Robertson formula and finite element analyses.

Under deflection control the longitudinal load then starts to diminish gradually, the values being about sixty per cent of the theoretical plastic collapse curve based on encastre supports. Mechanism curves are drawn for various $\tilde{\gamma}$ values, where

$$m_s' = \tilde{\gamma} m_s$$

and

$\tilde{\gamma} = 1$ for perfectly encastre supports
$\tilde{\gamma} = 0$ for zero moment at supports.

It is apparent that in this test

$$\tilde{\gamma} \approx 0.12 .$$

The probable reason for this is discussed in Section 4.4.2 below.

4.4.1.3 AXIAL FORCE DEVELOPMENT

The experimental axial force is computed from the strain gauge readings and is comparable to the load cell measurements, when the two are related using Eqn. (4.5). They are slightly different in that the strain gauge results are five or ten per cent higher than expected. However gauges placed both before and after the denting test give similar values. On future models, therefore, the same gauges can be used to monitor strains both during denting and in the longitudinal compression test.

Diagrams showing the variation of axial compression force with both end shortening and additional lateral deflection are very similar to their counterparts for longitudinal load. For this reason the axial force diagrams are not presented in this dissertation.

4.4.2 STIFFENER TRIPPING AT SUPPORTS

Because the preceding simplified analysis does not correlate well with the observed behaviour of the stiffened plate test it is necessary to introduce refinements. Probably the major cause of the discrepancy is the abrupt geometric imperfection in the stiffeners near each support and so these deserve closer scrutiny.

Substantial research has been undertaken into torsional buckling of stiffeners, as mentioned in Section 2.6.1. However no publications known to the present author consider sharp, localized initial deformations of finite size, such as those present at the end of the denting process. Murray's tripping mechanism (Ref. [105]) is concerned only with the development of this mode in

initially straight stiffeners. Hence it is again modified to suit the present situation.

An increment of lateral deflection requires shortening along the stiffener tip near the support and if the material is assumed to be relatively incompressible this is accommodated entirely by increasing the amplitude of the trip. Thus

$$d\theta.\tan\beta = \frac{2(\hat{w}/h_t)(d\hat{w}/h_t)}{\sqrt{1 - (\hat{w}/a_{tr})^2}} . \qquad (4.9)$$

If both θ and $\hat{w}/a_{tr}$ are considered to be small Eqn. (4.9) integrates to

$$\frac{\hat{w}^2 - \hat{w}_0^2}{h_t^2} \approx (\theta - \theta_0)\tan\beta .$$

This parallels Eqn. (3.25), but incorporates parameters which describe the initial damaged geometry existing before longitudinal loading starts. However the assumption of small deflections is rather dubious, and for accurate analysis the more rigorous incremental approach should be adopted.

The plastic capacity of the tripped section is now derived. Murray's approach is followed, although his theory is rewritten here using the notation of Fig. 4.6, which is consistent with that employed elsewhere in the dissertation. This facilitates presentation of the results in a concise nondimensionalized form.

The plastic interaction relationship between axial force and bending moment for a rectangular section is well known (see Ref. [68] for example). Employing the symbol "∂" to denote elemental quantities pertaining to a rectangular strip, the relationship becomes

$$\partial m + (\partial n)^2 = 1 \qquad (4.10)$$

where

$$\partial n = \partial N/\partial N_p \quad \& \quad \partial N_p = \sigma_y \partial A \quad \& \quad \partial A = t_l \partial y$$

$$\partial m = \partial M/\partial M_p \quad \& \quad \partial M_p = \sigma_y \partial Z_p \quad \& \quad \partial Z_p = \tfrac{1}{4} t_l^2 \partial y \ .$$

Moment equilibrium of a typical bilinear strip drawn in Fig. 4.6 requires

$$w\partial N = (1 + 1/\cos^2\beta)\partial M \ , \qquad (4.11)$$

allowing for the inclination of the outer hinge lines. Substituting (4.11) into (4.10) and solving the quadratic equation gives

$$\partial n = \sqrt{1 + (C_{14}')^2} - C_{14}' \qquad (4.12)$$

where

$$C_{14}' = \frac{2w/t_l}{1 + 1/\cos^2\beta}$$

and using

$$\partial A/\partial Z_p = 4/t_l \ . \qquad (4.13)$$

Equation (4.12) is integrated through the stiffener depth using the linear relation

$$w/\hat{w} = y/h_l$$

for the out-of-plane deflection of the stiffener at depth y . Firstly

$$\frac{N_l}{N_p} = n_l = \int_{y=0}^{h_l} \partial n . \frac{\partial N_p}{N_p}$$

$$= \frac{A_l}{2\hat{A}} \left[C_{15} - C_{14} + \frac{\ln(C_{15} + C_{14})}{C_{14}} \right]$$

where

$$C_{14} = \frac{2\hat{w}/t_t}{1 + 1/\cos^2\beta}$$

$$C_{15} = \sqrt{1 + C_{14}^2} \ .$$

Integrating moments about the stiffener/panel junction where $y = 0$ obtains

$$\frac{M_t}{M_p} = m_t = \frac{A_t h_t}{3Z_p}(C_{15}^3 - 1 - C_{14}^3)/C_{14}^2 \ .$$

With the aid of l'Hospital's rule it may be shown that n_t and m_t approach the values expected for a stiffener in pure compression as C_{14} tends to zero.

Again making use of the interaction relationship for a rectangular section, the moment in the panel is

$$\frac{M_{pa}}{M_p} = m_{pa} = \frac{A_p t}{4Z_p}(1 - (n_{pa}A/A_p)^2)$$

where N_{pa} is the net axial force in the panel.

Finally, equilibrium of the section at the centre line of the trip gives

$$n = n_t + n_{pa} \qquad (4.14)$$

$$m_s' = m_t + m_{pa} + \frac{n_t A t}{2Z_p} - n\frac{A_t(h_t + t)}{2Z_p} \ . \qquad (4.15)$$

Here hogging bending moments and compressive axial forces are assumed to be positive and moments are taken about the centroidal axis.

The interaction diagram defined by Eqns. (4.14) and (4.15) is plotted in Fig. 4.7 for typical values of $\hat{w}/t_t$.

The geometry of Plate P2 is used for the example with a β value of 0.3 radian, as observed experimentally. A series of approximately parallel lines result because m_{pa} is small and n_t and m_t are constant for a particular trip geometry.

Figs. 4.8(a) and (b) show the longitudinal load versus deflection response found by substituting Eqn. (4.15) into (4.8) and using the experimentally observed initial trip geometry caused by damage loading. Growth of the trip during compression is computed using Eqn. (4.9).

This modified theory, incorporating a reduced moment capacity at the support plastic hinges, gives a greatly improved estimate of the experimental load capacity although it is still a little optimistic. The agreement is better for longitudinal deflection than lateral deflection, partly because the theoretical end shortening at centroid level due to trip amplification is not included in the former.

Murray has found that the load capacity is insensitive to the β value and a small parametric study confirms this to be true here.

Other authors have also observed tripping mechanisms in similar experimental situations and have accounted for their effect theoretically. Carlsen et al [15] address tripping at the centre of straight T-section struts with pinned ends and find that Murray's analysis method correlates well with tests on slender stiffeners; that is

$$h_t/t_t > 0.5\sqrt{E/\sigma_Y}\ .$$

The present results agree with this.

Walker et al [181,182] have observed stiffener tripping near the end rings of stringer stiffened cylinders subjected to axial compression. The material and

geometry of the component stringer beams are similar to the present stiffened plate test although the cylinders contain no large initial imperfections. These researchers find that a close description of the experimentally observed behaviour is achieved if the moment capacity of the support is assumed to fall to zero when the stiffeners attain yield stress there. Further load is carried by the stringer beams, which are now considered to be simply supported, until yielding occurs at mid-span.

4.5 CONCLUSIONS

In Chapter 3 it is demonstrated that a straight forward mechanism analysis is able to predict the experimental response under lateral loading very well, even when stiffener tripping occurs. This chapter shows that the same cannot be said for longitudinal compressive loading. Material and geometric imperfections present after denting substantially affect the subsequent behaviour. The results may be adequately reproduced, however, by incorporating tripping into the collapse mechanism.

As shall be seen later in Chapter 6, the softness apparent in the loading path, and the low strength of the dented stringer beams, will be used to advantage to simplify the analysis of dented cylinders.

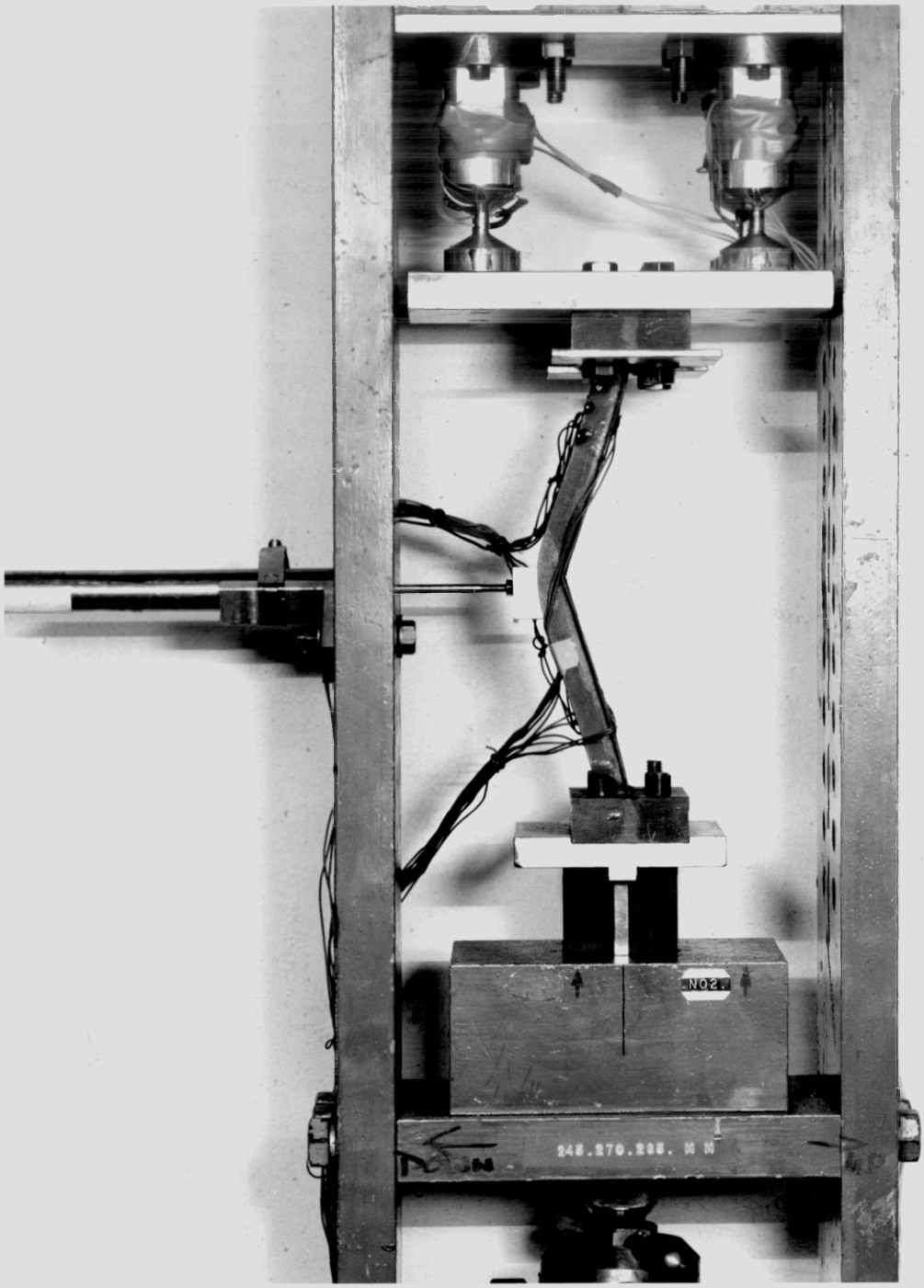


fig. 4.1
Test rig for longitudinal compression of dented plates

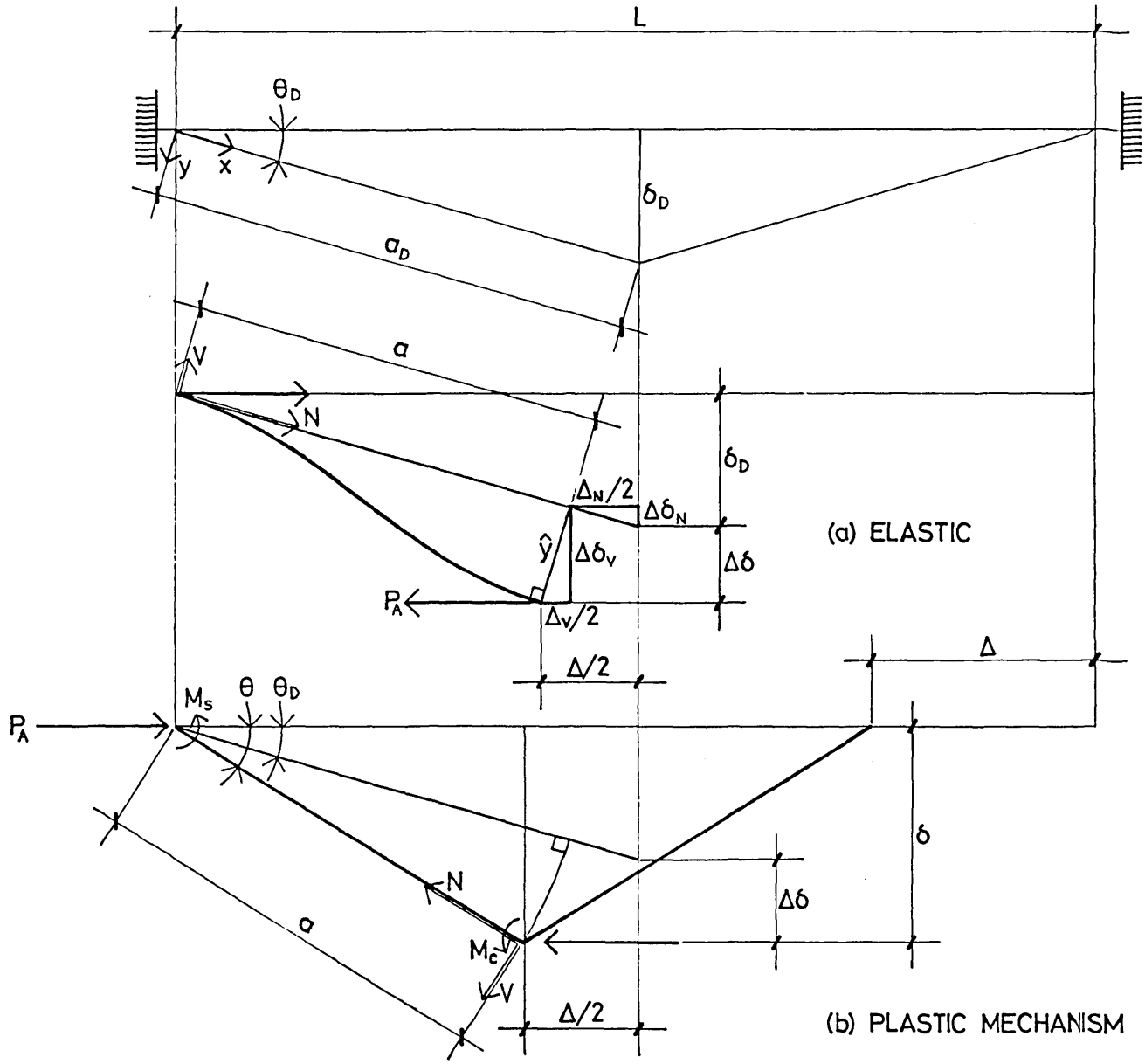


fig. 4.2
Longitudinal loading of V-shaped beam-column
Forces and deformations

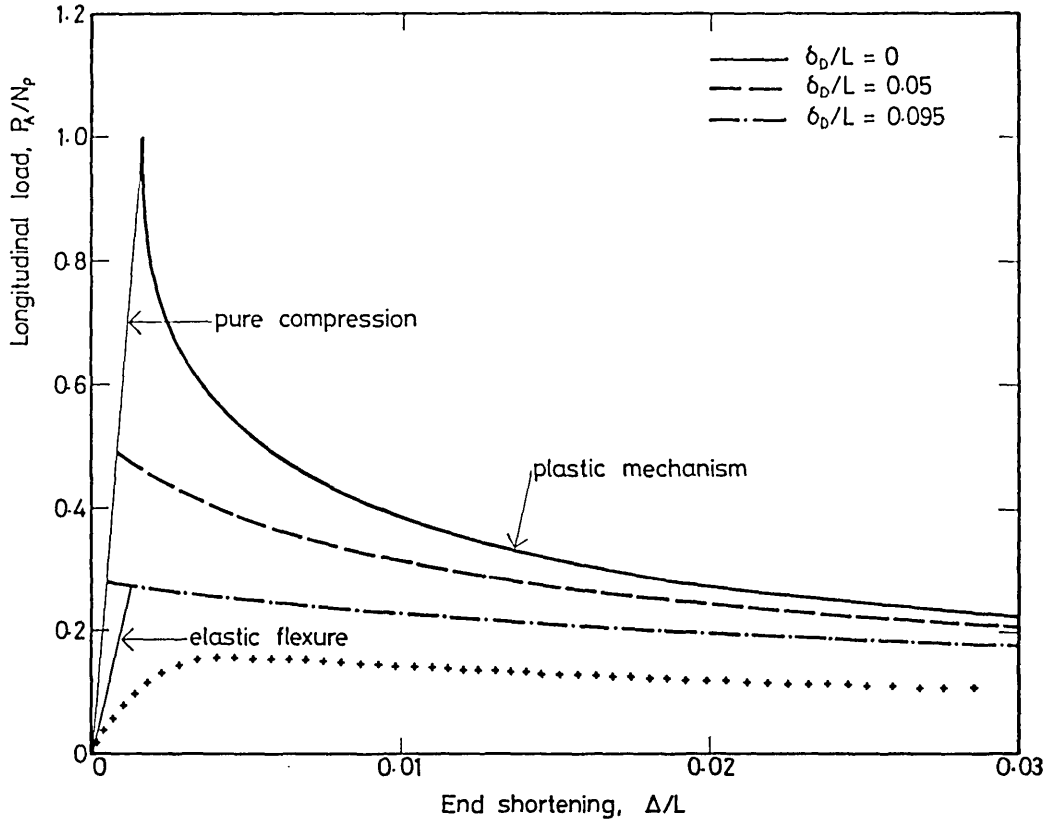


fig. 4.3(a)
Longitudinal load - end shortening curves for various initial dent depths

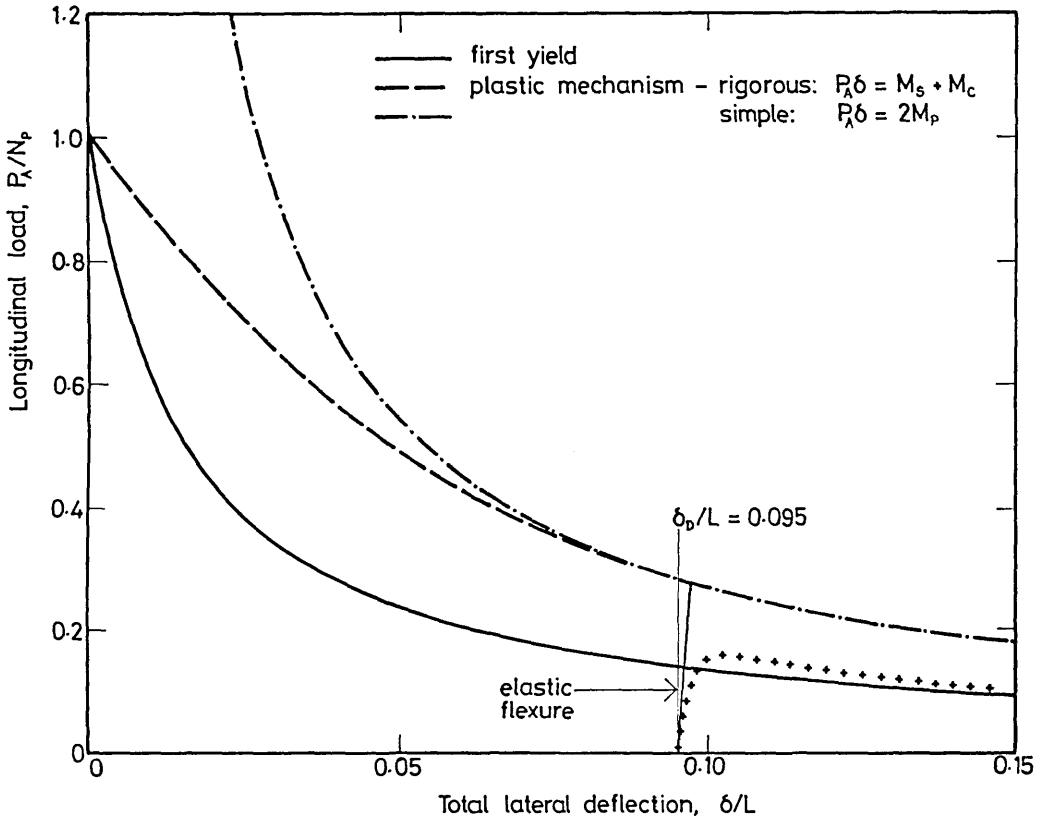


fig. 4.3(b)
Longitudinal load - lateral deflection curves

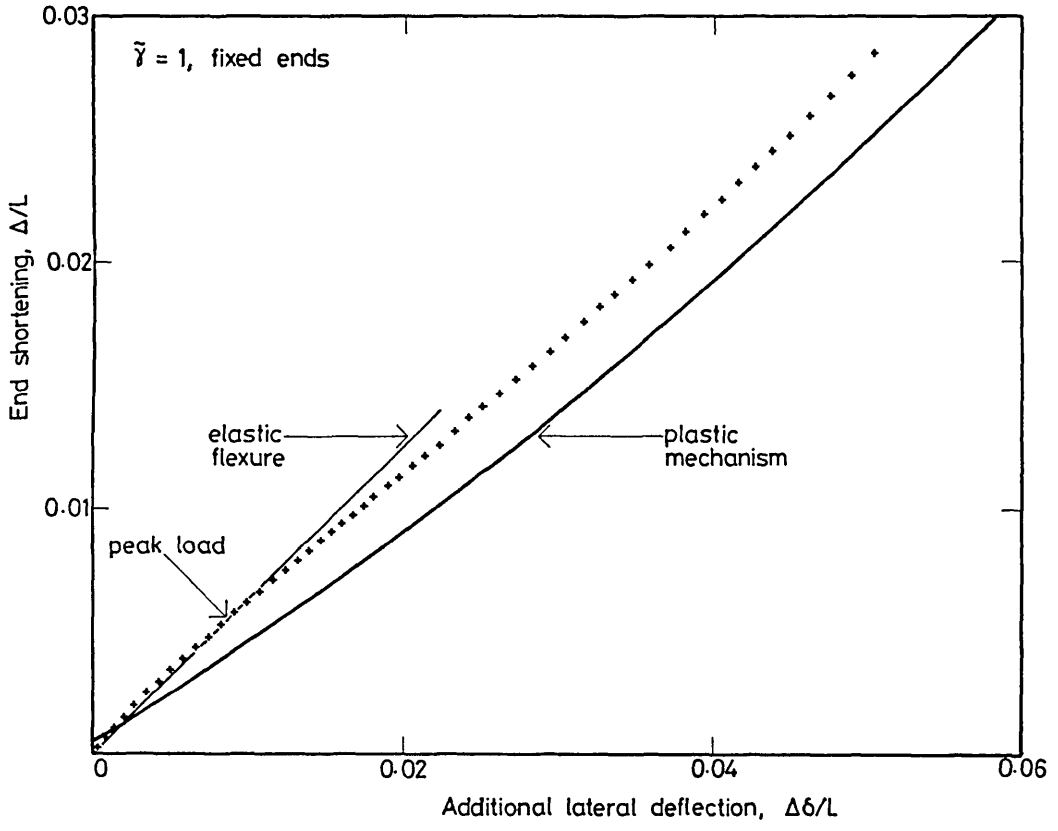


fig. 4.4
Theoretical and experimental deflection relationships

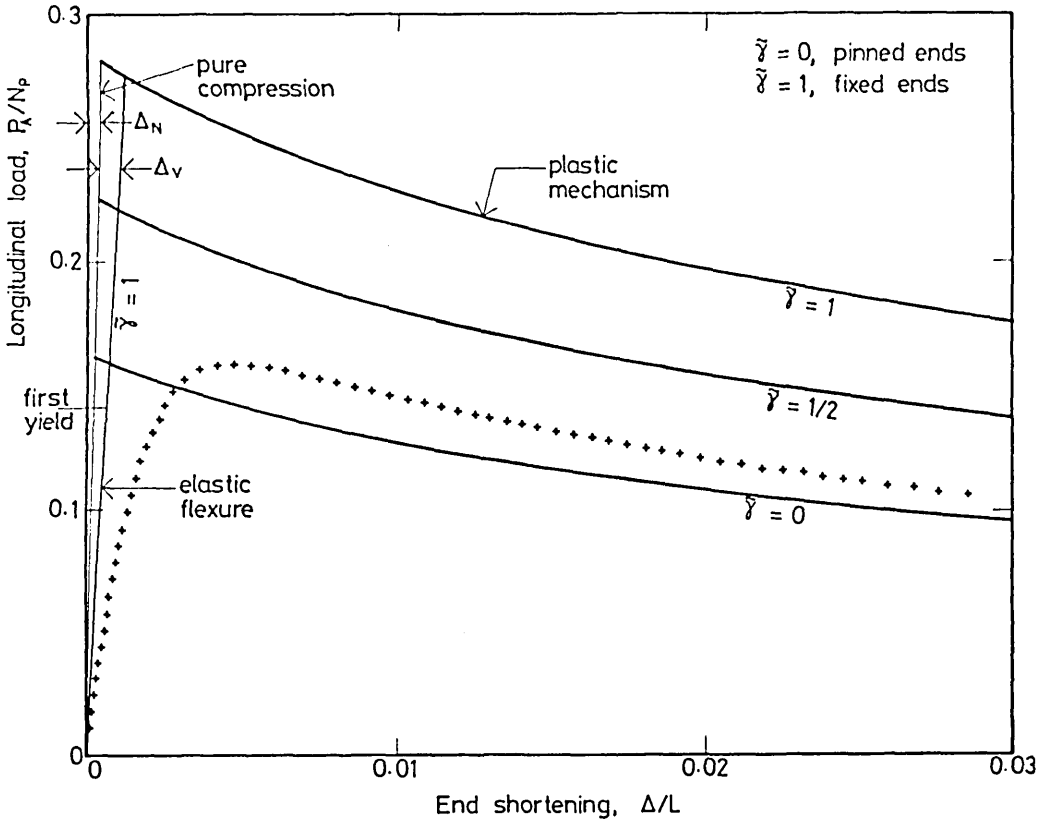


fig. 4.5 (a)
Theoretical and experimental longitudinal load - end shortening response

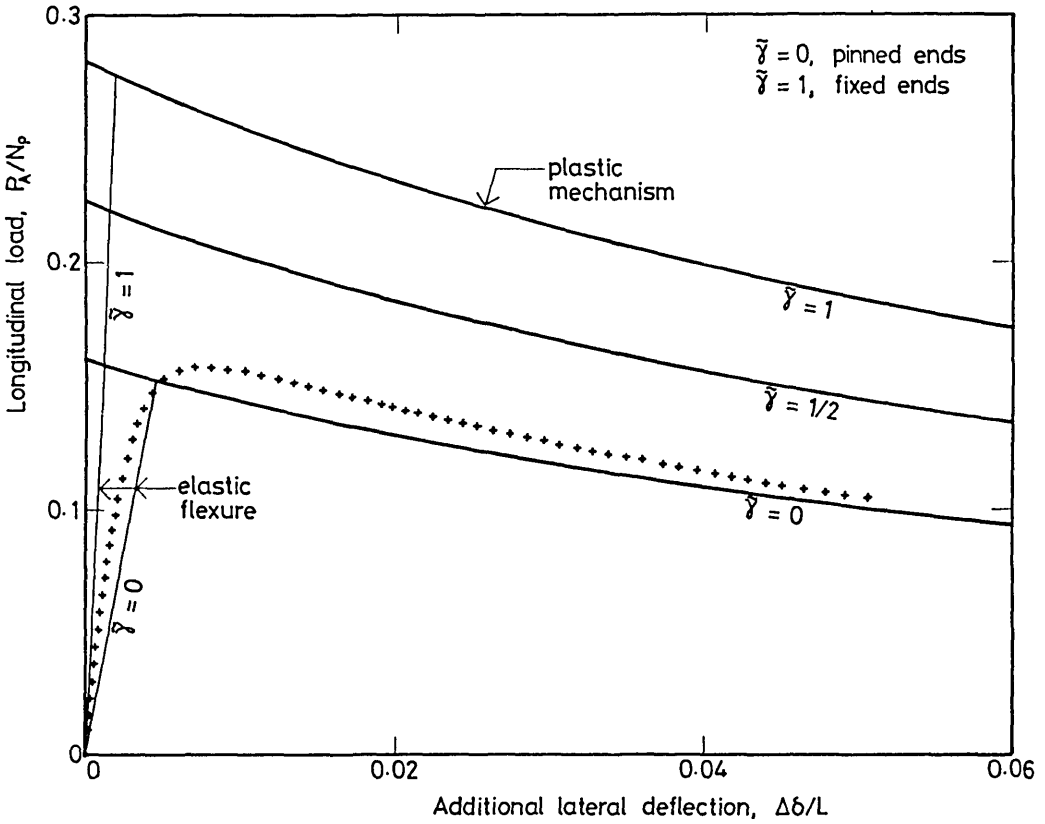


fig. 4.5 (b)
Theoretical and experimental longitudinal load - lateral deflection response

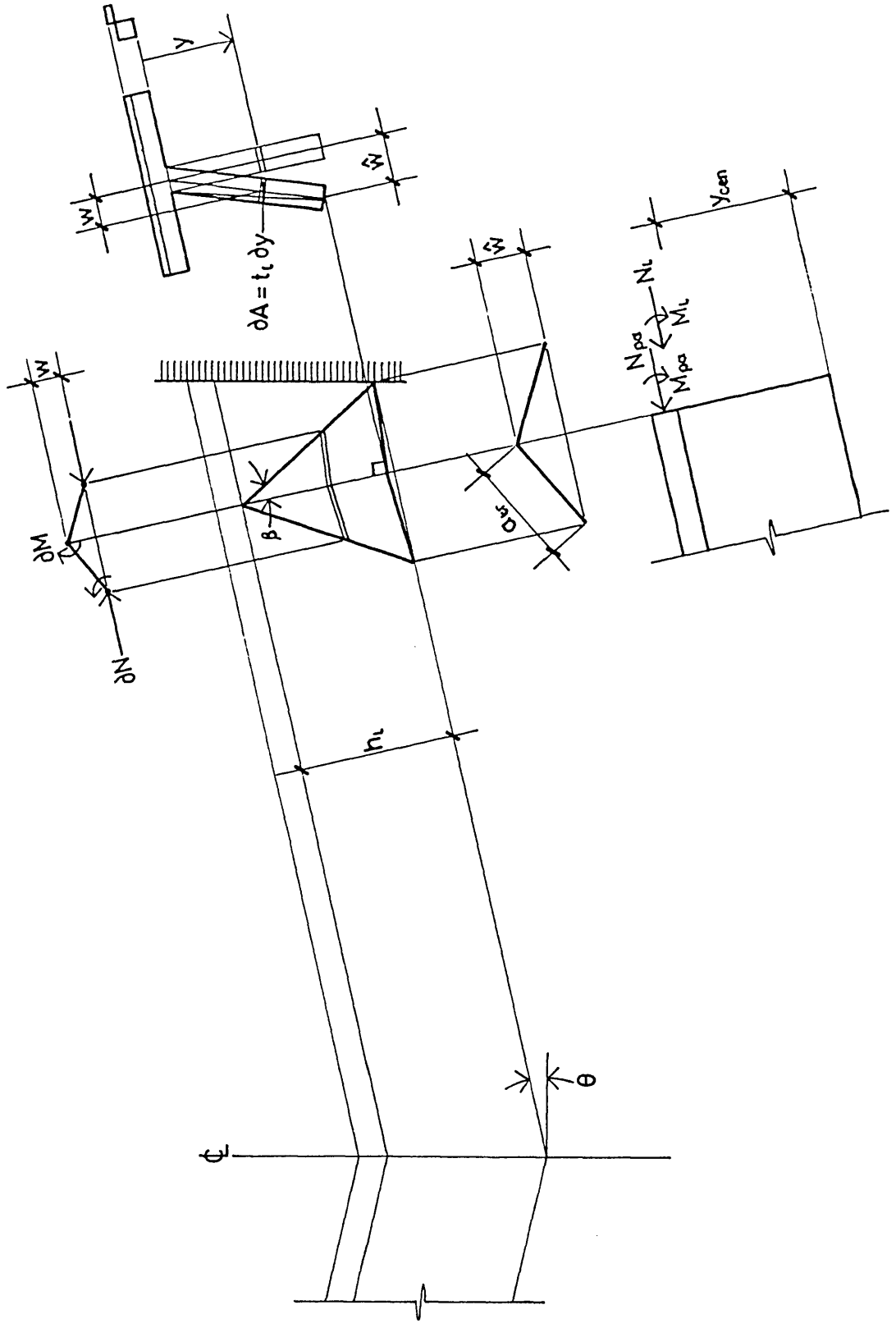


fig. 4.6
Stiffener tripping at support

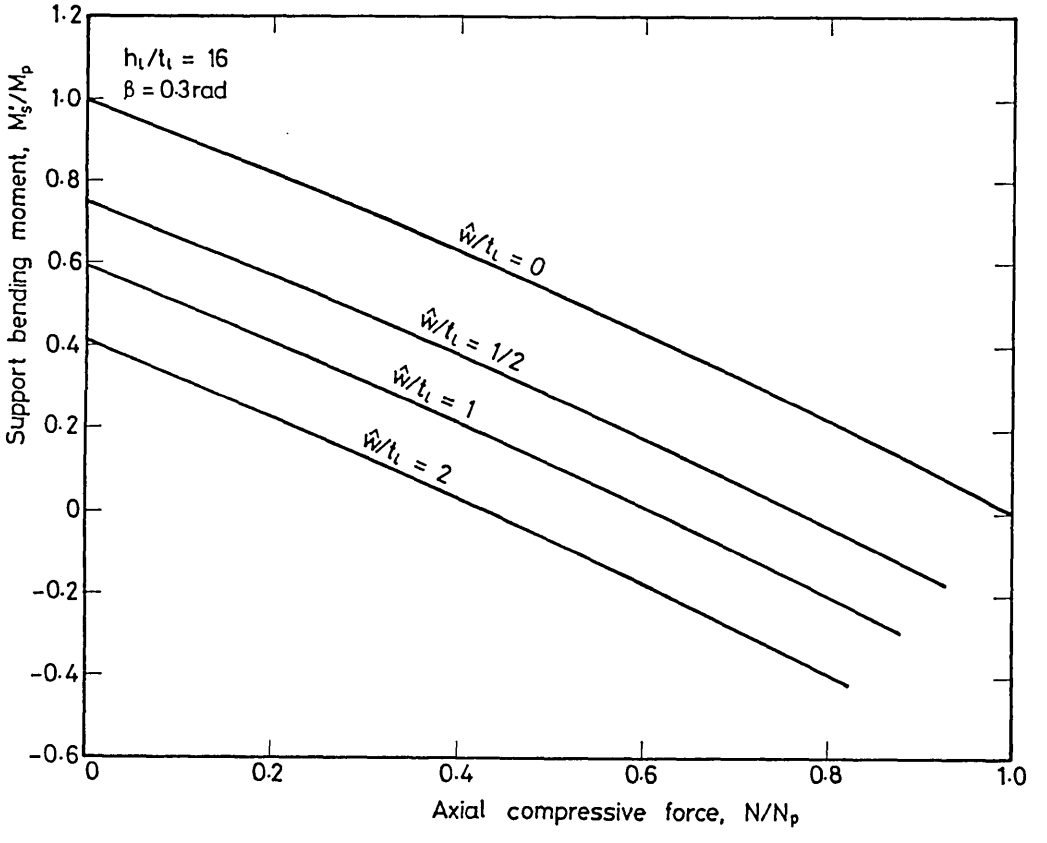


fig. 4·7
Tripped section plastic interaction curve
T-section geometry as for Test P2

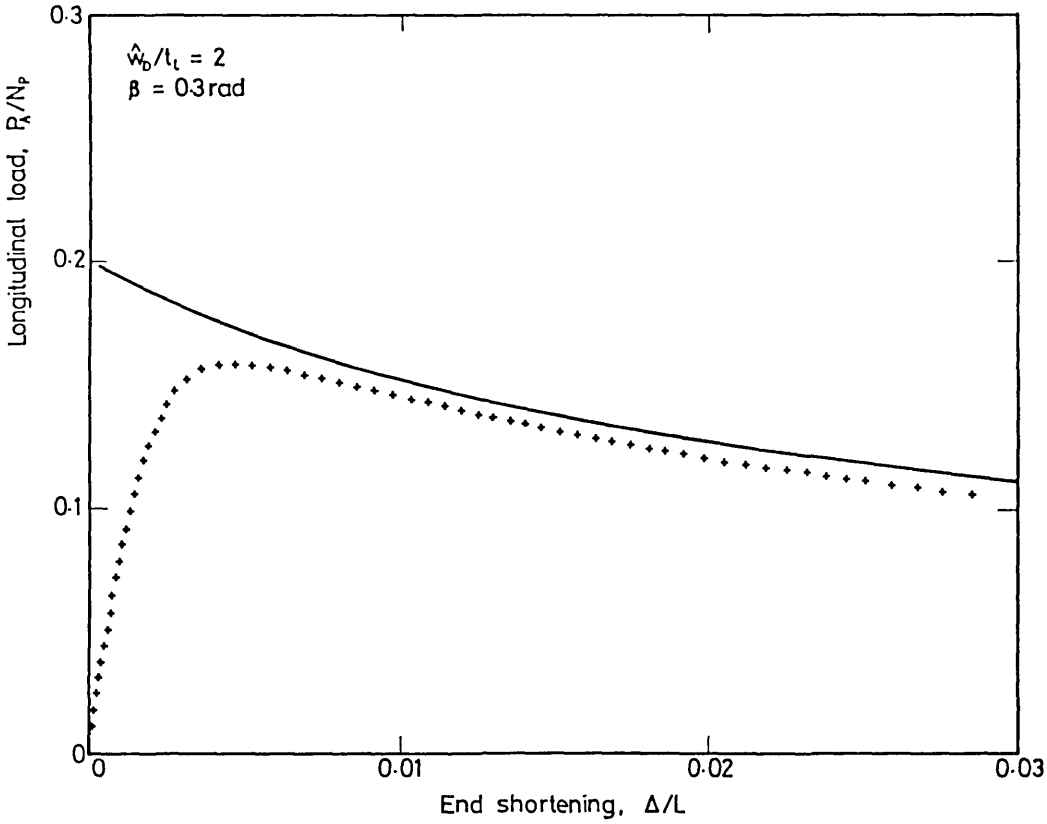


fig. 4·8 (a)
Longitudinal load versus end shortening incorporating support stiffener tripping

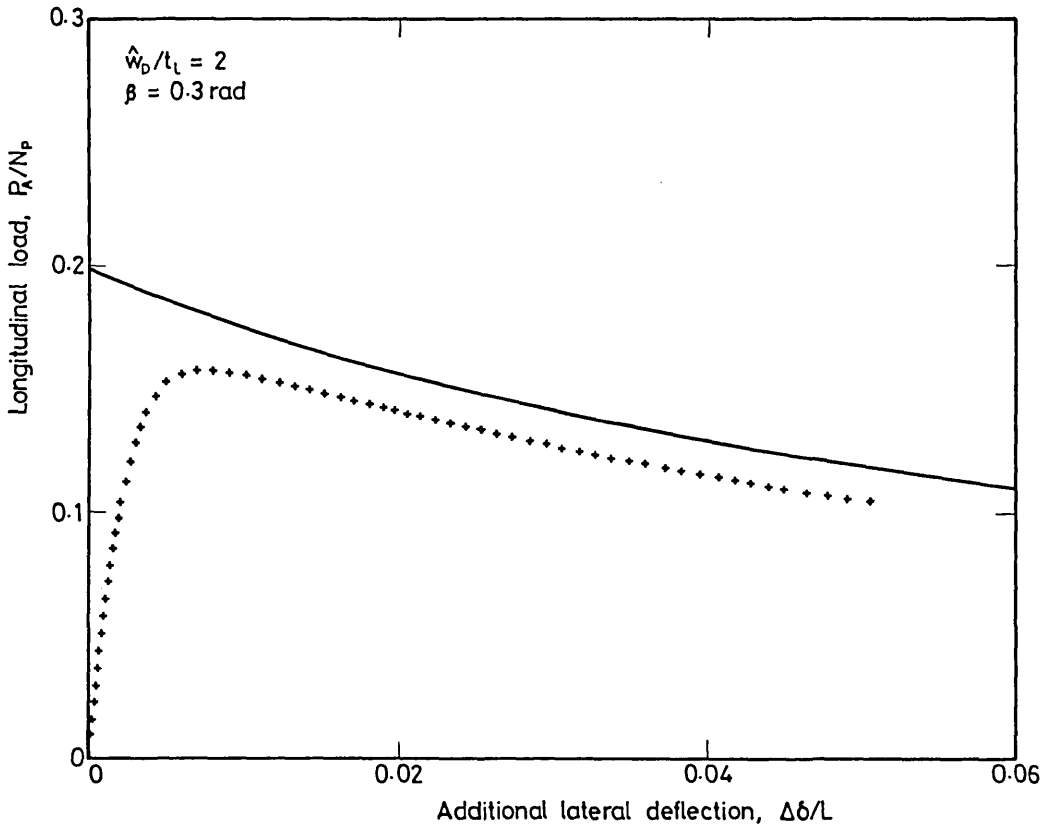


fig. 4·8 (b)
Longitudinal load versus lateral deflection incorporating support stiffener tripping

CHAPTER 5

DENTING OF STRINGER STIFFENED CYLINDERS

5.1 INTRODUCTION

The major concern of this dissertation is with stiffened shells of a type intended to be employed in compliant offshore structures. The two preceding chapters describe experimental and theoretical work on longitudinally stiffened plates which, being simpler structural units than cylinders, clarify many aspects of the denting process and its effect on subsequent longitudinal loading. The understanding gained from the study of plates is extended in this and the following chapter to suit orthogonally stiffened cylinders.

The present chapter begins with a description of the cylindrical models used in the experimental programme, and the set up for the lateral loading tests. The shape of the resulting dent determines how the mechanism analysis of Chapter 3 should be applied. The success of the new formulation is then assessed by undertaking a detailed comparison between experimental observations and theoretical predictions for many aspects of the denting process. The chapter concludes with a discussion of how a prototype stiffened cylinder might behave in practice, including the effects of member length and dynamic loading.

5.2 EXPERIMENTAL PROGRAMME

5.2.1 INTRODUCTION

Table 5.1 gives details of the cylinders dented in the test programme. In the model identification system the first digit is the number of bays and the letter represents the test series. Series A was made up of refurbished cylinders that had previously been tested in compression by Fahy [54] and Agelidis [1]. Series B models were new but of the same material and geometry as those in Agelidis' second, slender test series.

In contrast to the denting tests on unstiffened tubes undertaken by other researchers and discussed in Sections 2.7 to 2.9, it is clear that even the three bay models represent only part of an entire column, which has many bays.

The condition of the cylinders dictated two catagories of testing. Buckles were still present in Cylinders 1A1 and 3A1 after remodelling which limited the usefulness of any axial testing. They were therefore dented to failure in the unbuckled region, which furnished information on the strains that were achievable before rupture occurred. At this point the mechanism analysis becomes invalid, and in an actual structure flooding might occur leading to loss of buoyancy.

All other models made up the second group. These were unloaded prior to failure to give a range of dent depths within the limits suggested by the first tests. Unloading allowed a subsequent longitudinal compression test to determine the residual strength, as discussed in Chapter 6. Several of the cylinders in this group were also "second-hand". Realistic results in compression were expected for these models although some caution should be

exercised in interpreting the response of Cylinder 3A2 as the end bays were known to have imperfect welding between stringers and shell.

5.2.2 MODEL MANUFACTURE

One method that has been used to produce stiffened cylinders is to machine down a thick unstiffened tube at the required intervals to give a thinner shell with intermediate stiffening, as mentioned in Section 2.13.1. However this was not considered realistic for slender stringers located inside the cylinder, as found in offshore applications, and an alternative fabrication technique was employed.

Thin steel plate specifically designed to have mechanical properties representative of the thicker plate used in full scale construction was utilized. The stringers were attached to the shell by welding and during this process the model was jigged securely to keep the geometric distortions within the tolerance limits of the codes (Ref. [34] for example). However the residual stresses induced were unrealistically high and so the completed cylinders were heat treated.

A complete description of the fabrication process is given by Fahy [54] and only key points are mentioned here. Firstly a sheet of the thin plate was cut to a length equal to the circumference of the cylinder. Longitudinal stiffeners were cut from the same material and machined. They were sequentially attached to the plate with the aid of a spacing jig which ensured that each stringer was precisely positioned relative to the last. Only one side of the stiffener/plate junction was welded. A single pass fillet weld was produced using a tungsten-inert gas procedure with no filler wire, and results were of a consistently high standard. The weld size was comparable

to the fillet welds in a scaled full size member.

When all stringers were in place the plate was wrapped around a circular mandrel, using copper spacers between the stringers to protect them. A final T-butt weld along one of the stiffener/plate junctions closed the cylinder. Then an outer former was secured around the mandrel and in this tightly restrained state the model was stress relieved by heat treatment. Several tensile coupons were also included and the mechanical properties of the steel were later determined by testing these. In the treatment process the temperature was increased at a rate of 100 degrees per hour to 650 degrees Celcius, which was maintained for about an hour before the oven was allowed to cool.

Various repairs were carried out on Series A models. Cylinders 1A1, 1A2 and 3A1 had buckles at mid-length around about two-thirds of the circumference due to eccentric loading by Fahy [54]. With sparsely stiffened Cylinder 1A2 the buckles were successfully knocked out. This was not practicable for the other two cylinders and their deformed states were retained. Model 3A3 was modified by cutting off a uniform bulge near one end and straightening a shallow inward bow throughout the length. As with Cylinder 3A1, two slotted rings were fitted inside and welded from the outside to produce three bays. Excess weld metal was later removed to give a smooth surface. In contrast, three short cylinders were combined to make Cylinder 3A2. Each had buckles at one end which were cut off. When welded together two annular plates were sandwiched in between to form the ring frames and these were later spot welded to the stringers.

Although the methods of refurbishment were ad-hoc the high quality of the finished models gave confidence that they would yield useful results.

5.2.3 CHOICE OF GEOMETRY

The cross sectional geometries of all models were the same as for Fahy's and Agelidis' tests, which were chosen to typify present and possible future trends in orthogonally stiffened construction offshore. However the three bay models used for the first time in the current programme required ring frame dimensioning and this was done using the DnV Buckling Strength Analysis Notes [33] available at the time of design. The pertinent clause in this document is numbered 4.5.1 and stipulates a minimum ring frame cross sectional area, thus

$$A_r \geq Lt\left[\frac{\sigma}{E}\frac{R}{t}\sqrt{10^3/Z^2 + 60} - 1\right] . \qquad (5.1)$$

Here σ is the longitudinal stress acting and Z is the Batdorf length parameter, given by

$$Z = \sqrt{1-\nu^2}.L^2/Rt .$$

The notation is adjusted to suit that used herein.

The very sturdy rings in the models only just satisfy this requirement, presumably due to the presence of longitudinal stiffeners which allow both the applied longitudinal stress σ and the radius/thickness ratio to increase. When knife edge loading was applied to these models at mid-bay the ring frames exhibited negligible radial deflection and the stringers in the end bays did not deform. Thus the dent was confined to one bay, allowing these cylinders to be analysed in a manner similar to the single bay models.

The clause has been revised recently to read [34]

$$A_r \geq Lt(2/Z^2 + 0.06) \qquad (5.2)$$

which gives much smaller rings. It has been utilized in a new series of models recently commissioned. Only one of these has been tested and the rings deflected markedly during denting. However this work is outside the scope of the present dissertation.

The development of these formulae is not documented [156], but they are based on the desire to prevent general buckling involving in-plane deformations of the rings. Thus it is ensured that the general buckling stress is smaller than the stress causing buckling of the bays between rings [96], both stresses being determined from elastic criteria. The importance of plasticity in the relatively stocky models under consideration makes the concept conservative.

The rings were given a slenderness of

$$h_r/t_r = 8$$

to satisfy the local buckling requirements. There is also a limit on ring frame moment of inertia in the DnV Buckling Strength Analysis Notes. Because the shells were designed for compressive loading without external pressure, this clause is not critical if either Eqn. (5.1) or (5.2) is applied.

5.2.4 END CONDITIONS

Heavy steel rings were located on both ends of the models to provide full rotational and in-plane restraint. Not intended to be representative of actual structures, they gave a specifiable boundary condition which could be reproduced analytically. This parallels the decision to build the models using a procedure differing greatly from full scale construction, and then stress relieve them. When it is certain that the theoretical work accurately

describes the fundamental experimental behaviour, modifications may be incorporated to treat such aspects as residual stresses and ring frames of finite rigidity. An alternative end detail which provides perfectly pinned support is very difficult to achieve in practice [54].

Fahy [54] and Agelidis [1] used two different end ring details. In both the region near the stiffened shell was free of steel but filled instead with a mixture of sand and araldite epoxy resin. By this means, of course, there was no gap which might have allowed movement. One detail incorporated two rings and the cylinder passed between and extended beyond them. These protrusions became the loading surfaces and so were lapped flat and parallel. The other end connection method used a single grooved ring into which the cylinder ends butted. Thus longitudinal loading was applied to the end rings and these were lapped.

Both of these connections were unsuitable for the present test work as the sand-epoxy mix could not support the high membrane tensions generated during denting. Thus welded inner and outer rings were used (see Fig. 5.1) in a detail similar in principle to the stiffened plate end connection described in Section 3.2.3. Bolt holes were again drilled into the end rings to enable them to be connected to rigid end blocks.

After attaching the end rings Series A models were heat treated by the same process as when they were first fabricated. However the method of bracing varied. In this instance tension rods were passed through the bolt holes in the end rings and the nuts tightened. Each model was then placed in a box which was subsequently filled with firmly compacted sand. Re-heat treatment of the new Series B models after attaching the end rings was not considered necessary as the welding was on the outer side of the end ring. Thus stress build up within the clear span was assumed to have been minimal.

Before testing commenced the outer ends were made flat, parallel and smooth. The final thickness of the end rings on each model is listed in Table 5.2 as this dimension is required in Section 6.4.4.

5.2.5 MATERIAL PROPERTIES

Tensile tests were carried out on coupons cut from the material used for Agelidis' second series of models [1] and they exhibited very consistent mechanical properties. As the present Series B models were fabricated in the same programme the same results are used here.

Coupons were not available for the refurbished Series A steels. In the absence of other information the results of the original coupon tests were assumed to be still valid. This seemed reasonable as the cylinders were re-heat treated in the same way as when they were new.

For all tensile specimens the stress/strain plots exhibit a very extensive yield plateau and strain hardening effects are delayed. The important material characteristics are given in Table 5.1. Based on previous investigations [163] the compressive yield strength is considered to exceed the tensile yield strength, thus

$$\sigma_{YC} = \sigma_{YT} + 10 \ N/mm^2 \ .$$

5.3 DENTING TESTS

5.3.1 RIG ARRANGEMENT

Cylinders were dented lying horizontally with the arrangement drawn in Fig. 5.2. The end rings were bolted to massive end blocks with M8 bolts which were torqued for the same reasons as discussed in Section 3.3.1 regarding the stiffened plate tests. High strength socket head cap screws with 2.8m.kgf torque were closely spaced around the dent region where the membrane tension forces were large. Elsewhere Grade 8.8 bolts were used with only 2.2m.kgf torque to guard against thread stripping failure. Fig. 5.3, an end-on view of the denting rig, shows the bolting arrangement. Areas adjacent to the dent zone were in compression during lateral loading and so bolts were omitted.

Thick end blocks were chosen to minimize bending and shear deformation from the tensile forces in the dent. However compromise was necessary as the tension would also cause through-thickness stretching of the block and end ring pretensioned connection, of an amount proportional to the thickness. An optimum dimension was estimated but as this plate size was out of stock a somewhat greater thickness of 73mm was used.

Each end block rested on a bearing block which was free to run along a horizontal track parallel to the longitudinal axis of the cylinder. The bearing was also able to rotate about another horizontal axis perpendicular to this. Thus the cylinder ends could pull in and rotate but had to remain circular and at least approximately planar. This meant that the behaviour of the ends was dictated largely by the overall section response under lateral loading, with the end blocks moving as rigid bodies.

It was less preferable to leave the end rings free as they might have yielded under the high moment induced by the membrane tension and bent inwards substantially. Consequently they would not have provided a well defined boundary condition, nor would they have modelled the behaviour of actual ring frames. In a stiffened cylindrical column of many bays the ring frames may pull in toward the dent in a nonlinear manner but the deflection is also dependent on the stiffness of adjacent undamaged bays and the degree of restraint at the column ends. Some insight into such behaviour is furnished by the three bay models (Section 5.6.7.1) and these could be representative of actual columns where planar deformations may be enforced at the locations of stiff intermediate diaphragms.

It is of interest to compare the approach described with that of Onoufriou and Harding [110]. For their denting tests on ring stiffened cylinders the first of the sand and epoxy resin end rings discussed above was used. The rings rested on the steel loading platen with no additional support. Monitoring the end ring movement during lateral loading showed that little axial pull-in occurred. The shallow dent depth and low lateral stiffness precluded the development of large tensile forces, in contrast to the present tests where pull-in was a significant factor.

When positioned in the denting rig the end supports of the cylinders in the test programme discussed here were carried on a stiffened steel loading platen. To the lower side of the platen was attached a stocky plunger which slid smoothly but with very close fit through a greased guiding block. A screw jack below the plunger was turned via a chain and gear mechanism wound by hand. (Part of the wheel is seen in Fig. 5.3.) Thus slow, controlled deformation rates were achieved. The jack, although not included in Fig. 5.3, was located between two 45mm thick plates and supported by the lower one. The upper one

supported the guiding block.

Four threaded columns passed through these plates and upwards beyond them to form a square frame around the model. Column pairs were connected at the top by rectangular hollow section beams 120mm x 120mm x 10mm thick. Attached were bearing seats which carried the pinned ends of a central cross beam of the same cross section, and a knife edge indenter was screwed into the bottom face of this last beam. One of the pinned ends consisted of removable dowels which enabled the cross beam and indenter, when unloaded, to be swung out of the dent. Thus a bank of transducers could be positioned to monitor the dent shape in detail.

The knife edge geometry of the stiffened plate tests was retained here; namely an included angle of sixty degrees with a 3mm tip radius. This continued the trend of several tube denting experimental programmes as discussed in Section 2.7.1.1. However the adopted radius might be somewhat larger than expected; Smith et al [146] used 10mm radius for full scale tests and the present cylinders were about 1/20th. scale [42]. The larger radius guarded against premature tearing of the model beneath the wedge. Several other researchers have also used larger radii and their work has shown that this has little effect on the behaviour of the dent.

The choice of a rigid wedge having simple geometry again aids in developing a basic understanding of the behaviour. It is possible for additional complexities, including the shape of the contact zone on the impacting vessel and its deformation characteristics, to be incorporated at a later stage of the investigation.

The indenter was positioned at mid-span and oriented perpendicular to the cylinder's longitudinal axis. This was intended to simulate the broadside collision of the deck-edge of a boat into the leg of a tension leg platform

or semi-submersible. A dent shape produced in this way has similarity to the inward bowing associated with general buckling of a longitudinally stiffened bay and also encourages local shell buckling in the panels adjacent to the dent. Thus for both buckling modes, this form of large "initial imperfection" may have a marked influence on the cylinder strength in compression, which is another reason for its study.

As implied in Fig. 5.9 the knife edge initially rested directly above a stringer in all tests, and denting was symmetrical about this central stringer. The early loading behaviour obviously would have been weaker if the indenter had been located between stringers. However it is apparent from the lateral load response curves discussed later in the chapter (Section 5.6.3) that once the dent has reached reasonable depths its position with respect to the stringers has only small, localized effects on capacity.

Lateral load was applied by slowly raising the loading platen, and was measured with a ten tonne capacity load cell located above the jack. The denting arrangement is photographed in Fig. 5.4.

5.3.2 INSTRUMENTATION

5.3.2.1 STRAIN GAUGES

Strain gauges were aligned axially on several stringer beams in the region to be dented and just beyond it. Consistent with the stiffened plate tests these were placed both on the outer skin and on the longitudinal stiffener. The gauges were positioned at the quarter-point of the centre bay for the primary task of measuring the development of membrane tension. In Cyl 3A1, the same stringer beams were also gauged at the mid-point of one of

the outer bays in order to ascertain the degree of stress redistribution that occurred. Table 5.3 shows which stringer beams were monitored, using a numbering system defined in Fig. 5.9. These numbers are employed throughout the cylinder work.

In all cylinders except 1A1 and 3A1, which from the outset had buckles on the side opposite the dent, additional gauges were located well away from the dent to show the overall section response. These gauges were also oriented longitudinally; however they were placed on the outer skin only. Positions are given in Table 5.3 in terms of the parameter ϕ, which is the angle subtended at the location from the dent centre-line, as illustrated in Fig. 5.9. Usually they were placed at the bottom of the cylinder (diametrically opposite the dent) and at mid-depth.

Fig. 5.7 is a typical strain gauge diagram. It is apparent from the Figure that maximum use is made of symmetry in order to keep the gauge numbers within reasonable limits. It is understood that theoretical axes of symmetry are not necessarily followed exactly in experimental work. However in these models it was very likely that the chosen arrangement of gauges would provide a good indication of the complete cylinder behaviour.

Post-yield gauges designed to withstand very large elongations were chosen in the first tests, as for the stiffened plates, as it was desirable to follow the strain growth for as long as possible. As the central stringer beams most deformed by denting were not gauged in Cylinders 3A2 and 3A3 it was considered adequate to use cheaper polyester strain gauges which still work well beyond yield. Those used had relatively large bases as the smaller sizes were temporarily unavailable. This unavailability necessitated choosing small foil gauges for Cylinders 1B1 and 1B2 as larger bases would not have fitted onto the small stringers. All gauges used were

linear.

5.3.2.2 TRANSDUCERS

A Sangama linear transducer with 50mm travel, mounted vertically, monitored the central dent depth by measuring the relative movement of the loading platen and cross beam. Two longitudinally aligned transducers, clamped to horizontal bars connected to the vertical columns of the rig, measured the pull-in of each end block in line with the stringer beam at the dent centre. As the platen rose during denting the position of the transducer tip moved down relative to the cylinder. A small adjustment to the experimental readings was necessary to account for this, using the end block rotation indicated by the strain gauge readings.

A small linear transducer with 10mm travel was placed diametrically opposite the knife edge to measure any vertical deflection of the underside of the models. Where appropriate the ring frames were similarly monitored. The resulting readings were so small that deformation of the overall section might be considered negligible.

Several times during each test the cylinder was unloaded and the indenter swung out of the dent. This enabled a transducer frame, photographed in Fig. 5.5, to be located via three rounded legs into holes in the end blocks. One of these holes was slotted to accommodate axial pull-in. The longitudinal spacings of the legs and the transducers were adjustable to suit different cylinder lengths. There were three horizontal lines of small transducers, threaded together top and bottom with thin screw rods which were tightened using nuts to enhance rigidity. Each line monitored the vertical deformation of stringers in the region

$$0 \leq \phi \leq 3\pi/20$$

in one quadrant of the dent zone, and the panels between them.

Initially the height was set so that transducers near the dent centre-line were almost fully contracted but those further around the circumference did not touch the cylinder. As denting progressed the lines of transducers could be individually lowered (remaining horizontal) by loosening a screw at each end, after noting the prior transducer readings with the aid of the reset function incorporated into the data logging program. Thus the central dent growth could still be monitored and any deformation of the outer stringers was also able to be measured. The amount of lowering was controlled by slip gauges fitted behind the vertical supports of each line of transducers.

In the first three bay model to be tested, Cylinder 3A1, an arc was positioned over one ring frame, supported from the bottom platen. The outer edge of the steel strip forming the arc is visible in Fig. 5.3. Slotted holes in the strip allowed small transducers to be mounted radially on it at angular spacings of $\pi/20$. In this test transducers were set in line with stringers 4, 5, 6 and 10 only, to measure deformations outside the dent zone. As the arc did not interfere with either the wedge or the transducer bank it was left in position throughout the denting process.

Unfortunately the models were too small to enable transducers to be set up inside to measure stringer twist.

5.3.3 FINAL PREPARATION

Prior to testing the end blocks were bolted onto the end rings, one at a time, and then torqued up. The strain gauges were monitored during this process to see if any

nonuniform straining occurred due to incorrect torquing or the presence of local distortions. In all tests negligible overall prestress was induced in the cylinder, in contrast to the stiffened plate tests where the supports were not free to move.

Next the roller bearing caps were screwed onto the bases of the end blocks, and the assembly was lowered into the denting frame and located on the bearing seats. The vertical transducer bank was then postioned in the dent zone to obtain a set of zero readings. When removed, the cross beam was swung down and pinned in place and the loading platen height was adjusted so that a piece of paper just slid freely in the clearance between knife edge and cylinder. To ensure the indenter was at mid-span it was aligned with a circumferential line previously scribed onto the cylinder. After all the instrumentation was wired into the data logger the test was ready to proceed.

5.3.4 TESTING PROCEDURE

Lateral deflection was incremented in small steps as described in Section 3.3.4. When the knife edge approached additional stringers the step size was reduced to accurately follow the changing response. In between stringers the model was unloaded periodically to allow the dent shape to be measured with the transducer bank and viewed by eye. Final unloading took place either when fracture was observed (Cylinders 1A1 and 3A1) or when the dent reached a predetermined depth.

It was unfortunate, but largely unavoidable, that a small proportion of strain gauges failed under the extreme entensions induced by denting. This was in spite of the precautions taken in their attachment, as described in Section 3.3.2.1.

5.4 DENT GEOMETRY

In their knife edge denting tests on tubes, Thomas et al [161] and Smith et al [146,149] found an approximately exponential deflection decay moving away from the indenter along the longitudinal centre-line. However it is apparent from the discussion in Section 2.7.1.1 that this infers a dent length much greater than the actual cylinder length in the present test series, which precludes its applicability here.

Mechanism analyses of knife edge denting are often based on bilinear profiles [161,26,61]; that is:

$$\omega/\delta_0 = 1 - 2x/L_D \ . \qquad (5.3)$$

The notation is shown in Fig. 5.8. If all cross sections x are assumed to have straight dent lines then the geometry is defined by

$$\zeta/R = \sin\phi$$

$$\omega/R = 1 - \cos\phi \ .$$

Hence

$$\frac{\omega}{\delta_0} = \frac{1 - \cos\phi}{1 - \cos\eta}$$

$$= \frac{1 - \sqrt{1 - (\zeta/R)^2}}{1 - \sqrt{1 - (B/R)^2}}$$

$$\approx (\zeta/B)^2 \qquad (5.4)$$

for $B/R \ll 1$.

Substituting Eqn. (5.4) into (5.3) gives

$$2x/L \approx 1 - (z/B)^2 \ .$$

This parabolic plan shape is illustrated in Fig. 5.8.

Conversely, if the dent shape is rectangular in plan, cross sections other than the central one at $x = 0$ are curved. Thus the longitudinal fibres deflect at various angles θ_j as shown in Fig. 5.9.

The denting pattern observed in the present testing programme with the aid of the vertical transducer bank is somewhere between these idealizations. All stringer/panel intersections within the damaged region deflect in two straight segments between plastic hinges at the centre and each end of bay length L, but in plan part of a diamond-like pattern is apparent in the outermost dented panel. This is drawn schematically in Fig. 5.10 and is clearly apparent in the top half of Fig. 5.6, a photograph of Cylinder 3A1 after denting. Hence cross sections have slightly less curvature than in a purely rectangular dent.

This curvature is modified by the stringer behaviour. For models where

$$h_t/t_t = 8$$

a distinct kink occurs in all damaged stringers (except that on the longitudinal centre-line) at each ring, aligning them vertically. To maintain this orientation throughout the length the associated panel must deflect in double curvature as drawn in Fig. 5.10. This may give the appearance of shallow troughing between stiffeners. Additional curvature occurs near the dent edge to suit the first undamaged stringer which does not twist. The centre-line stringer also tends to trip at each end of the span but its out-of-plane deformation is smaller. This relieves the gross distortion here but does not alter the inclination of the stiffener. The lower half of Fig. 6.21, a photograph taken inside Cylinder 3A2 after the axial

compression test, shows these kinks, which were present before crushing.

The response is a little different for other stringer geometries. Cylinder 3A1 has slender stringers of

$$h_t/t_t = 16$$

which are too flexible to resist twisting. Stringers other than the central one have an initial inclination to the direction of deflection which encourages them to fold over inward. Before rupture has occurred both stringers 1 and 2 are lying on the ridge formed by the knife edge and stringer 3 is very close to being the same. This is seen in the view inside the dented model in Fig. 5.6.

In contrast, the stringers in Cylinders 1B1 and 1B2 do not trip noticeably at the supports because of their stockiness;

$$h_t/t_t = 6 .$$

They twist more gradually throughout the half span but still lie very nearly vertically, as indicated by the distortion in the flexible panels. At the large dent depths near the end of the lateral loading tests this panel distortion develops more fully. Troughs form in the dented panels of Cylinder 1B2, but for Cylinder 1B1 the wave is antisymmetrical about the longitudinal centre-line, producing an outward bow in the panel on one side. This last phenomenon is perhaps initiated by slight lack of symmetry in geometry or loading.

In all tests the skin beyond the edge of the dent is pushed out on the cross section under the knife edge, which produces a localized bulge in the dent's plan shape. This partly compensates for the circumferential shortening resulting from pressing an arc into a flat dent. Elsewhere outside the dent the lateral loading produces negligible

radial deformation.

5.5 THEORETICAL ANALYSIS

5.5.1 INITIAL ELASTIC ANALYSIS

Before undertaking the main plastic mechanism analysis of the denting process the early elastic response is examined briefly. For single bay models consideration of the central point loading of a single T-section beam with encastre supports gives an estimate of the elastic stiffness.

With three bay cylinders the initial elastic response is computed by modelling stringer 0 as a three span continuous beam with encastre ends. The elastic bending moment diagram drawn in Fig. 5.11 is easily constructed using the method of moment distribution. In this diagram M^F represents the fixed end moment and d is the moment distribution factor for the outer span at an intermediate support, taking account of symmetry in the model. Thus

$$d = \frac{L}{L + \frac{1}{4}L_U}$$

$$M^F = P_0 L/8 .$$

The moment-area method, amongst other approaches, gives the central deflection:

$$\delta_0 = \frac{P_0 L^3}{64EI}\left[d - \frac{2}{3} + d.\frac{L_U}{2L}\right] . \qquad (5.5)$$

Two extreme cases are considered for checking purposes. First

$$\text{if} \quad L_U \to 0 , \quad \text{then} \quad d \to 1$$

and Eqn. (5.5) simplifies to

$$\delta_0 = \frac{P_0 L^3}{192EI} ,$$

the expected result for an encastre beam of single span. In the second case

$$\text{if} \quad L_U \to \infty , \quad \text{then} \quad d \to 0 \quad \text{but} \quad d.L_U/L \to 4 .$$

The equation now becomes

$$\delta_0 = \frac{P_0 L^3}{48EI} ,$$

as required for a pin ended beam.

5.5.2 T-SECTION BEAM PLASTIC ANALYSIS

5.5.2.1 INTRODUCTION

The realignment of damaged longitudinal stiffeners having reasonable stockiness, discussed above in Section 5.4, suggests analysis of a series of T-section beams acting independently under lateral deflection. Thus the development, in Section 3.4, of the plastic behaviour of such beams may be utilized again here. This analytical approach to cylinder denting is believed to differ from earlier analyses in two aspects. First, beam mechanism ideas are applied to the local damage process rather than the overall bending response to lateral loading, where it usually finds application. Second, the section under consideration has longitudinal stiffeners whereas previous denting mechanisms have assumed unstiffened tubes.

5.5.2.2 STRINGER BEAM RESPONSE

Two general methods of quantifying the support pull-in are considered in Section 3.4.3. In the first approach, attributable to Jones [77], it is assumed that the axial displacement of the supports is proportional to the square of the lateral deflection. This is adapted to the present cylinder work in two different ways.

First, in what shall be referred to as version (ii) of Jones' formulation, it is generalized to define the pull-in of all stringer beams in terms of the central dent depth, thus:

$$\Delta_j/L = 2(1-\gamma_*)(\delta_0/L)^2 \ . \qquad (5.6)$$

Hence undented stringers experience axial compression, given by

$$n = n_I - \frac{E.\Delta_j}{\sigma_Y L}$$

$$= n_I - \frac{2E.(1-\gamma_*)(\delta_0/L)^2}{\sigma_Y} \qquad (5.7)$$

for $\delta_j/L \leq 0$.

Here

$$\frac{\delta_j}{L} = \frac{R(\delta_0/R - 1 + \cos\phi)}{L}$$

$$\phi = j\alpha$$

from the geometry of Fig. 5.9. It will be seen in Section 5.6.1 that this parabolic increase in force with dent depth is borne out by the test results, and enables the support axial stiffness parameter γ_* to be accurately estimated for each stiffener. Here n_I is the initial

pretension existing before denting begins, and is zero for all the present cylinder tests. In a prototype cylindrical member in service, n_I would represent the working loads.

Description of the axial stretching mode for

$$\delta_j/L > 0$$

is dependent on the conditions existing at the change-over point where

$$\delta_j/L = 0 ,$$

that is

$$\delta_0/R = 1 - \cos\phi . \qquad (5.8)$$

In particular, the new "initial" pretension is

$$n_I' = n_I - \frac{2E_*}{\sigma_Y}(1-\gamma_*)\left[\frac{R}{L}\right]^2(1 - \cos\phi)^2$$

from (5.7) and (5.8). Also the effective pull-in in this later regime is

$$\left[\frac{\Delta_j}{L}\right]' = \frac{\Delta_j}{L} - \left[\frac{\Delta_j}{L}\right]_c$$

$$= 2(1-\gamma_*)\left[\left[\frac{\delta_j}{L}\right]^2 + \frac{2R}{L}(1 - \cos\phi)\frac{\delta_j}{L}\right] \qquad (5.9)$$

where the pull-in existing at the change-over point is denoted by $\left[\frac{\Delta_j}{L}\right]_c$.

Whereas the axial compression mode of behaviour is governed by adjacent stringer beams, pull-in during denting is also very dependent on the deflections of the actual stringer. Thus there is no theoretical reason to

expect equality of the γ_* values in each mode. However results using a single γ_* value throughout for a particular stringer compare very well with the tests (refer Section 5.6.1) and so constant γ_* is assumed.

Incorporating the effective axial displacement of the supports into the method of analysis described in Section 3.4.3 leads to this modified governing differential equation:

$$C_{1*}\frac{dn}{d\delta_j/L} + (z_s + z_c)/L - \gamma_*\delta_j/L - C_8 = 0 \qquad (5.10)$$

where

$$C_8 = (1-\gamma_*)(1 - \cos\phi)R/L \ .$$

Other parameters are as defined in Section 3.4.3.

Sequential results of integration are given in Table 5.5 in a more condensed form than that used in Chapter 3. The first applicable integration constant C_i is computed using the "initial" condition

$$n = n_I' \quad \text{at} \quad \delta_j/L = 0$$

and subsequent ones are found by equating responses at

$$n = \pm C_0 \ .$$

One of the equations in Table 5.5 will be referred to specifically later in the chapter. It is therefore labelled Eqn. (5.11).

Using cylinder radius rather than ring frame spacing as the nondimensionalizing length parameter in Eqn. (5.10) gives

$$C_{1R*}\frac{dn}{d\delta_j/R} + (z_s + z_c)/R - \gamma_*\delta_j/R - C_{8R} = 0 \qquad (5.12)$$

where

$$C_{1R*} = (L/R)^2 C_{1*}$$

$$C_{8R} = (1-\gamma_*)(1 - \cos\phi) \ .$$

The various values of the term $(z_s + z_c)/R$ are listed in Table 5.4. These equations are simple variations of those quoted in Chapter 3, but are fully explicated because they will be found to be useful in the cylinder work. The solutions in Table 5.5 may be readily adapted to suit this new notation.

A second, and more literal, interpretation of Jones' criterion for support displacement is to assume the effective support pull-in during lateral loading of stringer j is related to its own lateral deflection. Unfortunately this eliminates the connection between the axial compression and denting response modes. How the seemingly independent pull-in of separate stringer beams concurs with the planar pull-in of rigid end blocks is discussed below and also at the conclusion of Section 5.6.7.1.

The relevant equation is

$$\Delta_j'/L = 2(1-\gamma_*)(\delta_j/L)^2 \qquad (5.13)$$

for $\delta_j/L > 0$.

Comparison of Eqns. (5.9) and (5.13) shows that less pull-in is stipulated in this latter version. Being equivalent to one of the approaches adopted in Chapter 3, the resulting differential equation (3.11) given there, and its solution, are applicable here. Because of its previous application this variation shall be labelled version (i)

for future reference.

It is apparent that the only difference between the two versions of Jones' pull-in approach is the addition of the parameter C_8. Its value is zero for $j = 0$ and very small for other stringers as both the relative dent depth and $1-\gamma_*$ are small for typical cylinders. Hence both approaches will give very similar results. In this chapter emphasis will be placed on version (ii) due to its elegance in combining compression and denting phases of behaviour.

An alternative and totally different treatment of support pull-in, following Hodge [72], assumes linear spring behaviour; that is

$$\Delta_j'/L = (1/\gamma - 1)\frac{\sigma_Y}{E}(n_j - n_{Ij}') \qquad (5.14)$$

for $\delta_j/L > 0$.

Results are again given in Chapter 3. By using the alternative length parameter the governing equation becomes

$$C_{1R}\frac{dn}{d\delta_j/R} + (z_s + z_c)/R - \delta_j/R = 0 \qquad (5.15)$$

where

$$C_{1R} = (L/R)^2 C_1 .$$

Again, these formulae describe the axial stretching mode only.

The lateral load response of dented stringer beam j is found from its moment equilibrium relationship. Thus, following Eqn. (3.7),

$$p_{Dj} = \tfrac{1}{2}(m_s + m_c + n\delta_j A/Z_p) \qquad (5.16)$$

for $\delta_j/L > 0$.

Stiffener tripping at the support hinges is discussed in Section 3.5.7 and is concluded to have negligible consequence for this loading configuration. Other distortions, including double curvature in the outer skin and gradual stiffener twist, are also assumed to cause no reduction in the load carrying capacity, which seems logical as tension is predominant.

The hinge moments in the presence of axial force are calculated from the formulae in Section 3.4.2.1, which are derived for T-shaped sections and ignore the panel curvature. Such curvature has the effect of reducing the width and increasing the effective thickness of the panel, at the expense of the stiffener height. Two consequences are that the value of C_0 marking the abrupt slope change in the interaction curve (Fig. 3.4) is increased, along with f which causes the bending moment value at this point to decrease. However the effects are small for the geometries under consideration. The curvature is diminished further during denting (especially at the central hinge) by the dual occurrences of overall arc flattening and panel distortion caused by the vertical alignment of stringers, as shown in Fig. 5.10. Thus the undertaking of a rigorous derivation of the interaction capacity, with its considerable extra complexity, does not seem to be justifiable.

When the membrane tension force reaches yield at

$$n = 1 ,$$

Eqn. (5.16) simplifies to

$$p_{Dj} = \delta_j A/2Z_p$$

or

$$P_{Dj}/N_p = 4\delta_j/L \ . \qquad (5.17)$$

5.5.2.3 TOTAL RESPONSE OF CYLINDER

Summing the individual responses of the dented stringer beams gives a total lateral load of

$$p_D = \sum_j^{s_D} p_{Dj} \qquad (5.18)$$

$$= p_{D0} + 2(p_{D1} + p_{D2} + \ldots)$$

over all stringers j where $\delta_j/L > 0$.

All stringer beams are considered to be orientated with a principal axis parallel to the direction of overall loading. This is largely achieved by stiffener twist and its accompanying panel distortion, described in Section 5.4. The beams are also assumed to deflect parallel to this principal axis, which must be at least approximately correct if not too many stringers are dented.

As is commonly done in mechanism analyses, the behaviour before plastic collapse is neglected as unimportant. Each stringer beam is assumed to carry zero load until the knife edge reaches its stiffener/panel intersection, at which time the plastic collapse load is attained instantly. Hence the contributions of longitudinal elastic bending and compression in the undented region, and hoop effects due to load dispersion, are ignored. These effects and others, including bending along the longitudinal dent edge and strain hardening, mean that the predicted damage load is likely to be an underestimation of the true response.

5.5.2.4 OVERALL SECTION BEHAVIOUR

Membrane tension in the dented stringer beams causes the end blocks to pull inwards. Because of the rigidity of the blocks and their method of support, they remain largely planar and move only as dictated by the cylinder response. Elementary combined load theory may therefore be applied to single bay models to determine the distribution of stresses throughout the remaining undamaged section, reflected by this movement. Such stresses equilibrate the axial force and bending moment applied to each end block by the dented stringers beams. The behaviour of the three bay models, being more complex, is not included here but is noted in Section 5.6.7.1.

Discussion of the various ways of determining the properties of the effective section comprising the undamaged material is postponed until Chapter 6, where it finds greater relevance. For convenience only, the principal results are transcribed here:

$$A_e/A = 1 - \eta/\pi \qquad (6.2)$$

$$I_e/A_e R^2 = \tfrac{1}{2} - \tfrac{1}{4}\sin 2\eta/(\pi-\eta) - (\bar{y}/R)^2 \ . \qquad (6.3)$$

A_e and I_e are, respectively, the cross sectional area and second moment of area of the effective section. The distance from the cylinder centre to the centroidal axis, considered positive when the latter is on the side opposite the dent, is denoted by $\bar{y}$, and given by

$$\bar{y}/R = \sin\eta/(\pi-\eta) \ . \qquad (6.4)$$

The elastic stress distribution around the effective section is

$$\sigma = \sum_j^{S_D} (N_j - N_{I\,j})/A_e - M_{\bar{y}}(\bar{y} + R\cos\phi)/I_e \ .$$

Here contributions to the applied membrane force are given by all dented stringer beams. However it is realized that these contributions may sometimes be compressive when δ_j/R is low. Consistent with earlier analyses deflections are assumed to be small and so the component of membrane force perpendicular to the end block is considered to approximate the total membrane force.

The bending moment about the effective centroid may be approximated by

$$M_{\bar{y}} \approx \sum_j^{S_D} (N_j - N_{Ij})(\bar{y} + R)$$

where it is assumed that the lever arm is nearly constant. This is valid if the dent is reasonably shallow.

Nondimensionalization leads to

$$\frac{\sigma}{\sigma_Y} = \frac{\epsilon}{\epsilon_Y} = \frac{\sum_j^{S_D} (n_j - n_{Ij})}{s} \left[1 + \frac{(\bar{y}/R + 1)(\bar{y}/R + \cos\phi)}{I_e/A_e R^2}\right] \cdot \frac{A}{A_e} \quad . \quad (5.19)$$

Eqn. (5.19) remains valid until first compressive yield occurs in the fibres adjacent to the dent. If, for simplicity, the dented stringer beams are included in the effective section, the equation reduces to

$$\sigma/\sigma_Y = \epsilon/\epsilon_Y \approx (1/s).\sum_j^{S_D} (n_j - n_{Ij})(1 + 2\cos\phi) \quad (5.20)$$

as now $\eta = 0$.

The resulting total longitudinal movement of both end blocks is given by

$$\frac{\Delta}{L} = \frac{\sigma_Y}{E} \cdot \frac{\sigma}{\sigma_Y} \quad . \quad (5.21)$$

The stress distribution described by Eqn. (5.20) and its corresponding pull-in are plotted in Fig. 5.39(a). It is seen that the neutral axis lies at

$$\cos\phi = -\tfrac{1}{2} .$$

Eqns. (5.21) and either (5.19) or (5.20) may be combined to predict the longitudinal pull-in at stringer beam 0; thus

$$\frac{\Delta_0}{L} = \frac{\sigma_Y}{E}.\frac{\sum_j^{s_0}(n_j - n_{Ij})}{s}\left[1 + \frac{(\bar{y}/R + 1)^2}{I_e/a_e R^2}\right].\frac{a}{a_e} \qquad (5.22)$$

$$\approx (\sigma_Y/E)(3/s).\sum_j^{s_0}(n_j - n_{Ij}) . \qquad (5.23)$$

The latter equation is reminiscent of Hodge's treatment of support pull-in (see Eqn. (5.14)), with the axial displacement linearly related to the membrane force. Summation over all dented stringer beams is a natural extension of his approach, as the membrane tension in these other stringers will obviously aid pull-in at the location of stringer 0. How the equations compare with the actual pull-in during the tests is investigated in Section 5.6.7.1.

5.5.3 ALTERNATIVE INCREMENTAL PLASTIC ANALYSIS

For comparative purposes an incremental mechanism analysis is also developed. Little importance is attached to this alternative formulation; in fact it is only applied once, to aid discussion of the lateral load versus dent depth response for Cylinder 1A2. In the development the cylinder skin is divided into a series of infinitesimal rectangular beam strips and the stringers are also treated as rectangles. Elements are assumed to

begin carrying lateral load when the dent depth reaches them.

The employment of differential notation gives

$$\partial p_D = \tfrac{1}{2}(\partial m_s + \partial m_c + \partial n.\delta.\partial A/\partial Z_p) \qquad (5.24)$$

following Eqn. (5.16). Meanings for many of the symbols are as given in Section 4.4.2, except that we are now considering a strip of panel rather than stiffener. For example:

$$\partial A/\partial Z_p = 4/t$$

after Eqn. (4.13). Also

$$\partial p_D = \partial P_D/\partial P_p$$

where

$$\partial P_p = 8\partial M_p/L \ .$$

In Eqn. (5.24), δ denotes the vertical deflection of element ∂A. Eqn. (4.10) implies

$$\partial m_s = \partial m_c - 1 - (\partial n)^2$$

and so

$$(z_s + z_c)/L = \partial n/C_2'$$

with

$$C_2' = L/t \ .$$

As expected, this shows that the T-section analysis derived in Section 3.4.3 and extended earlier in this chapter may be simplified to suit a rectangular cross section. Thus if Jones' version (ii) support pull-in

approach is adopted, for example, the form of Eqn. (5.11) in Table 5.5 applies now. When the integration constant C_i is evaluated this equation becomes

$$\partial n = C_2' \left[\gamma_* \frac{\delta}{L} + \left[\frac{\partial n_1'}{C_2'} + \gamma_* C_{1*} C_2' + C_8 \right] \exp(-1/(C_{1*} C_2')\delta/L - (\gamma_* C_{1*} C_2' + C_8)) \right]$$

incorporating the present notation.

Summing the contributions of all the elements making up the dented panels, each being given by Eqn. (5.24), and also the rectangular stringers, leads to the lateral load capacity of the cylinder for a particular dent depth.

5.6 THEORETICAL CORRELATION

Experimental results are now compared with the theoretical predictions. These are provided by the analysis based on individual stringer beams, derived in Section 5.5.2.

5.6.1 AXIAL FORCE DEVELOPMENT

5.6.1.1 CYLINDERS 1B1 AND 1B2

Fig. 5.12 shows the membrane tension build up in stringer 0 on the dent centre-line of Cylinders 1B1 and 1B2, for various values of support axial stiffness. Fig. 5.12(a) uses Jones' method (both variations of this method give identical results for $j = 0$). In the upper part of the curves excellent correlation with experiment is found using

$$\gamma_* = 0.62,\ 0.4$$

for Cylinders 1B1 and 1B2 respectively. Lower γ_* is

expected for cylinders with fewer stringers as there is less axial rigidity to resist pull-in. However the experimental points lie below the theoretical curves early in the response, for the same reasons as discussed in Section 3.5.2 with reference to the stiffened plate tests.

When computing the present experimental points from the linearized strain blocks the initial section shape, including panel curvature, is considered. This gives a better approximation of the true shape of the section at quarter-span, where the gauges are located, than would the assumption of straight panels.

The same experimental points are also shown in Fig. 5.12(b) along with results of Hodge's pull-in formulation. Comparison of Figs. 5.12(a) and (b) shows that the approaches of Jones and Hodge diverge when $n > C_0$. This is understood with the aid of the linear approximations to the upper part of the curves developed in Section 3.5.10.1. The approximate solutions for differential equations (5.12) and (5.15) are respectively

Jones (ii) :

$$n = C_{3R}(\gamma_* \delta_j / R + C_{4R} - \gamma_* C_{1R*} C_{3R} - C_{8R}) \qquad (5.25)$$

Hodge :

$$n = C_{3R}(\delta_j / R + C_{4R} - C_{1R} C_{3R}) \ .$$

Their gradients differ by factor γ_*.

The experimental responses also depart from Hodge's predictions for $n > C_0$, as they do in Chapter 3. In that chapter (Section 3.5.10) this is postulated to be attributable to elastic unload at the hinge locations as the neutral axis moves through the T-section. Curves using a simple flow rule based on total deformations, derived there as another extreme to account for elastic

effects, are also plotted in Fig. 5.12(b) for comparison with the traditional incremental deformation approach. Again, the two predictions diverge when $n > C_0$. For both Cylinders 1B1 and 1B2 the experimental response lies between the associated curves using actual and incremental flow rules.

It is, of course, possible to derive yet another response curve combining Jones' pull-in criterion with the total deformation flow rule. However with the Jones formulation the slope of the upper portion of the membrane response is not fixed, but may be adjusted to suit the experimental points by varying γ_* . Thus the additional slope variation that comes from using the alternative flow rule is, in a sense, superfluous.

The two unload/reload curves also included in Fig. 5.12(b) (and in many of the diagrams to follow) will be discussed in Section 5.6.4.

It is apparent from the theoretical curves in both Figs. 5.12(a) and (b) that the growth of membrane tension in twenty and forty stiffener models follow very similar form, the main difference being in the value of C_0 which locates the abrupt slope change.

Membrane tension development in stringer 1 of Cyl 1B1 is depicted in Fig. 5.13 using the major version (ii) of Jones' pull-in approach with

$$\gamma_* = 0.7 .$$

This value is chosen to give the best average fit to the test data both before and after the indenter reaches the stringer. Theory and experiment compare very well except in the region where $C_0 < n < 1$. Although not illustrated here, it may be envisaged from the location of the test points in this region that they fall in between the two predictions of the total and incremental flow rules using

Hodge's formulation, as they did for stringer 0 above.

Fig. 5.14 shows the membrane behaviour of stringers subtending angle

$$\phi = 2\pi/20$$

with the dent centre-line, in both Cylinders 1B1 and 1B2. Because the support axial stiffness parameter is put at

$$\gamma_* = 1 = \gamma ,$$

both Jones' and Hodge's formulations give identical predictions as there is no pull-in. Correlation with the experimental points is again very good for lower membrane tension values. The upper test response of Cylinder 1B2 is unfortunately curtailed as a result of strain gauge failure. However for Cylinder 1B1 the complete experimental response, including the region where $n > C_0$, is very closely followed by a curve developed from the actual deformations flow rule. This is also drawn in the Figure.

It appears from the foregoing evolution that elastic unloading at the hinges may have greater effect in stringer beams with higher ϕ. This is possibly due to reduced longitudinal restraint from adjacent stringers which have fully yielded; that is $n = 1$. Although the differences between flow rules base on actual and incremental deformations, and Jones' and Hodge's support pull-in formulations, are of theoretical interest, it will be shown that they have little effect on the most important issue in this chapter, namely the relationship between lateral load and dent depth. For simplicity, therefore, attention will be largely restricted to version (ii) of Jones' pull-in approach with the traditional incremental flow rule in the remaining experimental correlations. This will be seen to give adequate representations of the test data.

The parabolic increase of axial compression in undented longitudinal stiffeners at

$$\phi = 3\pi/20$$

for Cylinder 1B1, and

$$\phi = 4\pi/20$$

for both 1B1 and 1B2, is shown in Fig. 5.15. Circumferential load dispersion causes the experimental compression growth to level out earlier than expected.

All the preceding test results for Cylinder 1B1 are combined in Fig. 5.16 along with their Jones version (ii) predictions to give a general picture of the development of membrane forces in and beyond the dent zone.

5.6.1.2 CYLINDERS 1A1 AND 1A2

Fig. 5.17 shows the growth of membrane tension in the centre stringer

$$\phi = 0$$

of Cylinders 1A1 and 1A2. These fit Jones' theoretical curves using the incremental flow rule reasonably well, for γ_* values of 0.6 and 0.45 respectively. The shape of these curves is quite distinct from those for Cylinders 1B1 and 1B2 due to the different geometry.

Why the experimental points lie above the predicted lines at high membrane tensions is not entirely certain but may be attributable to panel curvature at the support plastic hinge. As discussed earlier, in Section 5.5.2.2, this increases the value of C_0 where the slope of the response changes markedly. In essence, the phenomenon should be more important for twenty stringer cylinders than forty because the broader panels curve further

downward. However the test results do not show the effect to be more pronounced for Cylinder 1A2 than 1A1. Also it is only slightly apparent for stringer O of Cylinder 1B2, (Fig. 5.12(a)), because the slope change is much less distinct for this geometry and occurs close to membrane yield. Another effect of curvature is to reduce the value of

$$C_2 = Lb/A$$

which is a strong indicator of the rate of increase of membrane tension in the range $-C_0 < n < C_0$. Little sign of this is seen.

The theoretical prediction for Cylinder 1A1 is also drawn in Figs. 5.23(a) and (b), alongside the responses resulting from doubling or halving the bay length whilst other dimensions remain unchanged. Thus the effect of length on the membrane response, plotted against dent depth nondimensionalized with respect to both cylinder radius and bay length, is illustrated. An interesting effect may be noticed.

The linearity of the upper part of each curve is obvious. In fact the approximate equation (5.25) for this portion of the response is added to Fig. 5.23(a) and the comparison is excellent. This linear equation readily shows why the response for $n > C_0$ is virtually independent of bay length in this Figure. Fig. 5.23(b) includes the counterpart of equation (5.25) in terms of bay length rather than radius which demonstrates that the slope is now proportional to bay length.

In contrast, the early responses for all lengths are similar when plotted as functions of δ_0/L rather than δ_0/R as the former parameter governs the axial extension.

Membrane tension development in stringer 1 of Cyl 1A1 is given in Fig. 5.18. The flow rule based on incremental

deformations is used and, for comparison, both versions of Jones' pull-in criterion are included. As expected, the resultant plots are very similar in shape. The small separation of the curves is due to differing rates of change in membrane tension just after denting reaches the stringer. This may be verified by referring to the differential equation (5.12). For δ_1/L only slightly greater than zero the slopes of the theoretical responses are highly dependent on the value of C_8 because $(z_s + z_c)/L$ is very small here. (It will be remembered that C_8 is the only parameter that causes versions (i) and (ii) of Jones' formulation to differ.)

Test points prior to strain gauge failure are also plotted in Fig. 5.18 and they match the theory well when $n < C_0$.

The experimental membrane responses of stringers in both Cylinders 1A1 and 1A2 at

$$\phi = 2\pi/20$$

are presented in Fig. 5.19 and they correlate very well throughout with version (ii) of Jones' theory with

$$\gamma_* = 0.97 .$$

A complete description of the build up of membrane forces in the dent zone of Cylinder 1A1 as the dent depth increases is given in Fig. 5.20. Several points deserve noting. Firstly, it is apparent that in all three of the responses already described, for stringer beams at

$$\phi = 0,\ \pi/20,\ 2\pi/20,$$

the test points lie above the theoretical line when $n > C_0$. However the experimental slopes here are very similar to those predicted, but tend to be slightly flatter. This indicates that some elastic unload may be

occurring as found in Cylinders 1B.

The other stringer beam in Fig. 5.20, at

$$\phi = 3\pi/20 ,$$

exhibits an almost perfect parabolic growth in compressive force right up until it yields uniformly at $n = -1$. This is due to the significant size of the longitudinal stiffeners, which ratifies their treatment as independent beams. As stringer 4 is not dented, it only experiences axial compression caused by the pull-in of the end blocks. This may be contrasted with Cylinders 1B1 and 1B2 (see Fig. 5.15) where some of the bending and tension in the dented region is transferred elastically to the adjacent undented fibres. Hence these latter models respond more like shells to the lateral loading because their stringers are so small. They also have a larger ratio L/R and this encourages load spreading.

Fig. 5.20 indicates, lastly, that the value of γ_* giving best fit of the theoretical curves to the test data increases with ϕ; that is, less pull-in occurs away from the dent centre, which is understandable. The variation of γ_* with ϕ for all denting tests is plotted in Fig. 5.24 and shows an exponential form roughly described by

$$1-\gamma_* = \tfrac{1}{2}\exp(-7.5\phi) .$$

The above equation does not find application in the work that follows because the lateral loading response is largely independent of variations in γ_*. It is included only because it gives a concise representation of a series of experimental observations.

5.6.1.3 CYLINDER 3A1

The membrane responses of stringers 0 to 4 in the dented region of Cylinder 3A1 are collected together in Fig. 5.21. The axial compression phase again closely follows a parabolic path up to uniform compressive yield; stringer 4 correlates especially well. However the experimental tension development bears less resemblance to theory. This is because the slender stringers,

$$h_t/t_t = 16 ,$$

cannot sustain finite deflections without twisting and eventually folding over. Uncontrolled twisting is signalled by the rapid growth, in opposing senses, of the readings of the strain gauges located on each side of the stiffener, and occurs soon after the indenter reaches each stringer. The average of the two measurements is used to compute the test points in Fig. 5.21 but these have little real worth as twisting invalidates the assumption of a T-shaped section. The main effect appears to be a delay in developing the second, stretching mode of behaviour when the stringer is reached.

No sign of this phenomenon is apparent in the second stiffened plate test although it has the same slender stringers. This is because the curvature of the cylinder gives the stiffeners incentive to twist inwards. Also the cylindrical model is deformed to a significantly higher dent inclination δ_0/L.

5.6.1.4 CYLINDERS 3A2 AND 3A3

Only stringer beams 2 and 3 are strain gauged in Cylinders 3A2 and 3A3 and the axial forces derived from their readings are plotted in Fig. 5.22. Results for the two models follow similar parabolic responses, which is to be expected as their central bays have identical geometries. When the indenter reaches stringer 2 in

Cylinder 3A3 the experimental points respond to stretching a little slower than predicted. Again this is attributable to stiffener twist, as demonstrated by the gauge readings. However the dramatic folding inwards found in Cylinder 3A1 does not occur here; in fact the stringer bows outwards slightly, motivated by the edge of the dent. This may be visualized with the aid of Fig. 5.10.

5.6.2 STRAIN DEVELOPMENT

Typical strain variations during denting are illustrated in Fig. 5.25, using stringer 1 of Cylinder 1B1 for the example. Quarter-span strains on the outer skin and the stiffener tip are plotted, the latter being computed by averaging the readings on each side of the stringer and extrapolating to the tip, assuming linearity. Several phases are apparent in the response. Initially the strains are small, but slight sagging bending moment is indicated by the stiffener test points lying above those for the panel, and Fig. 5.13 shows the existence of a small axial compression force.

Large hogging moments begin to develop at quarter-span when the indenter reaches stringer 1. This effect is noted in Section 3.5.2 and is due to a hogging shape being induced by knife edge loading. The hogging moment diminishes to zero when uniform tensile yield is attained; of course the stiffener tip strain reading may still be negative at this time as long as a strain change of $2\epsilon_y$ has occurred. Eventually, however, both panel and stiffener strain readings become tensile.

5.6.3 LATERAL LOAD RESPONSE

5.6.3.1 CYLINDER 1A1

Fig. 5.26 shows the lateral load versus dent depth response of Cylinder 1A1. In the theoretical curve, for simplicity, a constant value of

$$\gamma_* = 1 = \gamma$$

is chosen for all stringers. This is based on the conclusion in Section 3.5.4 that for axially stiff supports the damage load behaviour is insensitive to the actual values of γ_*. The discrete jumps in load capacity occurring when the dent reaches each additional pair of stringers (one on each side of the dent centre-line) are a result of assuming rigid-plasticity. The increments might be smaller than the present value of

$$P_D L/8M_p = 2$$

if γ_* was set at less than unity because the presence of significant compressive axial force would reduce the hinge moments.

The test points lie remarkably close to the theoretical response, but smooth out these steps. This is because, in practice, the stringer beams carry some load before the indenter reaches the stiffener/panel intersection.

Also drawn in Fig. 5.26 is a piecewise linear response resulting from the assumption that uniform membrane yield exists in all damaged stringers throughout the denting process. Although this is impossible in reality, the response is very similar to the true theoretical curve when the support axial stiffness is high, as found in Section 3.5.4 for stiffened plates. The

suite of lines is defined by combining equations (5.17) and (5.18) to give

$$\frac{P_D L}{N_p R} = 4.\sum_j^{S_D}(\delta_j/R) \ , \qquad (5.26)$$

summing over all stringers j where $\delta_j/R > 0$.

This describes all cylinders having the same number of longitudinal stiffeners with a single curve.

The present test results are combined in Figs. 5.31(a) and (b) for forty and twenty stringer cylinders respectively and all points lie above but fairly close to the linear approximation. Certainly the least successful correlation is shown by Cylinders 1B1 and 1B2 which have significantly higher strength than predicted. As discussed before this is due to their very small longitudinal stiffeners, which for Cylinder 1B2 contribute only

$$A_L/A = 0.07 \ .$$

Thus the importance of one dimensional "stringer beam" analysis is reduced and shell action comes into play.

It might be inferred from the scales on the axes of Figs. 5.31(a) and (b) that the lateral load which produces a specified damage is smaller for more sparsely stiffened cylinders. This is an illusion caused by dividing the load by the stringer beam cross sectional area as part of its nondimensionalization. In fact the lateral load response, and hence energy absorption, of cylinders differing only in the number of stringers (within reasonable bounds) are similar as the relatively small area of the stiffeners means that the area of the total stringer beam is roughly inversely proportional to the number of stringers.

It is useful to estimate the level of axial stiffness required at the supports to ensure that Eqn. (5.26) remains a valid approximation. Lateral load responses for several values of γ are given in Fig. 5.32 for the geometry of Cylinder 1A1. To enable the results to be related to a physical quantity Hodge's pull-in formulation is used. It is seen that all of the curves lie near the linear approximation even though the weakest response, defined by

$$\gamma = 0.05 ,$$

represents a support stiffness for each stringer beam of only five per cent of its axial stiffness.

The simple linear assumption is even more successful here than it is for stiffened plates (see Section 3.5.5) due to the periodic introduction of new stringers which strengthen the response. Additionally, the actual cylinder response lies above the theoretical prediction, for the reasons cited in Section 5.5.2.3, which further increases the range of conservatism of Eqn. (5.26).

5.6.3.2 CYLINDER 1A2

The damage loading response of Cylinder 1A2 is presented in Fig. 5.27. The rigorous plastic mechanism solution using

$$\gamma_* = 1 = \gamma$$

follows the test very closely at first. This indicates that the central stringer does in fact act as a T-section which adds substance to the individual stringer beam approach.

For comparison, the alternative incremental analysis formulated in Section 5.5.3 is also applied and the results drawn in Fig. 5.27. The curve falls well below the

test points near the central stiffener as it does not model the T-section response. However it produces a much closer estimate of the experimental behaviour at higher dent depths because it enables circumferential load spread to be continual rather than at discrete stiffener locations only. Despite this, the incremental procedure is not pursued any further as its extra finesse is not warranted when the simple piecewise linear approach gives adequate accuracy.

5.6.3.3 CYLINDERS 3A2 AND 3A3

The behaviour of Cylinders 3A2 and 3A3 under lateral loading is shown in Fig. 5.28. The predictions of plastic theory using

$$\gamma_* = 1 = \gamma$$

compare well with the experimental points for both models. These two experimental responses are also very similar in themselves, which is to be expected.

5.6.3.4 CYLINDER 3A1

The only model for which the plastic theory does not correlate favourably with test results is Cylinder 3A1; it is omitted from Fig. 5.31 (a). However Fig. 5.29 shows both the predicted and experimental responses for this cylinder. Although they compare very closely in the early stages, the test points eventually fall below the theoretical curve as stiffener twist takes its toll. Hence the application of the stringer beam theory of this chapter should be restricted to relatively stocky stiffener geometries when the deflections are large.

5.6.3.5 CYLINDERS 1B1 AND 1B2

Fig. 5.30 shows the experimental lateral loading behaviour of Cylinders 1B1 and 1B2. The vertical axis is nondimensionalized in a manner differing from all the above diagrams: by dividing the load by the tensile yield stress and an area parameter, Rt, chosen so as to be the same for both models. As asserted earlier the two responses are similar, even though Cylinder 1B2 contains only half as many stringers as 1B1. Small aberrations are visible in the responses when each additional pair of stringers is reached.

5.6.4 INTERMEDIATE UNLOADING AND RELOADING

In all tests the models are gradually unloaded at various times so that the indenter may be removed to survey the dent shape. Subsequent reloading returns the model to its original loading path. Many of these unload/reload curves are included in the diagrams discussed above, but not all as the clarity of the main response would then be impaired. They give information regarding the permanent set and residual stresses present after denting, which is important for the later axial compression tests.

The relaxation in membrane tension during rebound predicted by Eqn. (3.24) and able to be rewritten as

$$\frac{dn_j}{d\delta_j/R} = 4\gamma_* \frac{E}{\sigma_Y}\left[\frac{R}{L}\right]^2 \frac{\delta_j}{R}$$

compares well with the experimental observations. Aspects brought out by the theory are clearly apparent in the tests. One example is the linearity of the responses. Secondly, shorter cylinders have steeper unloading gradients, as seen by comparing the same stringer beams in

Cylinders 1A and 1B at similar dent depths. This is a result of nondimensionalizing the lateral deflection with respect to radius rather than length. A steeper slope also occurs when the stringer beam has higher lateral deflection as a larger component of the rebound deflection is parallel to the axis of the dented stringer. This is exhibited in Figs. 5.13 and 5.14.

All dented stringer beams rebound about the same amount so that at mid-span the dent cross section remains flat. When the lateral load is completely removed a new equilibrium situation exists with nett compression acting in the highly deflected stringer beams around the dent centre-line but some tension remaining in those near the edge of the dent. Again this is shown in Figs. 5.13 and 5.14.

As discussed in Section 3.5.8 the lateral load fall off during unloading is a little more complex as bending is produced as well as axial deflection. Elastic double curvature develops initially in each half span as there is no rotation at the support and central hinge positions. Soon, however, yielding occurs at these locations with the opposite sign of that caused by denting. The increased flexibility introduces nonlinearity into the lateral load versus dent depth unloading curve and also some hysteresis in the unload/reload loop. The nonlinearity is especially apparent in Cylinders 1B1 and 1B2 at low dent depth. The unloading response tends to duplicate the early loading path which is very flexible for these long, lightly stiffened models.

5.6.5 FAILURE

Two of the models, Cylinders 1A1 and 3A1, are loaded to failure. With the latter a tear starts at the tip of the central dented stringer at mid-span which grows upward through the section until panel rupture occurs. There is also a tear through part of the height of stringer 0 in Cylinder 1A1 at mid-span, accompanied by necking. However failure is caused here by rupture of the panel at one support. Final rupture occurs at

$$\delta_0/L = 0.229$$

for Cylinder 1A1, and

$$\delta_0/L = 0.344$$

for Cylinder 3A1. These values are somewhat higher than for the stiffened plate test.

5.6.6 ENERGY ABSORPTION

The piecewise linear approximation of the build up of lateral load with dent depth defined by Eqn. (5.26) enables the energy absorbed by denting to be easily estimated. For stringer beam j

$$W_j = 0$$

for $\delta_j/L < 0$

$$W_j = \tfrac{1}{2} P_{Dj} \delta_j$$

for $\delta_j/L > 0$

and so

$$W/M_p L = 2.\sum_j^{S_D} (\delta_j/L)^2 \qquad (5.27)$$

where W is the total energy absorbed by the cylinder.

Several publications give guidance on the energy that might be released in a ship collision with an offshore structure, as discussed in Section 2.2.2. DnV [31] cites a value of 14MJ as an extreme case and although it may be dissipated in several different processes it is conservatively assumed here that all work is involved in denting.

The dimensions of the quantity "work" mean that when it is scaled to suit small models rather than full sized structures, it has a dependence on the cube of the length scaling factor, if the yield stress is taken to be approximately constant. This cubic relationship is plotted on the left of Fig. 5.33 for the 14MJ collision energy. Different curves are produced for the geometries of Cylinders 1B1 and 1B2 because of the method of nondimensionalization used. Adjacent are graphs of Eqn. (5.27) for the same shells. It is readily apparent from the two diagrams what dent depth is produced by the assumed impact energy in any size of prototype cylinder scaled up from the models. This is exemplified by the lines drawn between the diagrams for scale factor

$$k = 1/10 .$$

The main purpose of Fig. 5.33 is to indicate how susceptible the stringer stiffened cylinders under consideration are (or, rather, are not) to denting in an offshore environment. It may be concluded that because the models in the present test series are small scale, only a small dent would occur in a full sized structure. An even smaller dent would be caused, of course, by a collision magnitude of greater probability than the 14MJ case.

Ref. [16] gives an exemplary collision energy versus indentation graph for a semi-submersible column. Before skin tearing occurs it follows a parabolic form similar to the right hand diagram of Fig. 5.33, although it is much less resistant to deformation. This is presumably due to the absence of stringers.

5.6.7 LONGITUDINAL PULL-IN

5.6.7.1 PULL-IN DURING LOADING

Throughout this chapter numerous references have been made to Jones' and Hodge's approaches for quantifying axial displacements at the supports. These theories are now put into context by comparing them with the measured movement of the end blocks during lateral loading.

As stated previously, the pull-in of each end block at the level of the centroid of stringer beam 0 is monitored by a horizontal transducer, aligned longitudinally. The sum of the two readings is plotted in relation to dent depth in Fig. 5.34 and 5.35, for Cylinders 3A3 and 3A1 respectively. Also drawn is the parabolic prediction of Jones' criterion, both versions of it giving identical results here. It is seen that the correlation between theory and experiment is excellent when using a γ_* value that roughly corresponds to the values describing the stringer beams within the dent zone, but away from its centre. Such values are indicated by the membrane force response curves. Other theoretical curves included in Fig. 5.34 indicate the sensitivity of the pull-in to the actual value of the support axial stiffness parameter, γ_*.

The application of the parameter γ_* to the end block movement of three bay models deserves some comment. Jones' criterion, specified in this chapter by Eqns.

(5.6) or (5.13), strictly defines the pull-in at the ends of the dented beam. Axial strains in the outer bays cause the longitudinal movement of the end blocks to differ from that at the internal ring frames. If unit extensions were constant in all three bays the end block pull-in would be greater by factor L_t/L. However it is shown later that at the level of stringer beam 0 the longitudinal displacement is probably smaller at the end blocks than at the ring frame. Thus the value of γ_* fitting the experimentally observed end block pull-in will be a little larger than the values inferred from the membrane tension response in the dent zone. This is seen in the results.

The correlation between test data and theory is not so obviously successful for the other models. Little useful information may be gleaned from Cylinder 3A2 as problems with the winding mechanism occurred early in the denting test and during its repair the longitudinal transducers were jarred.

The measured longitudinal pull-in for Cylinders 1B1 and 1B2 at stringer 0 is presented in Fig. 5.36. Although of the magnitude predicted using Jones' theory and a mean support stiffness value of

$$\gamma_* = 0.91 ,$$

the distribution of the test points is more linear than parabolic. This is because at higher dent depths the stringers near the centre-line have yielded uniformly, giving constant axial force. However the horizontal component of the force, which aids pull-in, decreases as the dent depth grows. Thus the rate of increase of support pull-in with dent depth may be expected to level out eventually. Discussion of the other theoretical lines drawn in Fig. 5.36 is set aside until later in this Section.

The same tendency to linearity occurs in the test data of Cylinders 1A1 and 1A2, although it is not illustrated here. Also, like Cylinders 1B1 and 1B2, the two experimental responses are very similar to each other and are of the magnitude predicted by Jones' approach.

The linear effect is not seen in the three bay models because the stringer beams abutting the end blocks are not dented and so the axial forces in them remain longitudinally aligned. Also stress redistribution means that the attainment of uniform membrane yield in the outer bays is delayed relative to its occurrence in the central, dented bay.

A phenomenon common to both single and triple bay models, however, is that the initial pull-in at the level of stringer beam 0 is negative. This is completely consistent with the earlier finding that the axial force in this stringer beam is compressive at the beginning of denting; see Figs. 5.12 and 5.17, for example.

Other indicators of end block movement are the longitudinally arranged strain gauges situated outside the dent region. Such gauges are present in Cylinders 1B1 and 1B2 on the outer skin only at

$$\phi = \pi/2, \pi$$

and on both the outer skin and the stiffener at

$$\phi = 4\pi/20 .$$

The gauge readings are presented in Figs. 5.38(a) and (b). For $\phi = 4\pi/20$ the nondimensionalized axial force N/N_p is actually plotted but this is equivalent, of course, to the mean axial strain ratio ϵ/ϵ_y in the elastic range. In these Figures the strains are related to the total membrane tension force acting over all the dented stringer beams, to facilitate comparison with the theoretical

predictions.

In these predictions, if the complete circular section is used to approximate the effective section, the strains within this section are linear functions of the sum of the dented stringer beam forces, as indicated by Eqn. (5.20). However if the more accurate Eqn. (5.19) is applied, the effective section properties are dependent on the dent depth and so the variation with dent depth of the membrane tension in the dented stringer beams must also be computed. This is done using

$$\gamma_* = 1 = \gamma$$

for simplicity, so that both Jones' and Hodge's pull-in criteria produce the same results.

The results are included in Figs. 5.38(a) and (b). The various horizontal offsets apparent in the diagrams occur when all dented stringer beams have attained uniform membrane yield, and are maintained until the dent depth reaches the next stringer. The overall section strains continue to grow at these times because the effective section on which the constant membrane tension force acts is diminishing. In between the discrete steps the curves are nearly linear, aping the approximate response mentioned above. A typical example of the approximation is given in Fig. 5.38(a).

Comparison of both Figures shows that the two cylinders behave very similarly. This is due to plotting, as the ordinate, the sum of the membrane tension forces divided by the number of stringers in the model. Thus the condition that more stringers are dented in Cylinder 1B1 than 1B2 at a particular dent depth is counteracted.

The correlation between theory and experiment is reasonably good, especially at $\phi = \pi/2$. The test points even mirror the horizontal offsets. Observing the strains

at $\phi = \pi/2$ and $\phi = \pi$ to have similar magnitude but opposite sign verifies an earlier statement (in Section 5.5.2.4) that the neutral axis lies at

$$\cos\phi \approx -\tfrac{1}{2} .$$

The slightly larger experimental tensile strains than predicted at $\phi = \pi$ may be attributable to the small sagging moment induced throughout the model by the applied lateral load. This would also contribute to the theoretical compressive strains being a significant underestimation of the observations at $\phi = 4\pi/20$, but there is another more important factor here. The end blocks are not, in fact, fully rigid and they bend inwards a little near the dented region under the action of the dented stringer forces.

The pull-in at stringer 0 of Cylinders 1B1 and 1B2, measured by transducers, is replotted in Fig. 5.37, this time in relation to the total membrane tension force in the dented stringer beams. The predictions of Eqns. (5.22) and (5.23), which are based on compatibility of the end blocks, are also included. The close similarity of the theoretical responses for the two models is apparent, the only difference being in the positions of the horizontal offsets. However the linear approximation, with its parallels in Hodge's approach to support pull-in, is a poor representation of the test data. The more rigorous Eqn. (5.22) is a better approximation because it considers the increasing axial flexibility of the end supports as the effective section resisting pull-in diminishes. However this curve still underestimates the test response because it does not allow for end block flexural and shear deformations which are superimposed onto the planar pull-in.

The theory of Eqn. (5.22) may be presented in another way as a function of dent depth rather than stringer beam membrane tension because they are mutually dependent

quantities. This is done in Fig. 5.36 for Cylinders 1B1 and 1B2, giving the two wavy lines hitherto not described. These new lines compare well with the test data at reasonably small dent depths, but increasingly underestimate the observed pull-in later in the response. The experimental points also smooth out the theoretical steps. This is partly because the actual development of membrane yield is more gradual than that predicted using the incremental deformation flow rule with

$$\gamma_* = 1 = \gamma ,$$

and so smears out the effects of individual stringer beam responses.

With other models Eqn. (5.22) underestimates the experimental pull-in of the end blocks even more. Their greater cross sectional areas allow larger membrane tension forces to be generated and so there is increased bending of the end blocks.

It may be possible to construe from Eqn. (5.22) that when lateral loading of a new stringer beam commences, the substantial pull-in caused by the sudden increase in membrane tension may induce unloading in stringers already dented. This hypothetical unloading of the span is quite distinct from the unloading at the plastic hinge locations discussed in Section 5.6.1.1, and does not occur. It is apparent from Figs. 5.34 to 5.36 that the dent depth, and hence axial extension, increase steadily along with the support pull-in and so the governing equations derived in Section 5.5.2.2 remain valid. Once uniform tensile yield has occurred the contribution of the hinges to the axial extension becomes indeterminate and so the membrane extension in the intermediate bars cannot be predicted either. However no reduction of membrane tension is expected, nor is it indicated by the strain gauges.

Cylinders 3A2 and 3A3 are the only other models with strain gauges at

$$\phi = \pi/2, \pi$$

and they are located in the central bay. It is of interest to compare their readings with those in Cylinders 1B1 and 1B2. The tensile strains at $\phi = \pi$ are a little smaller than expected. At $\phi = \pi/2$ the strains are much smaller still, in magnitude, and are also tensile, in contrast to Cylinders 1B. The stringer beam at $\phi = 3\pi/20$ which is also strain gauged, has compressive strains much larger than predicted by Eqn. (5.19).

An explanation for this is as follows. The stresses in stringer beams in the outer bays tend to be similar to their corresponding values in the dented bay, although some redistribution is likely. This is borne out by the results of Cylinder 3A1 where stringers 0 to 4 are strain gauged in an outer bay as well as the central one. For each dented stringer beam the associated axial force in the undamaged bay follows the form of that in the central bay as loading progresses, although the magnitudes are somewhat lower in both tension and compression as peaks in the distribution are smoothed out.

This implies that the form of the end block movement will be roughly as described by the single bay analysis, Eqn. (5.21), but that the internal ring frame lines must curve as illustrated in Fig. 5.39(b) to accommodate the tensile strains in the top stringers. Such nonlinearity produces extra compressive forces in the undented region adjacent to the dent in the central bay and simultaneously reduces the compression in the same region in the outer bays. For equilibrium between the two bays the stress distribution further down the section in the middle bay must become tensile sooner than predicted by the linear analysis. Both the larger compressive strains and the wider spread of tensile strains are apparent in the gauge

results.

It may be concluded that although Hodge's method of defining support pull-in has a sound general physical basis, in the experimental configuration under scrutiny in the present chapter it does not describe the observations well, even when the effects of all dented stringer beams are considered together. In contrast Jones' approach, although without clear physical roots [72], gives good correlation with the experimental pull-in of the end blocks, especially for the three bay models. It also predicts the observed parabolic growth of compressive forces in undented stringer beams near the dent zone.

Another point is worthy of note. If a very small value of γ_* is entered into Jones' formulation, in an attempt to quantify the effect of axially flexible supports, the large resulting pull-in implies the rapid development of compressive yield in undented stringers. This would not occur in practice. Flexible supports would pull in nonlinearly as they would not be able to resist large compressive forces. Thus the use of the same γ_* value in both the compressive and tensile modes of response becomes inappropriate, and a better approach is to assume that the axial force in each stringer beam is zero until the dent depth reaches it. This is done in computing the response curves in Fig. 5.32.

It remains to discuss why the values of γ and γ_* giving best fit to the experimental membrane tension responses of dented stringer beams may vary significantly. The end block pull-in is nearly constant throughout the dent region as the distance from the neutral axis varies very little. However yet another factor comes into effect: the through-thickness stiffness of the bolted connection between the blocks and the cylinder end rings.

In Section 3.5.2 it is determined that most of the support pull-in in the stiffened plate tests is

attributable to the bolted connection because the rig in which the models are held is very rigid. The compressive strains induced through the thickness of the connection during pretensioning decrease under the action of membrane tension. Another contributing factor is bending of the end plates between the bolts and the specimen, as discussed in Section 3.3.1. These effects are not small as the observed support axial stiffnesses in the two plate tests are reasonably low, namely

$$\gamma = 1/2,\ 1/3\ .$$

The effects would be expected to be less important in the cylinder tests, even though the end connections have very similar dimensions, because the latter are curved. In contrast to the simultaneous response of the stiffened plates, stringer beams in the cylinders acquire membrane tension sequentially during denting. The axial compression in adjacent undented stringer beams opposes the two tendencies for the connection to expand through its thickness and the end rings to bend. However the effects are still sufficiently pronounced to allow relatively wide variations in γ_* through the dent zone, as shown in Fig. 5.24. The supports are much more flexible axially when the dent depth is small because the compressive forces have not yet developed.

The same phenomenon also causes small fluctuations in the signs of the early membrane responses. These are illustrated in Fig. 5.20 for Cylinder 1A1. Because the axial force in stringer 0 is compressive at the beginning of denting the adjacent stringer 1 experiences a small tensile force. However the centre stringer soon becomes tensile; thus stringer 1 sees compression and the forces in the next stringers 2 and 3 are respectively tensile and compressive, with successively smaller magnitude. Such variations are quickly overwhelmed by overall end block pull-in, though, as denting progresses.

5.6.7.2 RESIDUAL PULL-IN

At the conclusion of each denting test, when the lateral load is finally removed, the model ends retain a small residual rotation. This is apparent from the unloading curves in Figs. 5.34 to 5.36. It is caused by the nett membrane tension remaining in the dent region (see Figs. 5.14 and 5.19 for example) and is equilibrated by small tensile forces diametrically opposite the dent and compression near mid-depth. It is mentioned in Section 5.6.4 that a small compressive force is also generated in the centre of the dent and thus an alternating pattern of compressive and tensile residual stresses exists through the cross section. This brings to mind the saw-tooth pattern found by Smith [148] in laterally bent tubes. However an important difference is that his residual stress block is opposite in sense, with tensile stresses under the point of load application. This has already been discussed in Section 2.7.2.3.

Detaching the end blocks produces additional strains, as demonstrated by the gauges, which give a new equilibrium configuration. These strain decrements are compressive in and opposite the dent zone with extension in between. Thus an outward bulging curve is superimposed onto the straight angle difference between the two cylinder ends. Combined with possible local distortions present from the outset due to welding on the end rings, the initial distribution of stresses under subsequent longitudinal loading is likely to be rather nonuniform.

5.7 COMPLETE CYLINDRICAL COLUMN RESPONSE

The support condition employed in the model denting tests gives essentially planar rotations at the ends, although some nonlinear pull-in occurs near the dent due to end block bending and flexibility in the bolted

connection. How applicable this arrangement is to full length columns found offshore is pertinent.

The three bay model tests show that in the central bay, where planarity is not enforced, the pull-in is more localized to the dented region. For longer cylinders with undamaged bays, therefore, greater pull-in would be seen at the dent and so the development of membrane tension may be slowed. This is automatically handled in the analysis by a reduced γ_* value, but further work is required to determine the relationship between member length and γ_* with various boundary conditions at the column ends. Also relevant is the distance along the member from the dent required for the tensile forces to die out through redistribution.

No noticeable diminution of the membrane behaviour occurs, however, in the three bay models. These might in fact be representative of actual columns in service, within which stiffened diaphragms are frequently spaced for various purposes including the provision of watertight compartments. Largely planar conditions would probably exist at these locations under collision loading. As a bottom line to all this, it should be remembered from Section 5.6.3.1 that while the restraint to longitudinal displacement remains reasonably stiff the actual pull-in has little real effect on the build up of lateral load with dent depth.

The energy involved in the collision between a boat and an offshore structure may be dissipated in a variety of processes, listed in Section 2.3. As mentioned there also, often only two of these processes are included when quantifying the consequences of hitting a member of a braced jacket structure. It has been observed experimentally [152,149] and analytically [26,48] that unstiffened tubes of the geometries typically used in these structures deform both locally, under the indenter, and in an overall bending mode. The beam response is

considered to be plastic with hinges at the supports and under the load.

However the stiffened columns of a tension leg platform or semi-submersible have much greater stockiness in the overall mode; that is, the length/radius ratio is significantly lower. The elastic bending deflections produced by lateral loading would be very small and plasticity would not develop in this overall mode. Thus the assumption that all collision energy is absorbed in the denting process investigated in the present chapter is conservative but not unreasonable for initial design purposes. Demonstrative numerical results [36] concur with this assertion.

The pull-in and rotation caused by denting might induce overall deflection, though, as suggested figuratively by the dotted line in Fig. 5.39(b). Such deflections are dependent on the degree of flexural and axial restraint provided at the member ends by the rest of the structure but are likely to be very small.

5.8 DYNAMIC EFFECTS

The applicability of static theory and test results using slow loading rates to the collision of a ship into another ship or oil rig requires some comment. Quasi-static analysis ignoring inertia forces is valid when the duration of impact is much greater than the period of vibration of the structure [82]. De Oliveira [25], Jones [78] and Valsgard and Pettersen [174] demonstrate this to be true for components of typical offshore structures but the dynamic properties of the overall structure should also be checked.

Another consideration is the effects of strain rate. A well known empirical formula for the strain rate

sensitivity of mild steel is due to Cowper and Symonds [19];

$$\sigma_Y'/\sigma_Y = 1 + (\dot{\epsilon}/40)^{1/5}$$

where σ_Y' is the elevated yield stress induced by strain rate $\dot{\epsilon}$. However the above equation overestimates the strength increase at high strains and low strain rates [82] representative of the present collision problem, and it may therefore be tentatively concluded that strain rate effects are not of critical concern. The dynamic lateral loading tests undertaken by Soreide and Amdahl [152] and discussed in Sections 2.7.1.1 and 2.12 substantiate this suggestion.

An interesting and related phenomenon is nonlinear scalability. Booth et al [7] have found from impact tests that larger models have greater deformations than expected from linear proportionality, which is attributed to the lower strain rate they experience. As well as increased yield stress, rapid straining produces an elongated yield plateau and a higher fracture stress [82]. This last phenomenon is also dependent on the material defects present, in the weld metal for example, and the shorter crack length likely in a scaled down model will retard rupture.

The prototype structure may further be affected in service by complex multidimensional stress fields [50] and the brittleness that accompanies low temperatures. Consideration of all these effects has led Valgard and Pettersen [174] to suggest an ultimate apparent strain of

$$(2e_a')/L = 0.015$$

as a realistic criterion for rupture at full scale. This value is significantly lower than those frequently adopted: an apparent strain [95,113] of

$$(2e_n')/L = 0.10$$

or a localized peak strain [62] of

$$\epsilon_n = 0.30 .$$

Booth et al [7] conclude that size effect is important in situations where the load falls off rapidly after plastic collapse and there is significant material tearing. Neither item applies to the problem presently under investigation.

5.9 CONCLUSIONS

It is found that knife edge loading normal to the longitudinal axis of an orthogonally stiffened cylinder produces bilinear deflections over one bay when the rings are substantial. The stringer deformations suggest an analysis of individual T-section beams which gives good correlation with the test results. Although the cylinder end blocks are free to pull in, the restraint provided by the undamaged material due to maintaining planarity and circularity of the ends causes the stringer beam supports to be very stiff axially. Thus a piecewise linear approximation describes the damage load response well, and in turn, the work done during denting may be easily estimated. Comparison with the possible impact energy in a ship collision shows that only a small dent would be formed, and whether twenty or forty stringers are present has little effect on the energy absorbing capability.

Care should be exercised in applying the approximate energy equation. With very light stiffening it underestimates the actual work done to reach a certain dent depth, but it may become unconservative for slender stiffeners, for example

$$h_t/t_t = 16 .$$

These fold over under gross deflection making the stringer beam analogy invalid.

TABLE 5.1 Cylinder properties

CYL NO.	MATERIAL	GEOMETRY							
	E/σ_{YT}	$t = t_l$	R/t	L/R	s	h_l/t_l	L_t/R	t_r/t	h_r/t_r
1A1	600	0.84mm	190	0.416	40	8			
1A2	600	0.84	190	0.416	20	8			
1B1	630	0.63	254	1.08	40	6			
1B2	630	0.63	254	1.08	20	6			
3A1	600	0.84	190	0.481	40	16	1.13	3.6	8
3A2	600	0.84	190	0.331	40	8	0.938	3.6	8
3A3	600	0.84	190	0.331	40	8	0.956	3.6	8

TABLE 5.2 End ring thickness

CYL NO.	END RING THICKNESS $\frac{1}{2}L_s$
1A2	19.3mm
1B1	15.4
1B2	15.5
3A2	14.5
3A3	14.3

TABLE 5.3 Strain gauging

CYL NO.	GAUGE TYPE	DESCRIPTION	GAUGE LOCATIONS	
			DENT STRINGERS	OVERALL SECTION
1A1	YL-3	post yield	$0 \leq j \leq 3$	
1A2	YL-3	post yield	$0 \leq j \leq 1$	$\phi = 3\pi/5$
1B1	FLA-2	foil	$0 \leq j \leq 4$	$\phi = \pi/2, \pi$
1B2	FLA-2	foil	$0 \leq j \leq 2$	$\phi = \pi/2, \pi$
3A1	FLA-2	foil	$0 \leq j \leq 4$	
3A2	PL-5	polyester	$2 \leq j \leq 3$	$\phi = \pi/2, \pi$
3A3	PL-5	polyester	$2 \leq j \leq 3$	$\phi = \pi/2, \pi$

TABLE 5.4 Parameter governing extension at hinges

AXIAL FORCE n	PARAMETER $(z_s + z_c)/R$
Encastre supports:	
$-1 \leq n \leq -C_0$	$n/C_{3R} + C_{4R}$
$-C_0 \leq n \leq C_0$	n/C_{2R}
$C_0 \leq n \leq 1$	$n/C_{3R} - C_{4R}$
Simple supports:	
$-1 \leq n \leq -C_0$	$n/C_{5R} + C_{6R}$
$-C_0 \leq n \leq 1$	$n/2C_{2R} + C_{7R}$

$$C_{2R} = Rb/A$$

$$C_{3R} = \frac{2R/A}{1/t_l + 1/b}$$

$$C_{4R} = (A_p - A_l)(1/t_l - 1/b)/2R$$

$$C_{5R} = 2Rt_l/A$$

$$C_{6R} = A_p^2(1/t_l - 1/b)/2RA$$

$$C_{7R} = (A_l/A_p)^2 C_{6R}$$

TABLE 5.5 Formulae for membrane tension development

JONES FORMULATION: Version (ii)

Pull-in of stringer beam j defined in terms of central dent depth

$$\frac{\Delta_j'}{L} = 2(1-\gamma_*)\left[\left[\frac{\delta_j}{L}\right]^2 + \frac{2R}{L}(1-\cos\phi)\frac{\delta_j}{L}\right]$$

Encastre supports:

$-1 \leq n \leq -C_0$	$n = C_3(\gamma_*\delta_j/L - C_{1*}C_3[\gamma_* + C_i\exp(-1/(C_{1*}C_3)\delta_j/L)] - C_4 - C_8)$
$-C_0 \leq n \leq C_0$	$n = C_2(\gamma_*\delta_j/L - C_{1*}C_2[\gamma_* + C_i\exp(-1/(C_{1*}C_2)\delta_j/L)] - C_8)$ (5.11)
$C_0 \leq n \leq 1$	$n = C_3(\gamma_*\delta_j/L - C_{1*}C_3[\gamma_* + C_i\exp(-1/(C_{1*}C_3)\delta_j/L)] + C_4 - C_8)$

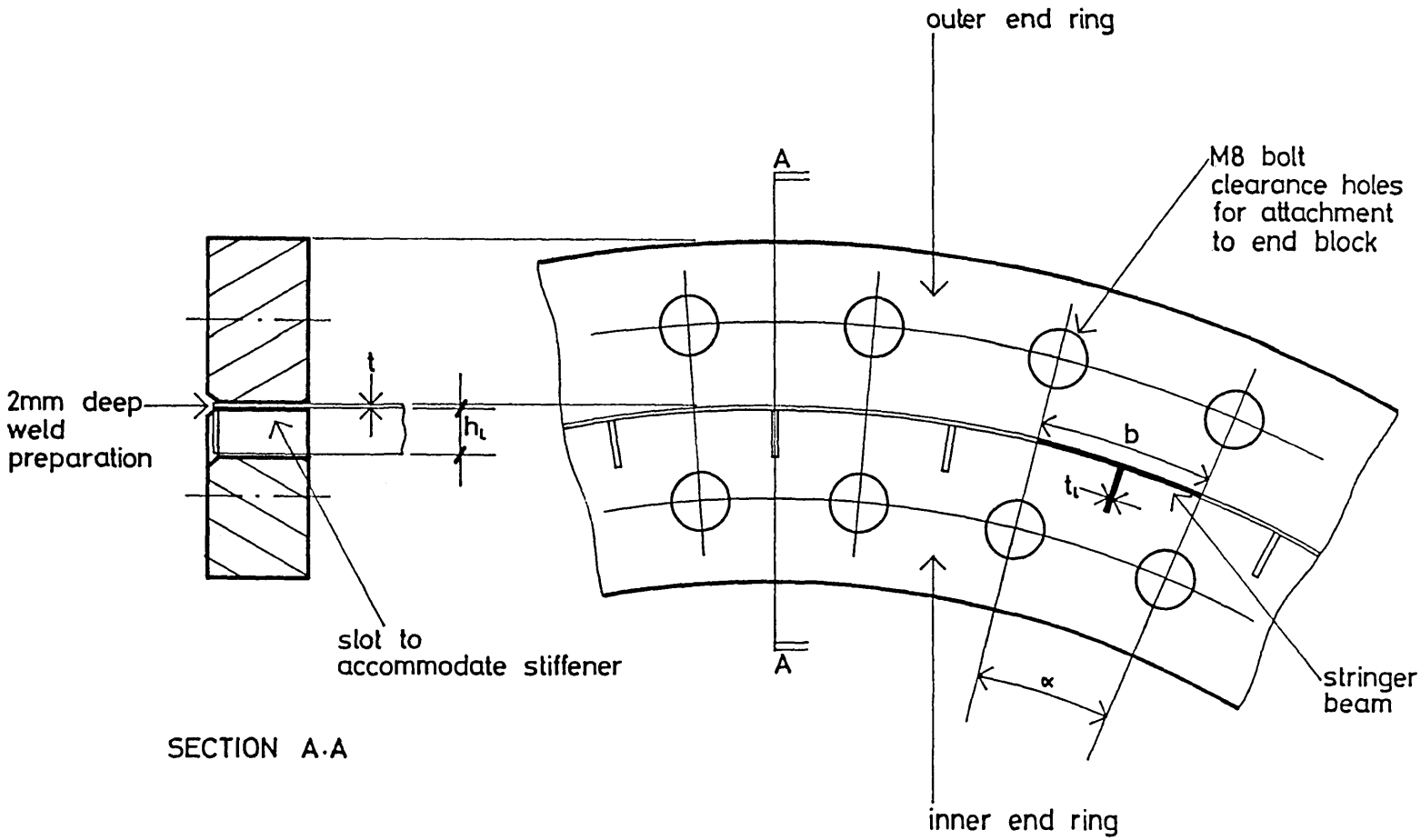


fig. 5.1
End ring detail

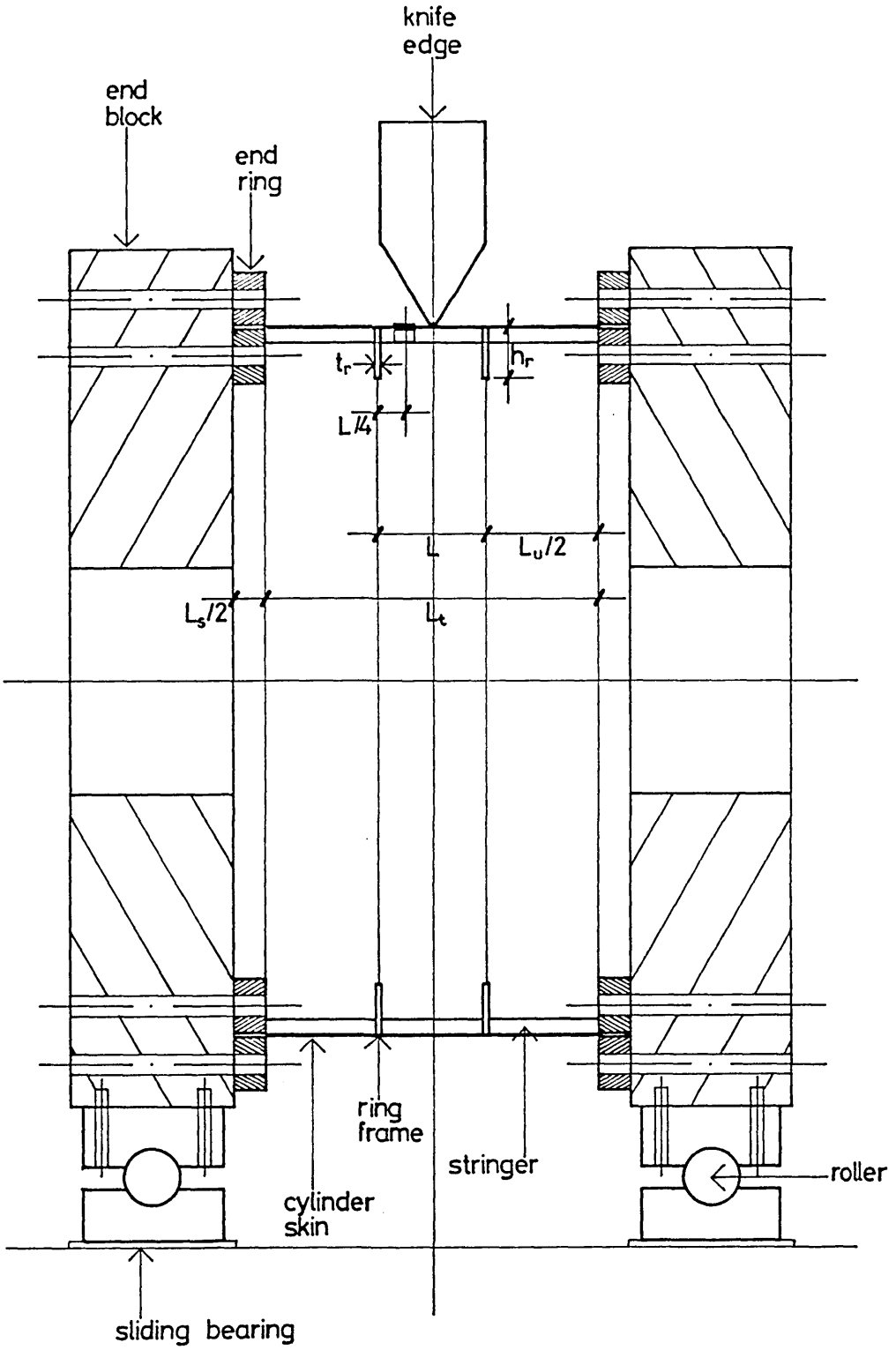


fig. 5.2
Arrangement for denting tests

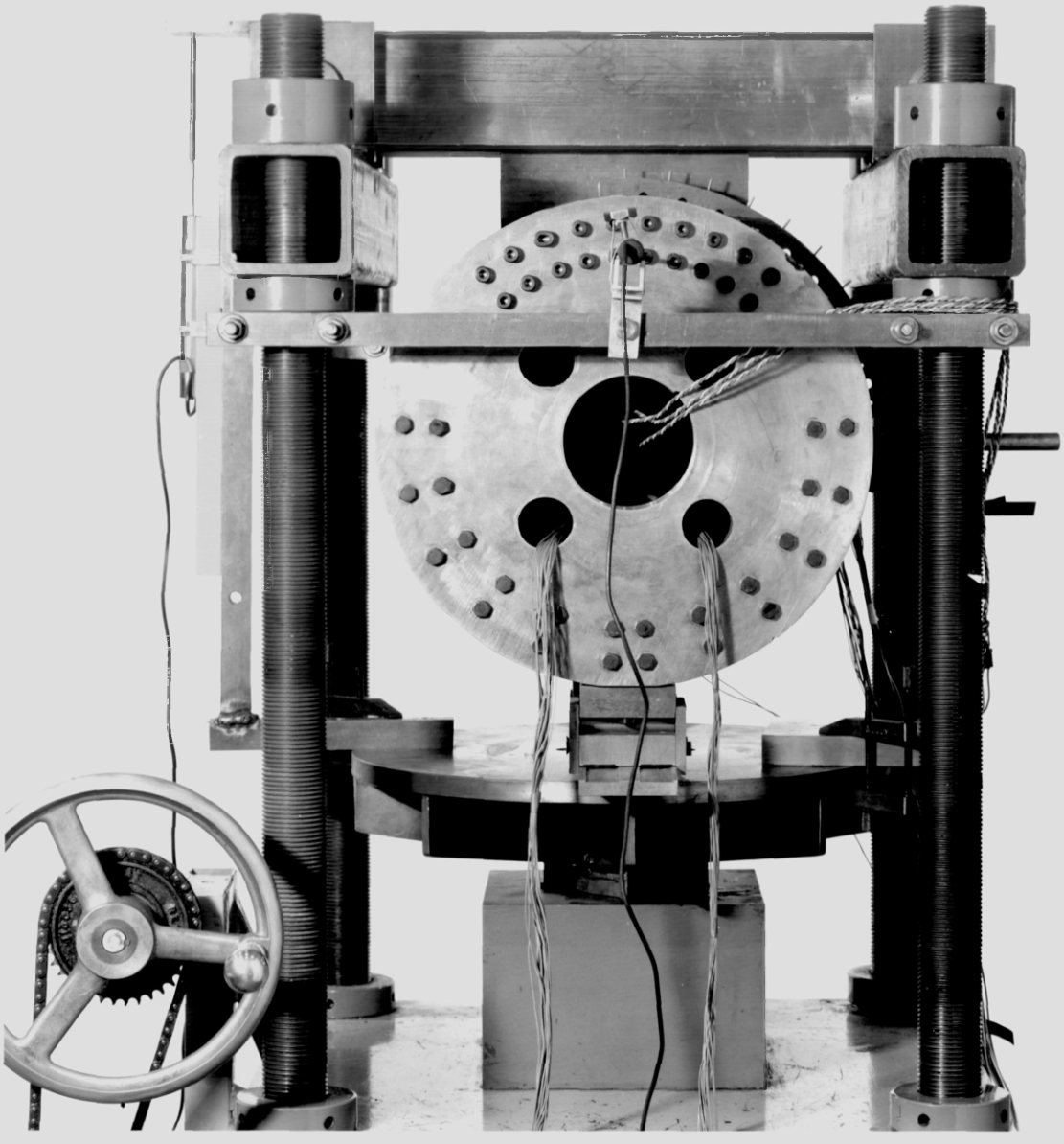


fig. 5.3
Test rig for denting stiffened cylinders

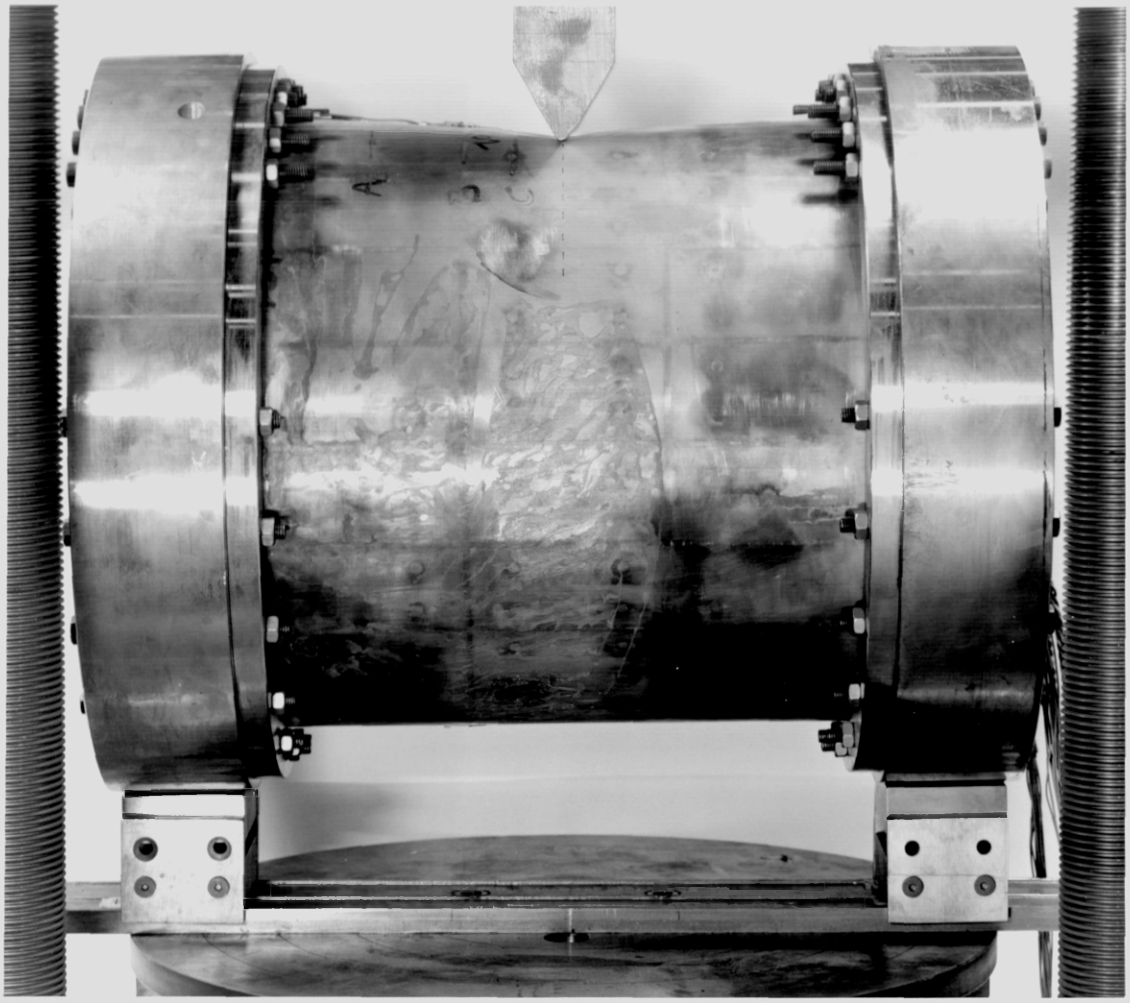


fig. 5.4
Lateral loading arrangement for stiffened cylinders

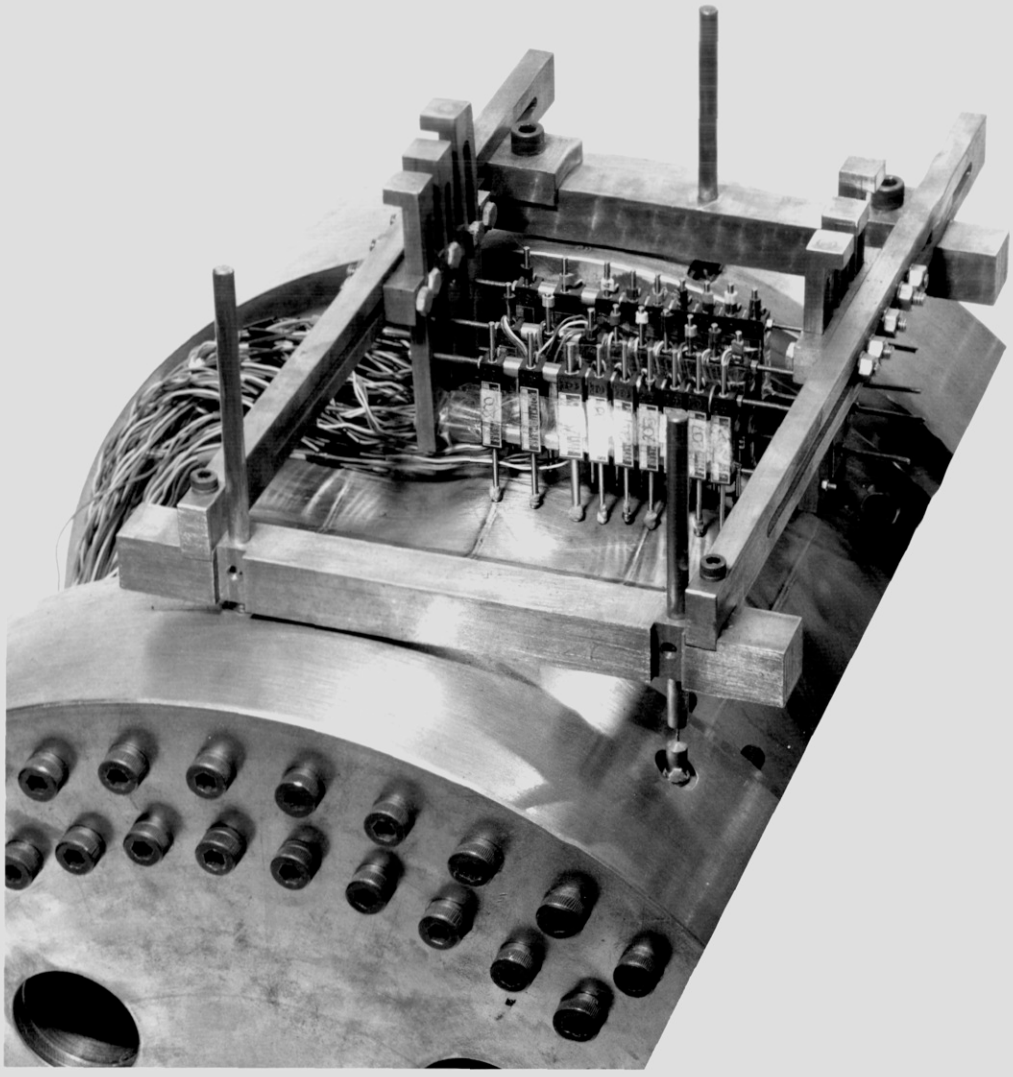
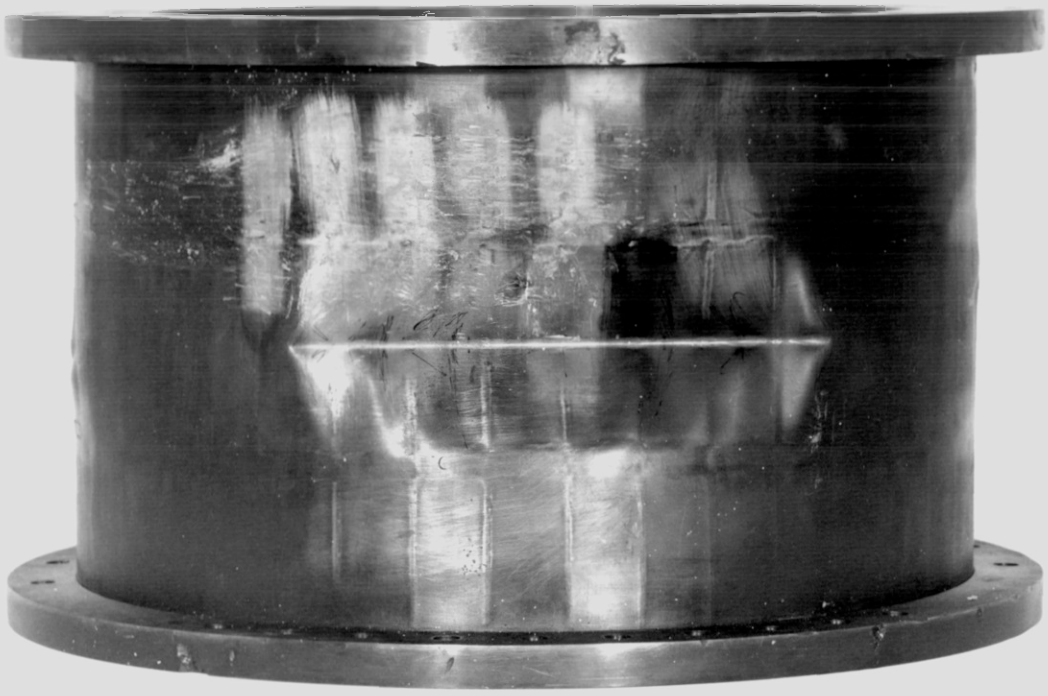


fig. 5.5
Bank of transducers to monitor dent shape



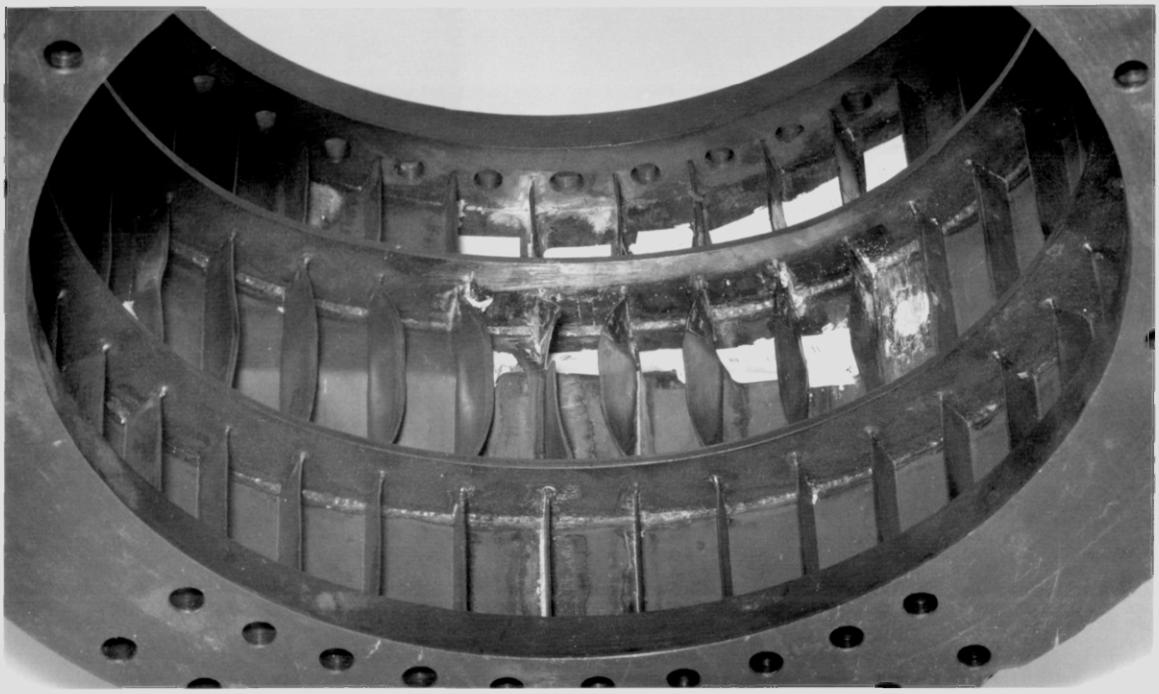


fig. 5.6
Deformation induced by lateral loading
Cyl. 3A1

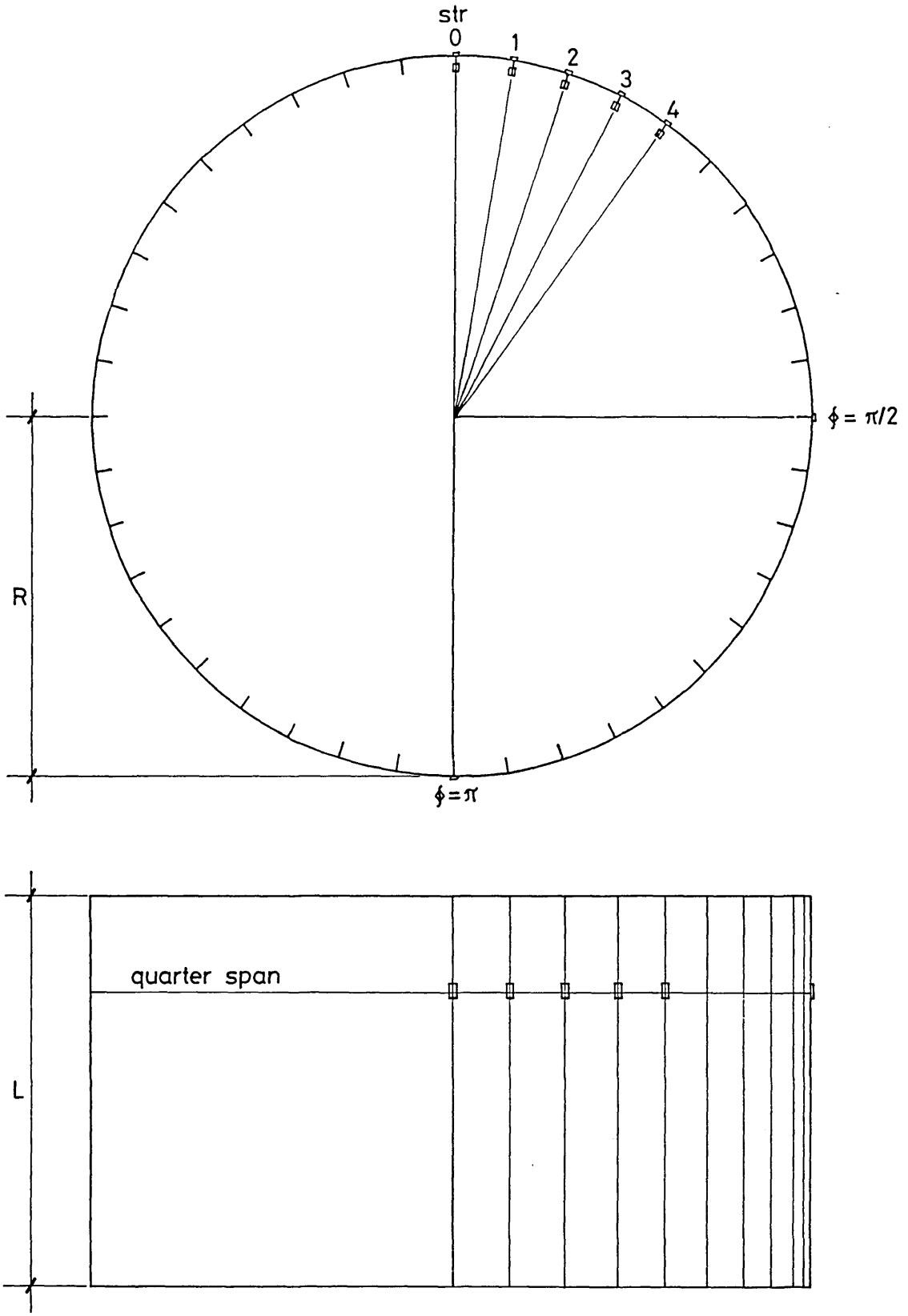


fig. 5.7
Typical strain gauge diagram
Cyl. 1B1

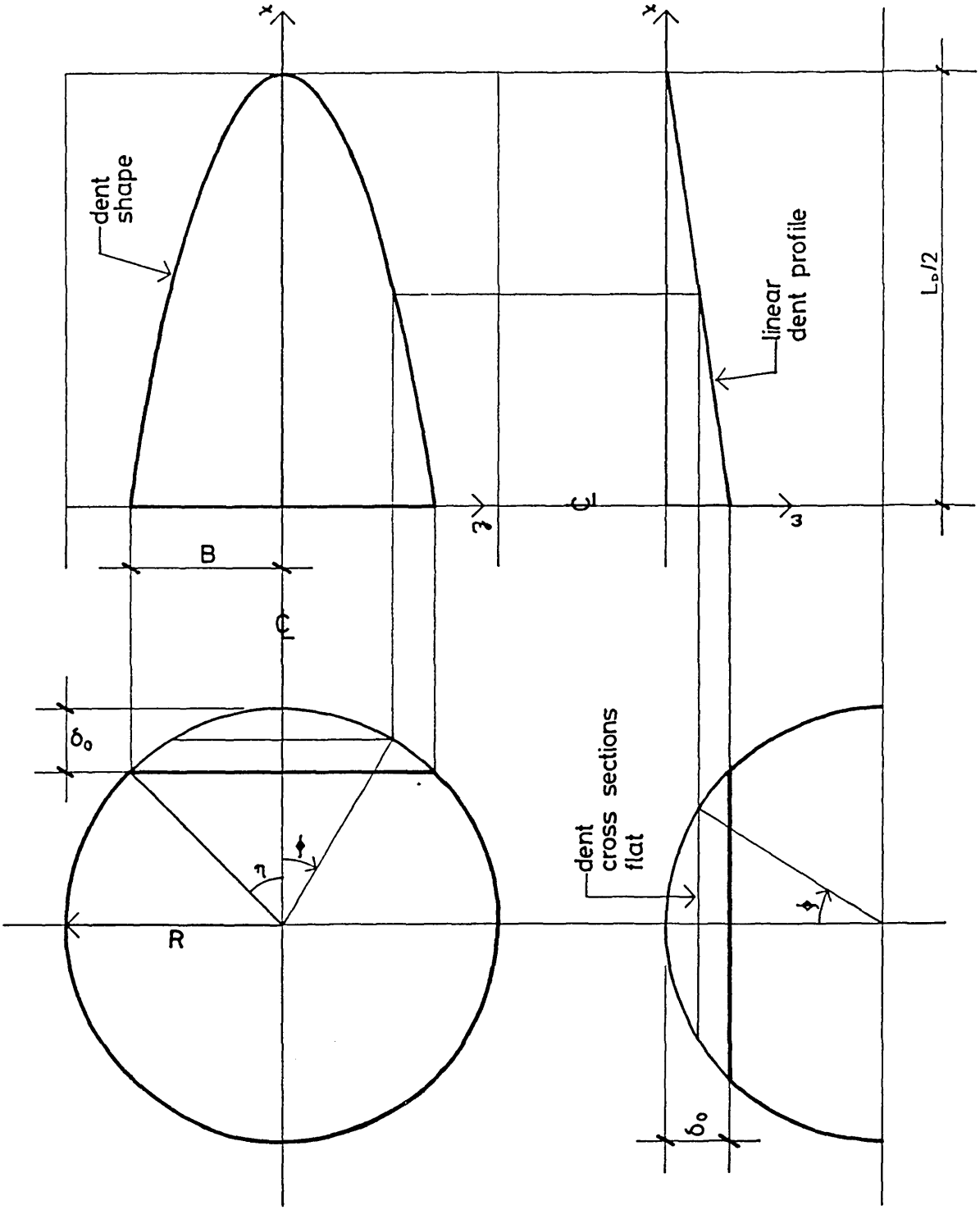


fig. 5·8
Dent shape produced by straight profile and cross sections

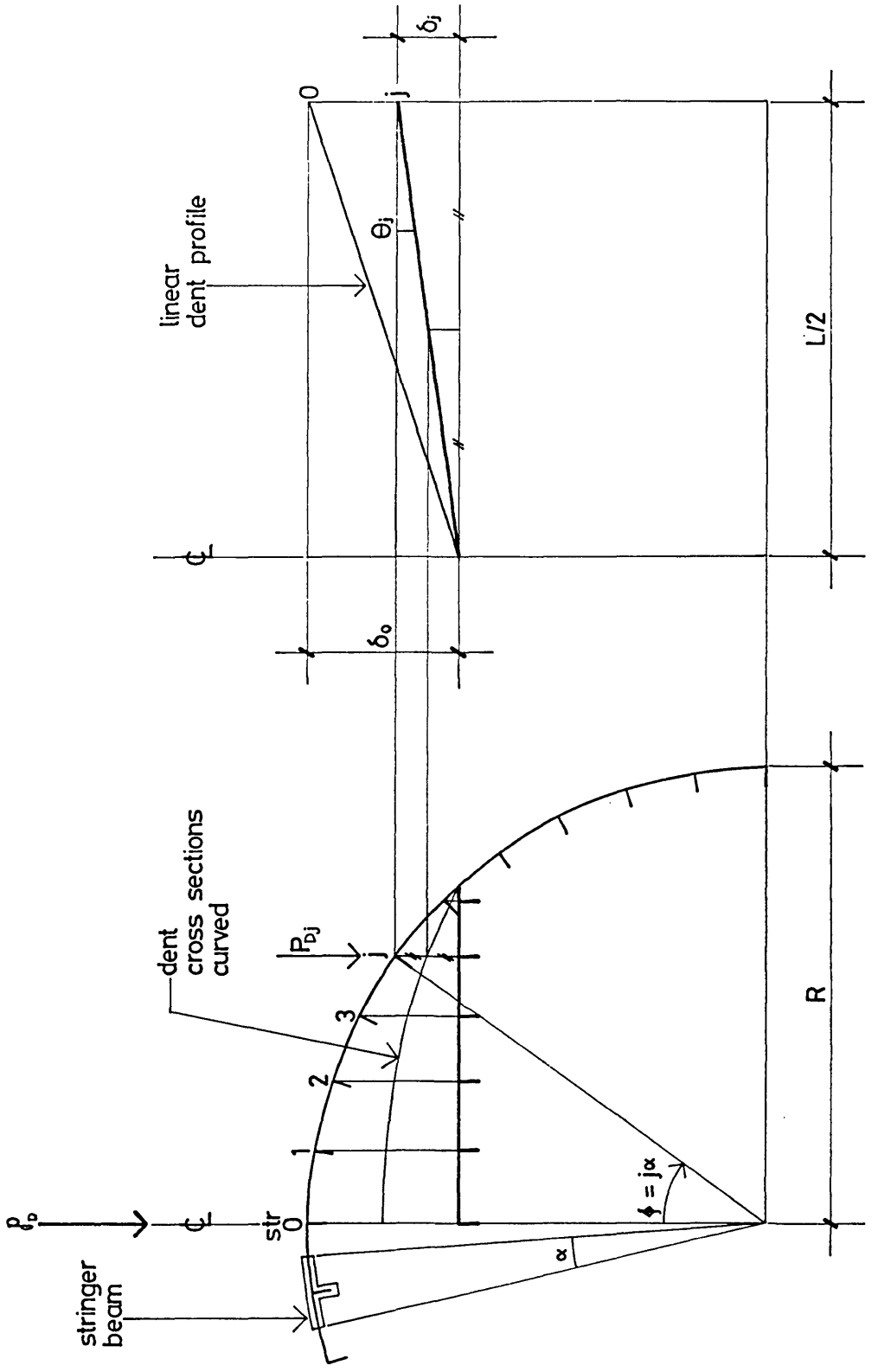


fig. 5.9
Cylinder geometry for rectangular dent shape with linear profile

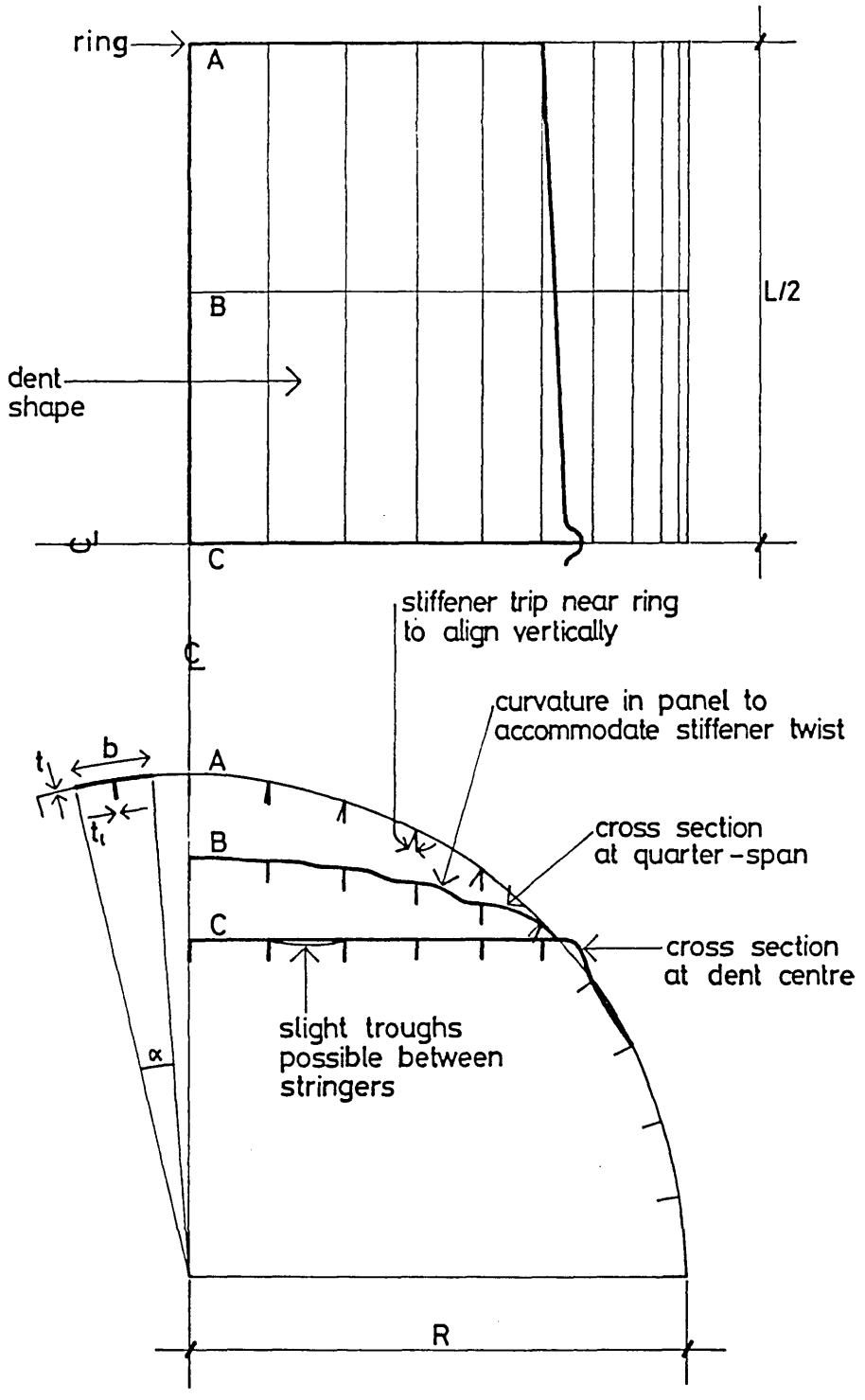


fig. 5.10
Representation of experimentally observed dent geometry

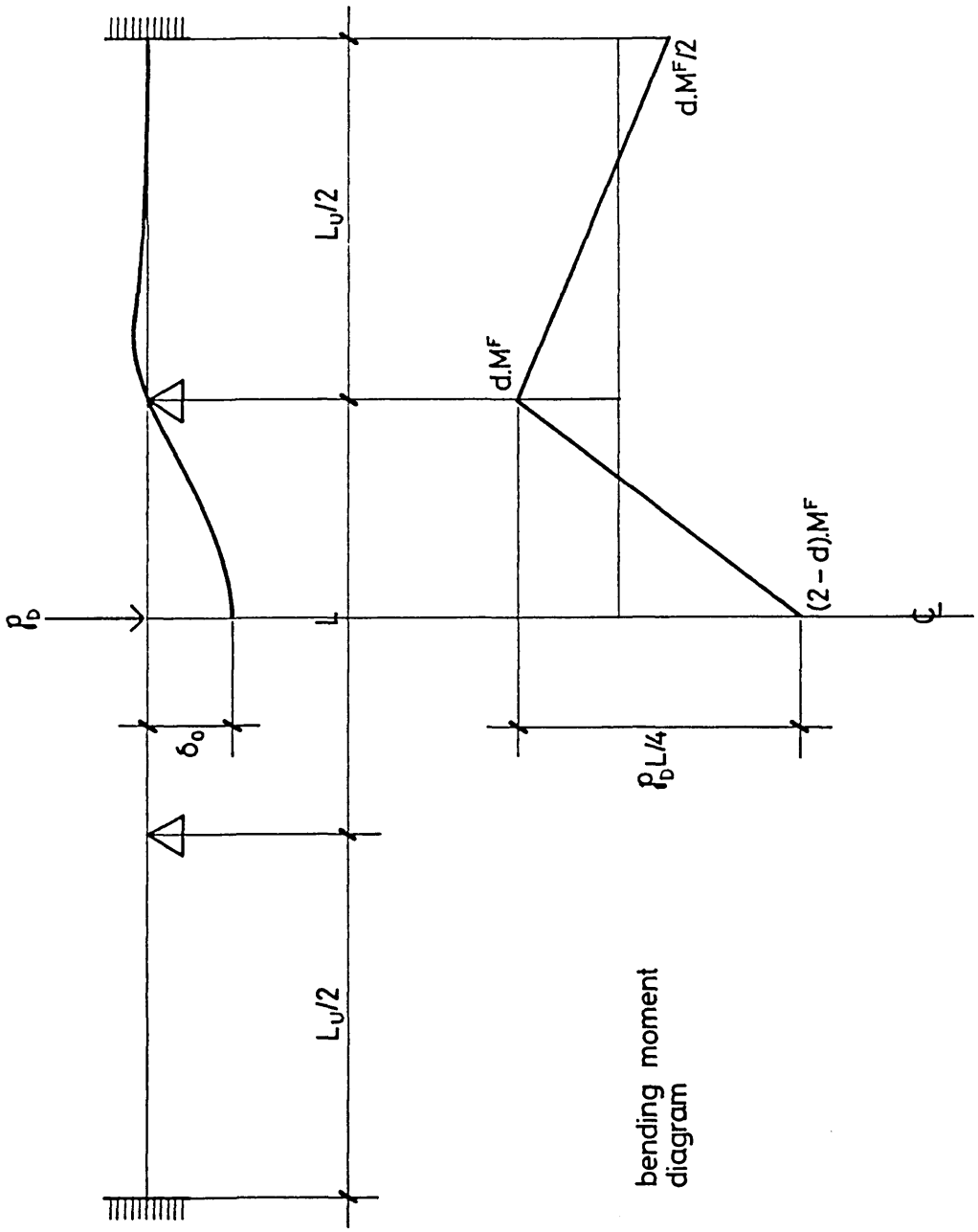
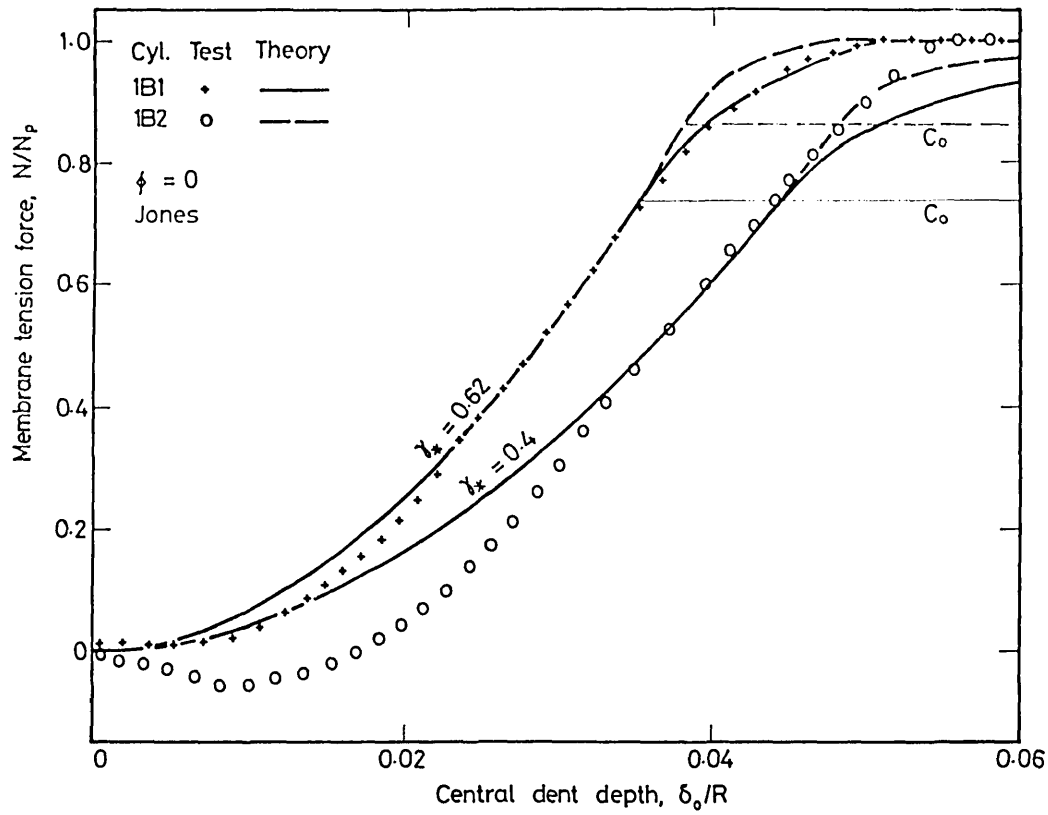


fig. 5.11
Initial elastic response of three bay models



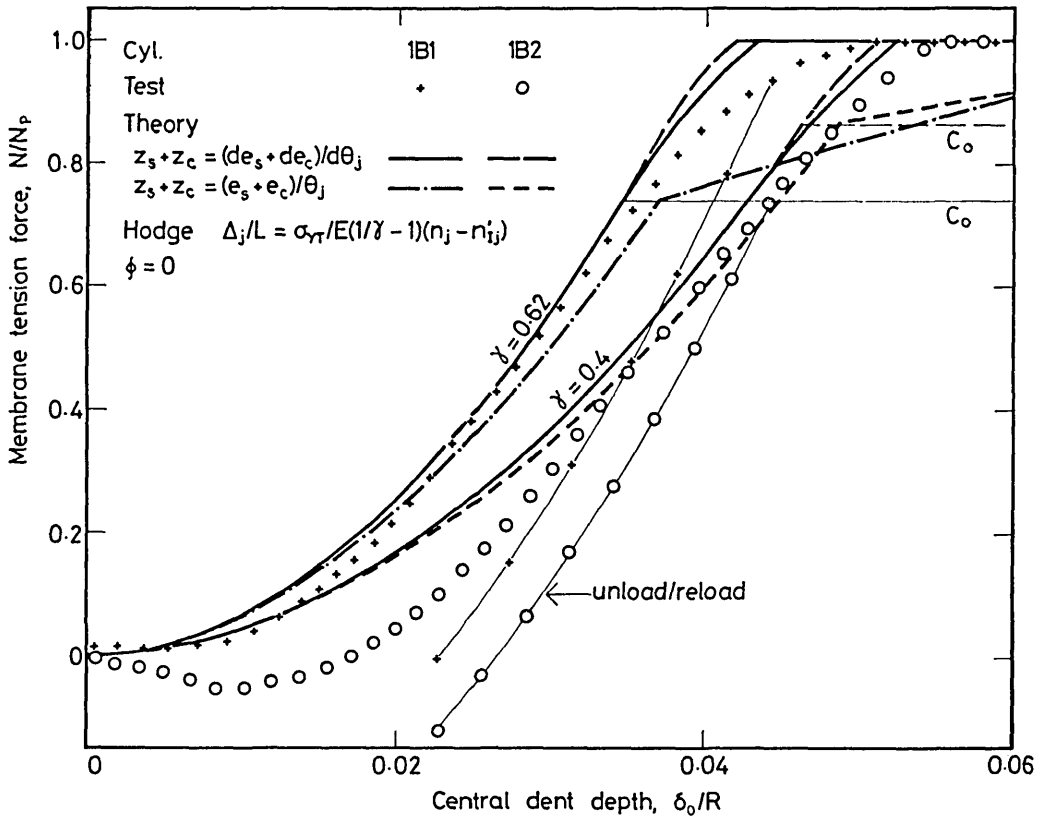


fig. 5.12 (a) and (b)
Theoretical and experimental membrane tension development with deflection
Cyls. 1B

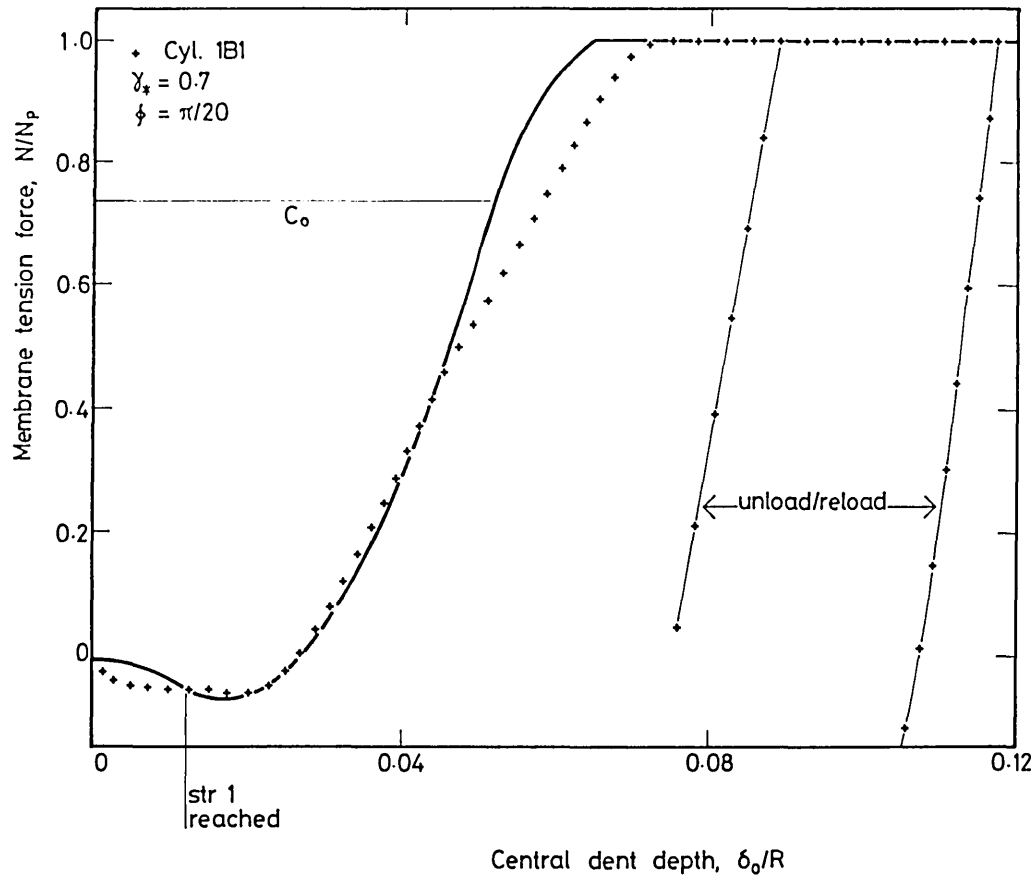


fig. 5·13
Theoretical and experimental membrane tension development with deflection Cyls. 1B

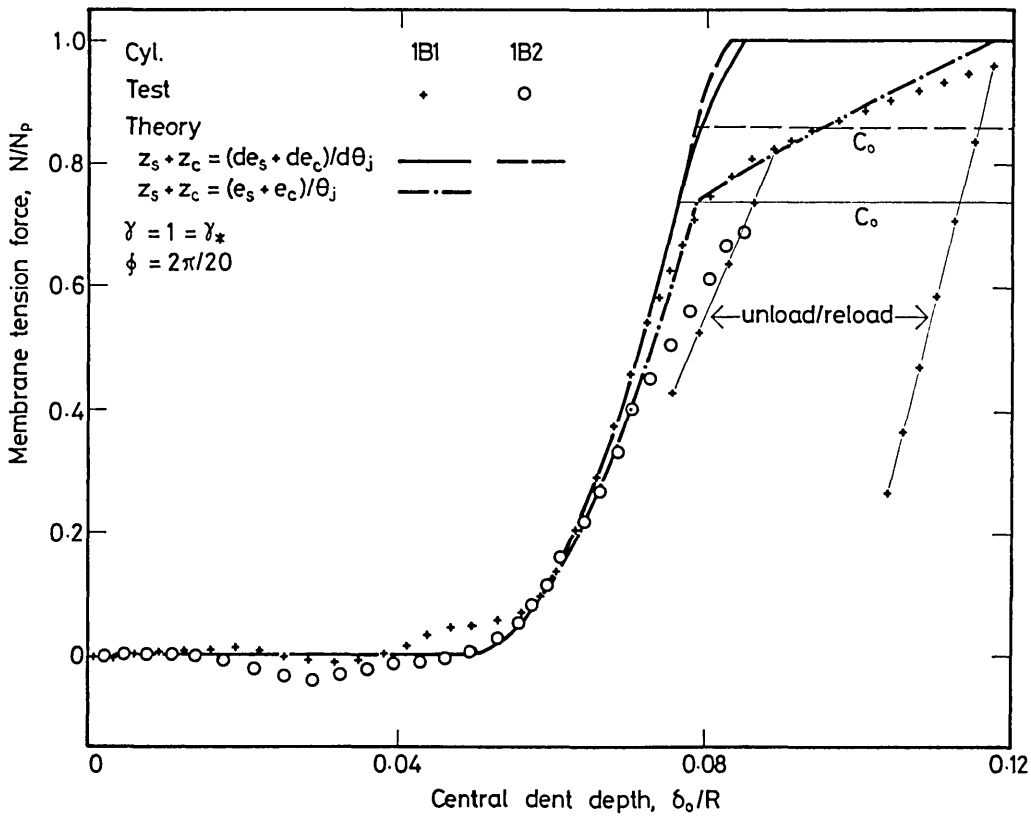


fig. 5·14
Theoretical and experimental membrane tension development with deflection Cyls. 1B

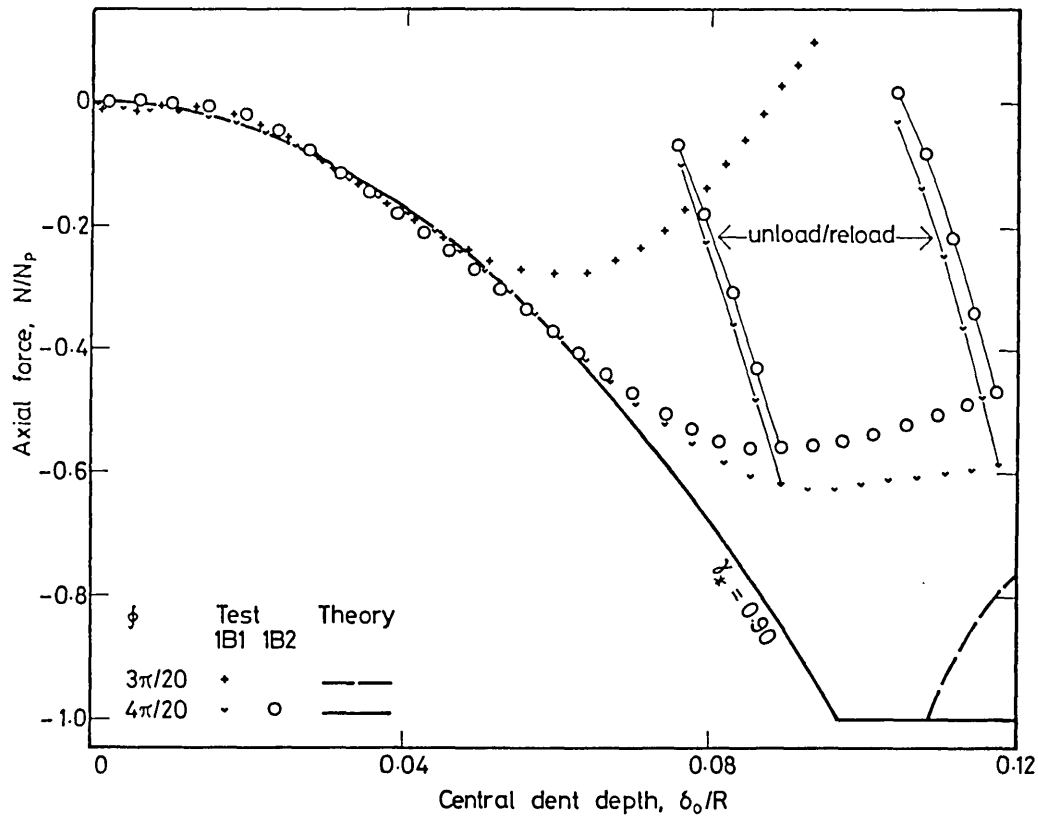


fig. 5·15
Theoretical and experimental membrane force development with dent depth
Cyls. 1B

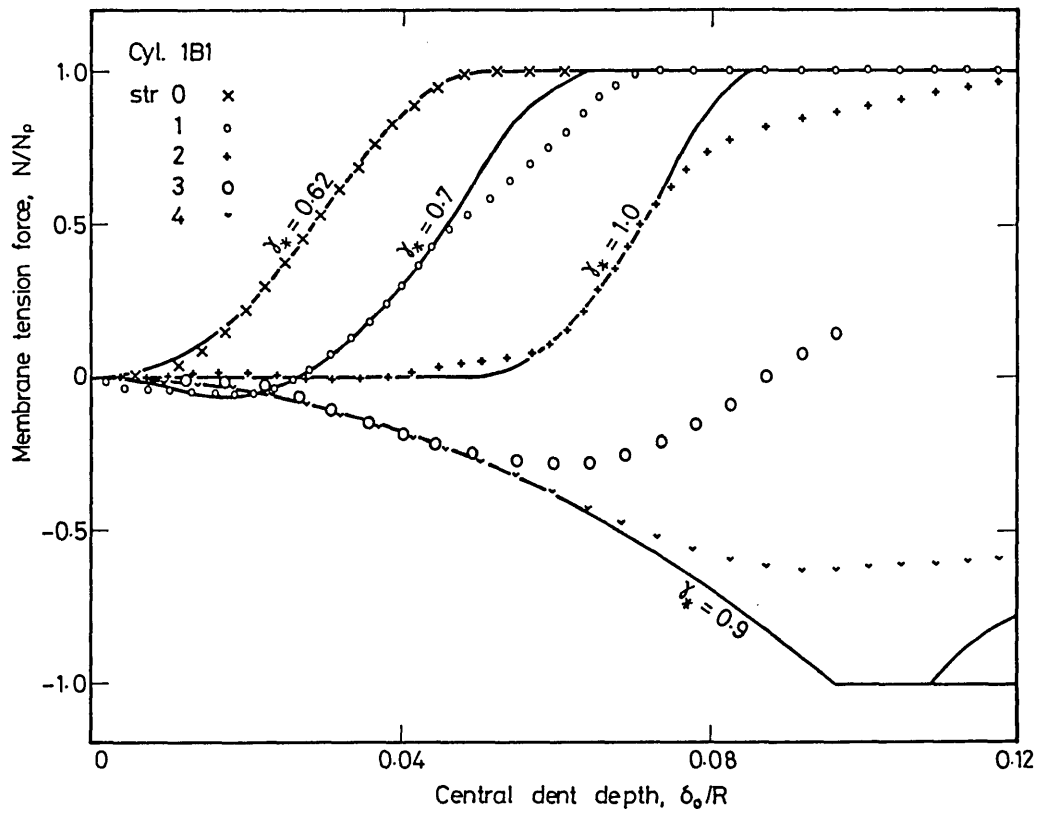


fig. 5·16
Theoretical and experimental membrane tension development with dent depth
Cyl. 1B1

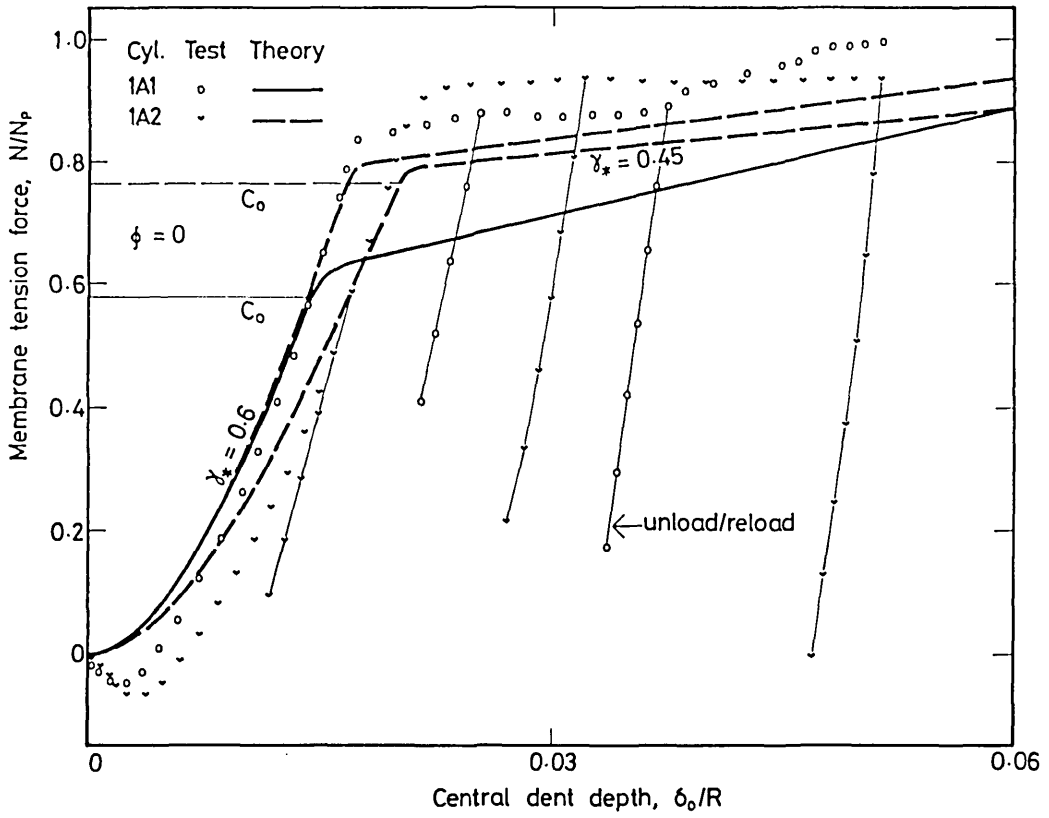


fig. 5·17
Theoretical and experimental membrane tension development with deflection
Cyls. 1A

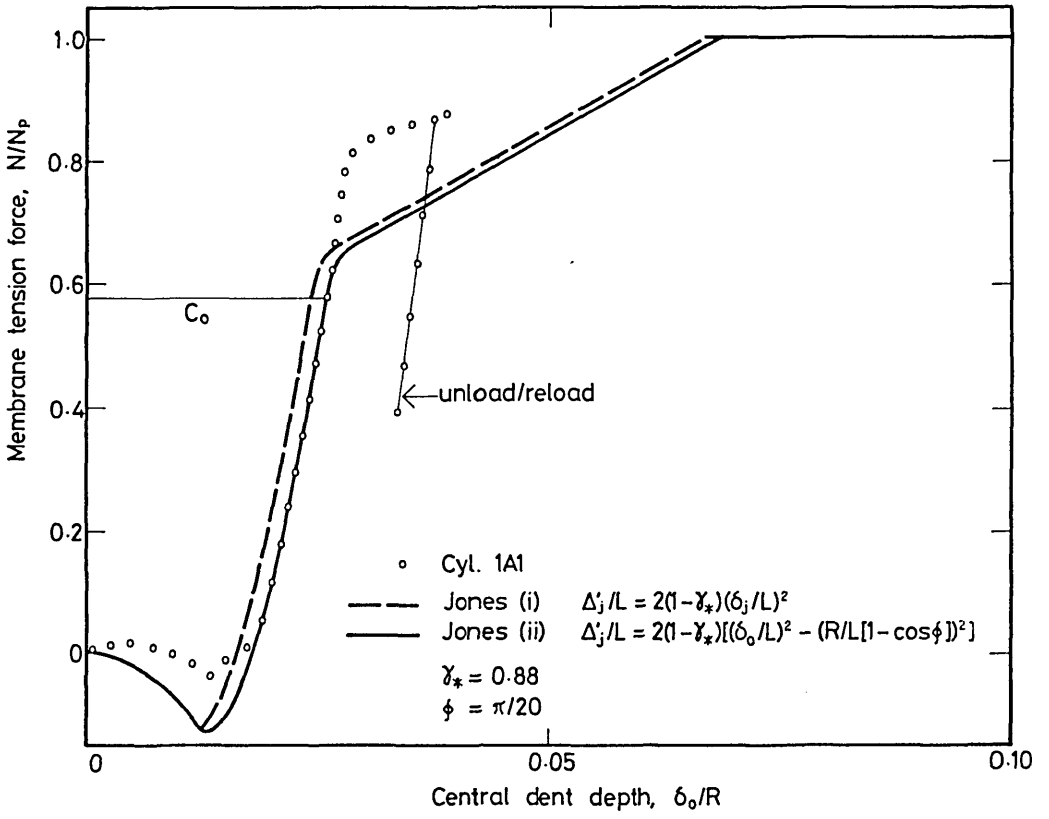


fig. 5·18
Theoretical and experimental membrane tension development with deflection
Cyls. 1A

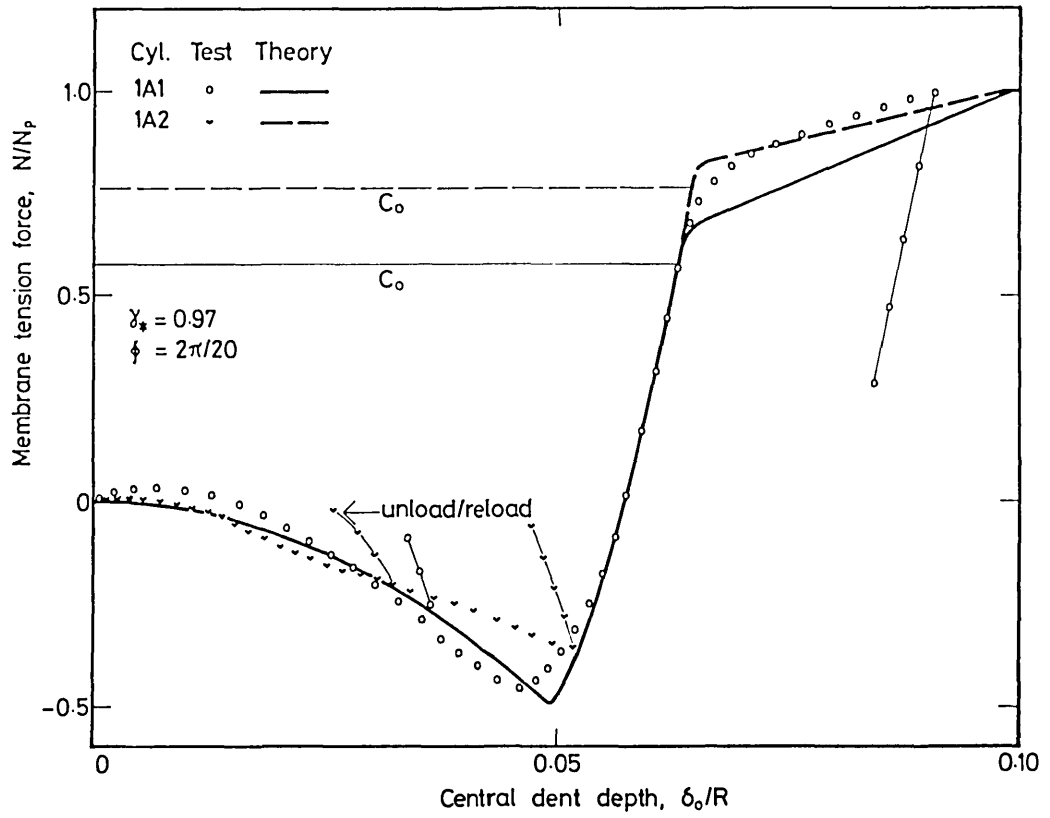


fig. 5·19
Theoretical and experimental membrane tension development with deflection
Cyls. 1A

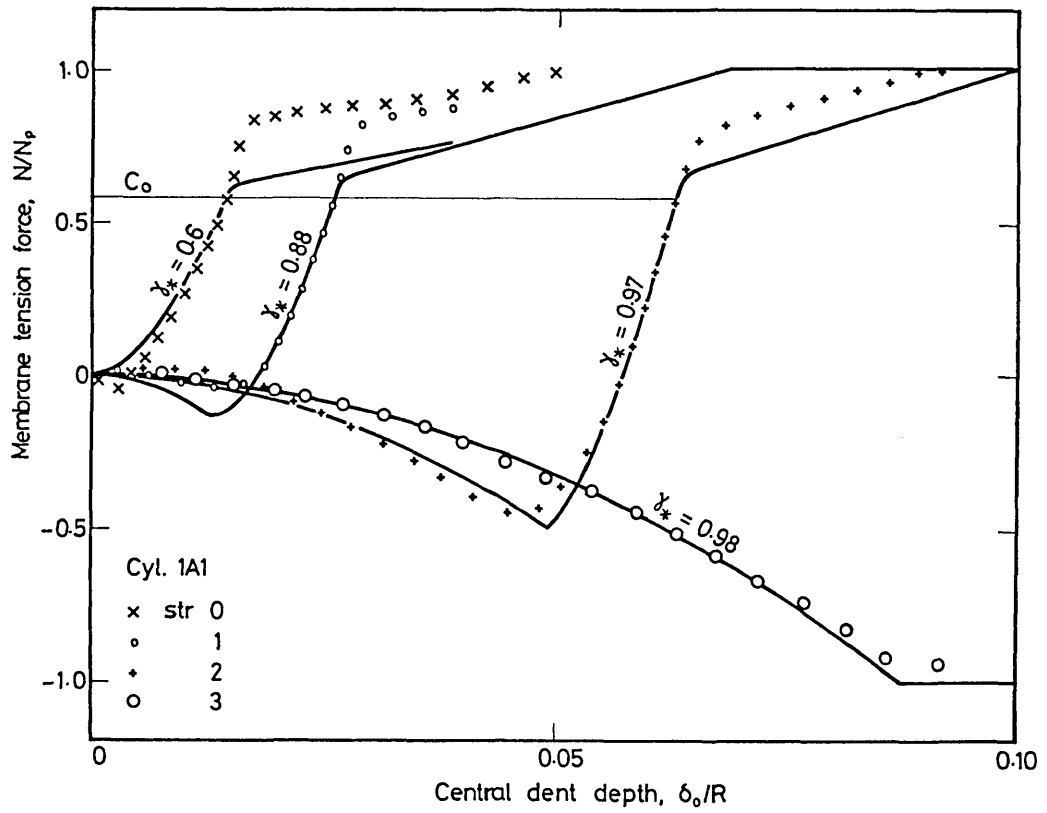


fig. 5·20
Membrane tension development with dent depth
Cyl. 1A1

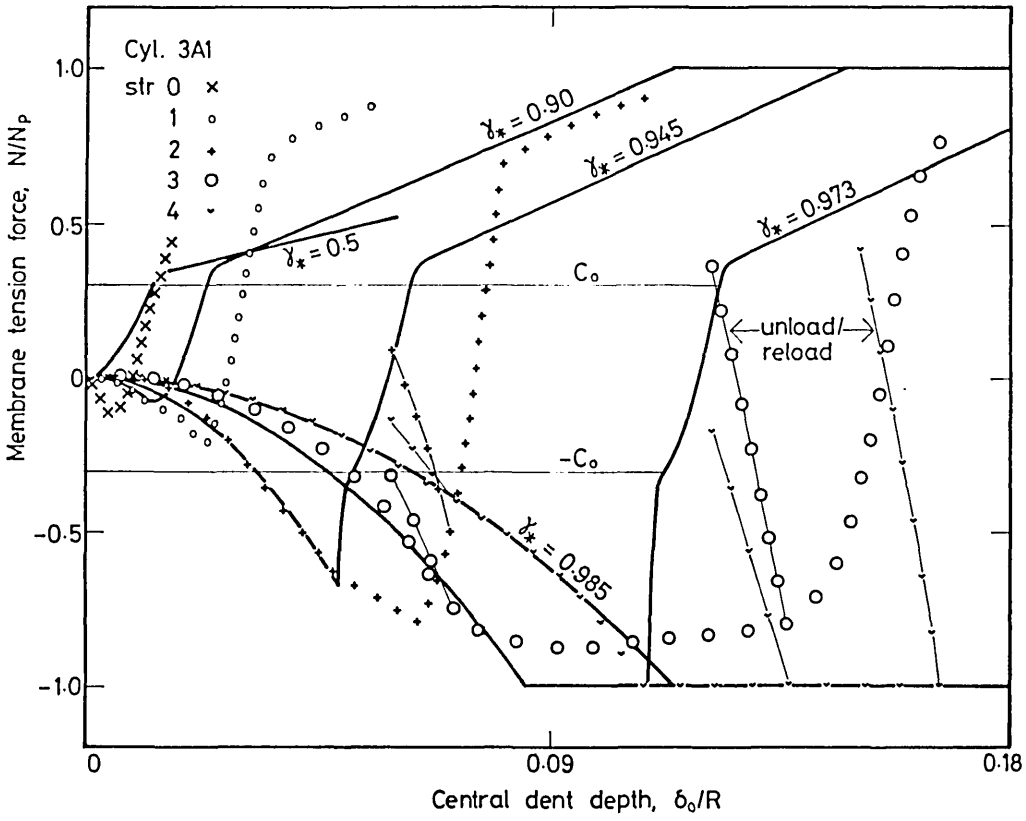


fig. 5·21
Theoretical and experimental membrane tension development with dent depth Cyl. 3A1

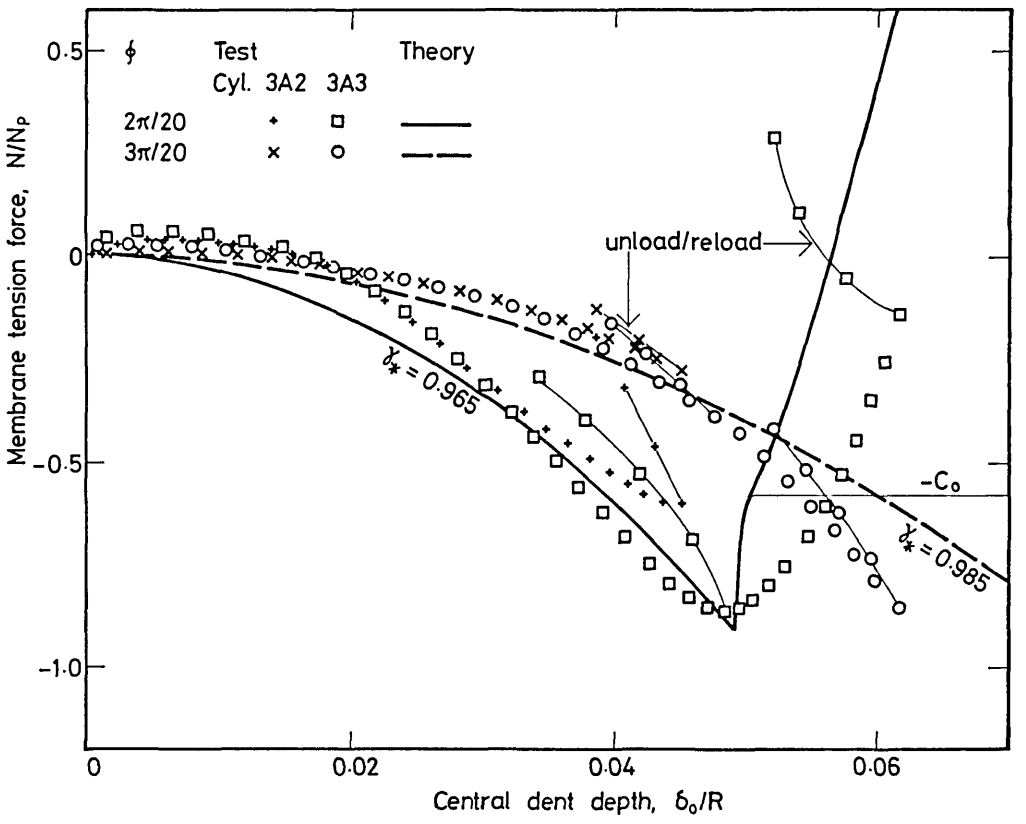
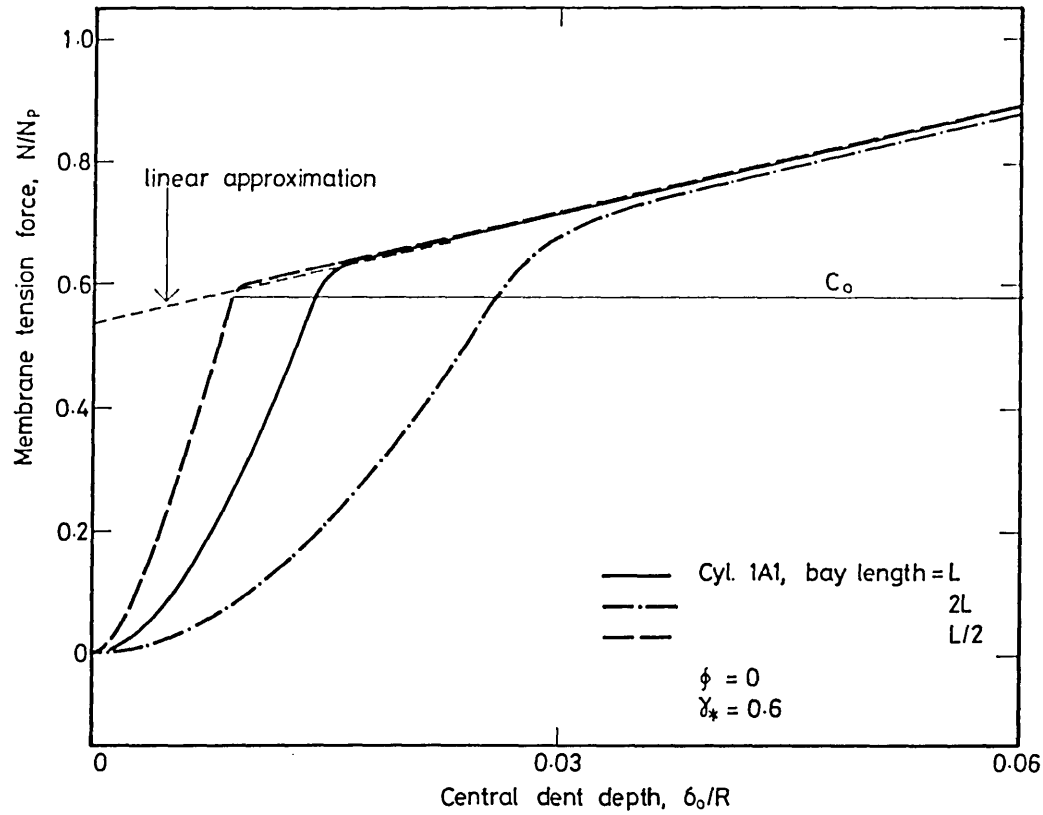


fig. 5·22
Theoretical and experimental membrane force development with dent depth Cyls. 3A2 and 3A3



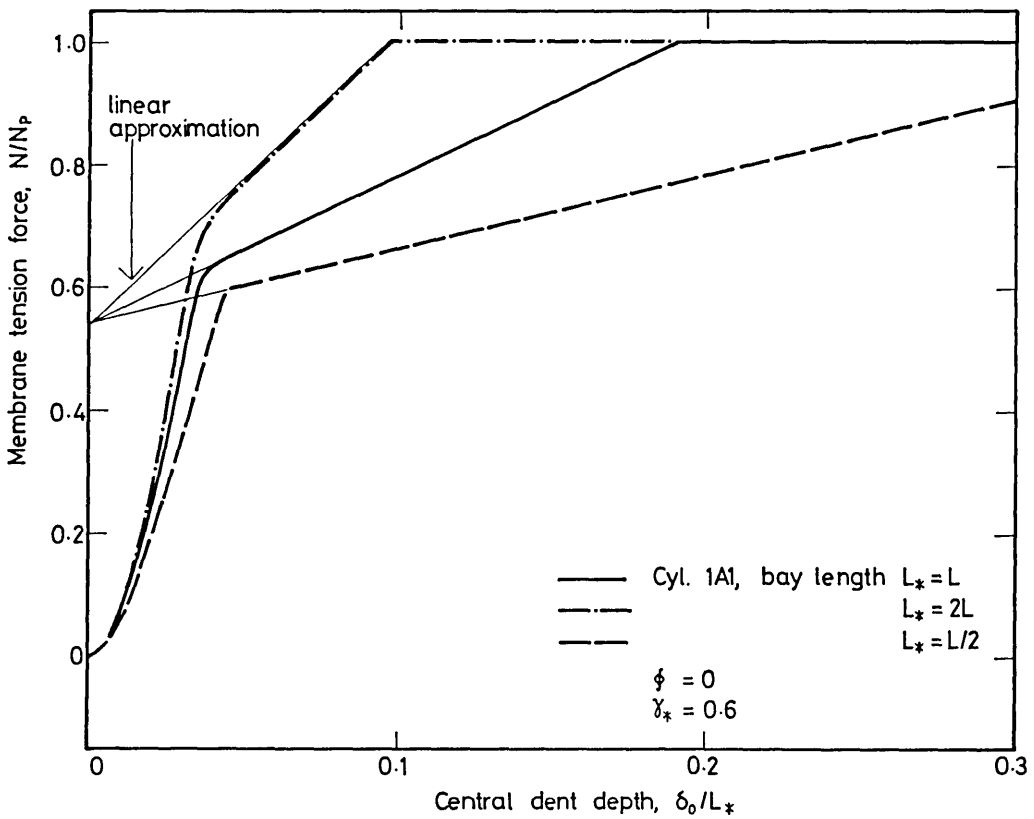


fig. 5·23 (a) and (b)
Membrane tension development for various bay lengths

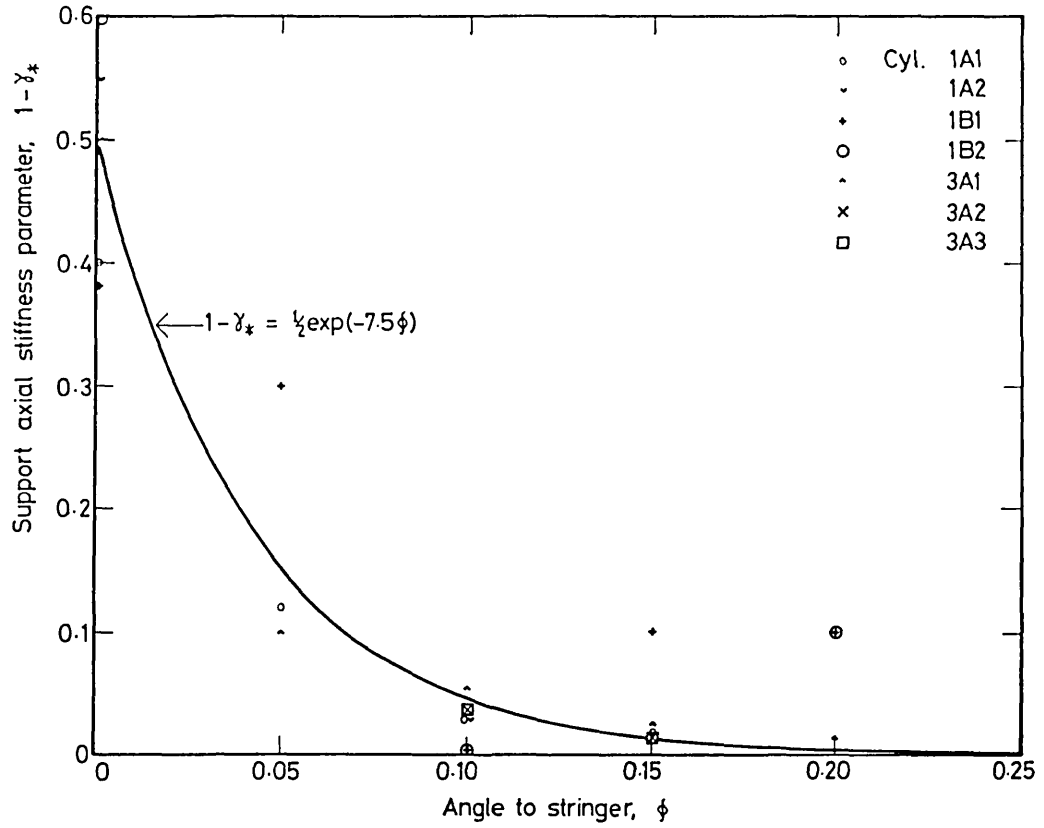


fig. 5·24
Variation of beam support axial stiffness with angle from dent centre

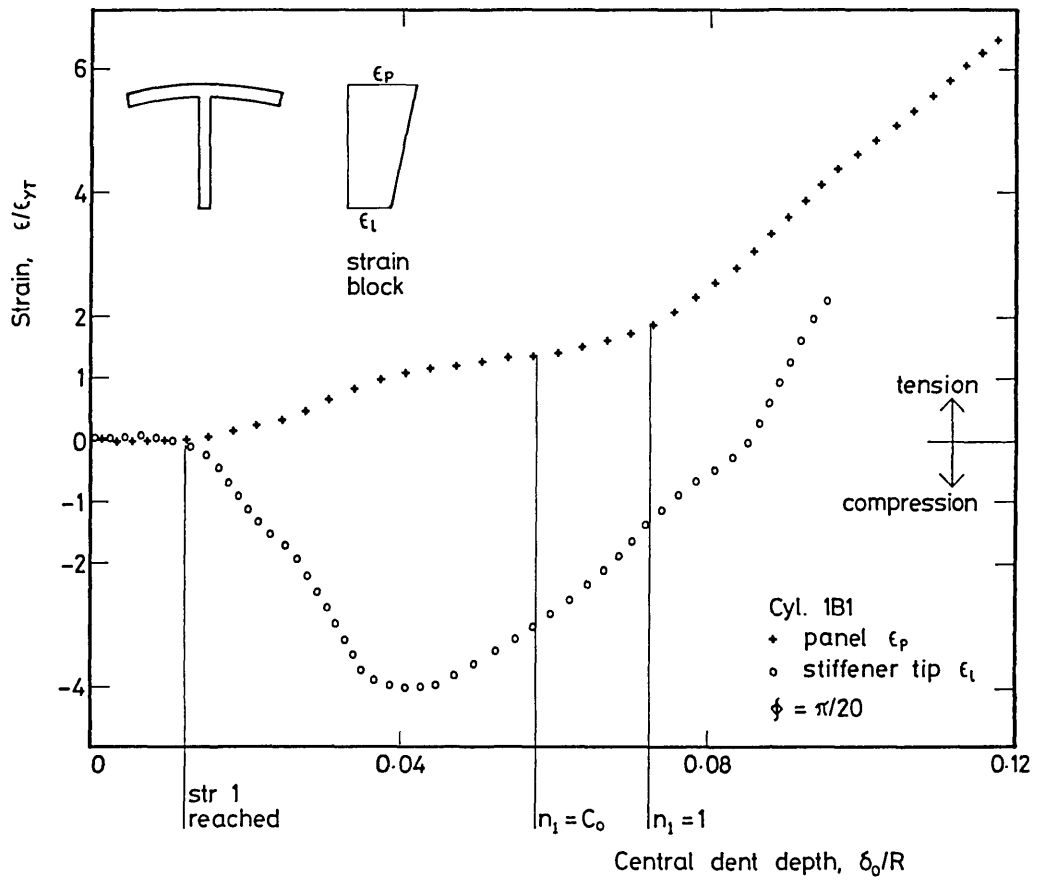


fig. 5·25
Strain development during denting
Cyl. 1B1

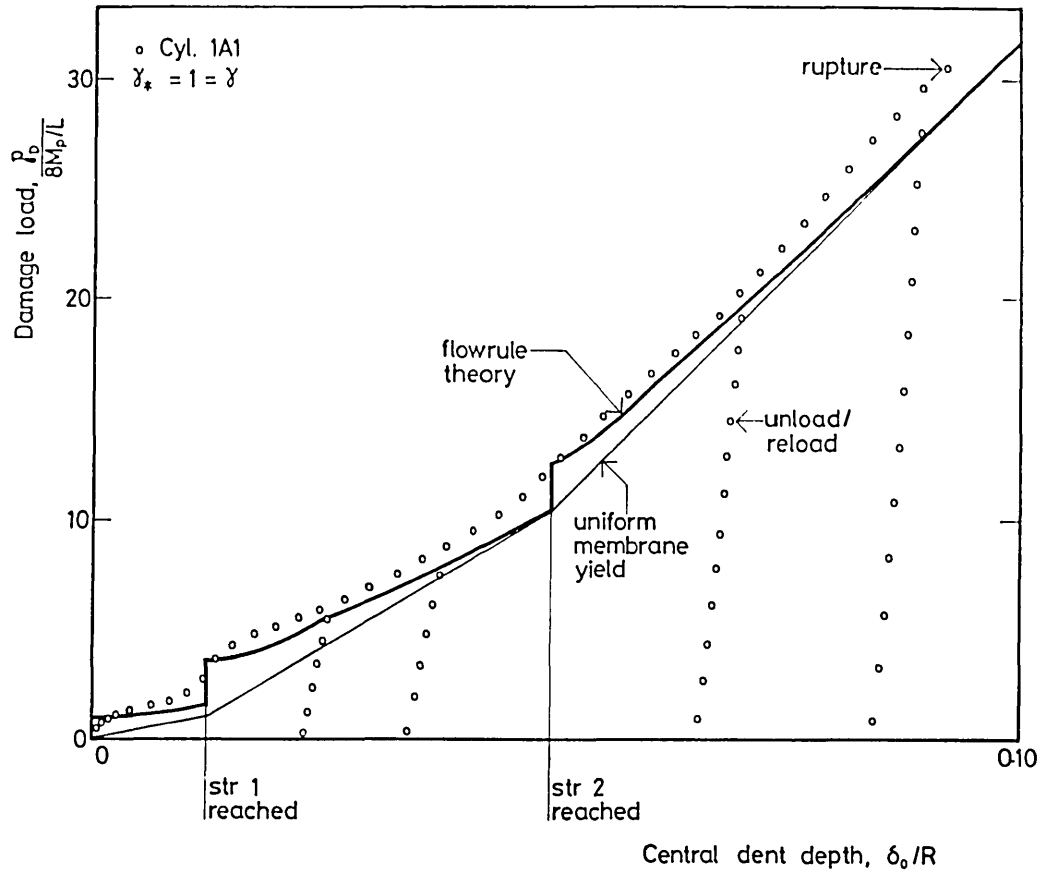


fig. 5.26
Theoretical and experimental lateral load - deflection relationship
Cyl. 1A1

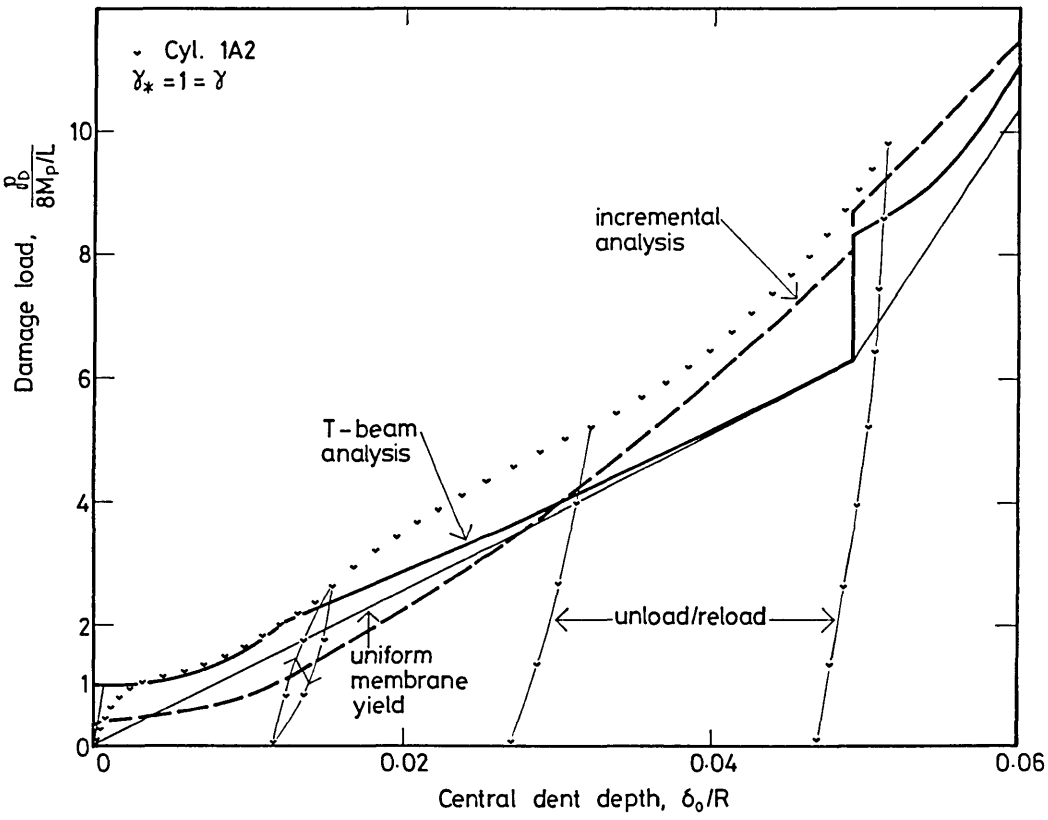


fig. 5.27
Theoretical and experimental lateral load - deflection relationship
Cyl. 1A2

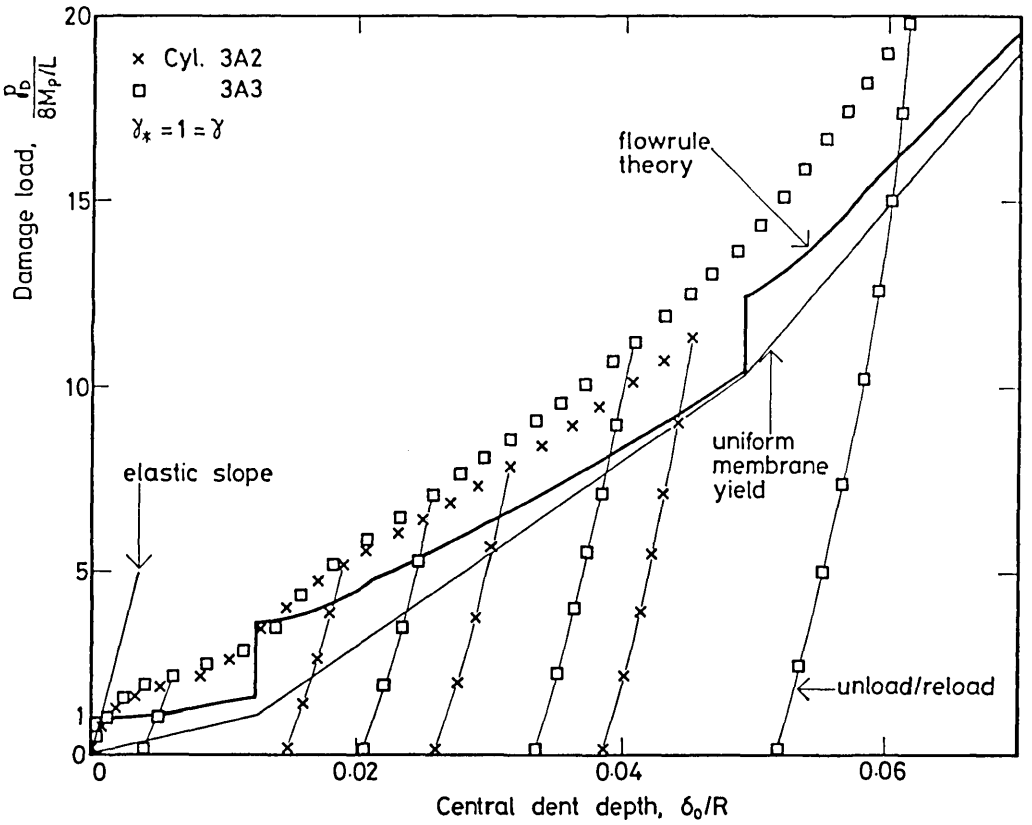


fig. 5·28
Theoretical and experimental lateral load - deflection relationship
Cyls. 3A2 and 3A3

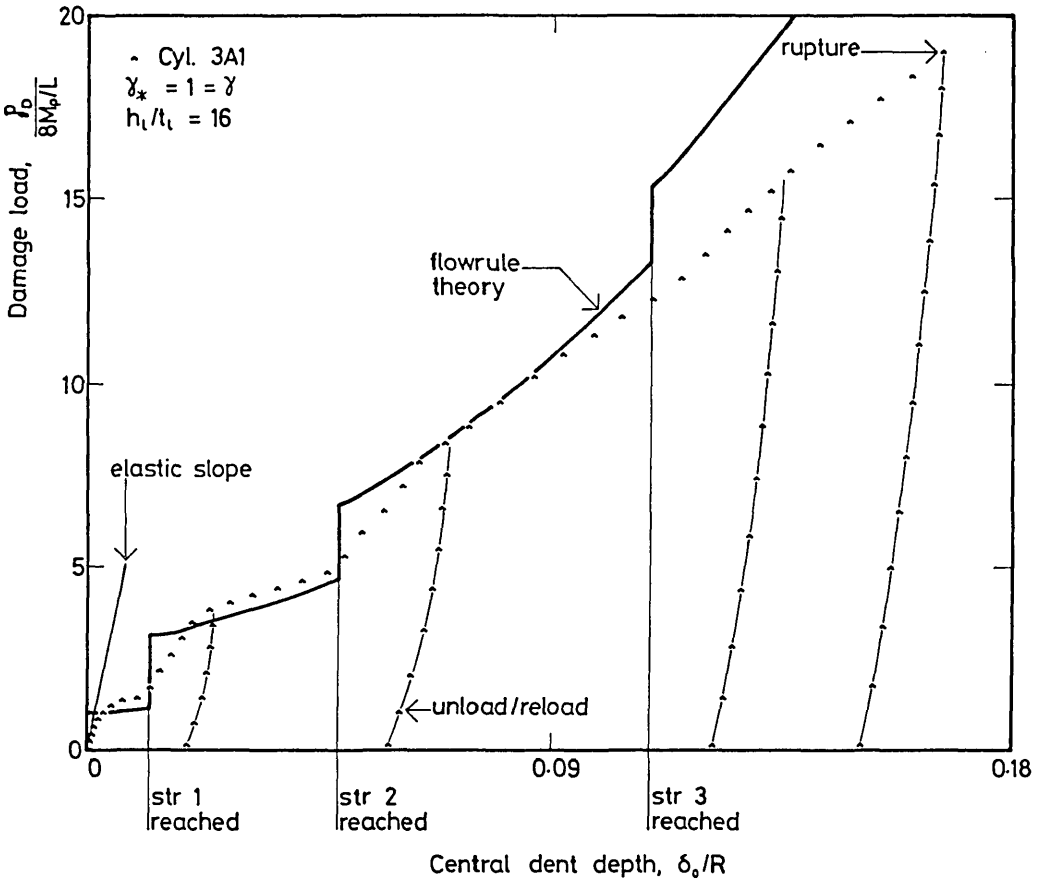


fig. 5·29
Theoretical and experimental lateral load - deflection relationship
Cyl. 3A1

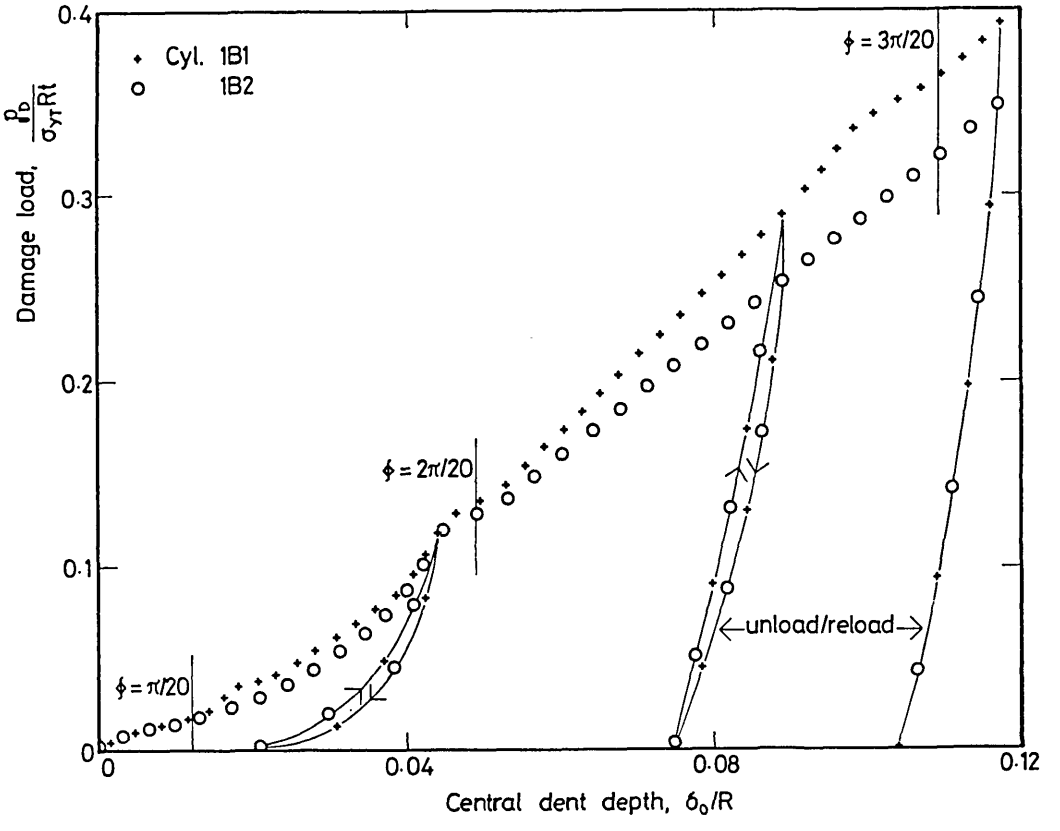
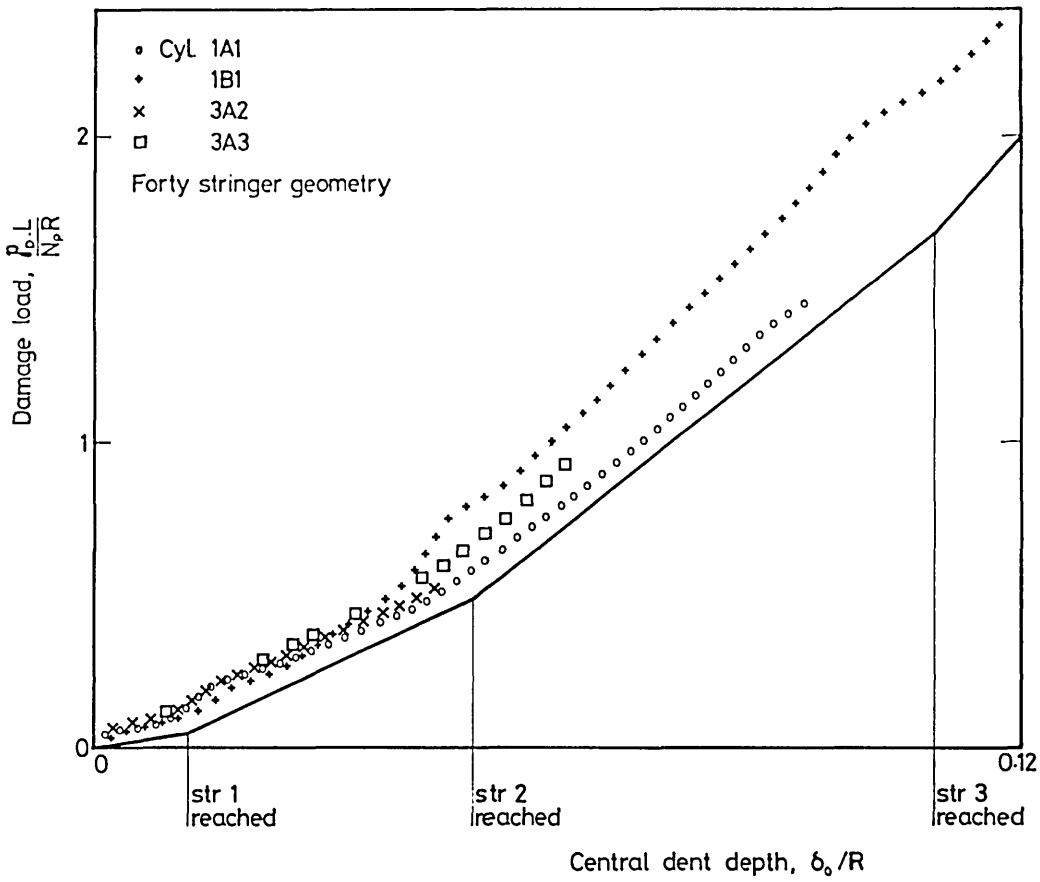


fig. 5·30
Theoretical and experimental lateral load - deflection relationship
Cyls. 1B



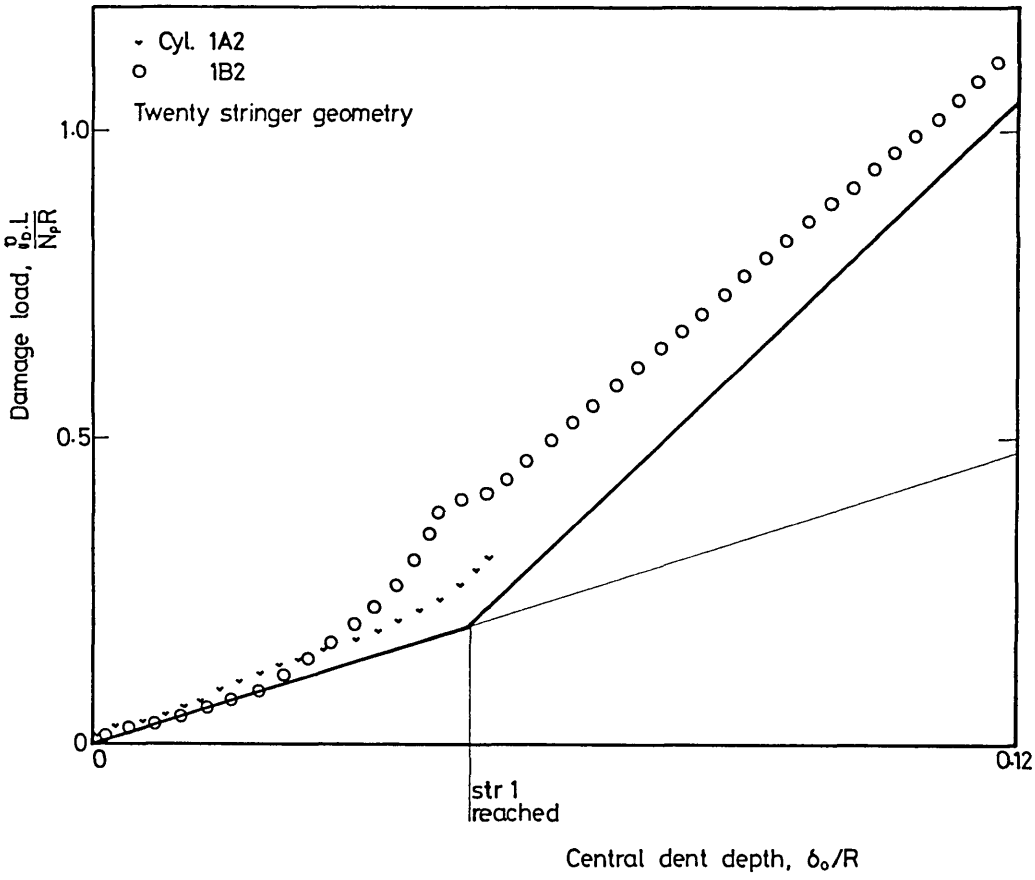


fig. 5·31 (a) and (b)
Simple membrane yield approximation of damage load response

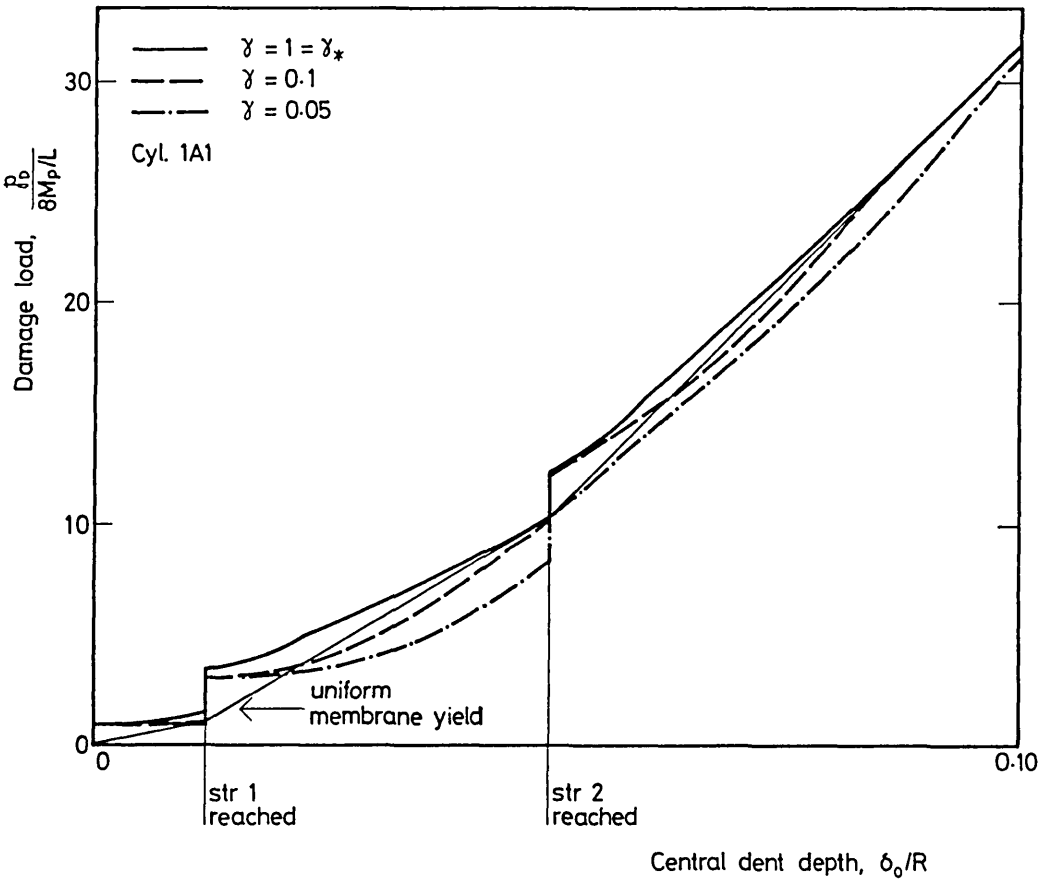


fig. 5·32
Variation of lateral load – dent depth response with support axial stiffness
Cyl. 1A1 geometry

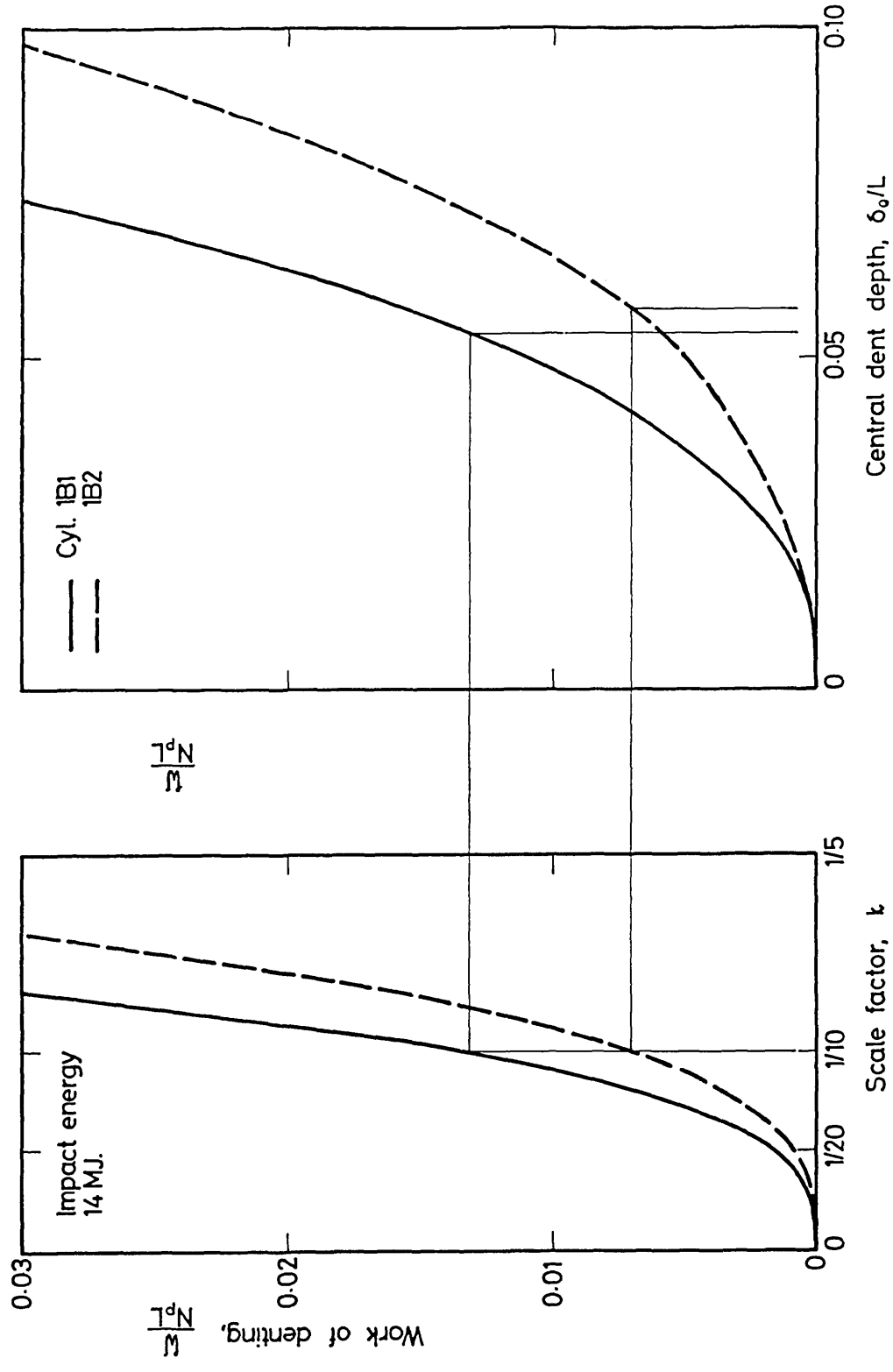


fig. 5.33
Relationship between dent depth and energy absorbed by cylinder
Cyls. 1B

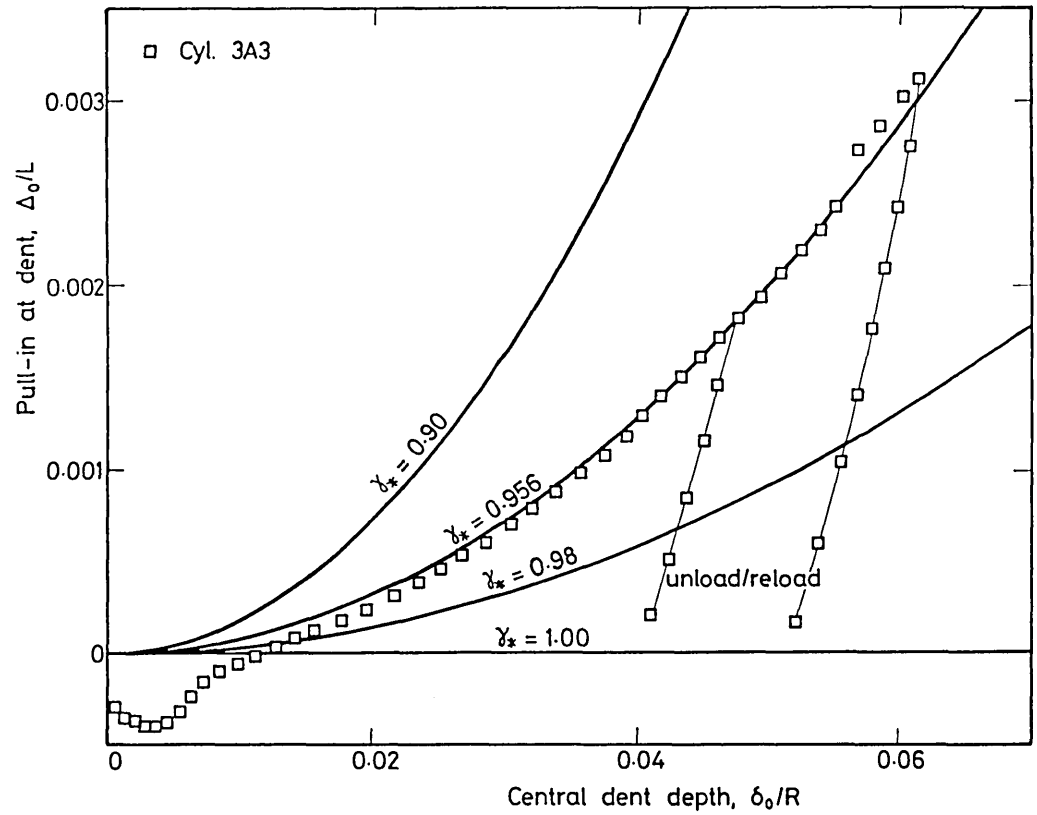


fig. 5.34
Axial pull-in at dent centre
Cyl. 3A3

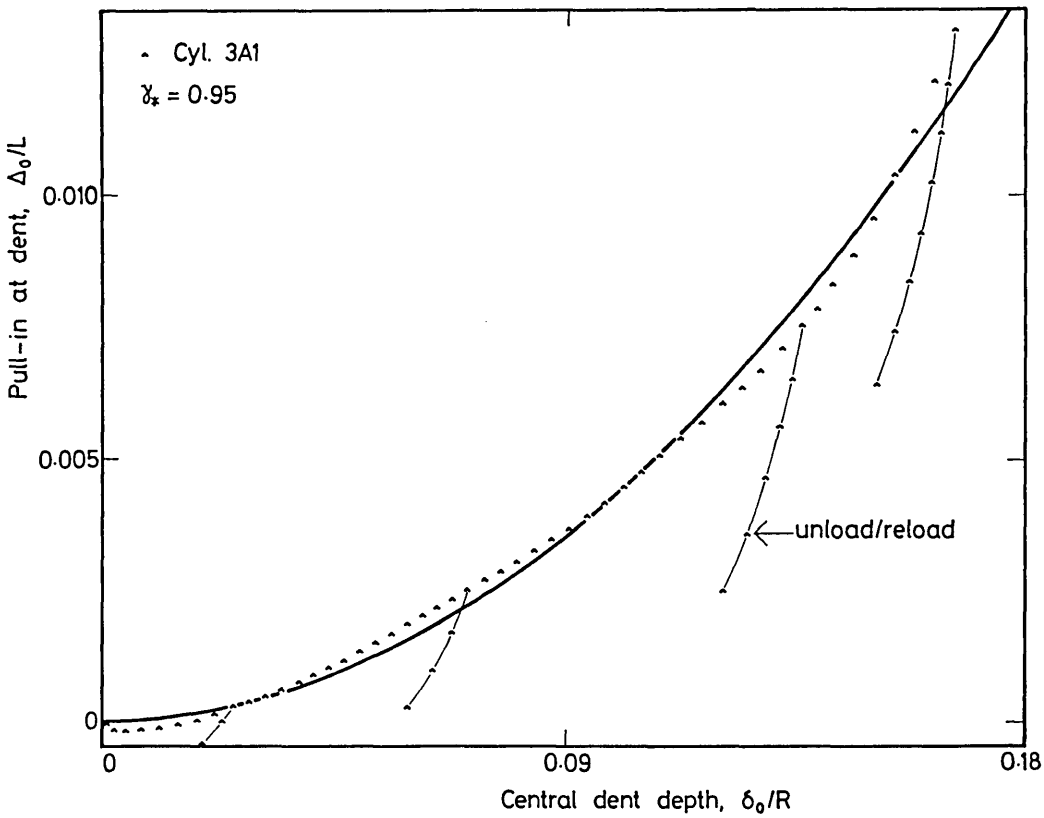


fig. 5.35
Axial pull-in at dent centre
Cyl. 3A1

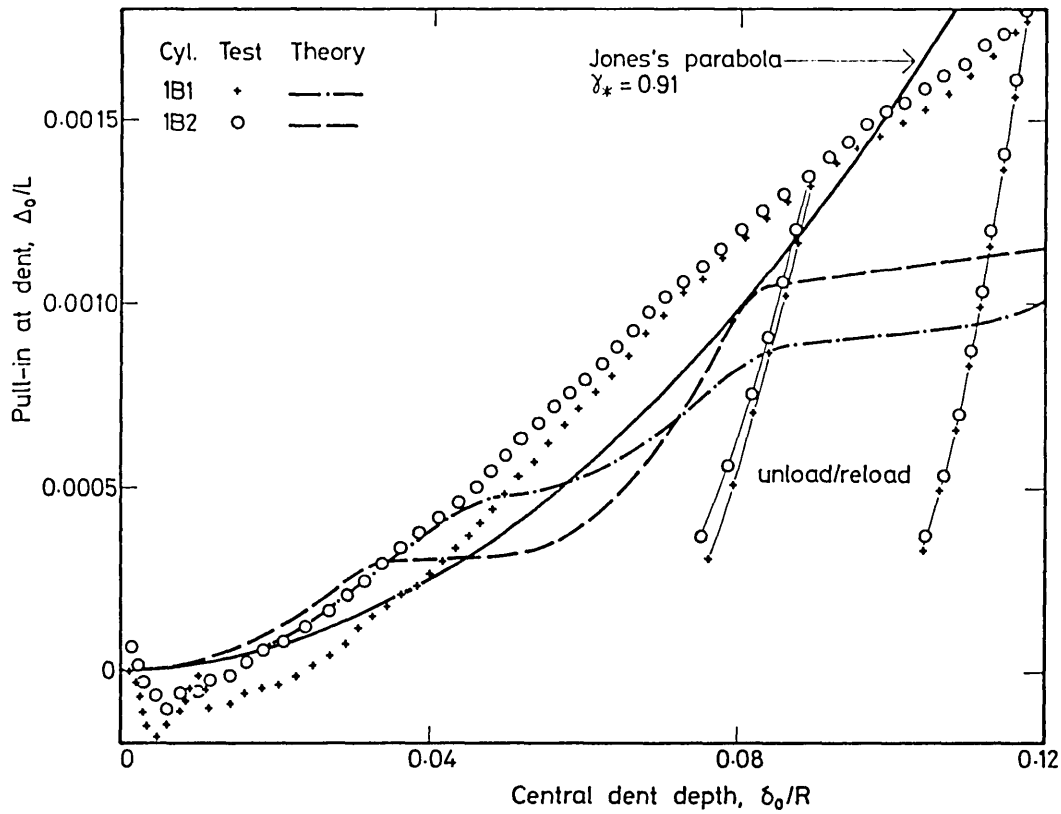


fig. 5·36
Axial pull-in at dent centre during lateral loading
Cyls. 1B

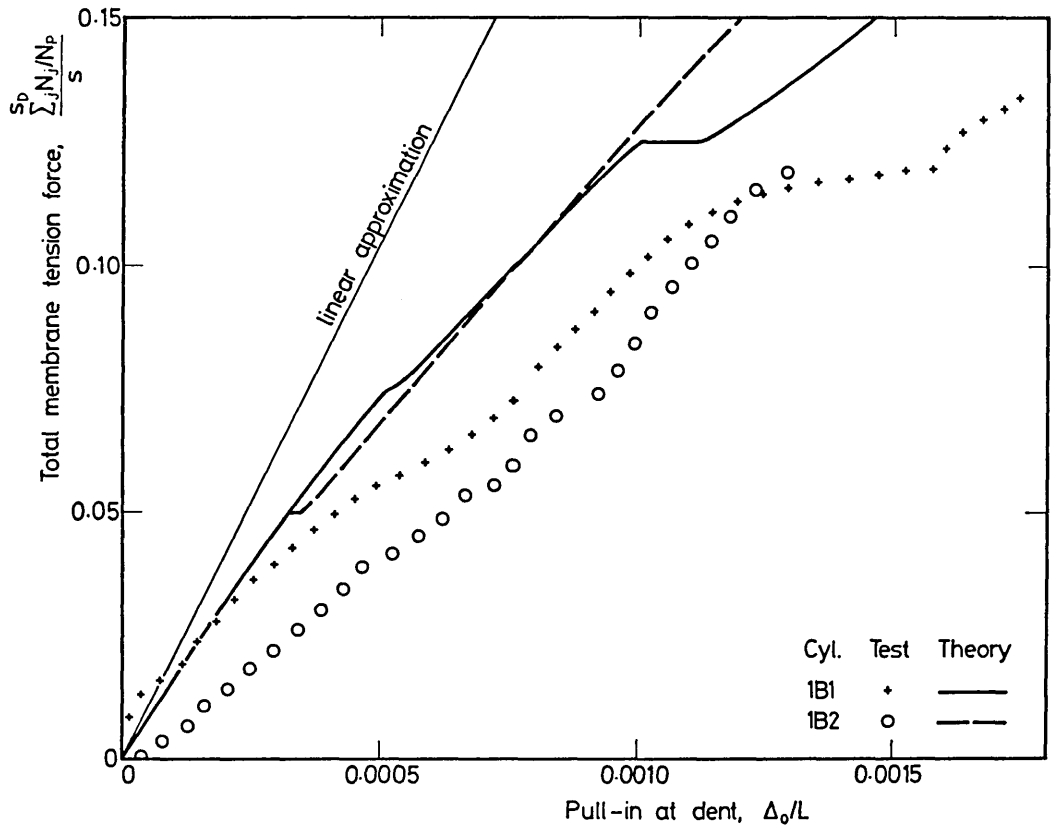
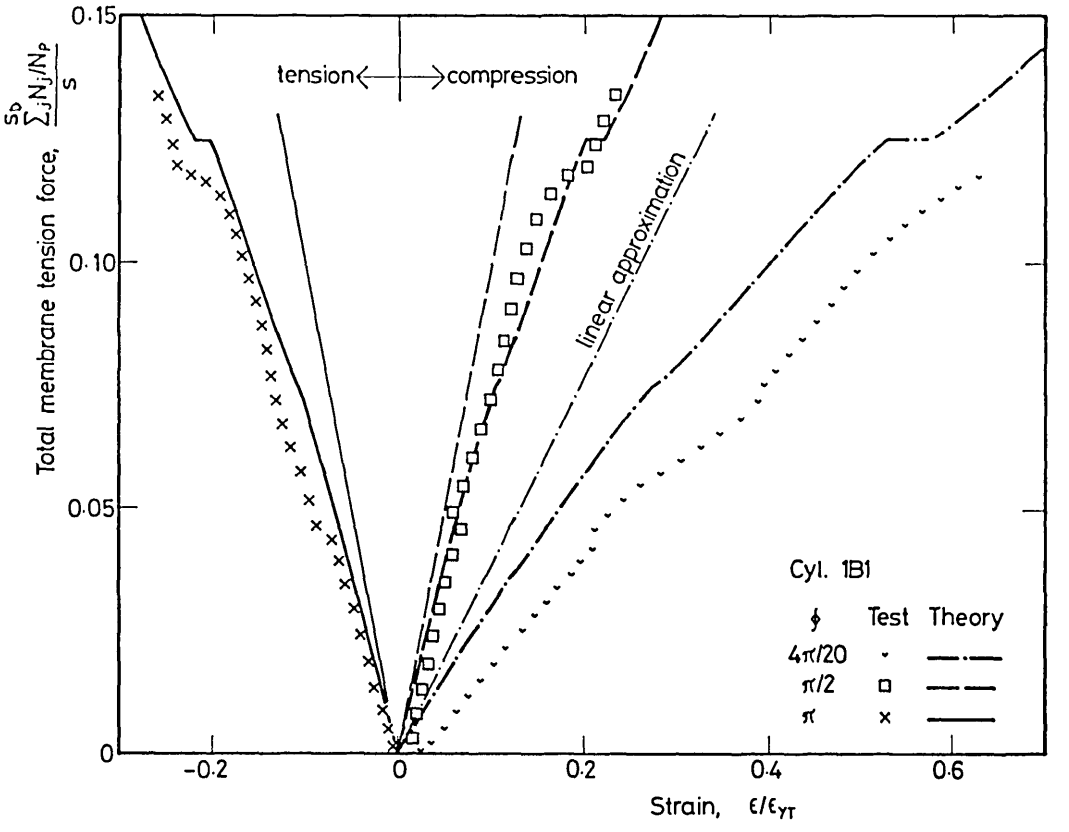


fig. 5·37
Axial pull-in at dent centre during lateral loading
Cyls. 1B



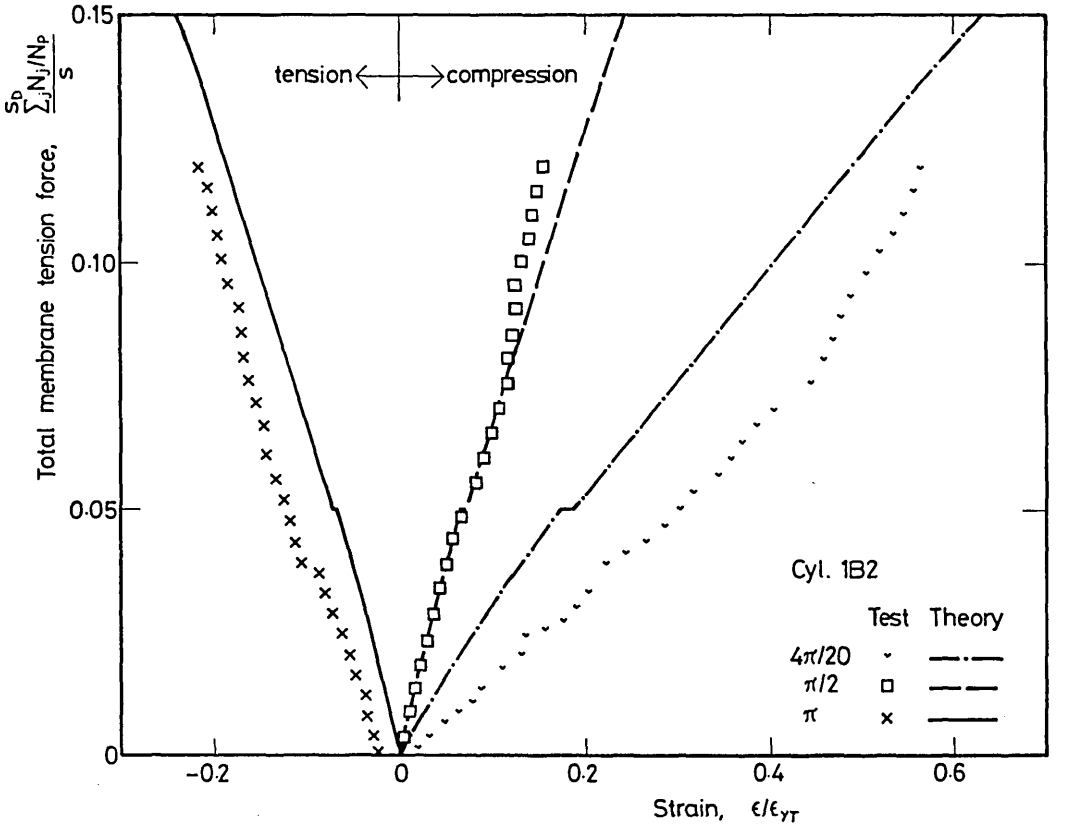
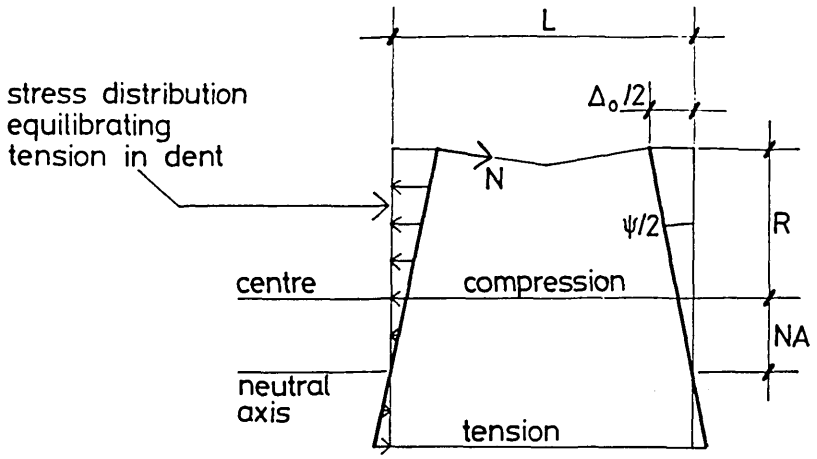
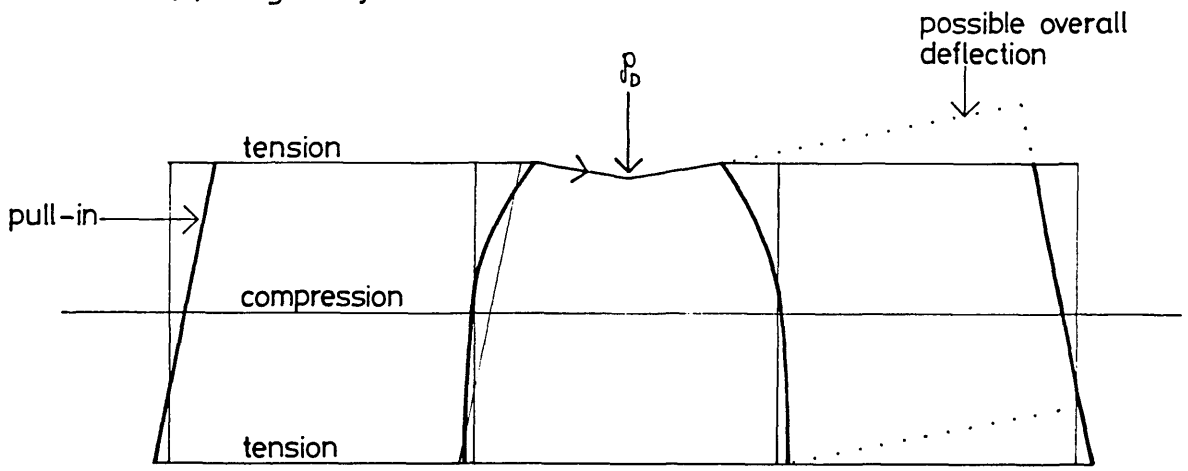


fig. 5.38 (a) and (b)
Strain distribution throughout section in terms of the tension force in the dent
Cyls. 1B



(a) single bay model



(b) three bay model

fig. 5.39
End rotation and pull-in during lateral loading

CHAPTER 6

LONGITUDINAL LOADING OF DENTED CYLINDERS

6.1 INTRODUCTION

The topic under consideration in this chapter is the residual strength of the cylindrical models dented without rupture as described in Chapter 5. First the method of compression testing is documented and this is followed by a qualitative description of the behaviour of each model. Quantitative details of the responses are presented after a corresponding analysis has been developed, to facilitate comparison between the two. Because the theoretical approach is analogous to a formulation by Rashed, Taby and Moan [120] for dented unstiffened tubes, a discussion of the similarities and differences between the methods is included. The chapter concludes with some comments on how a column with many bays might behave if it had a local dent.

6.2 LONGITUDINAL COMPRESSION TESTS

6.2.1 RIG ARRANGEMENT

The dented cylinders were crushed in a modified version of the circular frame used by Fahy [54] and Agelidis [1] for their cylinder tests. It is shown schematically in Fig. 6.1. The screw jack at the bottom was driven by a variable-speed electric motor through a low ratio gearbox which allowed very slow loading rates to be achieved. Load was applied by reaction against a cross-frame anchored to the laboratory strong floor. The rig was stiff enough to allow the post-collapse paths of most of the models to be followed accurately. Load measurement was achieved using three equilaterally arranged load cells which separated two 125mm thick plates and provided the

only support to the upper one. The cylinder was centrally located on a platen resting on this upper plate, with the dented region oriented vertically above one of the load cells. On top of the cylinder lay two more platens separated by a thick walled tube, and finally a 150mm diameter steel/PTFE spherical bearing which ensured concentricity of loading and allowed rotation of the model.

Such an end condition was intended to approximate the loading situation of a dented section within a longer column which has support restraints of reasonable flexibility. Also considered was an alternative arrangement of fixing the ends against rotation so that uniform longitudinal displacement was enforced. This was rejected, however. Not only would it have provided less satisfactory modelling of typical real components, but it would also have proven difficult to set up due to the small but varying initial rotation present in the dented models.

Lateral stability was ensured with the aid of three vertical columns which were clamped to the lower plate.

6.2.2 INSTRUMENTATION

6.2.2.1 STRAIN GAUGES

The strain gauges present during denting were reused during the axial loading test as only those in the most highly strained region along the dent centre-line were likely to have failed.

6.2.2.2 TRANSDUCERS

Three small linear transducers with 10mm travel were placed inside the model, close to the end rings and on the same radial lines as the load cells. They measured the relative displacement of the two end platens in contact with the cylinder. From this the model end shortening and rotation could be inferred. The wires from the transducers and internal strain gauges were passed through holes in the upper end platen and the wall of the thick tube to the external data logger.

A frame enclosing the model held a ring carrying forty 25mm travel Sangama linear transducers, arranged radially. These are photographed in Fig. 6.2. The ring could be moved vertically by turning the four threaded columns which supported it simultaneously through a chain and gear mechanism, using a winding handle. Cylinders were orientated so that the transducers coincided with the stiffeners in the forty stringer models, when the frame was in its "zero" position. However the frame could be rotated about the vertical axis and positioned, using a locating pin, at three successive angles of $\pi/80$. This enabled radial deformations at the quarter and mid-points of the panels to be read.

The same measuring frame was also used to obtain the shell surface readings before denting and compare them with a datum cylinder machined to a tolerance of ±0.0025mm on its diameter. The cylinders were measured from top to bottom at a particular angular rotation; between scans the ring was raised to the top and rotated to the next position. The sum of the squares of the differences between readings was minimized to determine the best-fit perfect cylinder and thus the initial imperfections of the real model from it.

Due to the depth of the dent the transducers in this region had to be moved in a little before the compression

test to ensure contact. This was of no concern as the dent geometry was known from the lateral loading test.

6.2.3 FINAL PREPARATION

When the model had been lowered onto its supporting platen and the internal transducers had been positioned, the upper platens and bearing were placed. The four quadrants of the radial transducer ring were then assembled. Instrumentation wiring was completed and checked. After scanning the cylinder to obtain a set of "initial" readings the transducers were raised to the dent centre. Just prior to testing the whole assembly was raised via the screw jack until the spherical bearing was brought into contact with the crosshead, whilst monitoring the load cells. Loading was then begun.

6.2.4 TESTING PROCEDURE

Load was applied in small increments, always less than 5kN. The step size was reduced as the models approached failure to ensure that nonlinearity in the response and the peak load were accurately recorded. The instrumentation was logged after each load increment. Generally the transducers were located at mid-span where the dent inclination changed abruptly. Before each reading all transducer rods in the dent zone were flicked in and out manually to check that they were still monitoring the deepest part of the dent, even though the cylinder length was decreasing. Complete scans of the model surface were taken only infrequently.

6.3 QUALITATIVE EXPERIMENTAL BEHAVIOUR

6.3.1 INTRODUCTION

General observations in the compression tests are discussed separately for each model, and compared with those of Fahy [54] and Agelidis [1] for nominally perfect stringer stiffened cylinders. Details of their models which have geometries similar to those in the present test series are given in Table 6.1 under their original names. For ease of comparison details of the dented models are also given in the same Table.

6.3.2 CYLINDER 1A2

Fig. 6.3 shows a nondimensionalized plot of experimental longitudinal compression load versus central end shortening for Cylinder 1A2. Central end shortening is defined as the longitudinal displacement at the centre of the formerly circular section. The theoretical lines also drawn in the Figure will be explained later in Section 6.5.1.

At the beginning of the test the response is significantly more flexible than expected. It is a result of nonuniform loading over the cross section caused by lack of planarity in the end bearing surfaces. This is discussed in Section 5.6.7.2. The effect is understandably much smaller in the nominally perfect cylinder tests of Fahy and Agelidis where every effort is made to make the ends flat and parallel.

After a few load steps the response becomes linear and remains so until just before peak load, when a very slight softening becomes apparent. During this linear

regime the dent bends inward, as expected, with the central stiffener deflecting a little less than the surrounding flexible panels. The restraint to bending provided by the undamaged stringer bordering the dent produces a localized dishing at each end of the circumferential dent centre-line, accompanied by outward bulging in the adjacent undamaged panel. The intermediate stringer twists in sympathy. An idealization of this mode of deformation is shown in Fig. 6.35. Most other panels also bulge out a little at mid-length, probably due to Poisson expansion, and the stringers bow just slightly inwards. Fig. 6.12, a typical set of prebuckling deflections at mid-span, illustrates all these effects.

Sudden unload occurs at collapse, too rapid for the rig to follow. Buckles form simultaneously in several panels around the dent, while the stiffeners remain essentially straight with no bowing. From the discussion in Section 2.13.3 unstable postbuckling is to be expected for the local failure of a number of these slender panels. The buckles are at mid-depth and alternately outward and in with corresponding twist in the stringers; similarity to the prebuckling deformations near the dent is obvious. Aided by the increased deflections the dent depth grows markedly, as shown in Fig. 6.13.

Further unloading is gradual and is followed by continuing to drive the screw jack. During each "load" step the axial load increases a little at first and then starts to fall when the current capacity is reached. Soon all panels have buckled. The rapid spread of buckling around the circumference is due to the small dent depth. As it occupies little of the circular section, relatively uniform stresses are maintained elsewhere.

Buckles on the side opposite the dent are closer to one end ring and several adjacent panels bulge out. This may be explained as follows. Poisson expansion constrained at the rings causes most of the cylinder length to barrel

out uniformly with high curvature near the ends. Combined with axial compression the maximum strains are likely to occur in the outer skin near the ends and so buckles here are understandable. Photographs in Fig. 6.18 taken outside and inside Cylinder 1A2 after testing is completed show the pattern of buckling.

The geometry of Cylinder 1A2 is very similar to Models 2 and 5 tested by Fahy [54]. They are nominally perfect and loaded concentrically, and at

$$ecc/R = 0.4 ,$$

respectively. In fact Model 5 is enjoying a second life as Cylinder 1A2. Pertinent details of the experimental behaviour of Fahy's models are summarized below.

Load increases linearly in Model 2 with simultaneous outward barrelling. The stiffness begins to decrease at

$$P_A/\Pi_P = p_A = 0.92$$

with sudden unloading occurring at

$$p_{A_B} = 0.96 ,$$

combined with alternate in and outward panel buckling right round the cylinder near one end ring.

Model 5 behaves rather as predicted by simple combined load theory:

$$\hat{\sigma} = P_A/A + M_A/Z \qquad (6.1)$$

where A and Z are the cross sectional area and elastic modulus, respectively, of the intact cylinder and $\hat{\sigma}$ is the stress at the critical location. Nonlinearity begins with first yield in the panel near the base at

$$\hat{\sigma}/\sigma_{YC} = 0.77 ,$$

and unloading, somewhat more gradual than in Model 2, occurs after failure at

$$\hat{\sigma}_{m}/\sigma_{YC} = 0.94 .$$

Initially only the critical location fails, but as postbuckling progresses panel buckles gradually extend around approximately two-thirds of the circumference. Again these are near the bottom end ring and alternately in and out.

It seems possible to conclude, therefore, that the eccentrically loaded cylinder collapses when the stress at the critical point reaches the failure stress of a uniformly loaded model with the same geometry. This behaviour is understandable as the slender panels have little capability of stress redistribution after first yield.

Another source of comparison with the test results is the numerical work presented by Harding and Dowling [65]. Using the method of finite differences they incorporate initial imperfections of various modes and magnitudes, and several types of flexural and membrane restraint along the boundaries. Longitudinal loading results are given for several three panel configurations with two intermediate stiffeners. The imperfections have the reasonably realistic "hungry horse" mode and are sized to just satisfy DnV tolerances [34].

For a geometry closely resembling Cylinder 1A2 the stress-strain curve of the central panel rises linearly but flattens out a little before peak load. Collapse occurs at

$$\sigma_{m}/\sigma_{YC} = 0.85$$

when the longitudinal edges are constrained such that they may move in-plane but must remain straight. In contrast, if these edges are fully restrained in position the strength is enhanced to

$$\sigma_u/\sigma_{yc} = 0.99 \ .$$

6.3.3 CYLINDERS 1B1 AND 1B2

The overall load versus deformation responses of Cylinders 1B1 and 1B2, differing only in their numbers of longitudinal stiffeners, are given in Fig. 6.4. After some initial "bedding in" the experimental plots are linear until slight softening occurs before the maximum load is attained. The gradient of Cylinder 1B2 is a little flatter than 1B1, perhaps due to Euler bending in this very slender model. During loading localized pull-in develops at the dent edges to accomodate the inward bending of all damaged fibres, together with an outward bulge in the adjacent undamaged strip and then an inward bulge in the region beyond that. The light stringers are included in these radial deformations.

Collapse is signalled by an audible bang and sudden growth of the aforementioned inward bow on one side of the dent. Figs. 6.14 and 6.16 show the distribution of radial deformations at mid-span just after peak load. The buckles extend around a small part of the surface only; uniform barrelling is apparent opposite the dent. Corresponding illustrations of the prebuckling deformations are not included as they are qualitatively similar to these, except in the depth of the inward bow.

Unlike Cylinder 1A2, there is no dramatic unloading at failure. With further axial deformation the postbuckling curves continue to be relatively flat, although several small jumps are discernable, particularly

for Cylinder 1B1. The jumps correspond with the development of other inward buckles, firstly on the other side of the dent and then further round the circumference. In this type of failure the buckles are prone to be inward because otherwise circumferential stretching of the shell plating would be necessary [108].

The final buckling patterns, containing eight full waves, are seen in Figs. 6.15 and 6.17. The major inward buckles are numbered in order of formation and these numbers are also located on the post-collapse curve. The dominating buckles are diamond-shaped and the dent region, which is largely rectangular before longitudinal loading commences, also takes on a slightly diamond-like appearance. The upper photographs in Figs. 6.19 and 6.20, of Cylinders 1B1 and 1B2 respectively, show the pattern.

Cylinders 1B1 and 1B2 are the same as Agelidis' undamaged Models E and A respectively [1], the only difference being in the marginally longer clear span produced by attaching different end rings. Both "nearly perfect" models have straight line loading responses with slight nonlinearity at higher loads. Peak load occurs at

$$p_{A\blacksquare} = 1.17$$

for Model E and

$$p_{A\blacksquare} = 0.81$$

for Model A, the values being slightly different from those quoted by Agelidis due to his alternative definition of compressive yield stress:

$$\sigma_{YC} = 1.1\sigma_{YT} \ .$$

There is no clear reason for the very high strength of Model E; indeed it is quite remarkable for a stringer geometry where

$$\frac{N_E}{N_P} = 4\pi^2 \frac{E}{\sigma_{YC}} \frac{I}{AL^2} = 0.69 .$$

Here N_E is the Euler buckling load for a stringer beam with encastre ends. For Model A the ratio N_E/N_P has a value of 0.40. Both values are of course four times smaller still if simple supports are assumed in computing the buckling load. This illustrates the high level of transverse restraint given to the stringer beams by the cylindrical skin, which makes the longitudinally stiffened shell a very efficient structural unit in compression.

Collapse brings a buckling pattern with nine circumferential waves in Model E and ten in A. (The slightly lower number of waves in the damaged cylinders is due to the inward bow at the dent being spread over more panels than would occur without the imperfection.) There is a dramatic load drop immediately after peak load, which is understandable as there is no strength reserve after buckling in a general mode. However the subsequent postbuckling response is fairly flat and all four cylinders retain a similar and significant strength.

Agelidis actually classes Model A as a local shell failure. The radial transducer readings show that the stiffeners remain essentially straight through most of the loading path and the first sign of distress is one of the panels popping inward, prior to maximum load. As the load increases again the buckle grows to form one of the waves and the stringers begin to bow. In contrast, stringers in Model E deflect from the commencement of loading, as they do in Cylinders 1B.

6.3.4 CYLINDERS 3A2 AND 3A3

Cylinders 3A2 and 3A3 have the same cross section and central bay length but different dent depths. Their longitudinal load versus deflection plots are given in Figs. 6.5 and 6.6. The early nonlinearity is much less pronounced for these three bay models because the undamaged end bays moderate the initial end ring curvature generated by the residual strains. After the usual linear response both models exhibit increasing flexibility to peak load and then gradual load fall off, all transitions following a smooth curve.

Photographs in Fig. 6.22 show part of the well developed pattern of buckles formed in Cylinder 3A3, with the characteristic inward bow in the damaged region, which includes the stringer running along each edge of the dent, accompanied with outward and then inward bulges in the next two panels. Twist of the stringers to suit these buckles is clearly apparent.

Theoretically, the two likely first yield locations are the outer skin near the rings due to the curvature induced by Poisson outward barrelling, and the stringer tip near mid-span. Because the dent, and the deflections induced by it, are at mid-span the latter is encouraged near the damaged region. Yielding then spreads through the stringer to produce ductile behaviour and buckling occurs after the plastic strains reach the panel. Unloading is gradual due to the stocky geometry.

The radial transducer bank positioned at mid-span indicates that elsewhere on the circumference the outward barrelling present before buckling is still existent. What the buckles do, in fact, is move gradually away from the centre-line further around the cylinder, lying closer to the lower ring frame on one side of the dent and on the other side migrating upwards and eventually crossing the

ring frame to lie just inside the end bay. The pattern is alternately in and outward at first but becomes predominantly outward bulging further away from the dent.

Cylinder 3A2 behaves differently. In this model the outward bulges in each of the panels adjacent to the dent are inclined towards the upper end ring and partnered by outward bulges near the centre of the top bay in the same panels. Generally in and out buckling continues most of the way around each side of the model, progressing towards the top end ring. Fig. 6.21 gives views of the pattern outside and inside the model.

Comparison with Cylinder 3A3 shows that in spite of Cylinder 3A2 having a smaller dent depth, this end bay failure occurs at lower load than the collapse of Cylinder 3A3. It is very probably due to flaws produced during fabrication, as mentioned in Section 5.3.4. Hence the failure of Cylinder 3A2 is classed as premature.

Models 1 and 4 of Fahy's tests and Agelidis' Model 1 have similar geometry to the central bay of Cylinder 3A3 and so their responses may profitably be compared. Examples of buckling both at mid-span and near an end ring occur.

The barrelling of Agelidis' model at low load becomes, at collapse, an outward bulge right round the the circumference near the bottom end ring. This mode is promoted by the end ring detail. Because the panels all deform more than the stringers it is classed as local shell buckling. The failure at

$$p_{AB} = 1.01$$

is soft with gradual load fall off and considerable postbuckling strength.

Fahy's Model 1 is compressed concentrically whereas Model 4 is loaded at eccentricity

$$ecc/R = 0.25 .$$

With Model 1 first yield occurs near the base in the panel at

$$p_A = 0.81 .$$

At

$$p_A = 0.89$$

the stiffener tips at mid-span begin to yield, and collapse occurs at

$$p_{Am} = 0.96 .$$

In Model 4 the stiffener outstand at the critical point yields at mid-span when

$$\hat{\sigma}/\sigma_{YC} = 0.85 .$$

At failure the strain here is calculated, from Eqn. (6.1), to be

$$\hat{\epsilon}_m/\epsilon_{YC} = 1.07 .$$

Thus collapse is delayed somewhat in comparison with the concentrically loaded cylinder because the stocky geometry allows a degree of stress redistribution to occur. In both Fahy's cylinders panel buckles develop at mid-span and the slope of the postbuckling path is gradual. Although all panels buckle almost instantaneously in the concentrically loaded cylinder, with Model 4 only the critical panel buckles initially. Failure gradually spreads outwards from the critical location as postbuckling continues, concurrent with elastic unloading

on the opposite side of the model to maintain equilibrium. Unloading eventually causes this opposite side of the model to lift off the platen.

Results relevant to Cylinder 3A3 may also be obtained from the finite difference analyses discussed by Harding and Dowling [65]. For a three panel model with very similar geometry to Cylinder 3A3, collapse is predicted to occur at

$$\sigma_a/\sigma_{yc} = 0.95$$

when the longitudinal edges are constrained to remain straight.

6.4 THEORETICAL ANALYSIS

6.4.1 INTRODUCTION

Vital to the following is the observation that all Fahy's and Agelidis' models load linearly with the stiffness expected of stub columns and exhibit capacities close to squash load. The only exception is the very slender geometry of Agelidis' Model A. This suggests the application of elementary combined load theory to the present dented cylinders without including second order effects.

6.4.2 SINGLE BAY MODELS

6.4.2.1 EFFECTIVE SECTION

As a first step in the analysis a single damaged bay is considered. Under compressive loading bending accompanies axial contraction in the dented region of this bay. Residual stresses are also present, of the same sign as those caused by the longitudinal loading. Thus the dent zone is very flexible axially and may reasonably be ignored. This assertion is supported by the results of the test discussed in Chapter 4, namely compressive loading of a dented stiffened plate. A prototype member might be further affected by the presence of other residual stresses, for example, those due to welding.

Conversely, the knife edge loading produces no significant radial deflections outside the dent zone that could reduce the axial stiffness of the undamaged region. Thus an effective section comprising all the undamaged material is assumed to dictate the overall end shortening response. The section is illustrated in Fig. 6.23(a) and this Figure includes much of the notation used below. Fig. 6.23(b) represents a quite different approach, discussion of which is left until Section 6.6.

The effective section properties may be estimated in several simple ways. Probably the best approach for the cylinder geometries under discussion in this dissertation is to assume the stringers are smeared to produce a shell of uniform equivalent thickness, t_e. Treatment as a thin arc gives the following results, which are adopted throughout this work:

$$a_e/a = 1 - \eta/\pi \qquad (6.2)$$

$$I_e = 2\int_{\eta}^{\pi} (y + \bar{y})^2 dA$$

where

$$\cos\phi = y/R$$

$$dA = t_e R d\phi$$

and ϕ is the angle between radii to the coordinate on the cylinder and the dent centre. Thus

$$I_e/A_e R^2 = \tfrac{1}{2} - \tfrac{1}{4}\sin 2\eta/(\pi-\eta) - (\bar{y}/R)^2 \ . \qquad (6.3)$$

Here

$$\cos\eta = 1 - \delta_{DD}/R$$

$$\bar{y}/R = \sin\eta/(\pi-\eta) \ . \qquad (6.4)$$

An alternative method considers individual stringer beams, giving

$$A_e/A = s_U/s$$

$$I_e/A_e R^2 = (1/s_U).\sum_j^{s_U} \cos^2\phi - (\bar{y}/R)^2 \qquad (6.5)$$

$$\bar{y}/R = \left|(1/s_U).\sum_j^{s_U} \cos\phi\right| = (1/s_U).\sum_j^{s_D} \cos\phi$$

where

$s = s_D + s_U$

$A = sA$

$A = A_p + A_t$ = cross sectional area of stringer beam.

For simplicity this formulation neglects the second moment of area of each stringer beam about its own centroidal axis. The relevant axis lies parallel to that of the overall section and so is at varying angles to the principal axes of the stringer beam.

Eqns. (6.3) and (6.5) are compared in Fig. 6.24 for a twenty stringer configuration. For denser stiffening the relationship is obviously closer as the steps inherent in Eqn. (6.5) become smaller and more frequent.

A more accurate compromise between the aforementioned approaches is to treat the continuous skin and discrete stiffeners separately using the first and second alternatives, respectively. However this furnishes results almost identical with Eqn. (6.3).

6.4.2.2 MECHANICS

A longitudinal force acting on the effective section produces a uniform component of end shortening given by

$$\frac{\Delta_u}{L} = \frac{P_A}{E a_e} \quad . \qquad (6.6)$$

It is implicitly assumed here that the cylinder is free to dilate, producing tensile hoop strains but negligible hoop stresses. Both the experimental and numerical stiffness results achieved by Agelidis [1] show such behaviour. This demonstrates that the radial restraint provided by the end rings is very localized and has little bearing on the overall response.

In contrast, the stiffnesses of Fahy's concentrically loaded models [42] seem to be better described using an effective panel width of $A_p/(1-\nu^2)$, which allows for hoop restaint in the cylinder skin. However his eccentrically loaded tests do not exhibit this enhanced stiffness. As the models in the present test series are also subjected

to bending moment the simple uniaxial stiffness assumption of Eqn. (6.6) seems applicable.

The bending moment acting is

$$M_{\bar{y}} = P_A(\bar{y} - ecc)$$

where ecc denotes the eccentricity of the load from the centre of the perfect cylinder, on the diameter passing through the dent centre-line. Positive ecc and $\bar{y}$ both occur on the opposite side of the cylinder centre to the dent, as illustrated in Fig. 6.23(a). The moment causes rotation ψ about the centroidal axis, which is related to the bending curvature by

$$\frac{\psi}{L} = \frac{M_{\bar{y}}}{EJ_e} .$$

The total end shortening at the cylinder centre is thus

$$\frac{\Delta_A}{L} = \frac{\Delta_{\bar{y}}}{L} + \frac{\psi\bar{y}}{L} .$$

Rearrangement gives

$$\frac{\Delta_A}{L} = \frac{p_A}{E}\sigma_{yc}\left[1 + \frac{(\bar{y}/R - ecc/R)\bar{y}/R}{J_e/A_eR^2}\right]\frac{A}{A_e} \qquad (6.7a)$$

$$= \frac{\psi R}{L}\left[\frac{J_e/A_eR^2}{\bar{y}/R - ecc/R} + \bar{y}/R\right] . \qquad (6.8a)$$

The stress distribution around the effective section that results from the combined loading is

$$\sigma = P_A/A_e + M_{\bar{y}}(y + \bar{y})/J_e$$

that is

$$\frac{\sigma}{\sigma_{yc}} = p_A\left[1 + \frac{(\bar{y}/R - ecc/R)(\bar{y}/R + \cos\phi)}{I_e/A_e R^2}\right]\frac{A}{A_e} \qquad (6.9)$$

Following on from Fahy's eccentric loading tests, this elastic distribution is assumed to remain valid until the stress in the undamaged region next to the dent reaches the failure stress of a uniformly loaded undamaged cylinder with the same geometry. This heralds collapse. The critical location may be considered to be either

$$\phi = \eta ,$$

or the first undamaged stringer, both giving very similar results. Thus

$$\frac{p_{Am}}{\sigma_m/\sigma_{yc}} = \Omega \qquad (6.10)$$

where

$$\Omega = 1/\left[1 + \frac{(\bar{y}/R - ecc/R)(\bar{y}/R + \cos\eta)}{I_e/A_e R^2}\right]\frac{A}{A_e} .$$

The undamaged capacity is assumed, for simplicity, to be

$$\sigma_m/\sigma_{yc} = 1$$

for all models except Cylinder 1B2, where

$$\sigma_m/\sigma_{yc} = 0.81$$

from the results of Agelidis' Model A.

The residual stresses introduced throughout the model by the denting process are discussed in Section 5.6.7.2. The axial force diagrams, Fig. 5.15 for example, indicate that such stresses are small near the critical location, especially after the end blocks are removed. No account,

therefore, is taken of them in determining the maximum applied stress levels.

6.4.2.3 LOAD ECCENTRICITY

It is implied in the previous Section that the longitudinal loading might have eccentricity. The actual eccentricity in each test is found from the group of three load cell readings in every loading increment, and two typical sets of results are presented in Fig. 6.25.

Initially the eccentricity of loading from the centre of Cylinder 1A2 is relatively large, whereas that of Cylinder 3A2 is negative, that is, toward the dent. This erratic behaviour is seen in the other tests too. It may be explained by remembering the convex curve of the end rings, induced by the residual strains at the end of the denting tests; the top platen might readily incline slightly either way when placed on the model, depending on the precise shape of the convexity.

When, after a few load steps, the curve is pressed out, the eccentricity settles to a small positive value in all tests. This is despite the spherical bearing being located centrally in the rig. Its point of contact with the platen is a little off-centre in the direction away from the dent because the end rings are still aligned at a relative angle inwards toward the damage. A similar effect is indicated by Fahy's eccentrically loaded tests. In his models the rotation resulting from the bending moment appears to cause the point of contact of the bearing to move "uphill" slightly and thus reduce the eccentricity.

Nearly constant eccentricity is maintained until buckling, when it increases rapidly along with the rotation. The steady prebuckling eccentricity for each cylinder is quoted in Table 6.2.

6.4.3 THREE BAY MODELS

If only part of the cylinder length is dented (the three bay models tested here are examples) deformation of the intact portions must also be considered.

The inner end of each undamaged length sees the stress distribution generated in the dented bay. It has the shape drawn in Fig. 6.23(a). The highest stresses are immediately adjacent to the dent and they taper downwards as $\phi = \pi$ is approached. The outer end of the model is subjected to point loading at small eccentricity, as described above. Acting on an undented section, the location of the eccentricity suggests a stress block sloping in the opposite way. Redistribution must therefore take place along the length of intact bay. The simplest conclusion which may be drawn is that the two stress systems counteract each other; that is, the total longitudinal shortening resulting from the stresses is approximately uniform over the section, with magnitude

$$\frac{\Delta_U}{L_U} = \frac{P_A}{Ea}$$

where L_U is the length of undamaged cylinder.

The end shortening of the complete model resulting from this inference is thus

$$\frac{\Delta_A}{L_t} = \frac{p_A \sigma_{YC}}{E}\left[\left[1 + \frac{(\bar{y}/R - ecc/R)\bar{y}/R}{I_e/a_e R^2}\right]\cdot\frac{a}{a_e}\frac{L}{L_t} + \frac{L_U}{L_t}\right] \qquad (6.7b)$$

$$= \frac{\psi R}{L_t}\left[\frac{I_e/a_e R^2}{\bar{y}/R - ecc/R}\cdot(1 + (L_U/L)(a_e/a)) + \bar{y}/R\right] \cdot \qquad (6.8b)$$

Here

$$L_t = L + L_U$$

is the overall cylinder length. Naturally these equations simplify to their counterparts, Eqns. (6.7a) and (6.8a), when $L_U = 0$.

The postulate that undamaged bays compress uniformly has no bearing on Eqn. (6.7b) as any rotation which may occur in these bays does not alter the central end shortening. Only Eqn. (6.8b) is affected because rotation is made an explicit parameter.

6.4.4 MODIFICATION TO ACCOUNT FOR END RINGS

An adjustment to Eqns. (6.7) and (6.8) is required to enable comparison with the test results. In the experiments transducers measure the displacement of the platens which sandwich the model and its end rings, whereas the analysis considers the shortening of the clear length only, between end rings. The contribution of the supports must, therefore, be incorporated. At each end ring the cylinder experiences radial restraint, causing compressive hoop stresses. These reduce the strain in the axial direction produced by the axial stress.

Agelidis [1] makes different assumptions concerning the axial stress in each of two end ring details. Both types of end condition are described in Section 5.2.4. For the arrangement which causes the compression rig to apply axial load to the end ring, good correlation with experiment is found by considering the load to be transferred to the cylinder by uniform shear through the ring thickness, giving an average axial stress there of half the total value in the cylinder. If, on the other hand, the load acts directly on the cylinder because its ends extend slightly beyond the rings, the axial stress equals the applied stress.

A third end ring configuration is used in the present test series. The cylinder is loaded via the rings, suggesting the former assumption, and so the axial shortening within the total thickness L_s of both end rings is given by

$$\frac{\Delta_s}{L_s} = \tfrac{1}{2}(1-\nu^2)\frac{\sigma}{E} .$$

Here σ is the axial stress in the cylinder. The modifying factor $\frac{1}{2}$ disappears from the above equation if the second of Agelidis' assumptions is employed.

For single bay models σ is defined by Eqn. (6.9). The distribution of stresses in the end rings is assumed to mirror that in the adjacent cylinder material, which is quite logical as little redistribution could be expected to occur in the circumferential direction over such a short length. The end rings thus behave in keeping with the dented section and give it an extra effective length of $\frac{1}{2}(1-\nu^2)L_s$.

In consequence the stiffness of the longitudinal load versus end shortening response in Eqn. (6.7a) decreases by factor

$$1/[1 + \tfrac{1}{2}(1-\nu^2).L_s/L] . \qquad (6.11)$$

The ratio of end shortening to rotation in Eqn. (6.8a) is unaffected, of course, as both deformations are adjusted in the same proportion.

The situation is somewhat different for the three bay models. In these cases the behaviour of the end rings is governed by the stress distribution in the outer undamaged bays, which results in an increase in the effective length of intact cylinder. Reference to Eqns. (6.7b) and (6.8b) shows that both relationships are thereby influenced.

The applicability of Agelidis' ideas to dented cylinders might well be called into question. As the models are no longer axisymmetric the hoop stresses will be modified. However it is apparent that different assumptions concerning the degree of radial restraint and the variation of axial stress within the end rings bring little variation to the results, and that only a small portion of the total axial shortening occurs at the supports. Thus an approximate treatment of end ring behaviour is adequate.

6.5 THEORETICAL CORRELATION

6.5.1 OVERALL LOAD AND DEFORMATION CHARACTERISTICS

The applicable version of Eqn. (6.8) with an adjustment for the end rings, where appropriate, gives an excellent approximation to the prebuckling experimental ratio of end-shortening to rotation, for all models. This is shown in Figs. 6.7 to 6.11. The deflection ratio later decreases markedly to a new roughly constant value. The change occurs just prior to peak load for the slender cylinders. However stress redistribution ability in the stocky Models 3A2 and 3A3 delays maximum load until significantly after the stiffness change. Other lines drawn in Fig. 6.7 indicate the sensitivity of Eqn. (6.8) to the dent depth.

This linear growth in rotation from the outset of loading is in direct contrast to the behaviour of dented unstiffened tubes [120]. These are assumed to compress uniformly at low loads as the entire cross sectional area is considered to be effective.

Eqn. (6.7a), incorporating the end ring reduction factor defined by (6.11), is plotted in Figs. 6.3 and 6.4.

Two alternative factors are also included for comparative purposes in Fig. 6.3. For the line labelled 3 the factor is an opposite extreme of that in (6.11); namely, radial restraint is neglected and the axial stress is assumed to be invariant through the end ring thickness. In line number 2 no account at all is taken of the end ring. The factor in (6.11), which is included in the emphasized line 1, gives the best agreement with the experimental stiffness. The divergence of the three examples is much less distinct for the other models as the end rings occupy significantly smaller proportions of the overall length.

Eqn. (6.7b), with its pertinent end ring modification to give a larger undamaged length, is drawn in Figs. 6.5 and 6.6. It may be concluded from all the models that only the very slender Cylinder 1B2 is more flexible than predicted by Eqn. (6.7), and this is probably due to second order elastic deflections.

In Figs. 6.3 to 6.6 the lines defined by Eqn. (6.7) terminate at the peak load found from Eqn. (6.10) when the undamaged cylinder capacity is reached at the critical location. For Cylinder 3A3 the experimental strength is a little higher than the theoretical limit because the section is stocky enough to allow stress redistribution. However all other predictions overestimate the test results. This is attributed to premature failure in an end bay for Cylinder 3A2, and the slender geometries of the other cylinders which render them imperfection sensitive.

A parametric study undertaken by Agelidis [1] contains some data relevant to this. In considering several sizes of initial imperfection he demonstrates their importance for the geometries of Cylinders 1A2 and 1B2 under longitudinal compressive loading. Cylinder 1B1, however, is not included in his study as it fails in a general buckling mode which cannot be duplicated by his simple finite element mesh.

The theoretical and observed strengths are listed in Table 6.2 and they do not differ greatly. The largest discrepancy is for Cylinder 1B2. All predictions would become conservative if a factor of 0.8 was applied to the intact cylinder capacity to give an allowable critical location stress.

Fig. 6.26 shows the theoretical variation of residual strength with dent depth, without incorporation of the above knock-down factor. Several curves are drawn for longitudinal loading at different eccentricities. In this context residual strength is represented as the load capacity of the dented cylinder as a fraction of the corresponding intact cylinder capacity. This ratio is seen to drop to about 0.5 at a dent depth of

$$\delta_{DD}/R = 0.2 \ .$$

Due to bending moments induced by the relocation of the centroid of the dented section this strength erosion is significantly steeper than that contributed by loss in area alone.

The enhanced capacity given by an increased load eccentricity is a result of the advantageous definition in Fig. 6.23(a) of positive eccentricity lying away from the dent. The bonus is lost when the dent depth is so small that

$$\bar{y} < ecc$$

because first yield then occurs diametrically opposite the dent centre. It is this alternative failure criterion that produces the abrupt slope changes in Fig. 6.26.

Fig. 6.27 is the linear interaction diagram for the elastic section capacity under axial load combined with the bending moment produced by its eccentricity. Lines are included for various dent depths. The test results are

also plotted in both Figs. 6.26 and 6.27 for comparison, although their dent depths and loading eccentricities do not precisely tally with the values for which the lines are drawn.

Because the formulae derived in Section 6.4 may be applied without modification to ring stiffened and unstiffened cylindrical sections, it is easy to compare the experimentally observed capacity of the dented ring stiffened cylinder in Ref. [110] with that predicted here. The test point is included in Figs. 6.26 and 6.27 and in the former diagram is seen to lie on the curve defined by zero eccentricity. This model was in fact loaded concentrically.

6.5.2 DETAILS OF LOCAL BEHAVIOUR

6.5.2.1 MATERIAL REMOTE FROM DENT

It is stated in Section 5.3.2.1 that strain gauges are scattered round the circumference of the models. These aid detailed understanding of cylinder behaviour by monitoring the distribution of stresses. In this Section attention is given to those gauges situated well away from the dent zone, all of which are longitudinally aligned at the quarter-point of the central bay. They are positioned in line with stringers but on the outer surface. In Cylinders 1B1, 1B2, 3A2 and 3A3 locations are

$$\phi = \pi/2, \pi$$

whereas Cylinder 1A2 carries one at

$$\phi = 3\pi/5 .$$

The results for all models exhibit the same essential features. To avoid repetition emphasis is placed on

Cylinders 1B1 and 1B2. These two models incur almost identical theoretical strain predictions due to their very similar dent depths, and so presentation is simplified. Also, being the most slender models, they give the theory a rigorous trial. Figs. 6.28 and 6.29 show the nondimensionalized readings of the gauges on these cylinders, alongside the predictions of Eqn. (6.9).

The strains diametrically opposite the dent are discussed first (Fig. 6.28). Initially they are smaller than expected because the convex curve of the end rings produced by the denting process means that there is little early contact with the platens in this part of the cylinder. Thereafter straining occurs at the estimated rate until peak load, when unloading begins. Unloading equilibrates the loss of capacity in the region adjacent to the dent caused by buckling. The same phenomenon is noted in Fahy's eccentrically loaded tests [54]. As the fibres at $\phi = \pi$ are still elastic almost the same slope is followed by the unloading path, until some tendency for tensile straining occurs at very small load.

In Cylinder 3A2, only, the commencement of unload is delayed until a little after peak load. This is attributable to a combination of end bay failure and stocky geometry, which means that the panels next to the dent do not shed load immediately after failure.

In contrast, the prebuckling strains are slightly higher than predicted in Cylinders 1B1 and 1B2 at $\phi = \pi/2$ (see Fig. 6.29). Here the platens always rest on the cylinder due to its convex ends. Thus overall equilibrium with the applied load is maintained by compensating for reduced loading rates elsewhere. However the increase required is small and, in fact, even less apparent in the mid-depth gauge readings of Cylinders 3A2, 3A3 and 1A2. After peak load the strains continue to rise until a buckle forms that includes the stringer at the gauge location. The resulting deformation is large enough in

Cylinder 1B1 to make the strain tensile.

Increasing compressive strain readings continue significantly longer in the corresponding gauges on Cylinders 1A2 and 3A3 because local shell buckles form which do not bend the stiffeners longitudinally. Strain measurements up to

$$\epsilon/\epsilon_{yc} = 8$$

are attained. The Cylinder 1A2 results are plotted in Fig. 6.30 for comparison.

The three Figures discussed in this Section serve to confirm the assumptions on which the stress distribution defined by Eqn. (6.9) are founded. Apart form the minor initial anomalies introduced by the curved end rings, experimental strains throughout the section increase at the expected rates during loading.

6.5.2.2 STRINGER BEAMS ADJACENT TO DENT ZONE

Undamaged stringer beams close to the dent are also gauged both on the stiffener and the panel. Fig. 6.32 shows the response of stringer 3 on the edge of the dent in Cylinder 1B1. At first the observed axial compressive force in this stringer beam is smaller than predicted by Eqn. (6.9), again due to the curved end rings which delay the application of load to this region. Further loading is linear to just reach yield at peak load. As the stringer beam lies at the critical location this behaviour is entirely consistent with the simple first yield criterion for model collapse outlined in Section 6.4.2.2. Unloading then occurs along the same path. The stringer is pulled inwards by the deflecting dent during the response.

The variation of axial force with applied load in stringers at

$\phi = 4\pi/20$

in Cylinders 1B1 and 1B2 is given in Fig. 6.33. While the two responses are very similar to each other, the forces supported are significantly less than predicted, throughout the prebuckling range. Their magnitude begins to decrease before the overall capacity is reached and they become tensile a little later, due to buckling deflections.

Comparison with stringer 3 above shows, somewhat unexpectedly, that the stringer further away from the dent is weaker. This is due to severe distortion here, where the stringer/panel intersection bulges out between the bow-in at the dent and the adjacent inward buckle, as illustrated in the radial deformation diagrams (Figs. 6.14 to 6.17). The sharp ridges formed are clearly seen in the upper photographs of Figs. 6.19 and 6.20. Such reshaping must impair the stiffness and strength of the two half panels associated with the stringer. The capacity of the stringer itself is reduced by its sympathetic local tripping which is also apparent in Figs. 6.19 and 6.20.

The loading of stringer beams 2 and 3 of Cylinder 3A3 in Fig. 6.31 is quite different. One theoretical line suffices for both stringers as $\cos\phi$ is virtually unchanged. The test points follow this line extremely closely, especially for stringer 2. The slightly larger experimental axial force in stringer 3 at higher loads is probably a result of its method of computation. The strain measured at the stringer/panel intersection is assumed to act uniformly over each associated half panel width. When the panels begin to deflect out-of-plane this is no longer valid as more stress is carried at the stiff stringer junction. The test points therefore overestimate the actual load supported by the stringer beam.

Both stringer beams attain uniform yield before the overall section capacity is reached and maintain it for as

long as monitoring is possible. Eventually the gauges begin to peel at strains many times greater than yield. Stringer 2 bows inward with the dent whereas stringer 3 bulges out slightly.

The stringer beams spaced just a little away from the dent and depicted in Figs. 6.31 and 6.33 hold the key to understanding the variety of complete cylinder responses observed, because they are the only ones that deviate markedly from the expectations of simple linear theory. The geometry of Cylinder 3A3 is sufficiently stocky to restrain the detrimental out-of-plane prebuckling deflections encouraged by the presence of the dent. It is able to support localized compressive strains well in excess of yield as ductile stress redistribution takes place. A first yield failure criterion thus underestimates the section capacity. The corresponding stringer beams in Cylinders 1B, on the other hand, are weakened by such deflections and fail early. In these cases the predictions of linear analysis are optimistic.

It is likely that a better estimate of the residual strength of damaged cylinders might be obtained by modelling the critical stringer beams in a numerical analysis, incorporating the deformations induced by the pull-in of the dented region during loading. Accurate reproduction of the dent shape would be required, as would a fine mesh of finite elements. However this is beyond the scope of the present work, and would constitute only a rather expensive refinement of the substantially accurate means of assessing residual strength enunciated above.

6.5.3 DENT ZONE

6.5.3.1 INTRODUCTION

The behaviour under longitudinal compression of bilinear struts with T-shaped cross sections is discussed in Chapter 4. After an initial elastic response plastic hinges develop both at the centre and at the encastre supports and a V-shaped mechanism forms. For stringer beam j the mechanism is defined by

$$\frac{\Delta\delta_j}{R} = \frac{a_j}{a_{Dj}}\cdot\frac{L}{R}\cdot\frac{\sin\theta_j}{2\cos\theta_{Dj}} - \frac{\delta_{Dj}}{R} \qquad (6.12)$$

$$\frac{\Delta_j}{L} = 1 - \frac{a_j}{a_{Dj}}\cdot\frac{\cos\theta_j}{\cos\theta_{Dj}} \quad . \qquad (6.13)$$

These equations follow directly from Eqns. (4.6) and (4.7), but incorporate slightly different notation which better suits the cylinder work. The notation is illustrated in Fig. 6.34. The springs drawn in the Figure represent an elastic foundation which will be utilized later. In the formulae

$$\tan\theta_{Dj} = 2\delta_{Dj}/L$$

and

$$a_j/a_{Dj} = 1 - n_j\sigma_{YC}/E \qquad (6.14)$$

$$\approx 1 \qquad (6.15)$$

for the material characteristics of steel. Eqn. (6.15) is equivalent to the assumption of rigid links between hinges.

When the mechanism is part of a cylinder relative rotation of the end rings could cause additional growth in

lateral deflection and strut inclination. This behaviour is neglected, consistent with the postulate of small deflections, and the above equations assume that the supports are subject only to longitudinal shortening.

6.5.3.2 CYLINDER 1A2

Cylinder 1A2 is discussed first as only one stringer is dented. The end shortening versus lateral deflection relationship predicted for this stringer beam by Eqns. (6.12) and (6.13), and incorporating approximation (6.15), is drawn as a broken line in Fig. 6.36. Also plotted are the test points monitored by longitudinally and radially aligned transducers. Although the two plots are very similar in form, the experimentally observed additional lateral deflection of the dent during crushing is somewhat smaller. The same effect is observed in Section 4.4.1.1 for the compressive loading test of the dented stiffened plate. It is thought to be due to extra compressibility caused by the presence of geometric and material imperfections induced during the denting process. In the cylinder tests, however, restraint to inward bowing provided by the adjacent undamaged region also has an effect.

To understand such restraint, attention is given to the mode of deformation induced circumferentially by dent growth. This is sketched schematically in Fig. 6.35. The inward bending dent and the undamaged stringer nearby, which provides a point of resistance, are bridged by a strip where there is severe localized pull-in. The material here is likely to reach yield in circumferential tension soon after longitudinal loading begins. Idealizing the dishing to a uniform slope ζ implies a total transverse force per unit length on stringer O of

$$q = 2\sigma_y t.\zeta$$

$$= k_2 y \ .$$

Here

$$\zeta = y/d_1$$

within the bounds of small deflection theory, and therefore

$$k_2 = 2\sigma_y t/d_1 \ . \qquad (6.16)$$

If the distorted width d_1 is assumed to remain constant along the length of the cylinder it is apparent that stringer 0 is supported by an elastic foundation of unit spring stiffness k_2 .

Referring to Fig. 6.34, moment equilibrium at the end of the dented length under this loading configuration gives

$$P_A\delta_j = M_s + M_c + \int_0^{a_{0j}} qx.dx \ .$$

Rearrangement leads to

$$\tan\theta_j = \frac{2\cos\theta_{0j}}{C_{13}} \frac{(m_s + m_c + Q(\theta_j - \theta_{0j}))}{n(1 - n\sigma_{yc}/E)}$$

$$\approx \frac{2\cos\theta_{0j}}{C_{13}} \frac{(m_s + m_c + Q(\theta_j - \theta_{0j}))}{n} \ . \qquad (6.17)$$

This is an extension of the earlier Eqn. (4.8), allowing now for the transverse support provided by the foundation.

Hinge moments are given in terms of the axial force by formulae in Section 4.3.4. Panel curvature is again neglected in employing these equations, consistent with the arguments put forward near the conclusion of Section 5.5.2.2. A modification to the moment capacity at the support hinge to allow for stiffener tripping is discussed

in Section 4.4.2. It need not be incorporated here, however, because stringer 0 does not trip, as may be seen in Fig. 6.18.

The following result is also incorporated:

$$\int_0^{a_{0j}} \frac{q_x . dx}{\sigma_Y Z_p} = Q(\theta_j - \theta_{0j})$$

where

$$Q = \frac{k_2 a_{0j}^3}{3\sigma_Y Z_p} \qquad (6.18)$$

is a nondimensionalized stiffness parameter for the elastic foundation, and

$$y = x(\theta_j - \theta_{0j}) .$$

It is assumed in this last equation that the springs remain normal to the legs of the mechanism as they rotate. The struts are also considered to be stiff enough axially that the half-length a_{0j} remains virtually unchanged.

Dimension d_1 may be roughly estimated by equating the localized dishing slope to the angle of twist of stringer 1 (see Fig. 6.35). At the circumferential dent centre-line

$$w/h_1 \approx \Delta s_0/d_1 .$$

During loading the stiffeners are out of sight. However at the end of the compression test when

$$\Delta s_0/R = 0.021$$

the maximum out-of-plane displacement of the pertinent outstand tip is observed to be about 4mm. Using Eqns.

(6.16) and (6.18) a value of 125 is thus obtained for Q.

By putting this value into Eqn. (6.17) the response of stringer beam 0 on the dent centre-line of Cylinder 1A2 is obtained. The axial force is presented as a function of end shortening in Fig. 6.37 with the aid of Eqn. (6.13). The curve describes the experimental axial force development remarkably well after buckling. Similar correlation is achieved if the additional lateral deflection $\Delta S_j/R$ is plotted on the abscissa rather than the end shortening, because both deflections are adequately modelled by the analysis. As shown in Section 4.4.1, the two plots have the same form due to the nearly linear relationship between the two deflections. It is therefore unnecessary to include both plots.

The actual relationship between the two deflection parameters is shown in Fig. 6.36 using a full line. This time Eqn. (6.14) is used, rather than its approximation Eqn. (6.15), by inserting the axial force values computed from Eqn. (6.17). The resulting curve lies closer to the test points, but the reduction in lateral deflection caused by taking account of the foundation is small nonetheless.

The prediction of Eqn. (6.17) for

$$Q = 0 ,$$

representing a free mechanism, is also included in Fig. 6.37 for comparison. In Fig. 6.36 the corresponding curve is virtually coincident with the dashed line described earlier, which is computed without consideration of the axial force present. This is due to the accuracy of Eqn. (6.15) when this force is small.

Pure elastic compression of a stringer beam in a longitudinally stiffened cylinder is given by

$$\Delta_j/L = n_j \sigma_{yc}/E \ .$$

This equation is drawn in Fig. 6.37 as well and it is apparent that the dent is much more flexible longitudinally than the rest of the cylinder, as asserted in Section 6.4.2.1. Thus, although significant axial forces are supported in the dent zone, the region may be rationally neglected when estimating the elastic stiffness of the overall section for these models. These forces supplement, to a small degree, deficits in the load carried by the stringer beams adjacent to the dent, which are caused by out-of-plane deflections prior to buckling.

The actual longitudinal load supported at the ends of the bilinear mechanism is even less than implied by the computed axial force, due to the presence of a transverse reaction which equilibrates the elastic foundation force. The reaction is included in Fig. 6.34. However its longitudinal component is relatively small and, thus, its effect is also small.

Despite the agreement between theory and experiment discussed above, there is certainly no claim of accuracy or general applicability in the notion of an elastic foundation in this context. Indeed no consideration is given to the mode of transfer of the transverse force to stringer beam O from the strip of localized dishing. The point of interest is simply that dented stringers are able to support increased axial force after buckling of the section, due to the restraint provided by the undented stringer beams nearby.

6.5.3.3 CYLINDERS 1B1 AND 1B2

Several stringers are dented in these models and so it is possible to observe how the individual mechanisms behave in relation to each other.

If the legs of each mechanism are able to deform freely during compressive loading, and if they are assumed to be axially stiff, each point on them would move in a direction perpendicular to the strut axis. Thus those stringer beams further from the dent centre-line would have to deflect a greater lateral distance for a particular end-shortening as their initial inclination is more gradual. This is seen in the deflection plots, in Fig. 6.39, of stringers at

$$\phi = 0,\ \pi/20,\ 2\pi/20$$

in Cylinders 1B1 and 1B2. These are derived using Eqns. (6.12) and (6.13) and incorporating approximation (6.15).

Free inward bending is counteracted, however, by the restraining effect of the rest of the cylinder, which is likely to increase across the width of the dent as the undamaged material is approached. Thus it might be expected that all the stringers in the dent will actually have similar additional lateral deflections, and this is borne out by the test results in Fig. 6.39.

The experimentally observed bow-in is initially very small, or even negative, although the end shortening increases. Because the end rings curve inwards slightly at the dent after damage loading, the end platens of the compression rig do not touch the dented material at first. Thus the axial force there remains very small but may be either compressive, or tensile along with slight outward bulging, as the point of loading through the spherical bearing encourages the end rings to possibly separate a little at the dent. However this region appears to shorten as the transducers measure the changing separation of the platens. The same behaviour is also apparent in Fig. 6.40(b), as well as Figs. 6.36 and 6.37 for Cylinder 1A2. When uniform contact is achieved after a few load steps the deflections follow the theoretical prediction for stringer 0 reasonably closely.

Unfortunately gauges on stringer 0 of both Cylinders 1B1 and 1B2 fail during the denting test and so their axial force responses during compression loading cannot be followed. Results for the other dented stringers are available however. It is possible to consider them to be resting on elastic foundations, consistent with the above analysis for Cylinder 1A2, but empirical input is again required in order to obtain quantitative results. This is avoided if an alternative approach is pursued as follows.

Fig. 6.38 illustrates the assumed deflections under longitudinal compression of dented stringers 0, at the centre-line, and j, at

$$\phi = j\alpha \ .$$

Both stringers have very similar end shortening

$$\Delta_0/L = \Delta_A/L + \psi R/L$$

for reasonably small ϕ, as seen in Fig. 6.23(a). The test points in Fig. 6.39 demonstrate that the stringer beams also exhibit the same additional lateral deflection $\Delta\delta_0$.

The same Figure also shows that the use of approximation (6.15) for stringer beam 0 gives a good estimate of the observed behaviour, which implies that its leg length a_{00} remains essentially constant. However for compatibility stringer beam j must shorten axially, causing a compressive force defined by Eqn. (6.14).

The growth of this compressive force with dent depth is readily determined from Eqns. (6.12) to (6.15). It is possible, though, to rearrange them to give a simple explicit solution

$$1 - a_j/a_{0j} = 1 - \sqrt{1 - 2d_2\Delta\delta_0/a_{0j}^2}$$

$$\approx d_2\Delta\delta_0/a_{0j}^2$$

where

$$d_2/R = 1 - \cos(j\alpha) \approx \tfrac{1}{2}(j\alpha)^2 \ .$$

Thus

$$n_j = \frac{E}{\sigma_{YC}}\left[\frac{2R\cos\theta_{0j}}{L}\right]^2 \frac{d_2}{R}.\frac{\Delta\delta_0}{R} \qquad (6.19)$$

$$\approx \frac{2E}{\sigma_{YC}}\left[\frac{j\alpha R\cos\theta_{0j}}{L}\right]^2 .\frac{\Delta\delta_0}{R} \ . \qquad (6.20)$$

In arriving at these equations use is made of the following geometric properties of the system

$$a_{0j}\cos\theta_{0j} = a_{00}\cos\theta_{00}$$

$$a_j\cos\theta_j = a_{00}\cos\theta_0$$

$$\Delta\delta_0 = a_{00}\sin\theta_0 - a_{00}\sin\theta_{00} = a_j\sin\theta_j - a_{0j}\sin\theta_{0j}$$

$$d_2 = a_{00}\sin\theta_{00} - a_{0j}\sin\theta_{0j} = a_{00}\sin\theta_0 - a_j\sin\theta_j \ .$$

Fig. 6.38 clearly illustrates these relationships.

Eqns. (6.19) and (6.20) predict much higher axial forces in stringers further from the dent centre. The predictions for stringers 1 and 2 of Cylinder 1B1 and stringer 1 of Cylinder 1B2 are presented in Fig. 6.40(a) and the slopes compare well with the test points.

Similar correlation is obtained if the axial force is plotted in terms of end shortening rather than additional lateral deflection, as shown in Fig. 6.40(b). Because the relationship between the two deflections is not exactly linear, however, neither is the theoretical axial force versus end shortening response perfectly linear for Cylinders 1B1 and 1B2. The deflections are approximately related by

$$\frac{\Delta_0}{L} \approx 4\left[\frac{R}{L}\right]^2 \frac{\delta_{D0}}{R}\frac{\Delta\delta_0}{R} ,$$

which at low deflections is tangential to the true response drawn in Fig. 6.39. Insertion of this equation into Eqn. (6.19) gives

$$n_j \approx \frac{E}{\sigma_{yc}} . \cos^2\theta_{Dj} . \frac{d_2/R}{\delta_{D0}/R} . \frac{\Delta_0}{L} .$$

The stringer beams at $\phi = 2\pi/20$ eventually attain uniform compressive yield. Thus restraint gives these dented stringer beams greater strength than the adjacent undamaged ones. This is aided by the ridge formed by the knige edge at mid-span, which reduces the effective length of the dented stringer beams by providing a line of stiffness. There is no indication of Euler buckling of the dented stringer beams in the tests, only the bilinear mechanism deformations on which the above analysis is based. Dent buckling is apparent, however, in the ring stiffened model of Onoufriou and Harding [110]. An antisymmetric pattern forms longitudinally, with one half wave in each half of the bay between ring frames but very little deflection at the mid-span ridge.

Although the legs of stringer beam 0 are assumed not to compress in the theory derived in this Section, it should not be inferred that they carry no axial force. It is shown for the same stringer beam in Cylinder 1A2 that substantial axial force may be supported with little alteration to the end shortening versus additional lateral deflection response derived using approximation (6.15), and hence little effect on the theory above.

6.5.3.4 CYLINDER 3A3

The predicted end shortening of the dented stringers in Cylinder 3A3 is plotted in Fig. 6.41 as functions of additional lateral deflection, assuming no transverse

restraint. The correlation with experimental values is adequate for stringer beam O, although the lateral deflection is overestimated. However for stringer 1 the measured lateral movement is slightly smaller still. This is probably due to the extra restraint provided by the adjacent undamaged material in this stocky cylinder with very short bay length. These stringer beams are not strain gauged and so their axial compression forces cannot be compared with theory.

6.5.4 SUMMARY

The strain gauge data presented throughout Sections 6.5.2 and 6.5.3 may be collated conveniently by plotting axial stress blocks for the cylindrical sections. Fig. 6.42 overlays the linear predictions with the test results of Cylinders 3A3 and 1B1. Excellent correlation is obtained with the former cylinder. This serves to verify the implicit assumption that for the testing arrangement adopted the presence of undamaged bays does not alter the response of the dented bay, and hence, its distribution of stresses.

The slender Cylinder 1B1, in contrast, demonstrates nonlinearity. As implied in earlier discussions within Section 6.5.2.1, the generally convex form of the stress block ensures overall equilibrium when there is weakness near the dent. Of particular interest is the double peak just outside the dent zone. The intermediate trough is caused by the distortion of the stringer beam at

$$\phi = 4\pi/20 ,$$

as described in Section 6.5.2.2.

A similar phenomenon is found by Onoufriou and Harding [110] in their numerical analyses of a dented ring

stiffened cylinder under axial loading. They find, as well, that the dent carries very little force. The uniform fall-off in stress towards $\phi = \pi$ after the second peak in Fig. 6.42 is duplicated in some of Onoufriou and Harding's numerical work, but not all, as rotation of the ends is inhibited in one of their methods of load application. Stress tapering is apparent in their test result but forms a concave rather than linear profile at higher loads.

It has become apparent during this chapter that the behaviour of the dent, including its plastification, does not induce failure of the cylinder. Nor does its presence act soley as a large imperfection which develops to form part of a complete buckling pattern. Rather, it causes stress concentration in the undamaged region adjacent to the dent and buckling occurs when the strength of the section is reached here. Additionally, however, this strength may be eroded by deformations encouraged by the dent.

6.6 COMPARISON WITH AN ALTERNATIVE APPROACH

That the response of the dent zone helps dictate the behaviour of the entire cylinder is manifest. It is of interest, therefore, to compare the dent behaviour observed in this chapter with that of dented unstiffened tubes investigated by Rashed, Taby and Moan [120] and described briefly in Section 2.8.2.

The authors of Ref. [120] state that inward bending of the dent is restrained at the beginning of loading and so the dent is forced to compress with the same stiffness as the rest of the tube. The dual effects of uniform stressing and restraint to lateral deflection mean that the arcs at the ends of the dent spanned by the dented longitudinal fibres may be treated as an integral unit with the resultant longitudinal force acting through the

centre of area of the arcs. The distance of the centre of area above the bottom of the dent is denoted by $\hat{\delta}_{00}$. Fundamentals of the approach, including this dimension, are illustrated in Fig. 6.23(b).

Using this model it may be computed when a plastic hinge line forms at the dent centre. (No similar hinge lines are assumed to develop at the ends of the dent as the lateral deflection peters out gradually.) With the advent of plasticity the dent is considered to lose its stiffness and support no extra load. Additional load is carried only by the remaining section which has the same shape as the effective section discussed in this chapter. However the slope of the complete stress block differs from that derived earlier due to the addition of the constant component σ_{0P}, which represents the stress acting at dent plastification.

There appears to be a slight contradiction here. The assumption that the dent zone has no stiffness after hinge plastification implies that it bends in freely when the adjacent undamaged fibres are further compressed. However the growth in dent depth would cause the load capacity of the mechanism to fall a little, but σ_{0P} is assumed to remain invariant.

In contrast, Smith [149] has noted that there is negligible dent growth before collapse in his compression tests on dented unstiffened tubes. This means that the dent is still restrained by the surrounding material. In this situation the load carried by the dent must increase greatly after plastification and its longitudinal stiffness remains significant.

Although the overall lateral deflection caused by rotation in the dented segment and its amplification in the presence of axial load are considered by Rashed et al [120], these factors may be neglected in applying their approach to stub columns. This leads to a simplified

strength equation

$$\frac{p_{Am}}{\sigma_m/\sigma_{YC}} = \Omega + (1-\Omega).\frac{\sigma_{DP}/\sigma_{YC}}{\sigma_m/\sigma_{YC}} \quad . \qquad (6.21)$$

By adapting the postulate of uniform stressing to the dented stringer beams of longitudinally stiffened cylinders and assuming they act together, the load producing dent plastification may be found by putting

$$\tan\theta = \tan\tilde{\theta}_{DO} = 2\tilde{\delta}_{DO}/L$$

into Eqn. (4.8). Rearrangement leads to

$$\sigma_{DP}/\sigma_{YC} = \sqrt{\xi^2 + 1/f} - \xi \qquad (6.22)$$

where

$$\xi = \frac{\tilde{\delta}_{DO}.b/A}{\cos\tilde{\theta}_{DO}} \quad . \qquad (6.23)$$

Eqns. (6.22) and (6.23) are valid for

$$n \leq C_0 \quad ,$$

which is very likely for the dent depths under consideration.

The similarity of Eqns. (6.22) and (6.23) to the corresponding ones used by Rashed et al, and rewritten in Chapter 2 as Eqns. (2.2) and (2.3), is obvious. The factor of two absent now from the parameter ξ follows from the assumption that plastic hinges form at the ends of the mechanism as well as at the centre. Included is another factor, $\cos\tilde{\theta}_{DO}$, which allows for the axial load in the mechanism being at an angle to the longitudinal axis.

The point of application of the longitudinal load acting on the dent zone is defined by

$$\frac{\tilde{\delta}_{00}}{\delta_{00}} = \frac{(1/\eta)\sin\eta - \cos\eta}{1 - \cos\eta}$$

$$\rightarrow 2/3$$

from below for very small dent depths.

The theory of Rashed et al [120] implies several changes in behaviour at the point of dent plastification. Firstly, it predicts an abrupt reduction in overall axial stiffness. This is not apparent in their results; however the dent occupies only a small portion of the length of their models and so the stiffness is dictated largely by the predominant intact material. Increasing lateral deflection of the dent would also be expected at the onset of plasticity whereas there should be no growth before this point.

Observations in the current test series are quite different. No sudden loss of axial stiffness occurs, despite the dented bay being a major portion of all models. Concerning the second factor, Fig. 6.43 combines a sample selection of plots showing the development of lateral deflection in the dent during longitudinal loading. The dent depth is able to grow from the beginning of loading in these models due to their slender sections. For Cylinders 1B2 and 3A3 the growth curve is very smooth, both before and after buckling. The prebuckling gradient softens a little with the former model, but at a load much greater than that causing dent plastification. It is due to reduced stiffness of the effective section rather than increasing bending of the dent. Cylinder 1A2 does exhibit sudden dent growth, but it occurs at the point of dynamic buckling, aided by the buckling deflections, and not with the formation of plastic hinges.

Whereas the method of Ref. [120] considers that the surrounding undamaged material checks dent bending completely before plastification and then not at all, the

opposite trend is seen in the present stringer stiffened dents. The initial response is highly flexible. Thereafter, the dent growth is controlled such that the axial force it supports increases steadily even after dent plastification and later cylinder buckling have occurred. Both sets of tests exhibit uniform additional lateral deflections across the dent. In the present series, however, axial stresses are not uniform: stringer beams with larger inclinations near the longitudinal centre-line carry much less force, which appears to be logical.

Comparison of the method of Ref. [120] (Eqn. (6.21)) with Eqn. (6.10) shows that the former predicts greater strength, due to the addition of a second term. In actuality, however, the discrepancy is small, especially at larger dent depths where the load required to produce dent plastification is small. The dents put into the current models are deep enough to fall within this region of similarity, and those used in the tests of Rashed et al are comparable or even deeper. Results from the two equations are drawn in Fig. 6.44 for the case of concentric loading. Whereas Eqn. (6.10) is independent of cylinder geometry, the approach of Rashed et al is not, and so is plotted using Cylinders 1B1 and 3A3 as examples. The prediction for Model 1A2 lies in between these two curves, and Cylinder 1B2 is very similar to 1B1, but just slightly weaker.

6.7 COMPLETE CYLINDRICAL COLUMN RESPONSE

The compression tests undertaken on dented stub columns give insight into the likely response of the dented portion of a longer member in service. Attention is now directed, briefly, towards the behaviour of the entire member in the presence of the weakened zone.

The locally dented unstiffened tubes considered by Rashed et al [120] are relatively slender in the overall bending mode. The rotation of the dented segment during compression loading causes overall deflections of the entire column which must be added to any initial deformations and, in turn, produce additional bending moments throughout the member length. Rashed et al quantify this behaviour using simple analytical techniques that assume implicitly that plane sections remain plane.

However the overall stockiness of typical members forming the legs of floating offshore structures prevents any significant second order deflections. Instead another phenomenon gains importance; namely, the redistribution of axial stress around the cross section along the intact bays. This is promoted by the requirement that both compatibility and equilibrium must be satisfied at the border to the dented bay. To illustrate: if the intact bay next to the dented one carried uniform stress and hence strain throughout, the stressing would cause very large axial deflections in the weak dent zone, and compatibility would be violated. It means that the undamaged bays will deform in a nonplanar manner, which complicates the accurate estimation of the stiffness of the total column. Whether the member ends are constrained to remain planar and circular affects the response.

In contrast, the residual strength should be little affected by the addition of intact bays, as exemplified by the three bay models. However the degree of rotational restraint afforded to the dented bay is of relevance. The models discussed in this chapter are loaded through a spherical bearing and so they will mirror the capacities of corresponding prototype columns having reasonably little flexural end restraint. On the other hand, if the in situ supports are effectively encastre and the column is short, rotation of the dented bay may be retarded and a somewhat greater capacity would be expected due to uniform stressing of the effective section. This behaviour could

also be emulated in a stub column test by using a different loading configuration. The configuration adopted in the test series is clearly conservative in these instances.

6.8 CONCLUSIONS

Many aspects of the experimental behaviour of dented stringer stiffened cylinders under longitudinal compression are accurately described by making simple assumptions. Before buckling the cylinders act as if the dented region is not present; the axial load, end-shortening and rotation of the ends may all be predicted using an effective cross section of undamaged material. Failure is deemed to occur when the stress at the critical point adjacent to the dent attains the "perfect" cylinder capacity.

For stocky geometries this is conservative as stress distribution occurs after yield. However for slender geometries this method will overestimate the residual strength, due to local distortions in the critical region. Incorporation of a twenty per cent knock-down factor here will make the predictions safe. Exactly where the behaviour changes is very difficult to quantify from this limited test series but geometries which are imperfection sensitive under axial load may be regarded as "slender".

At failure the damaged cylinders buckle into modes very similar to their nominally perfect counterparts and examples of both local and general buckling patterns occur. Stringers in the dent continue to carry increasing axial force after peak load as they are restrained by the nearby material. Many details of the observed behaviour differ markedly from those concerning unstiffened tubes discussed elsewhere [120].

It is also worth noting that the refurbished cylinders (with the exception of Cylinder 3A2) adequately characterize the response of new models and thus provide a relatively inexpensive source of useful data.

TABLE 6.1 Cylinder properties

CYL NO.	MATERIAL	GEOMETRY							
	E/σ_{YC}	$t = t_i$	R/t	L/R	s	h_i/t_i	L_t/R	t_r/t	h_r/t_r
(a) DENTED MODELS									
1A2	580	0.84	190	0.416	20	8			
1B1	610	0.63	254	1.08	40	6			
1B2	610	0.63	254	1.08	20	6			
3A2	580	0.84	190	0.331	40	8	0.938	3.6	8
3A3	580	0.84	190	0.331	40	8	0.956	3.6	8
(b) UNDAMAGED MODELS WITH SIMILAR GEOMETRY									
Fahy's series									
1,4	580	0.84	190	0.406	40	8			
2,5	580	0.84	190	0.406	20	8			
Agelidis' series									
1	580	0.84	190	0.40	40	8			
E	610	0.63	254	1.00	40	6			
A	610	0.63	254	1.00	20	6			

TABLE 6.2 Compression test results

CYL NO.	DENT δ_{DO}/R	ECC ecc/R	STRENGTH p_{Am}		
			UNDAMAGED	DAMAGED	
				TEST	THEORY
1A2	0.047	0.055	0.96	0.76	0.77
1B1	0.104	0.067	1.17	0.59	0.67
1B2	0.104	0.086	0.81	0.46	0.57
3A2	0.038	0.045	1.01	0.71	0.81
3A3	0.051	0.055	1.01	0.86	0.79

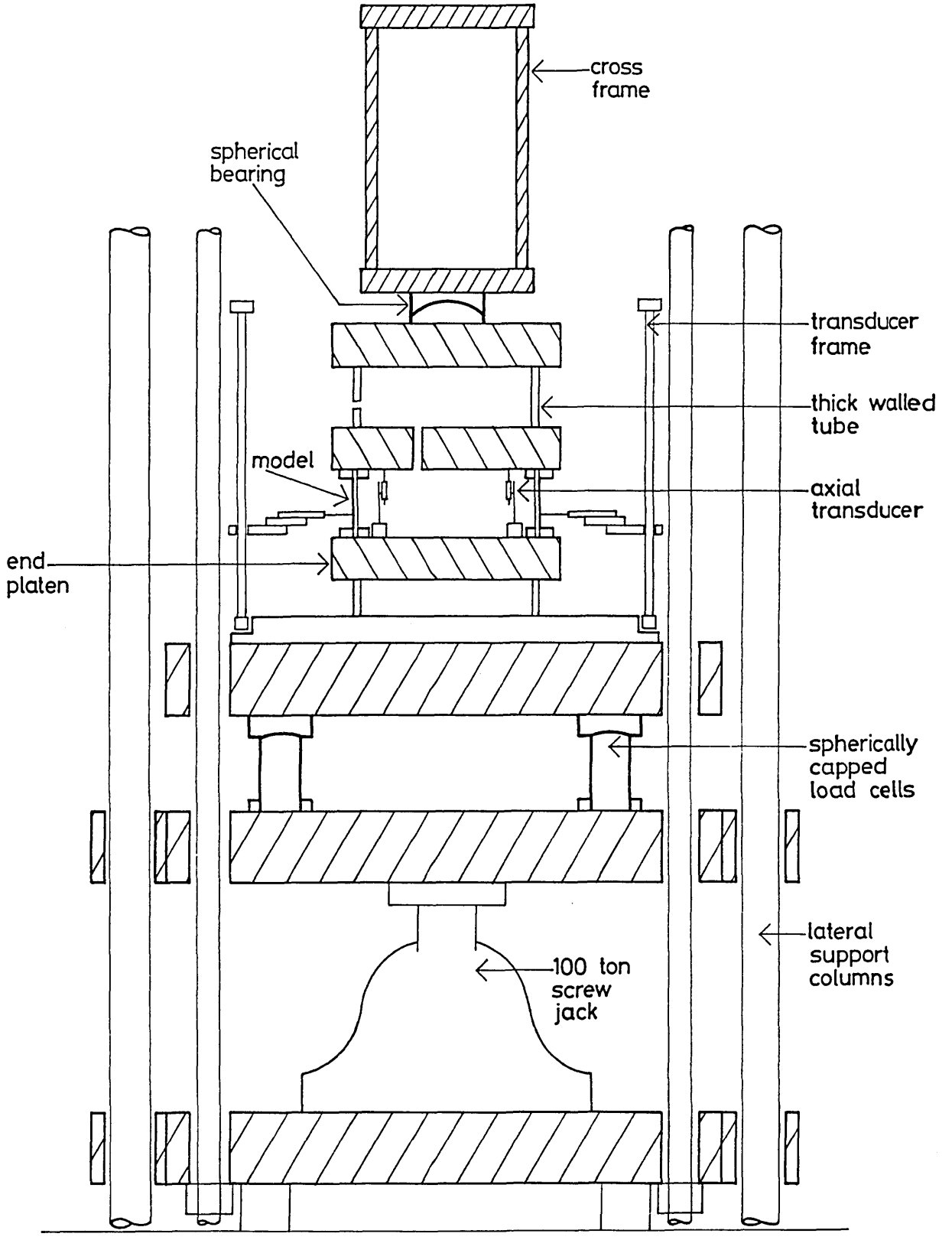


fig. 6·1
Arrangement for compression tests

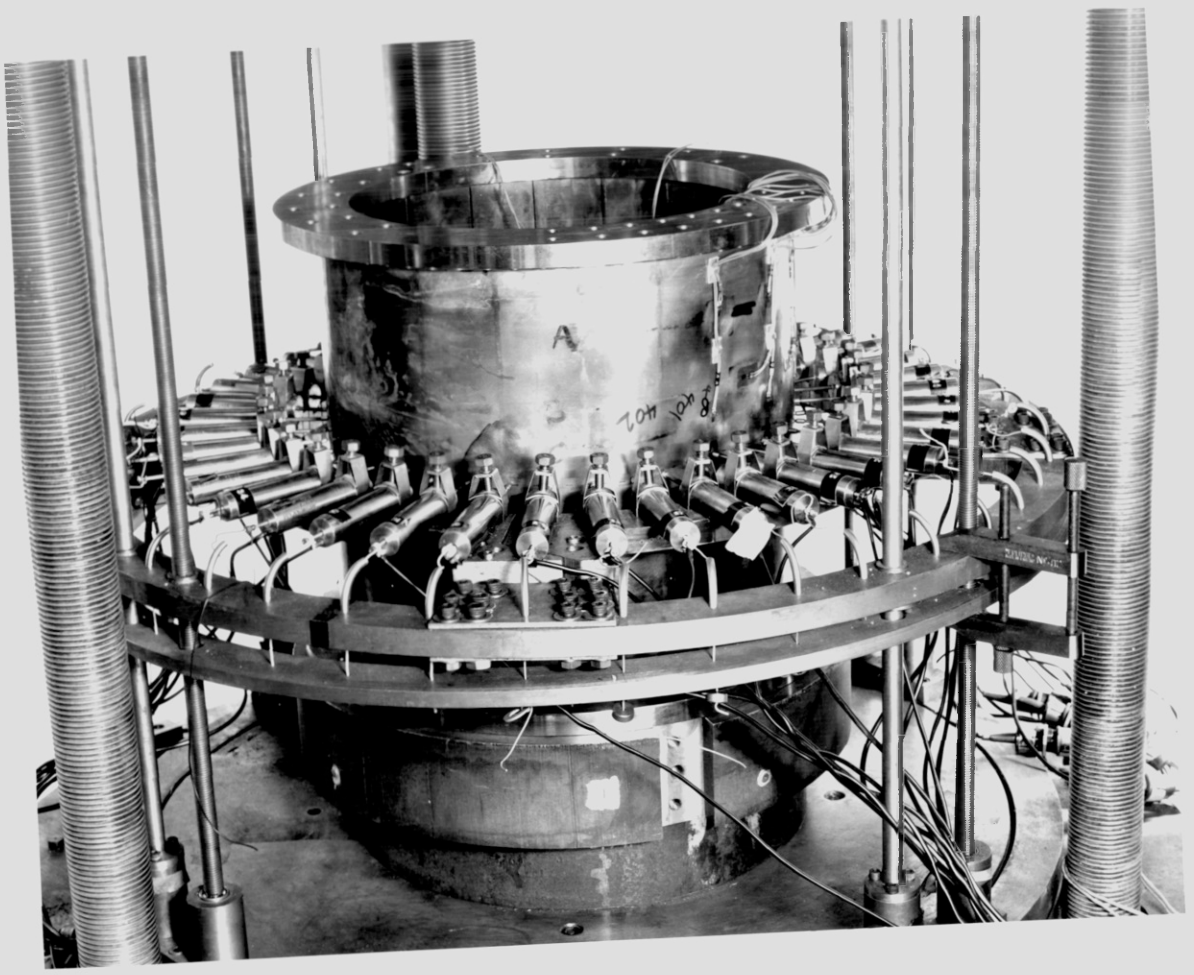


fig. 6.2
Bank of transducers to monitor buckling deformations

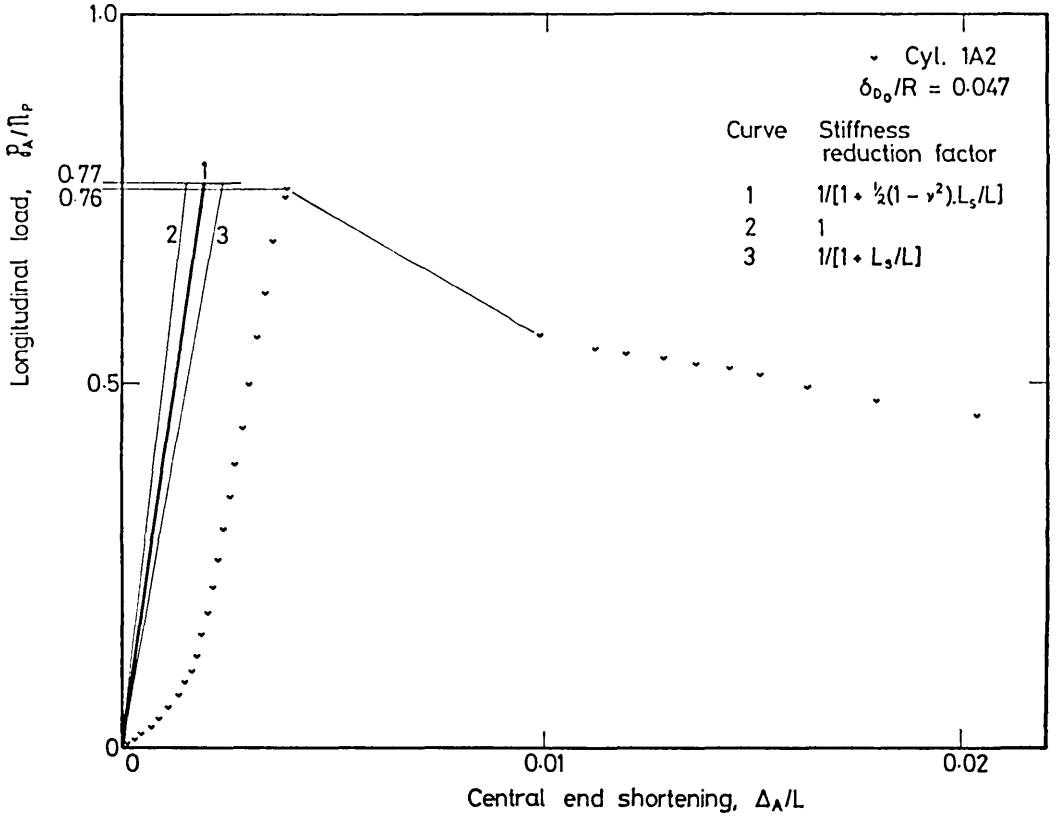


fig. 6·3
Longitudinal load - end shortening response for various end ring conditions
Cyl. 1A2

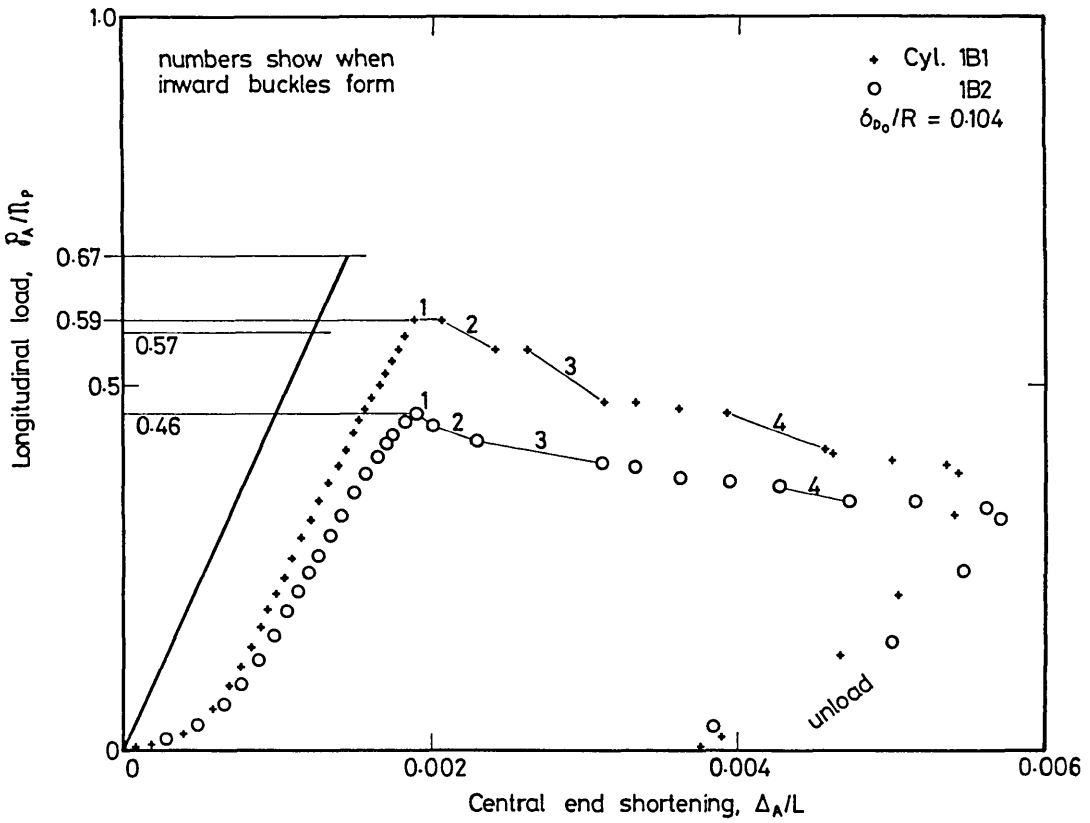


fig. 6·4
Longitudinal load - end shortening response
Cyls. 1B

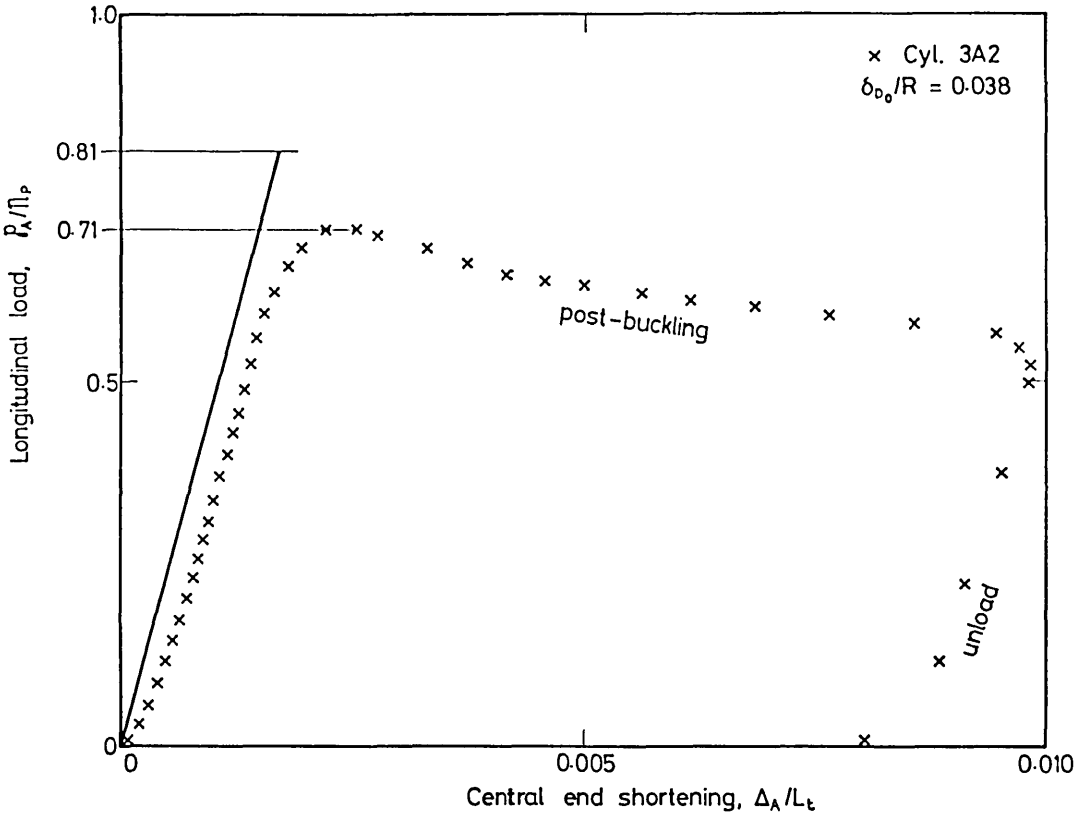


fig. 6·5
Longitudinal load - end shortening response
Cyl. 3A2

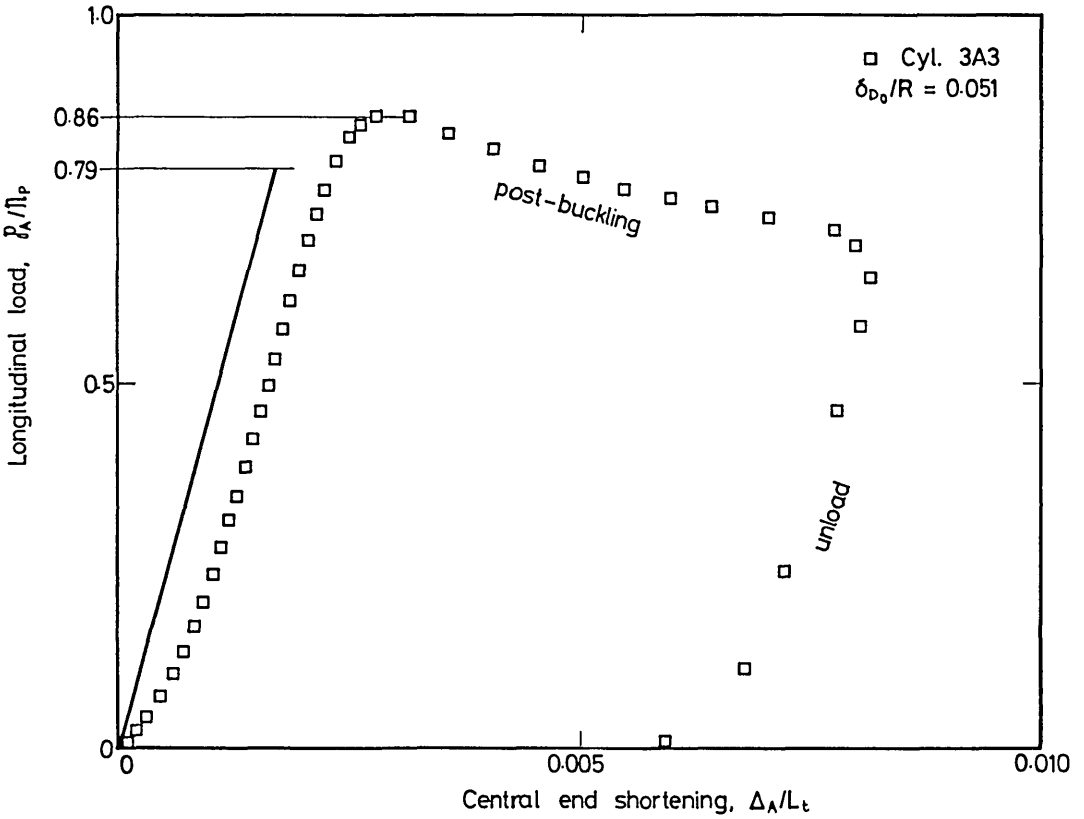


fig. 6·6
Longitudinal load - end shortening response
Cyl. 3A3

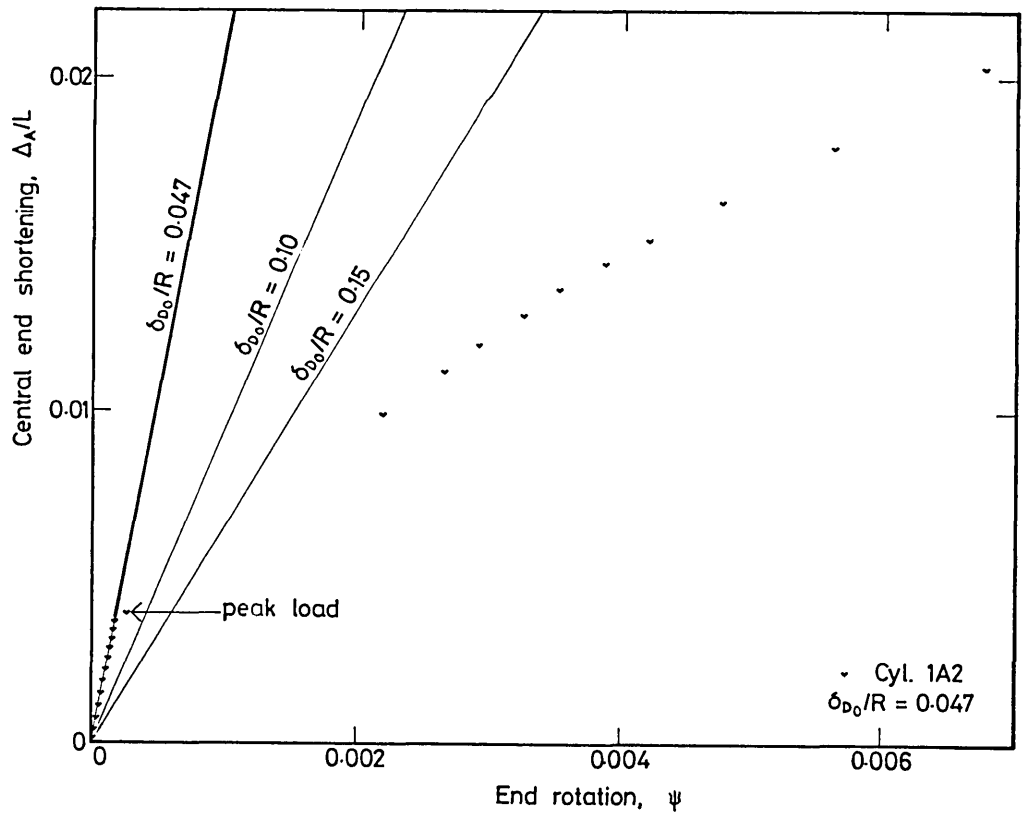


fig. 6.7
Theoretical and experimental relationship between end shortening and rotation Cyl. 1A2

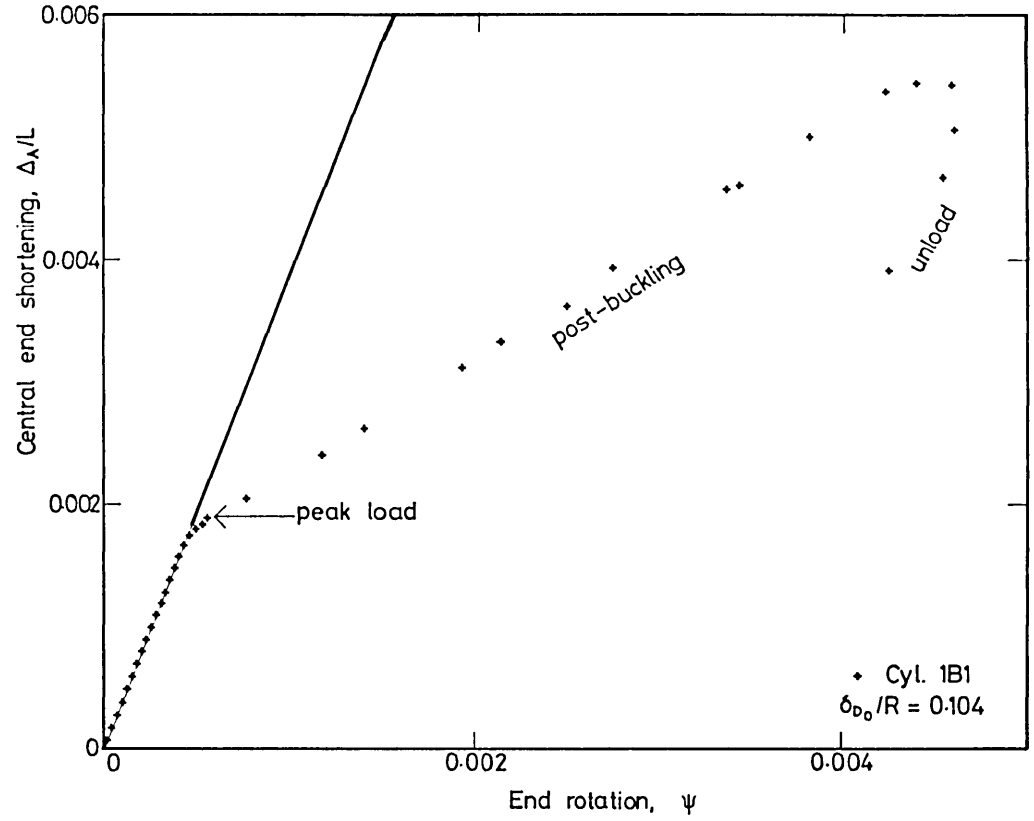


fig. 6·8
Relationship between end shortening and rotation
Cyl. 1B1

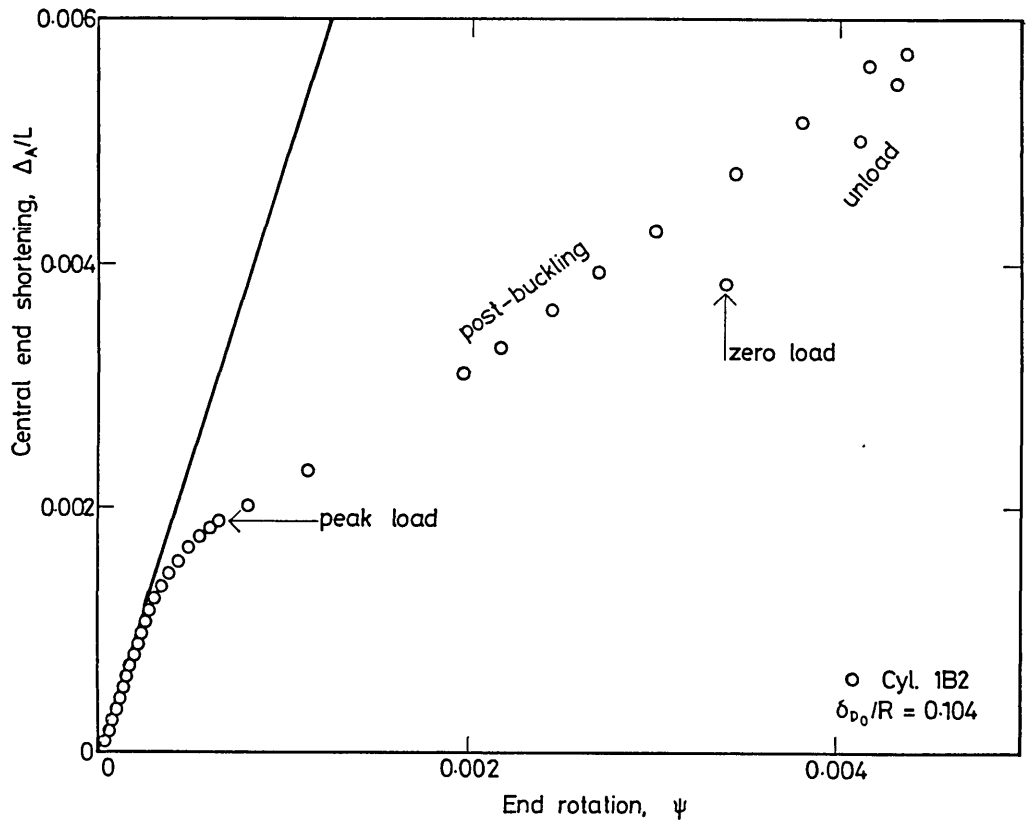


fig. 6·9
Relationship between end shortening and rotation
Cyl. 1B2

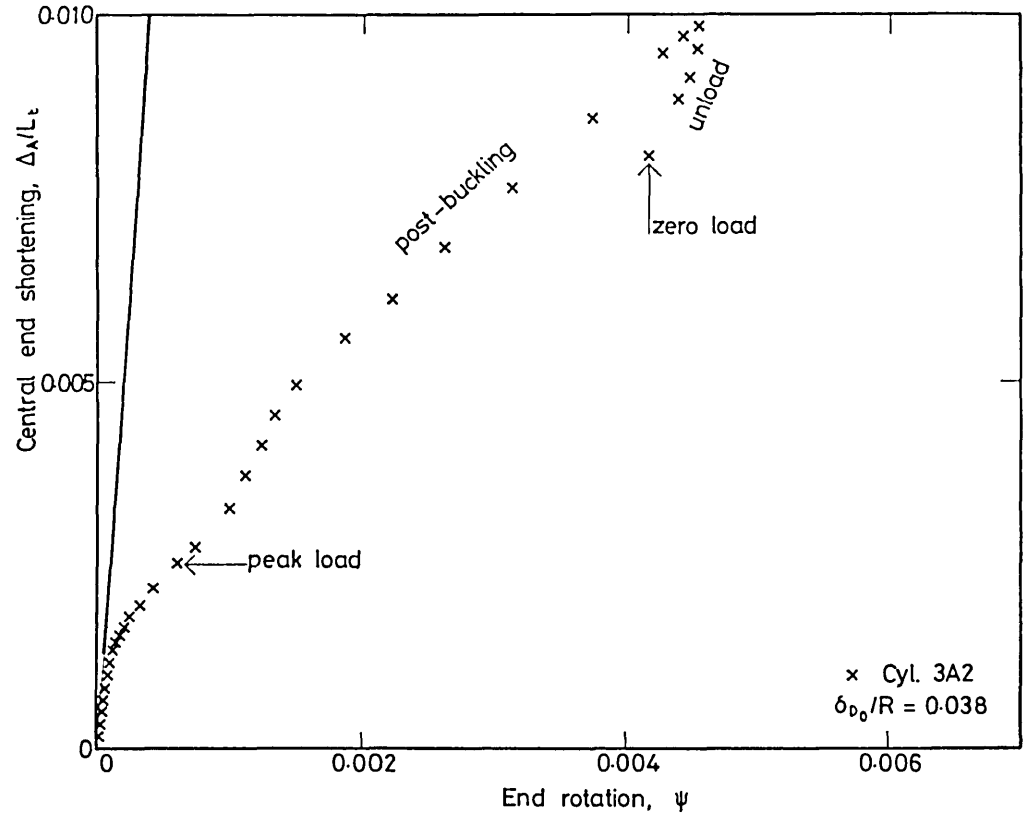


fig. 6·10
Theoretical and experimental relationship between end shortening and rotation Cyl. 3A2

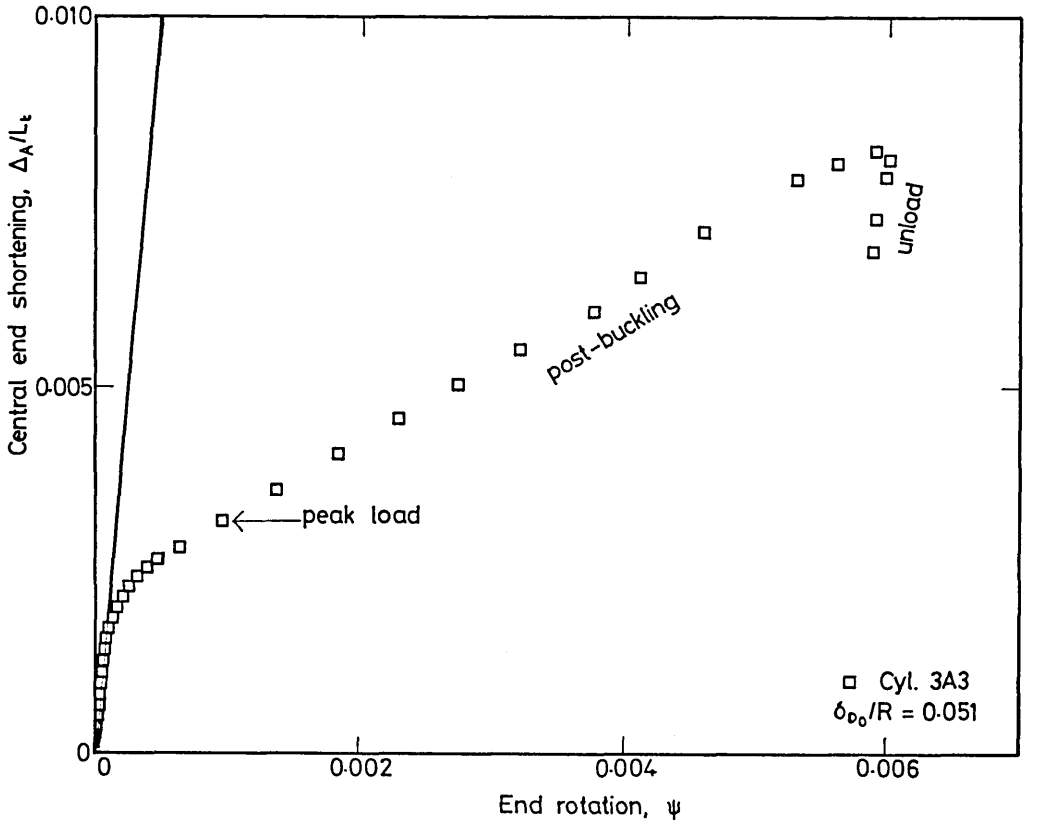


fig. 6·11
Relationship between end shortening and rotation Cyl. 3A3

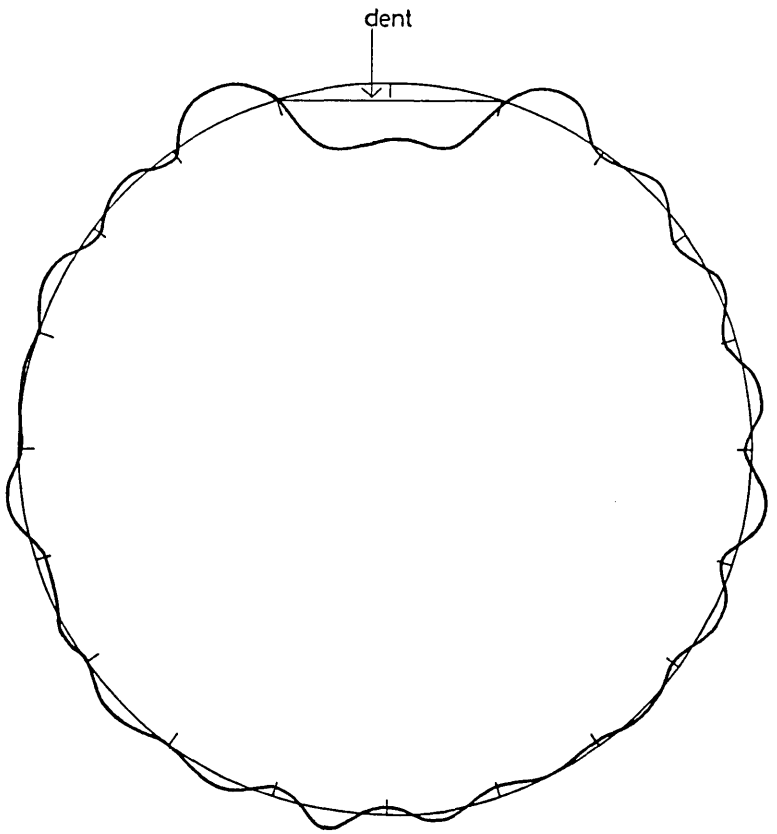


fig. 6·12
Typical pre-buckling deformations at mid-depth
Cyl. 1A2
Exaggeration x200

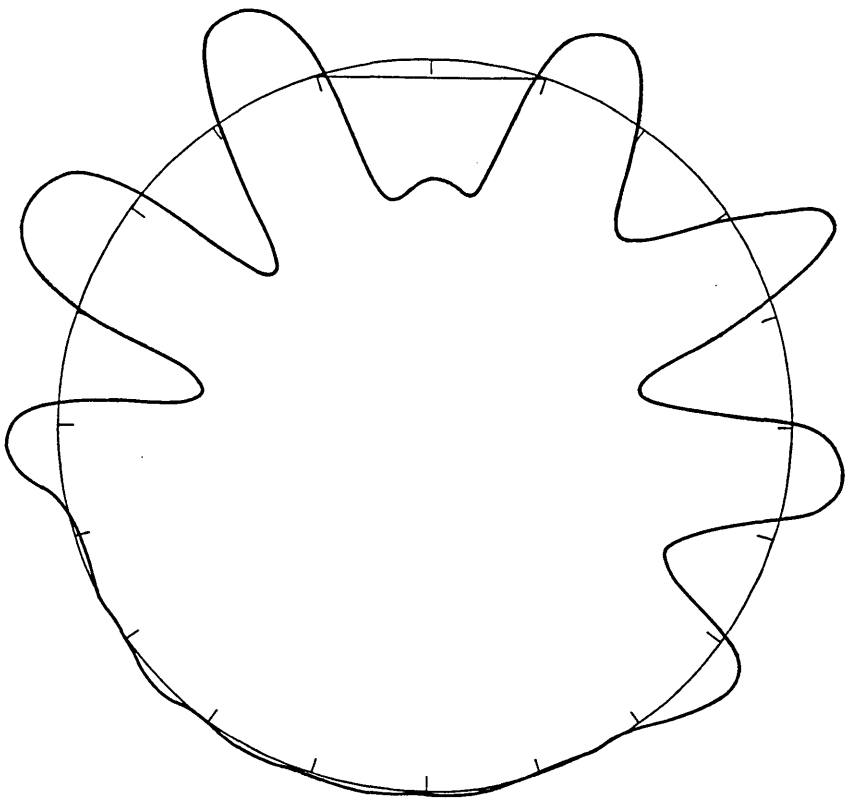


fig. 6·13
Radial deformations at mid-depth immediately after peak load
Cyl. 1A2
Exaggeration x30

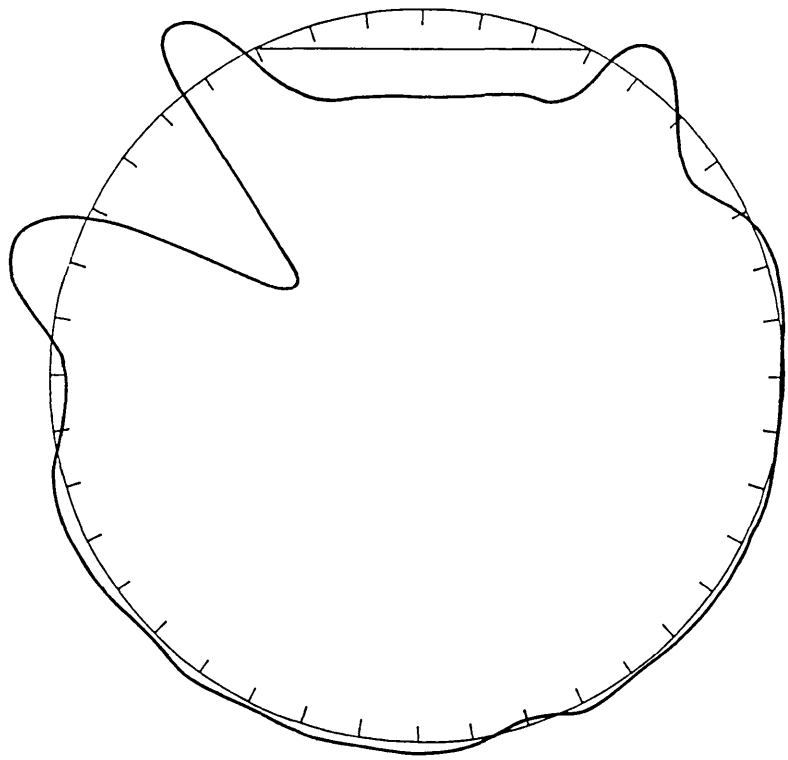
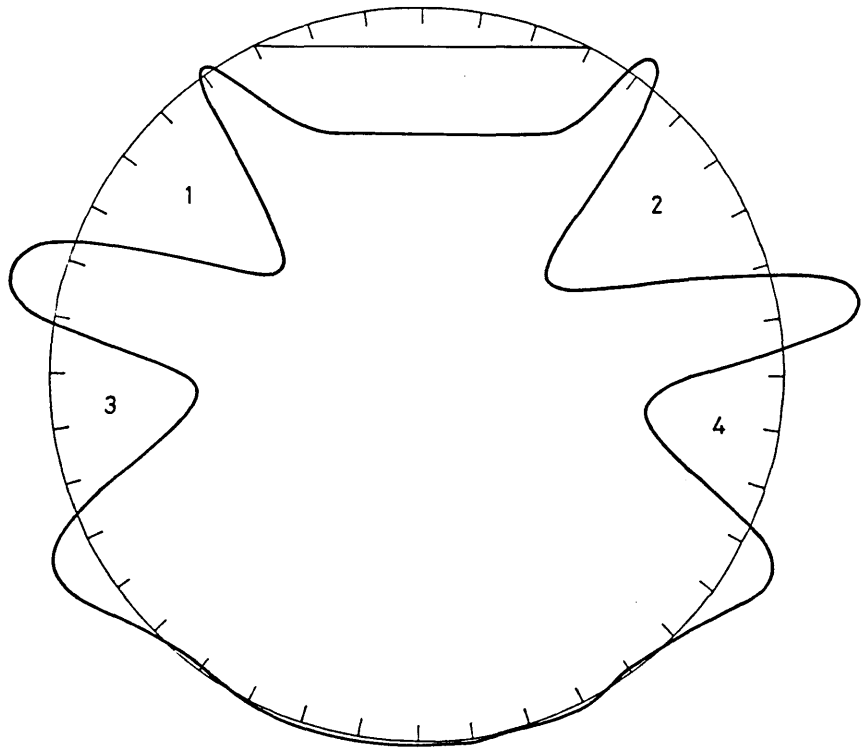


fig. 6.14
Radial deformations immediately after peak load
Cyl. 1B1
Exaggeration ×25



numbers give order of formation of inward buckles

fig. 6.15
Buckling pattern well beyond peak load
Cyl. 1B1
Exaggeration ×10

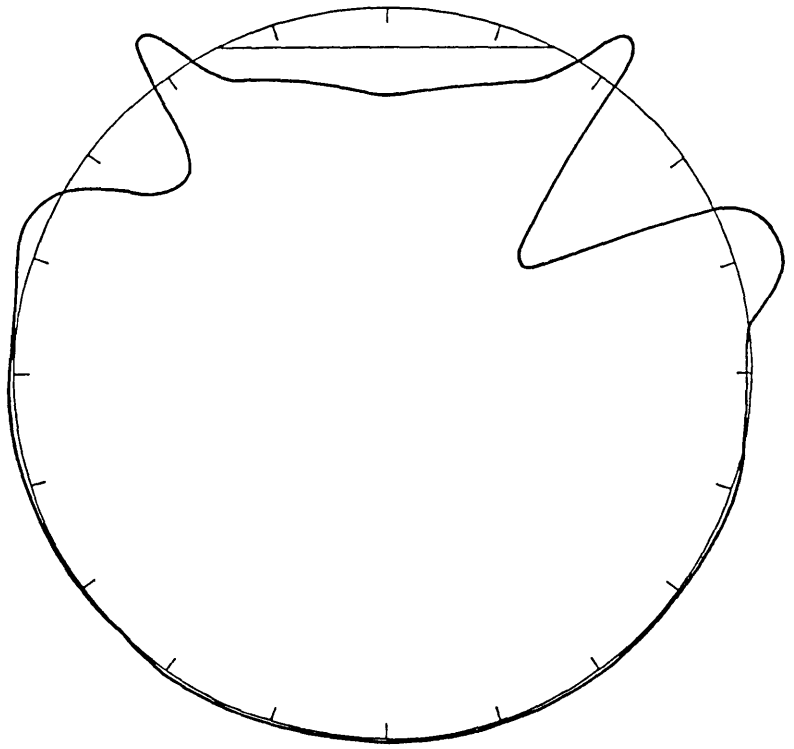
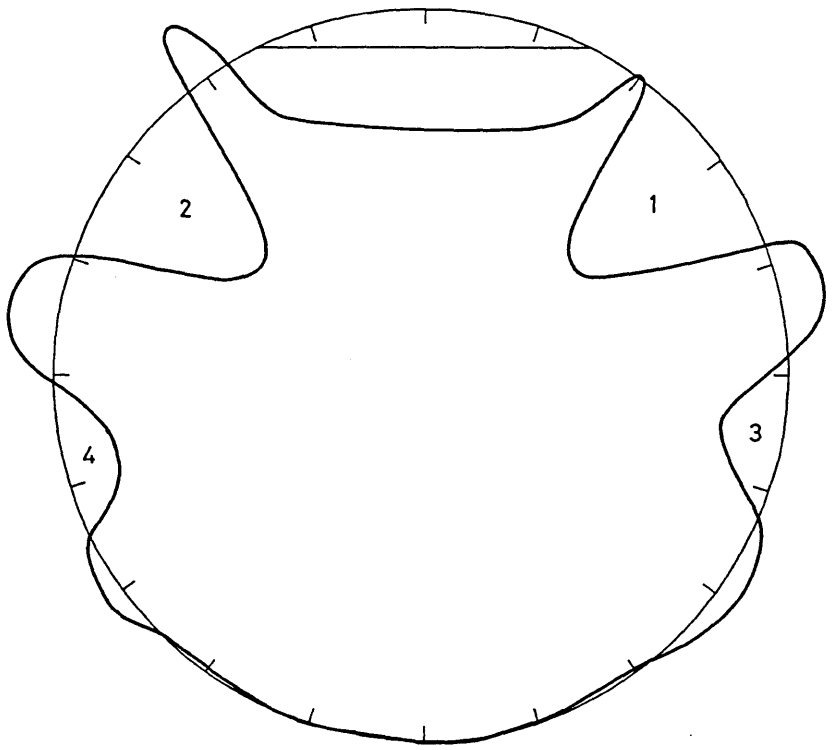


fig. 6.16
Radial deformations immediately after peak load
Cyl. 1B2
Exaggeration ×25



numbers give order of formation of inward buckles

fig. 6.17
Buckling pattern well beyond peak load
Cyl. 1B2
Exaggeration ×10

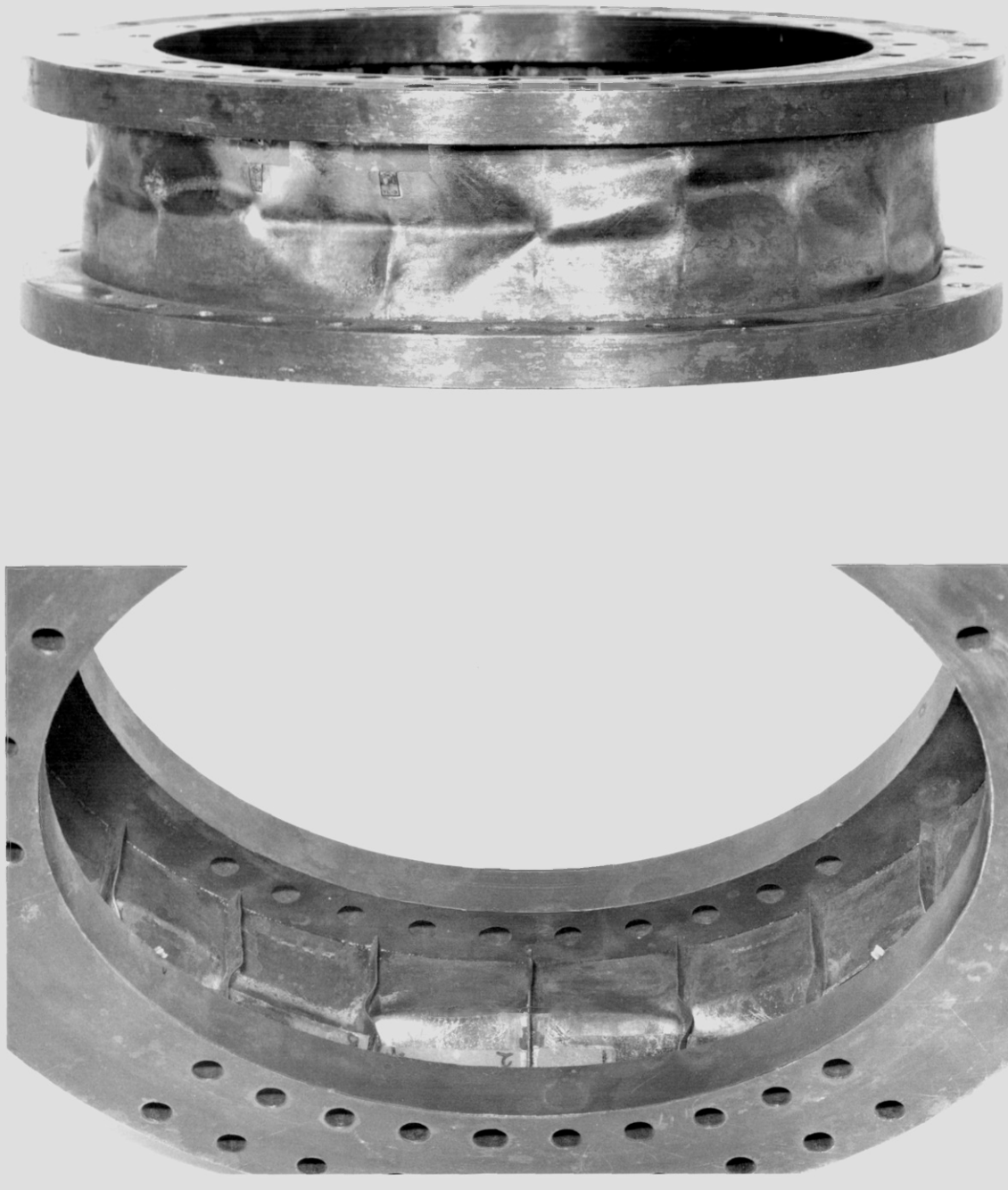


fig. 6-18
Buckling deformations induced by compressive loading
Cyl. 1A2

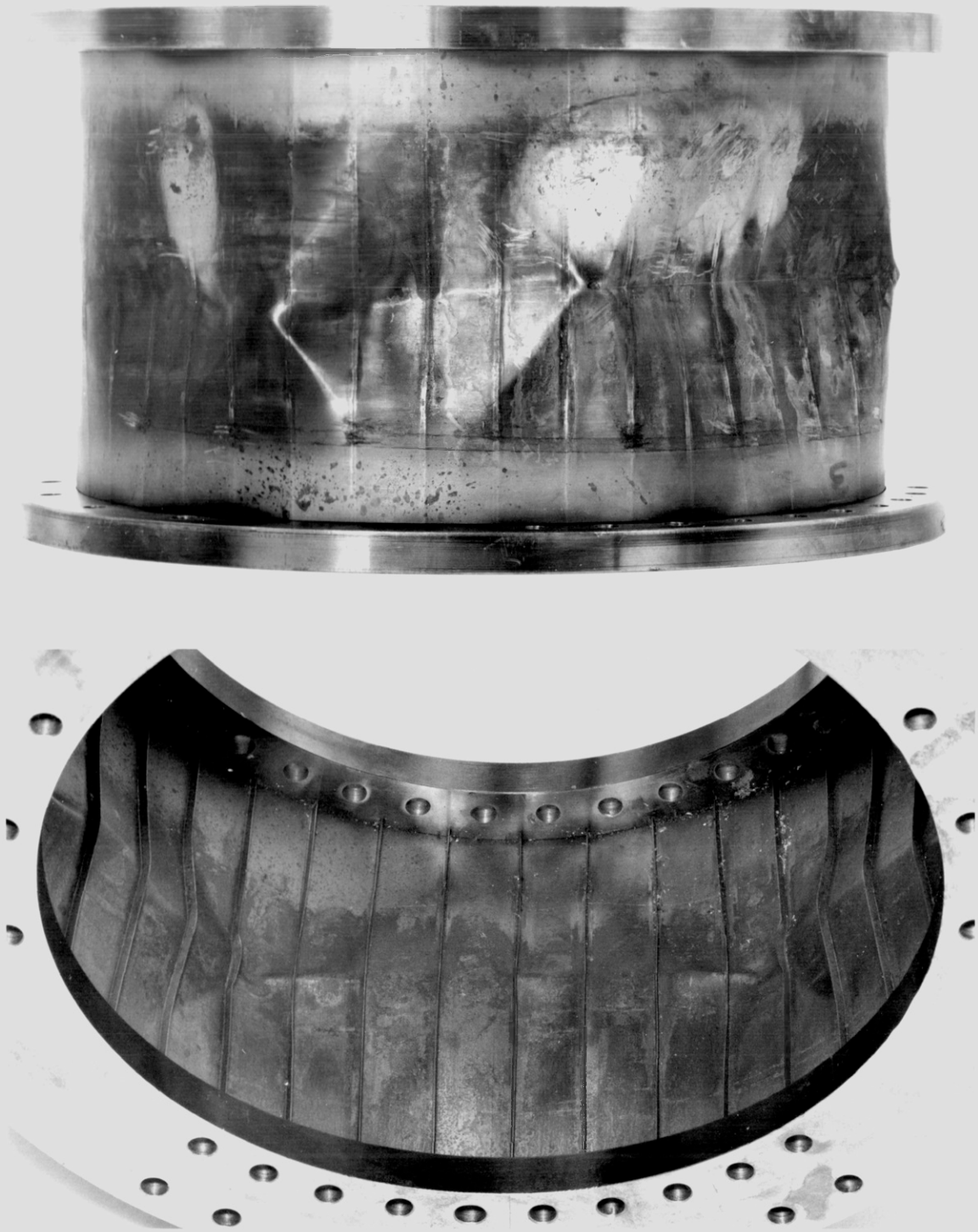


fig. 6.19
Buckling deformations induced by compressive loading
Cyl. 1B1

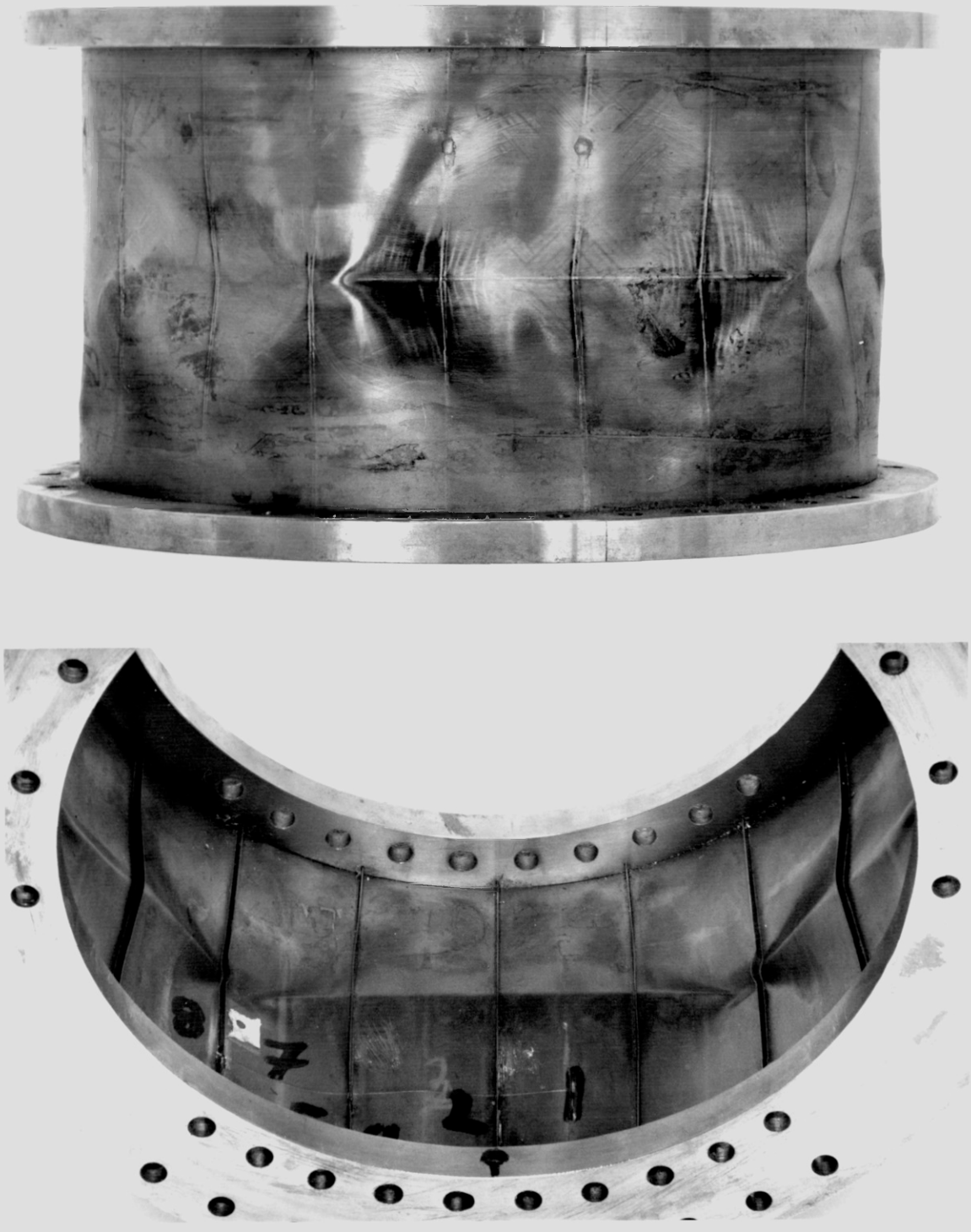


fig. 6.20
Buckling deformations induced by compressive loading
Cyl. 1B2

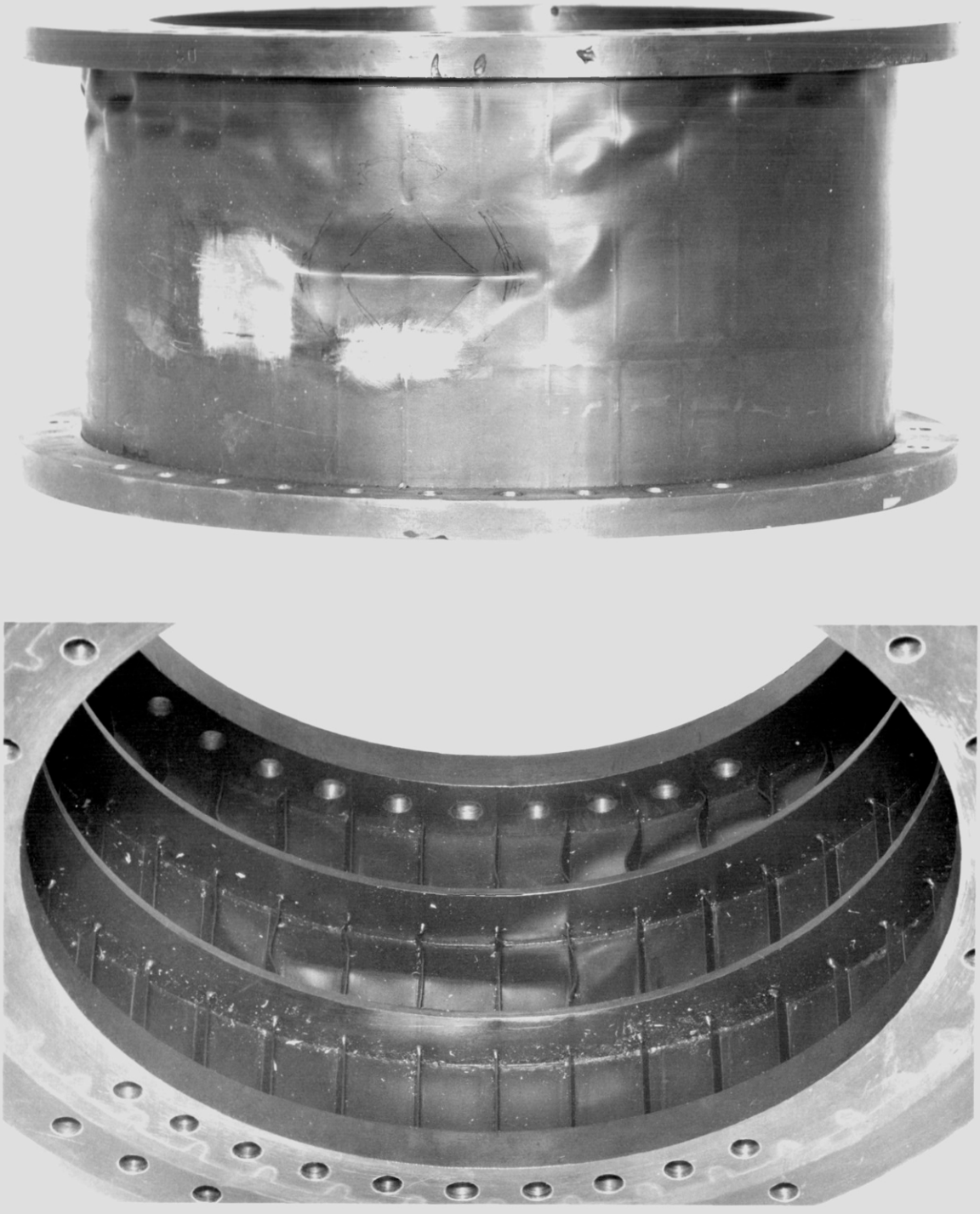


fig. 6.21
Buckling deformations induced by compressive loading
Cyl. 3A2

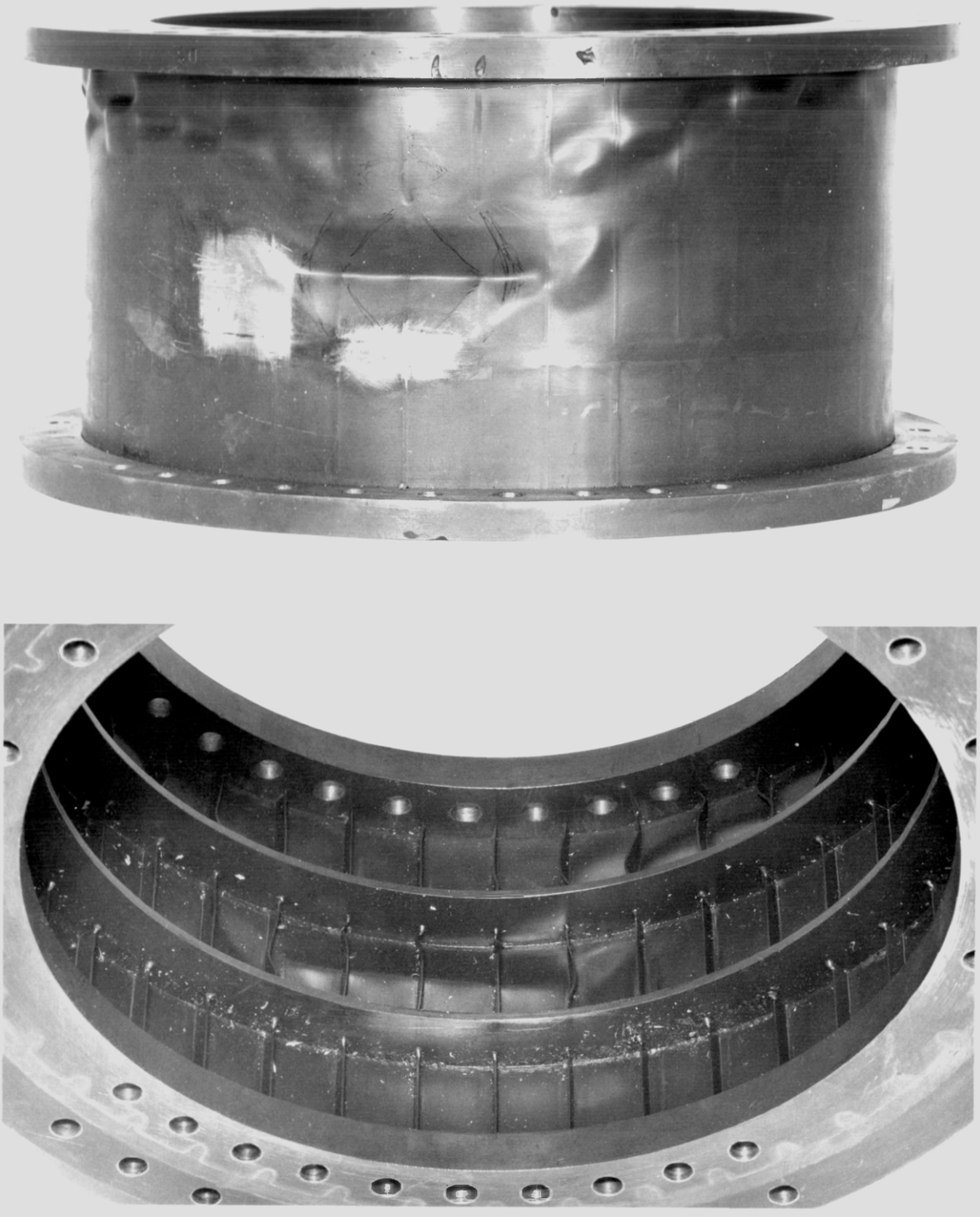


fig. 6-21
Buckling deformations induced by compressive loading
Cyl. 3A2

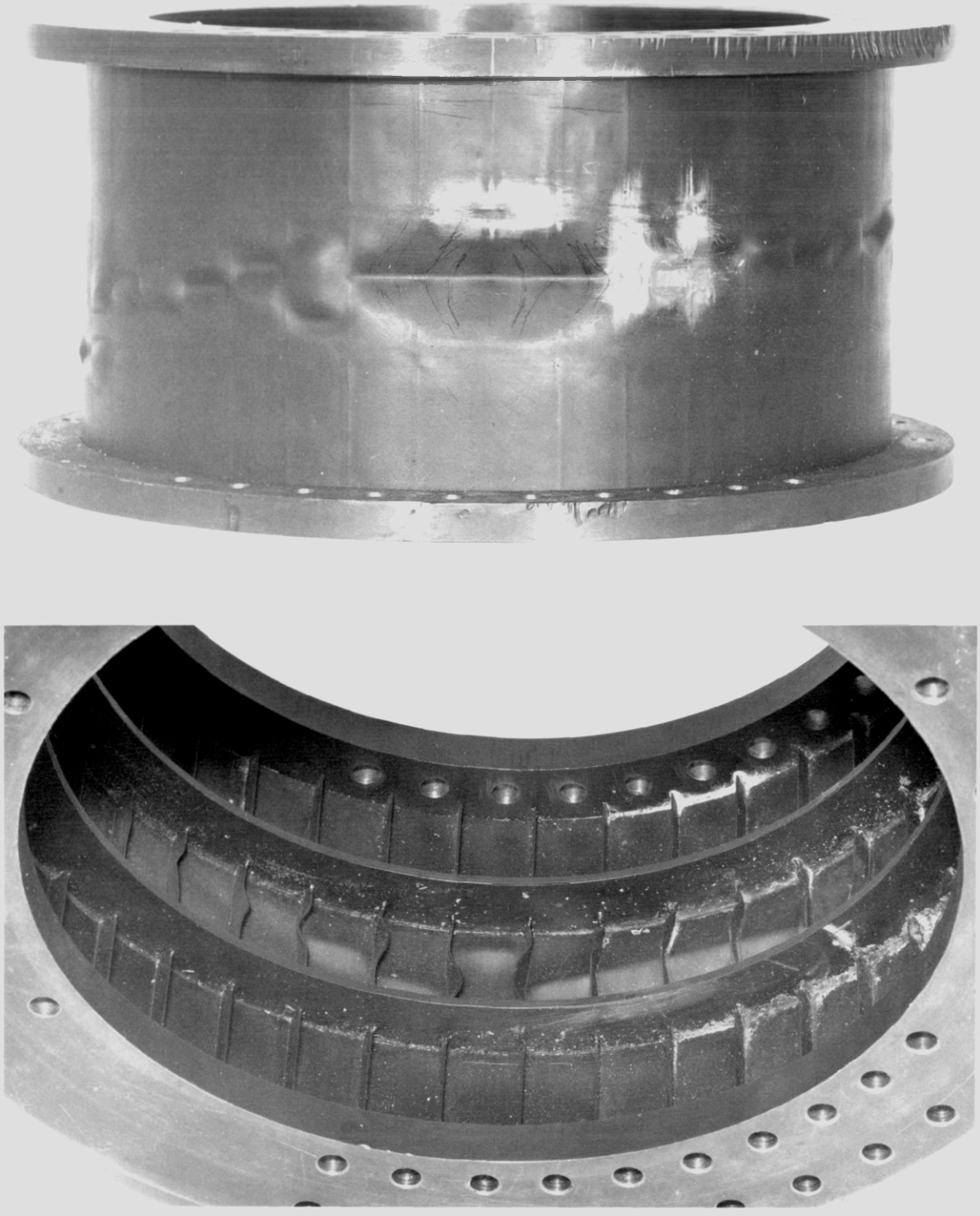


fig. 6-22
Buckling deformations induced by compressive loading
Cyl. 3A3

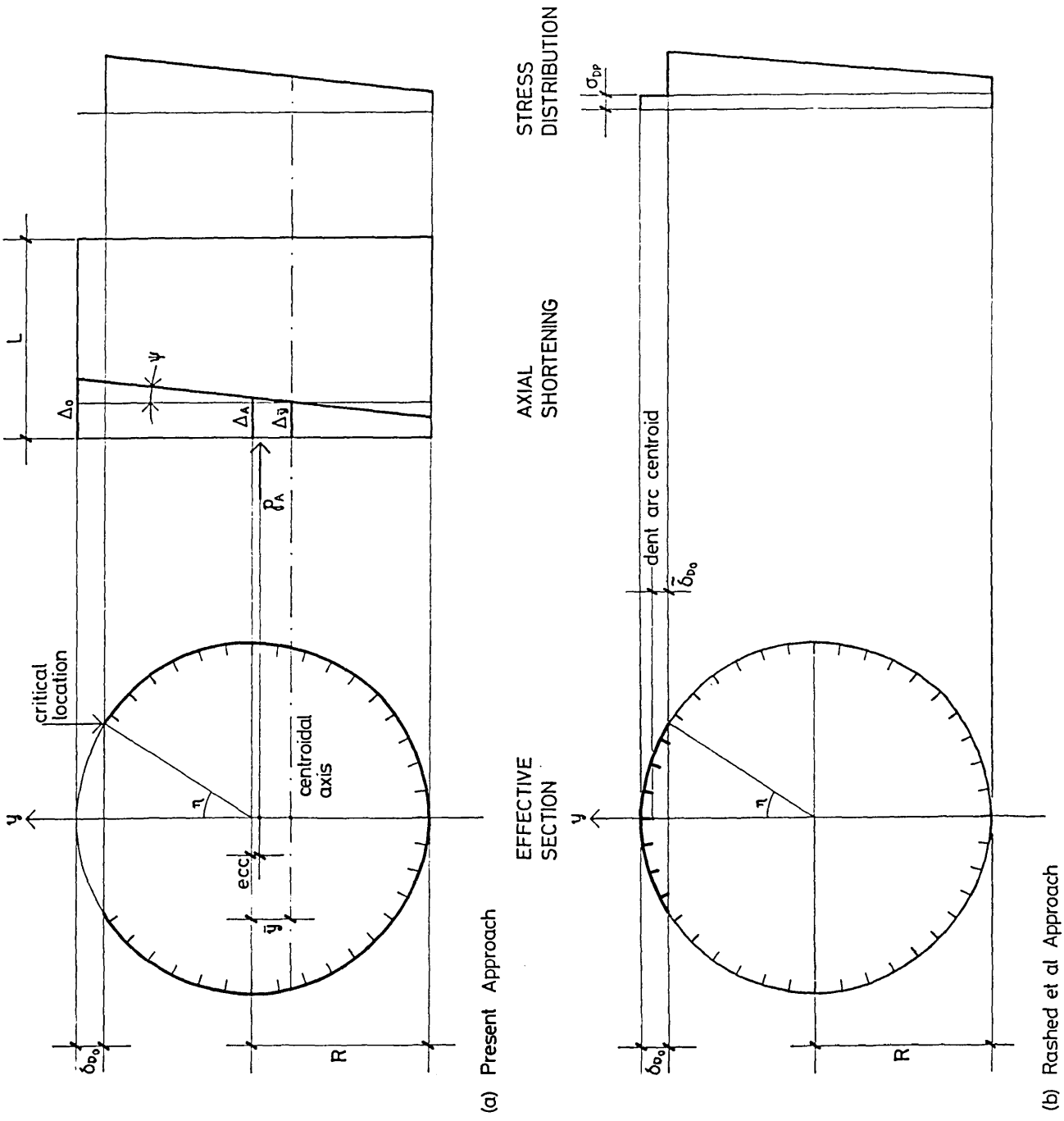


fig. 6.23
Effective section response under longitudinal compression

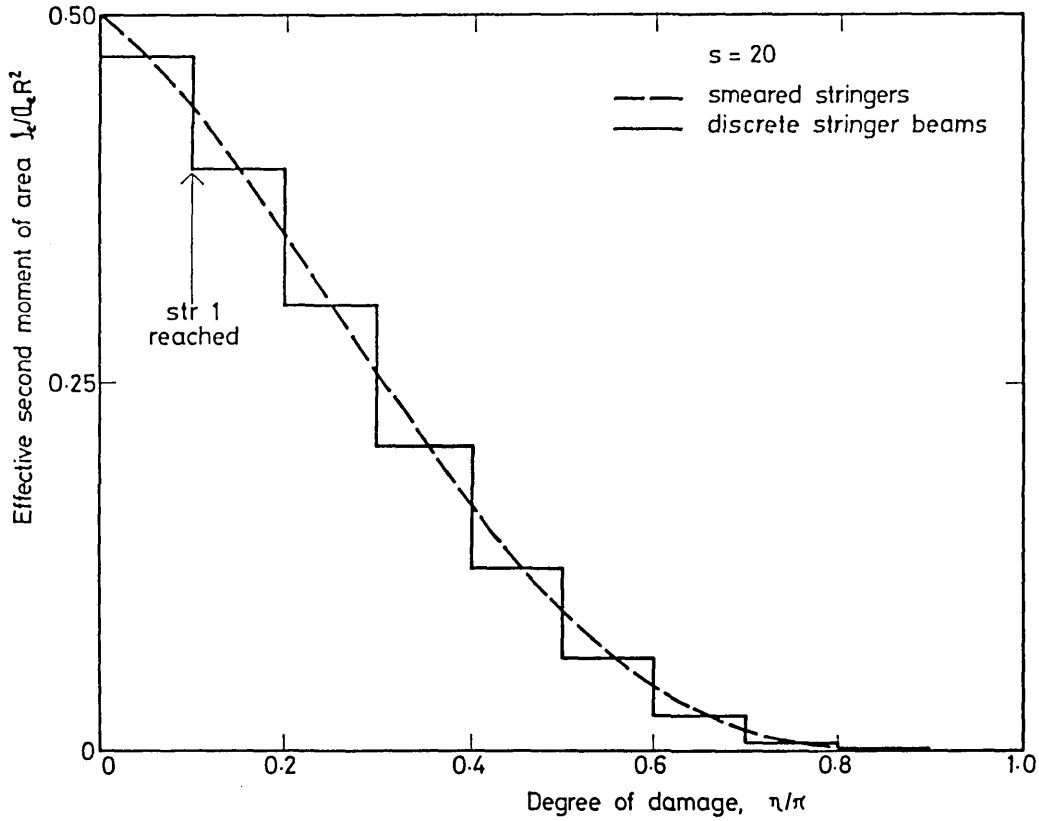


fig. 6·24
Variation of second moment of area with degree of damage

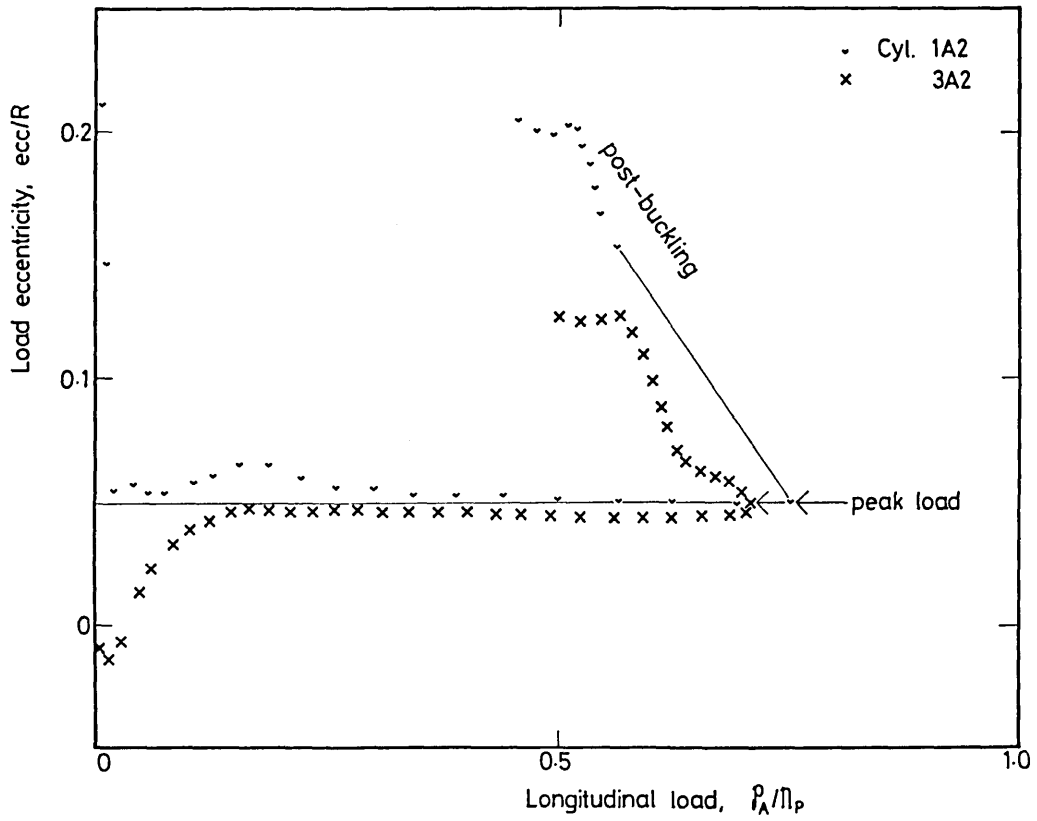


fig. 6·25
Eccentricity of longitudinal load from cylinder centre during response

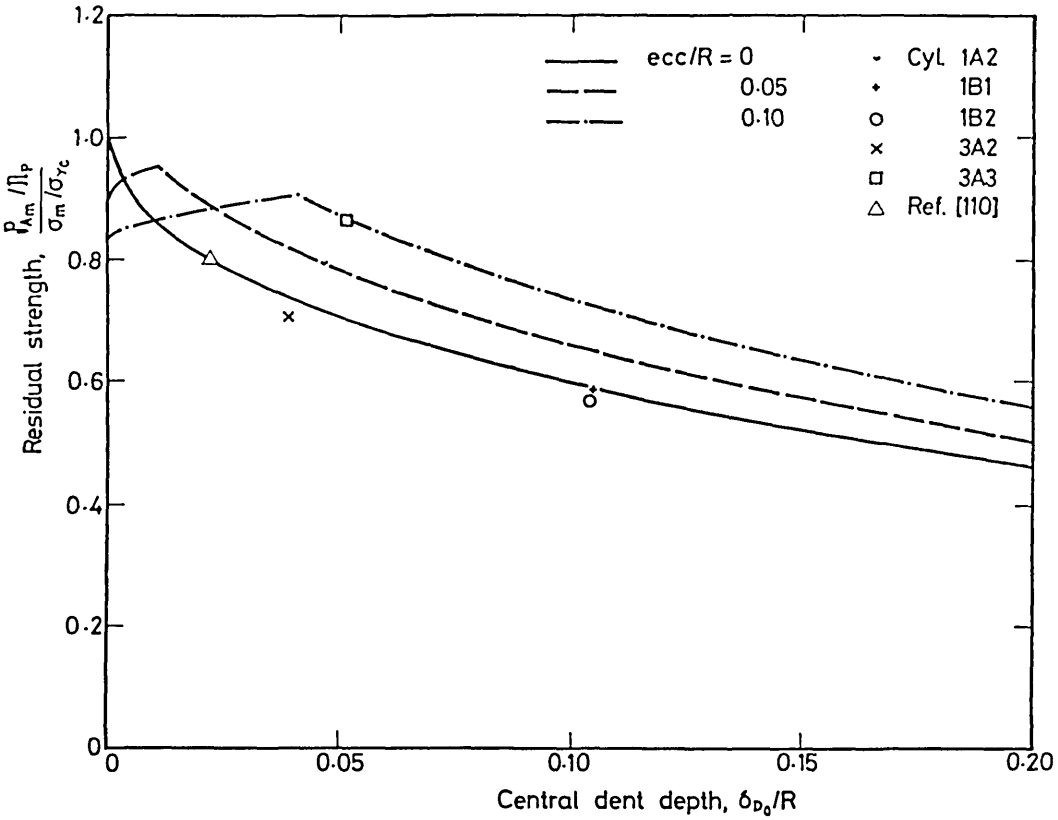


fig. 6·26
Effect of dent depth on the residual compressive strength

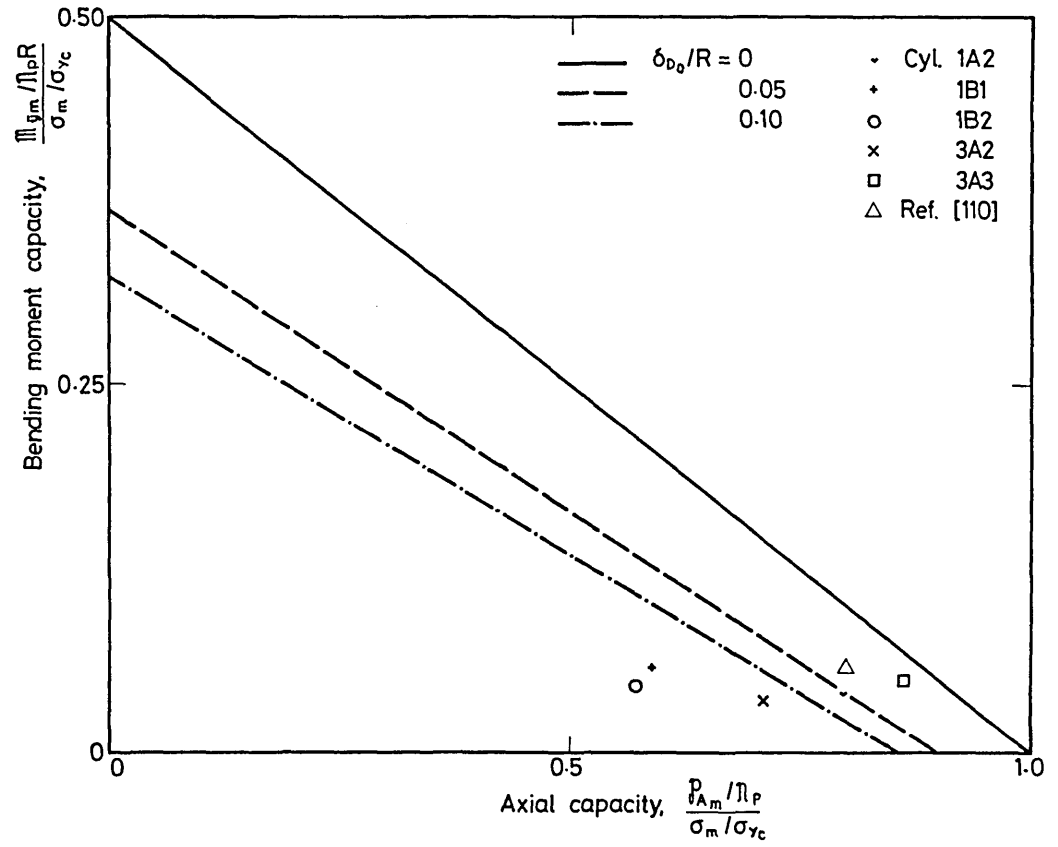


fig. 6·27
Bending moment and axial load interaction capacity

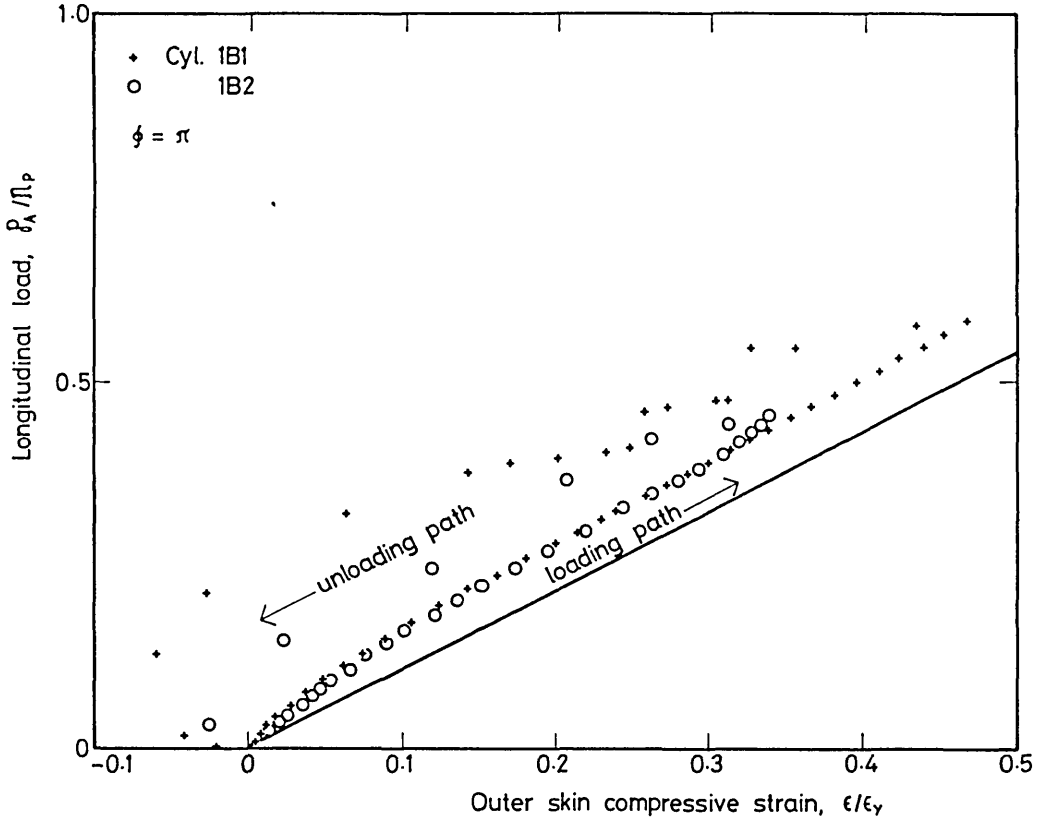


fig. 6·28
Strain development in undamaged region opposite dent
Cyls. 1B

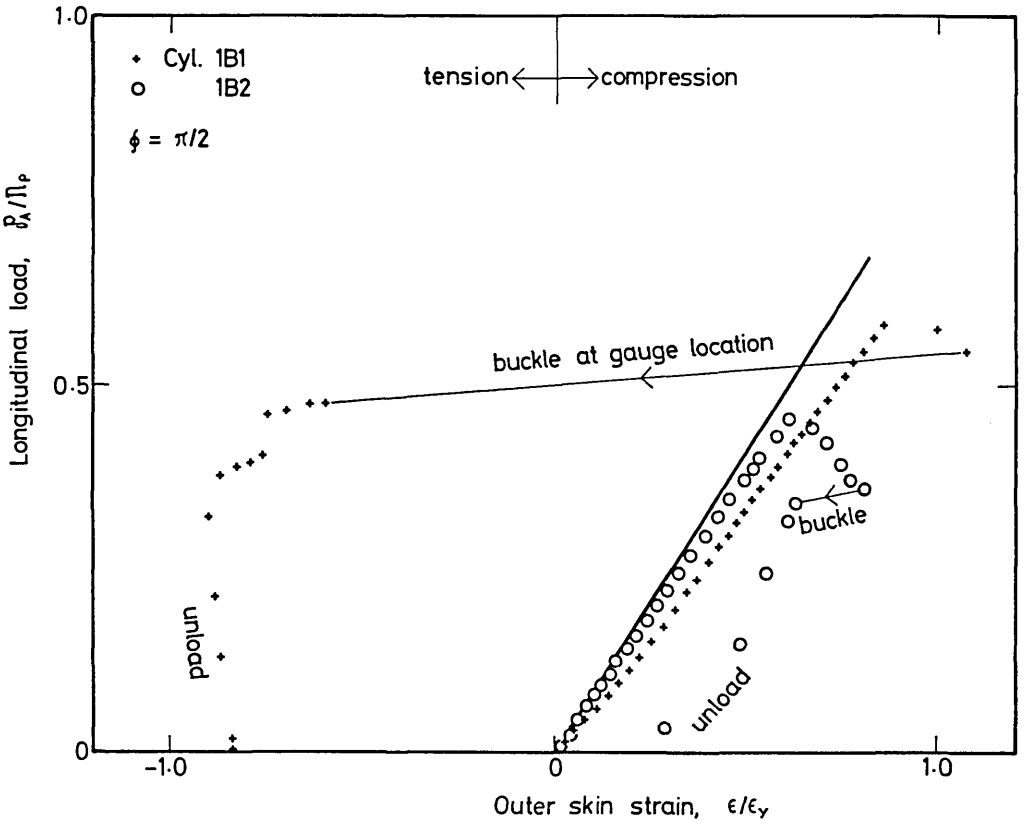


fig. 6·29
Strain development in undamaged region
Cyls. 1B

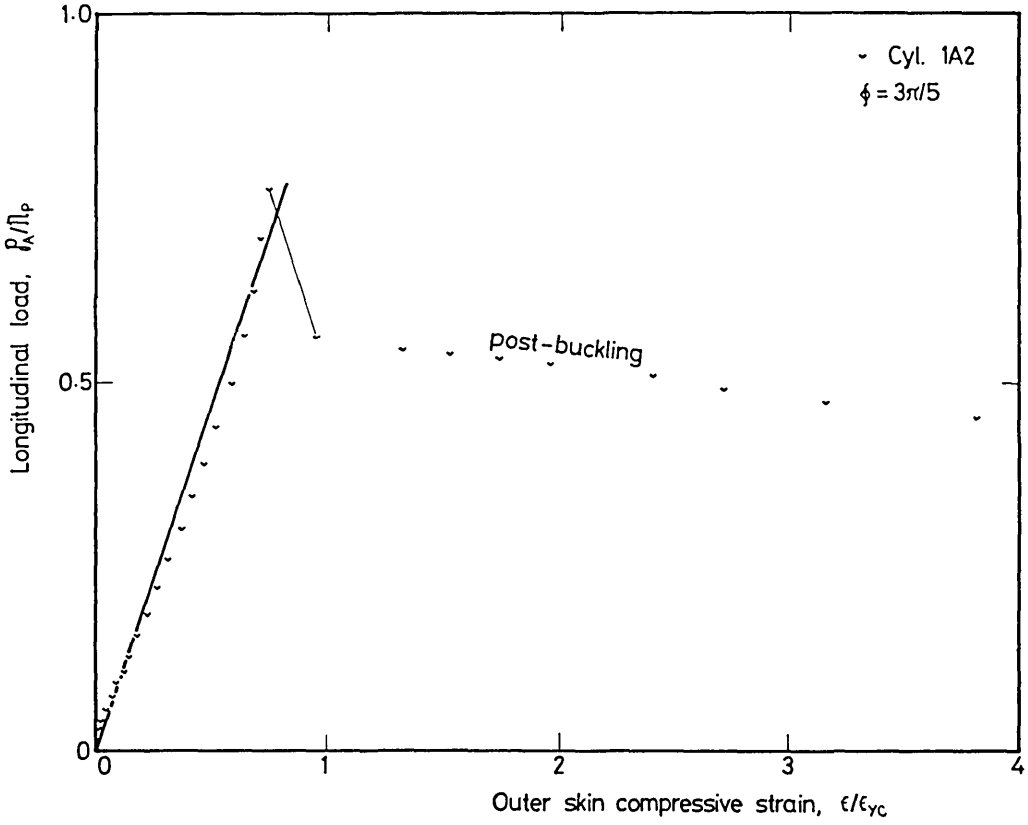


fig. 6·30
Strain development in undamaged region
Cyl. 1A2

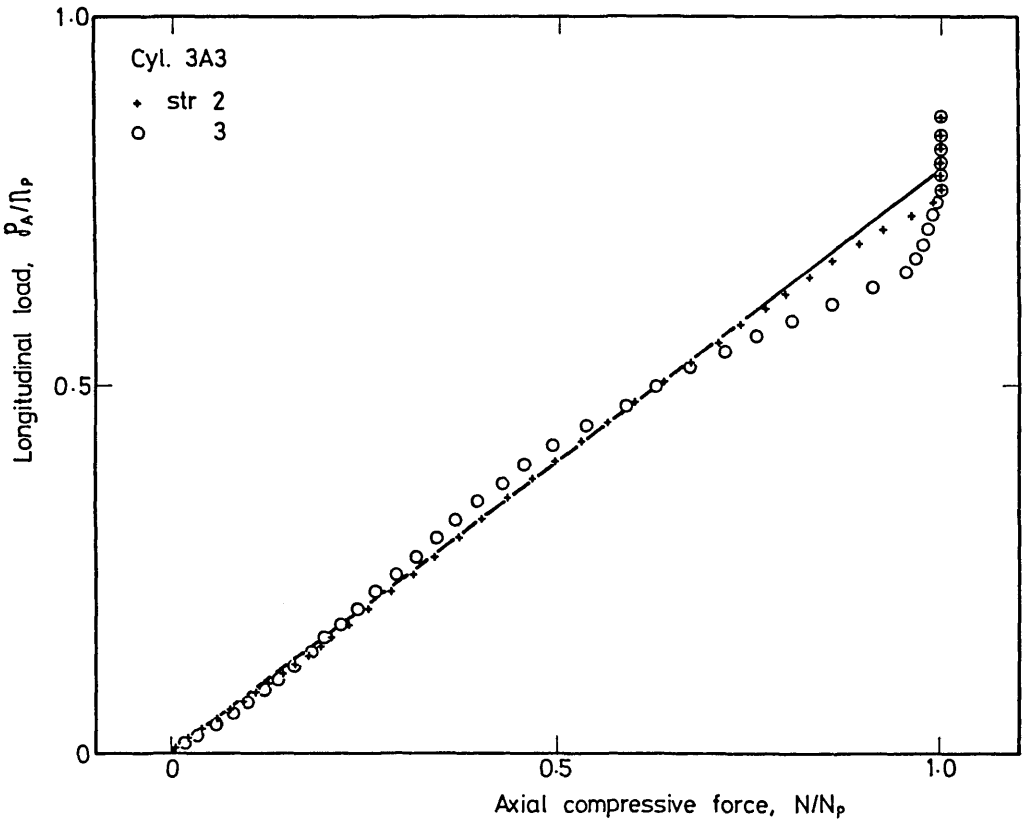


fig. 6·31
Forces in undamaged stringer beams near dent
Cyl. 3A3

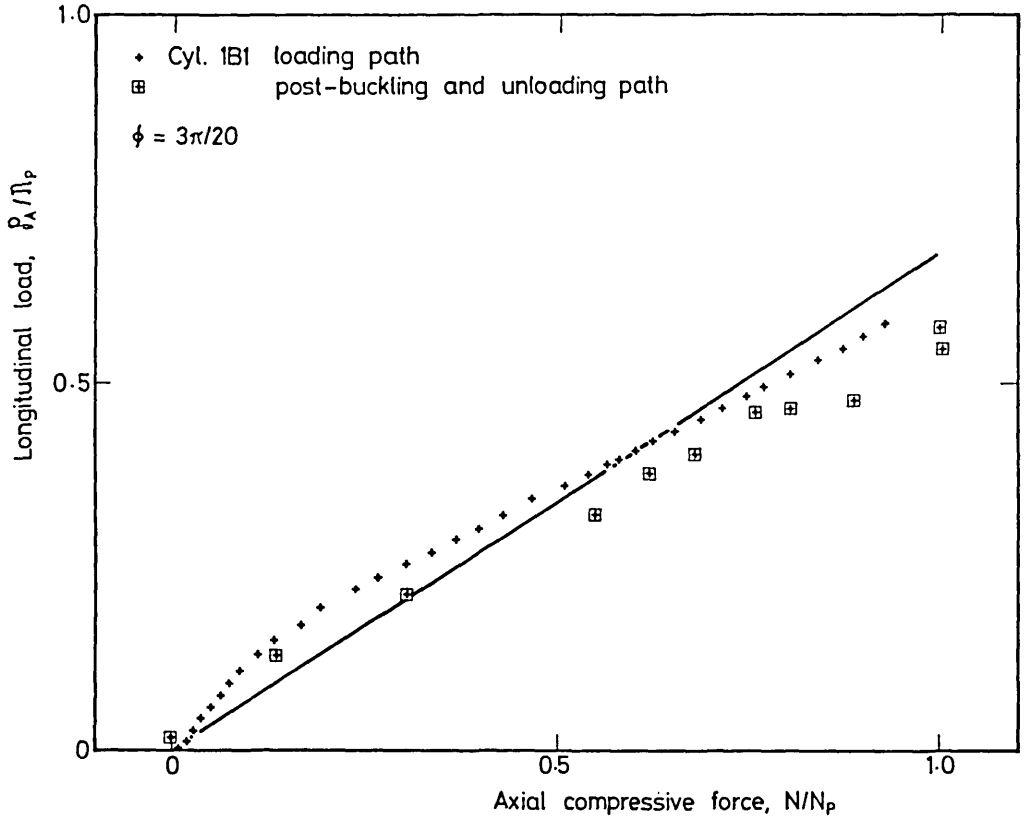


Fig. 6·32
Force in undamaged stringer beam at edge of dent
Cyl. 1B1

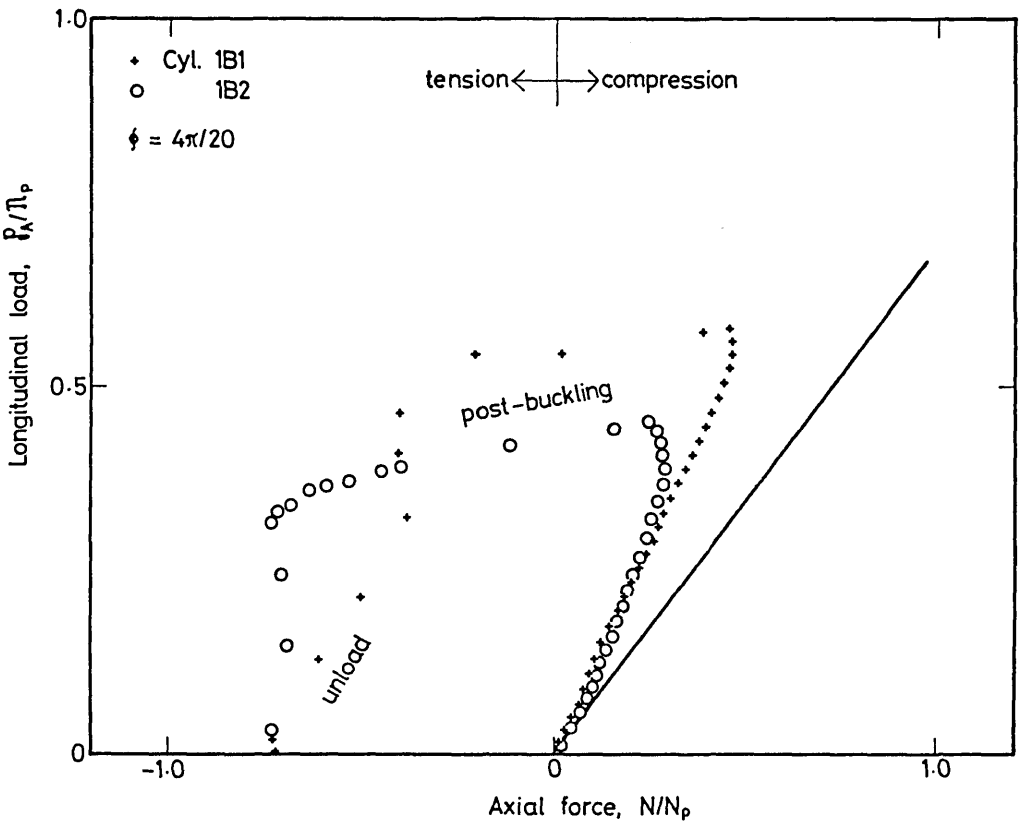


fig. 6·33
Forces in undamaged stringer beams near dent
Cyls. 1B

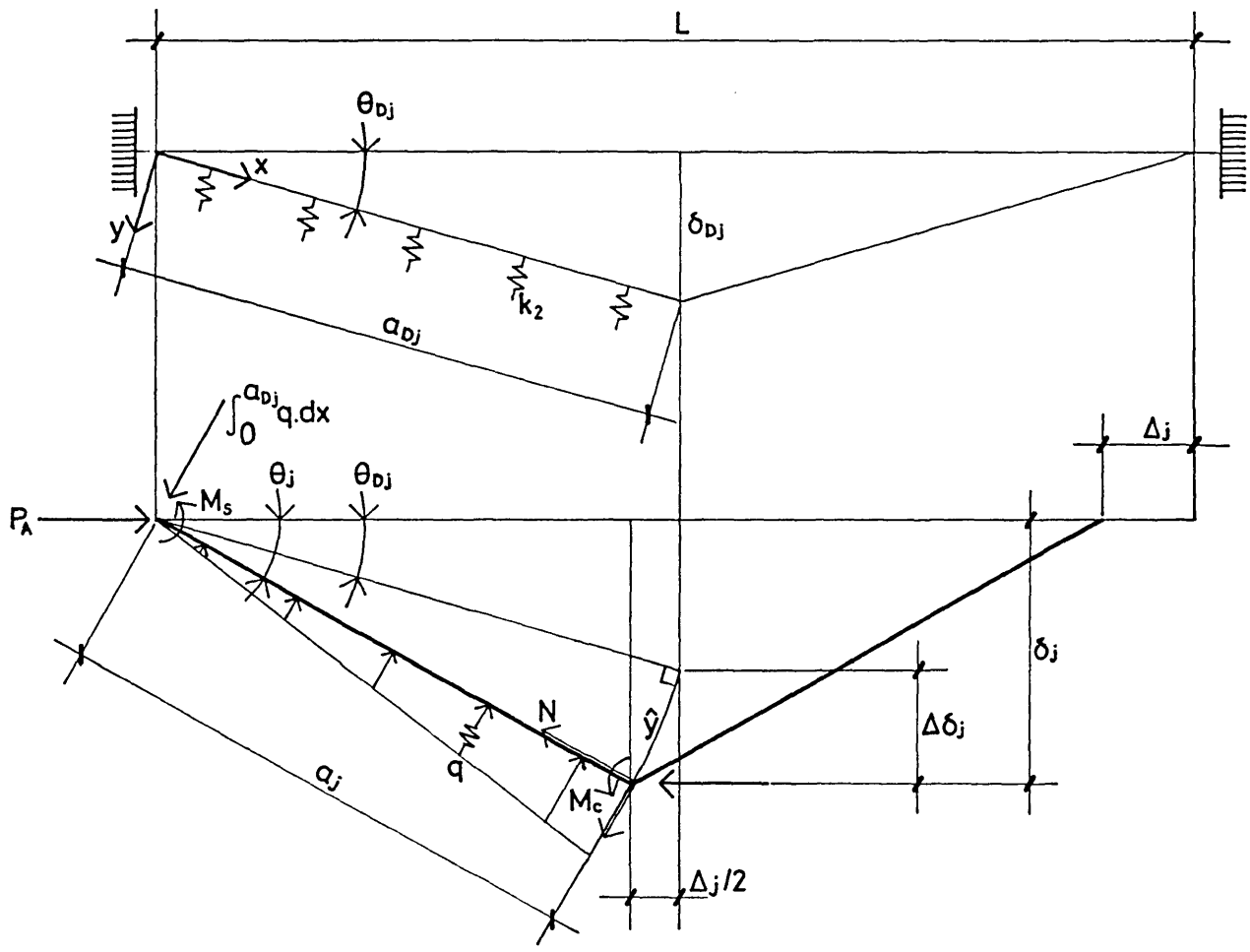


fig. 6.34
Longitudinal loading of V-shaped beam-column on elastic foundation
Forces and deformations

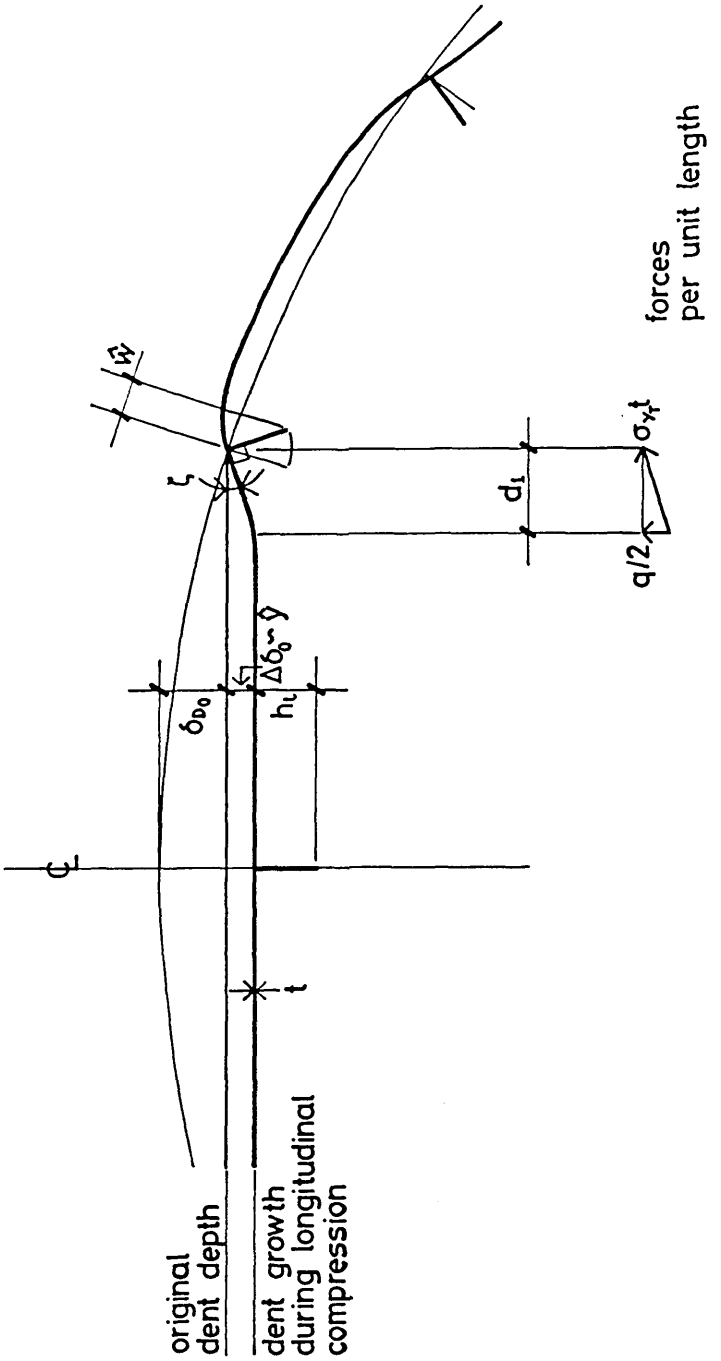


fig. 6-35
Deformations at dent centre under compressive loading
Cyl. 1A2

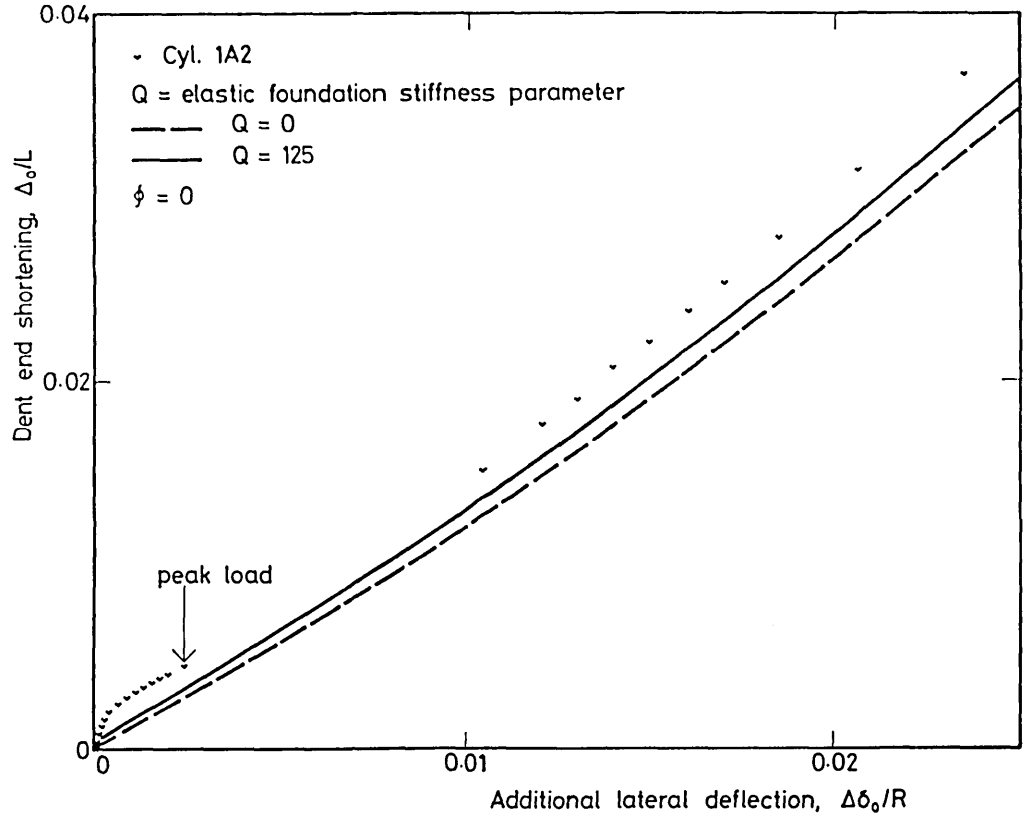


fig. 6.36
Relationship between additional lateral deflection and end shortening in dent Cyl. 1A2

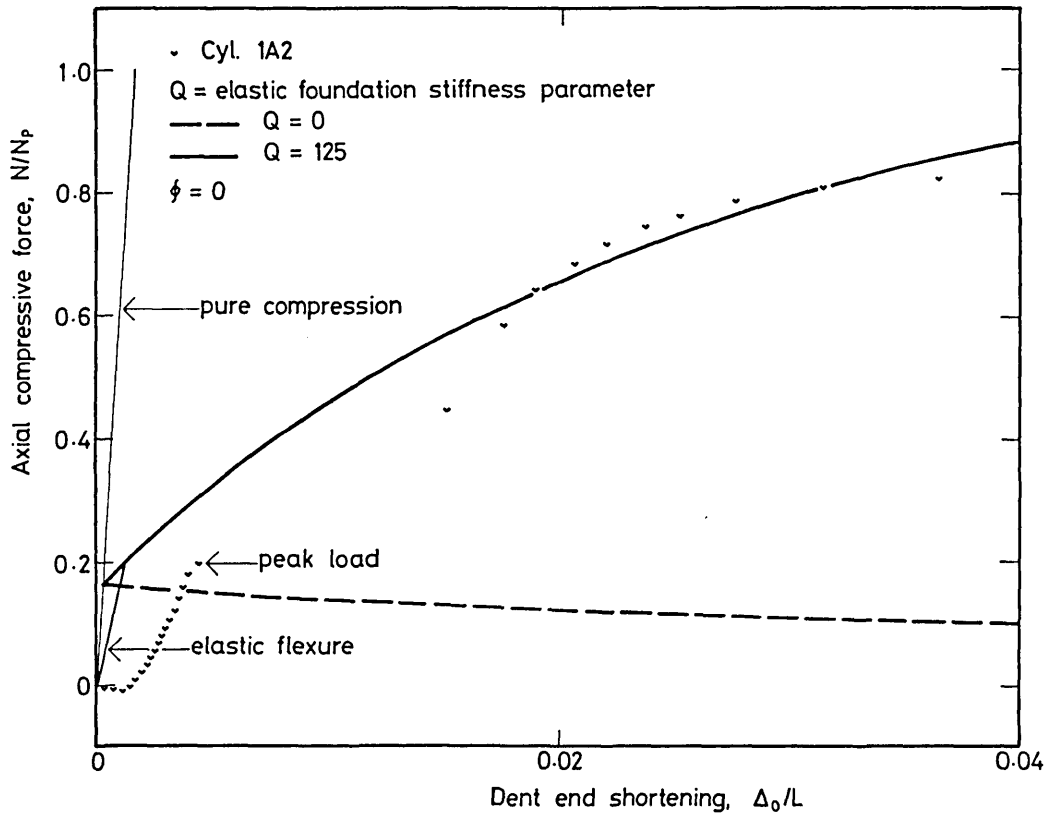


fig. 6.37
Build up of compressive force with end shortening in dent Cyl. 1A2

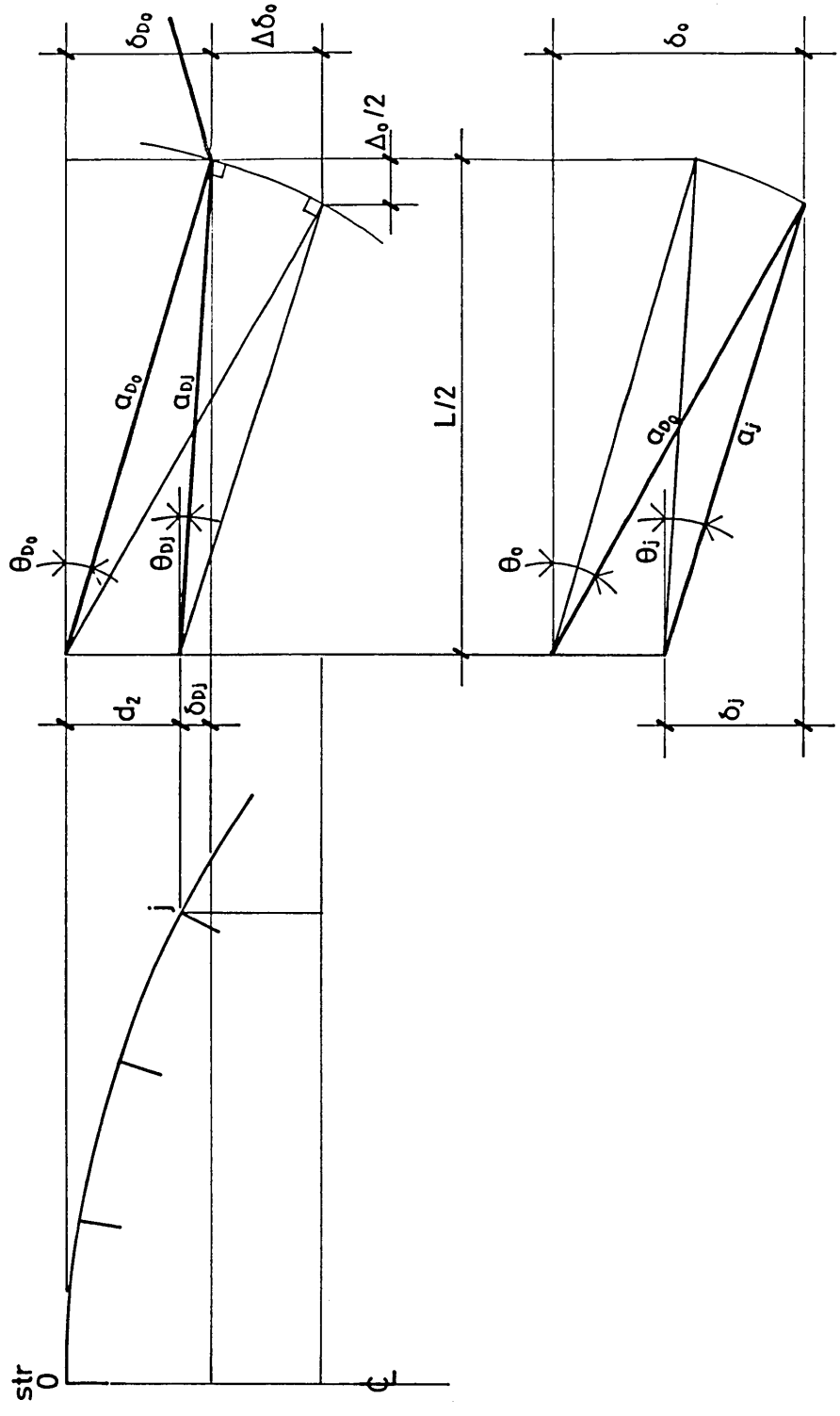


fig. 6.38
Deformation of dented T - beams

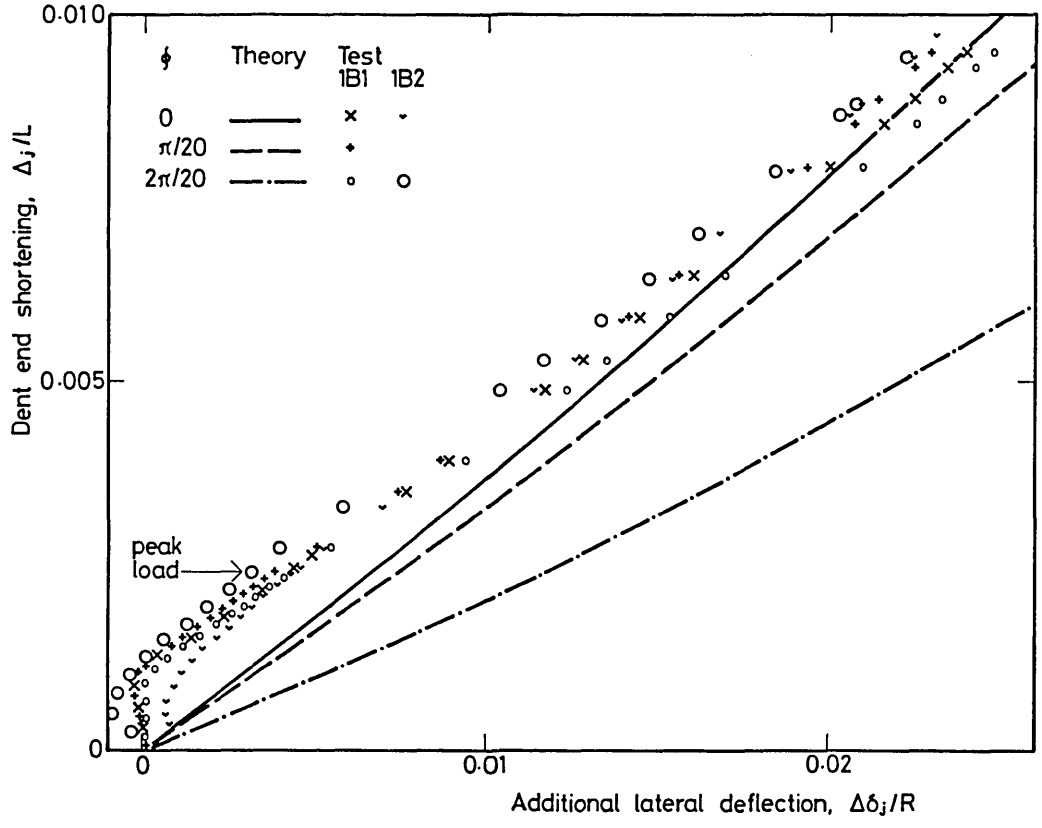


fig. 6·39
Relationship between additional lateral deflection and end shortening in dent Cyls. 1B

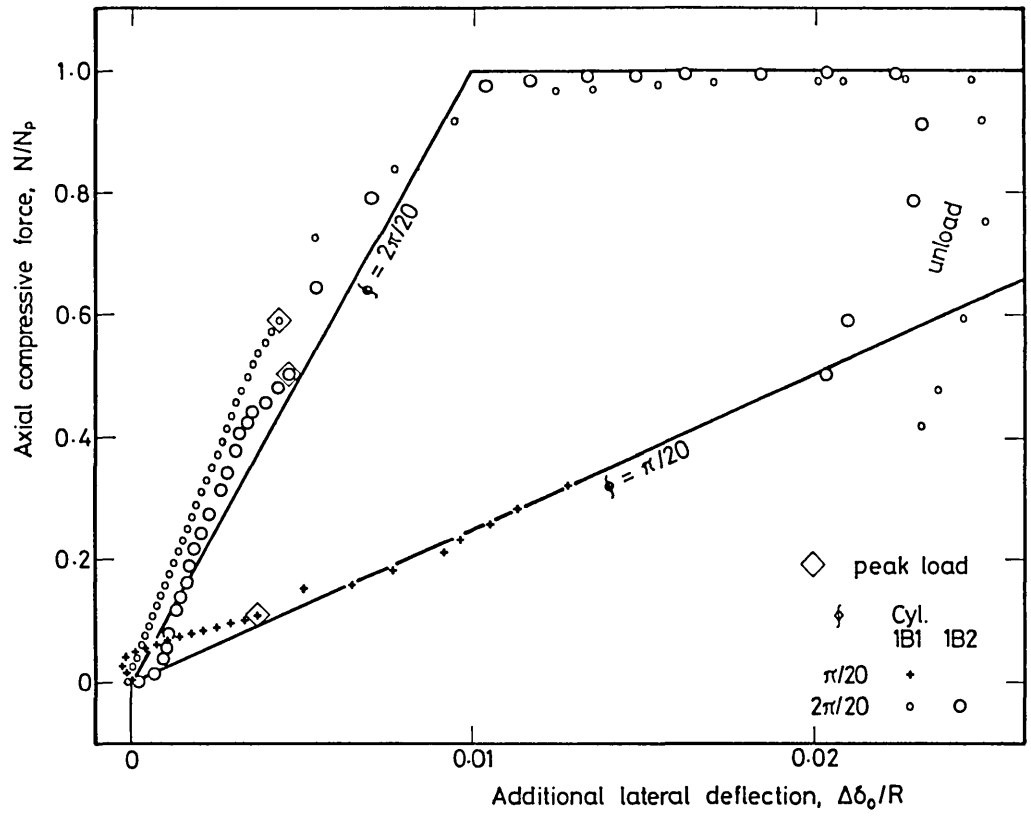


fig. 6·40 (a)
Build up of compressive force with additional dent deflection in damaged region Cyls. 1B

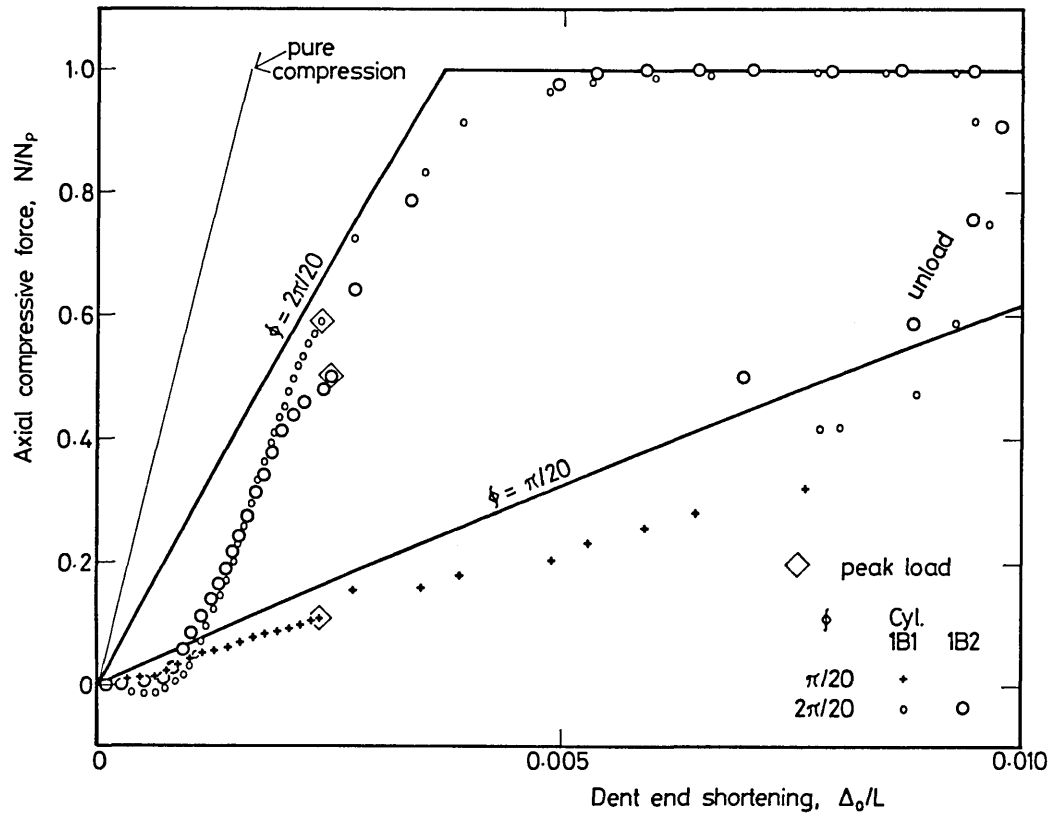


fig. 6·40 (b)
Build up of compressive force in damaged region with respect to dent deflection Cyls. 1B

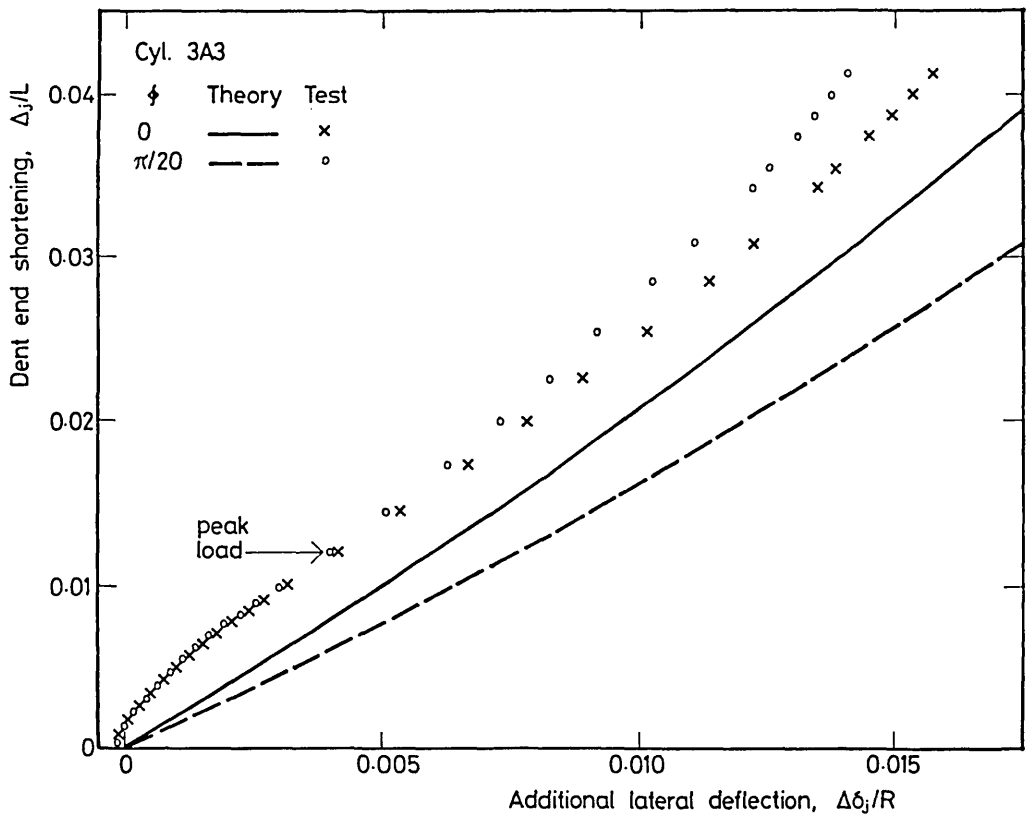


fig. 6·41
Relationship between additional lateral deflection and end shortening in dent Cyl. 3A3

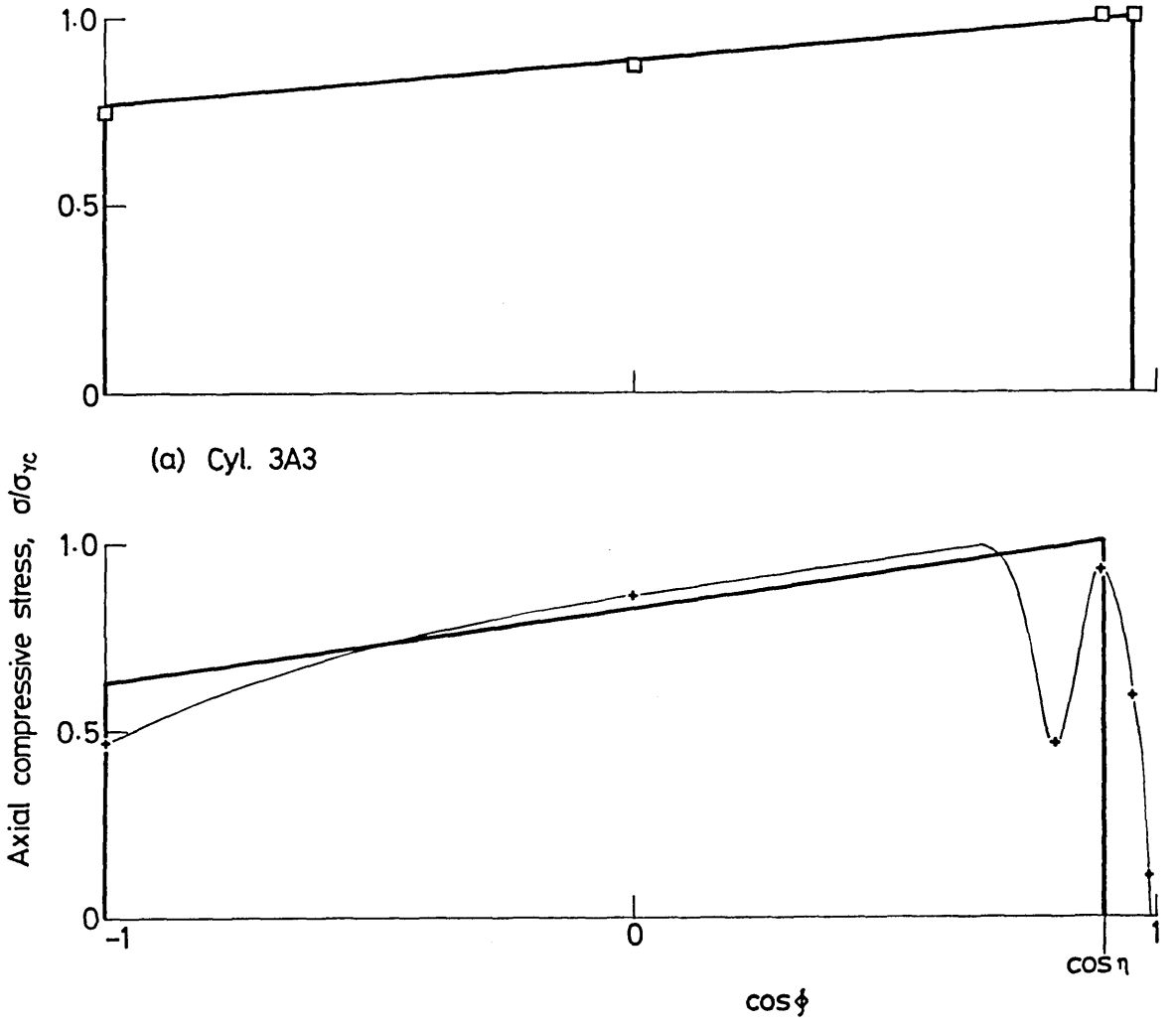


fig. 6·42
Axial stress distribution in dented bay just before peak load

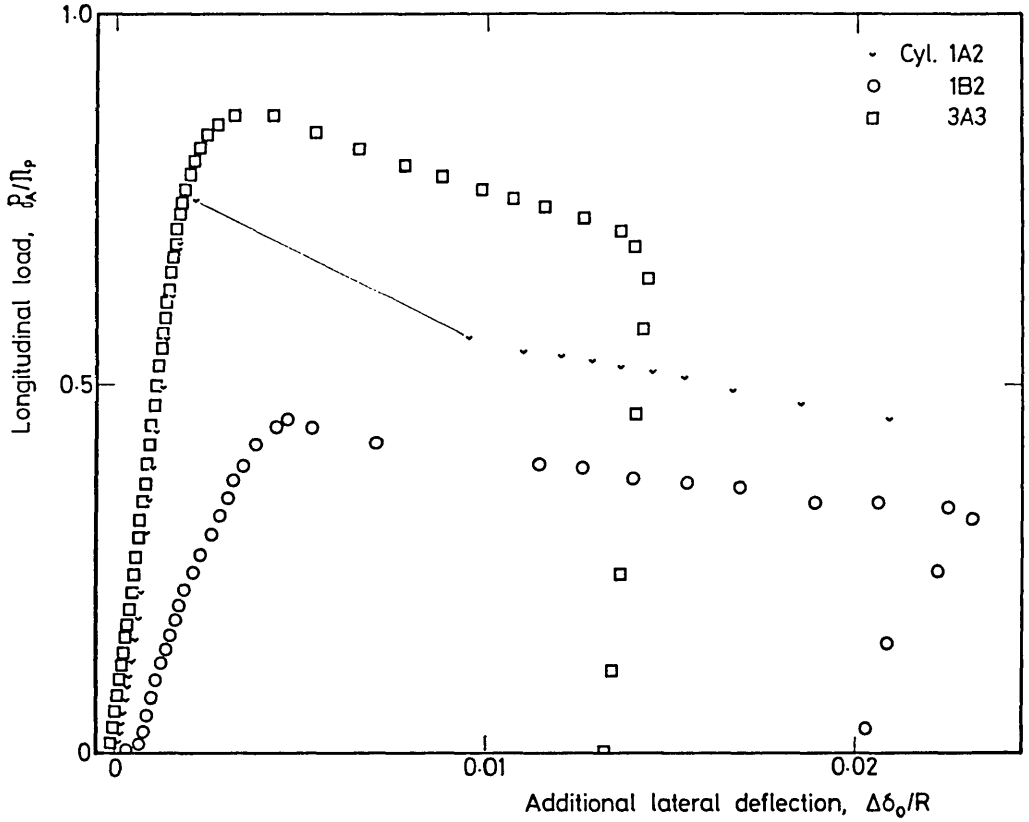


fig. 6·43
Growth of dent deflection during longitudinal loading

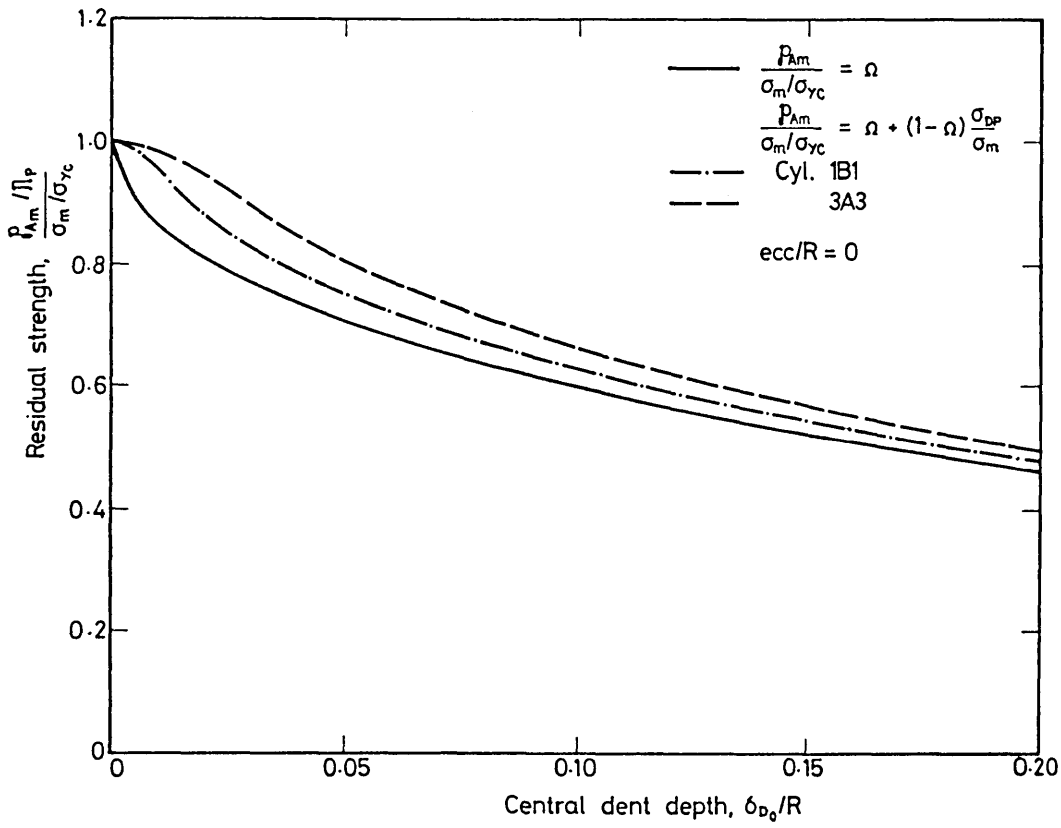


fig. 6·44
Effect of dent depth on the residual compressive strength

CHAPTER 7

CONCLUSIONS OF RESEARCH

7.1 GENERAL CONCLUSIONS

7.1.1 COLLISION LOADING

The response of a T-section beam to finite deflections under central point loading is presented as a closed form solution. Variable axial restraint and both rotationally fixed and pinned supports are treated. The analysis is used to predict the behaviour of stringer stiffened plates and cylindrical shells during knife edge loading perpendicular to the stiffening. In turn, it gives an accurate description of experimental observations.

It is apparent that as long as there is reasonable restraint to longitudinal pull-in the lateral load increases approximately linearly with dent depth, which facilitates the computation of energy dissipation. This is significant as several Codes now specify energy absorption capability as a design criterion. Orthogonally stiffened cylinders typical of those used to form the legs of floating offshore platforms are demonstrated to be robust against the energy that might be released in a supply vessel berthing impact.

7.1.2 RESIDUAL STRENGTH AFTER COLLISION

The development of relatively simple analytical techniques continues in the investigation of the compressive strength of damaged components. This enables the importance of factors other than the primary shape imperfection to be ascertained. The residual stiffness of severely dented stringer stiffened plating is reduced significantly below the level that might be expected, due

to the presence of residual stresses. Local out-of-plane twisting of the stringers makes an important contribution to the similarly significant reduction in strength.

This behaviour means that the dented region of an orthogonally stiffened cylinder carries little compressive load and may be ignored. The effective undamaged material is shown to dictate the axial and flexural stiffness of the models. In addition, failure may be equated with the attainment of the collapse stress of a nominally identical model that is not dented.

This last postulate appears to toss aside the knowledge, of fifty years standing, that thin-walled cylinders are imperfection sensitive. In fact the situation is more complicated than it might seem because, although the dent is a large initial deviation from the the ideal geometric shape, it does not primarily act out the role expected of an imperfection to instigate failure within its confines. Instead, the adjacent undamaged material is forced to distort sharply to provide compatibility between the inward growth of the dent and the developing deflection pattern predisposed by the overall cylinder geometry. Collapse occurs when the stress carried by this formerly intact region reaches its modified capacity in the deformed state.

The deflections that promote failure are unrelated to the initial imperfections existing in the intact region and tend to be much larger. Another point is that the location of failure is largely predetermined in a dented cylinder, whereas for undamaged models the critical point may be anywhere and depends the distribution of imperfections. This implies that the scatter of failure loads found in nominally identical intact cylinders, due to their different imperfections, bears little relation to their residual strengths in a dented state.

Sophisticated theoretical techniques would be required to simulate the growth of distortion near the dent and determine its deleterious effect. However, by completely neglecting the phenomenon the very simple method employed in this dissertation is demonstrated to give reasonable estimates of the response and indicate when and why a more accurate analysis may be of benefit.

Several of the cylinders that have been tested fail at loads close to the simple prediction because they are not imperfection sensitive. They may be even stronger than the analysis suggests if they are able to redistribute stress after yield. Other models are weakened by the enforced deflections and a somewhat unconservative strength estimate results from neglecting these deformations. It should be emphasized, however, that these latter geometries are extremely slender and are not likely to be employed in platform construction in the foreseeable future. They are included mainly to ascertain the limits of the analysis.

In selecting any analytical technique it is sensible to find a compromise between the additional accuracy and the extra computational complexity that usually comes with refinement. Bearing in mind the uncertain nature of actual collision damage, the method developed would seem to have value for the geometries currently in use offshore, facilitating rapid assessment of the loss of stiffness and strength resulting from damage.

7.2 FUTURE RESEARCH

Several areas in which further research is desirable suggest themselves. How the transverse frames in orthogonally stiffened plates and shells deflect under concentrated lateral loading, and the effect of this deflection on the compressive strength of the components,

are both very relevant. It is mentioned in Section 5.2.3 that testing has commenced on a new series of cylinders with very light ring frames. These deform markedly under knife edge loading at mid-bay. With the benefit of an understanding of both in-plane and out-of-plane buckling of the rings gained through this experimental programme, it should be possible to study the problem parametrically and determine a relationship between the degree of restraint afforded by transverse stiffening and its geometry. Offshore, it may even be found prudent to use sturdy ring frames in zones where ship collision is possible, to guard against substantial dent depths which will excessively weaken the column.

The range of parameters under study could be enlarged almost indefinitely. Geometric parameters other than the ring frame size should be varied and an obvious direction of uncertainty is towards very slender models. For these geometries the deformations induced near the dent zone will markedly influence the response. The simple method of strength prediction adopted in this dissertation is likely to become increasingly inaccurate as the slenderness increases and the development of a more rigorous analysis would be important. However an extensive pursuit of this course of action is only justifiable if such light sections are to be utilized in offshore construction. As mentioned in Section 7.1.2 above, this is doubtful.

Another facet of the problem is the type of lateral loading, including the shape of the indenter and its location with respect to the transverse frames. Loading speed is also pertinent to determine the effects of strain rate. Although of interest, the author does not emphasize the investigation of variations in these items, as the loading configuration adopted herein is probably the most critical and therefore suitable for design purposes. In addition, tests have recently been carried out at Imperial College on ring stiffened cylinders where knife edge loading is applied close to a ring frame, and these should

provide supplementary guidance when they are documented.

Perhaps of higher priority would be an investigation of the residual strength of the dented member under various loadings. In the sea external pressure loading is important, and, in fact, is currently under study at the University of Surrey. Forming part of the same cohesive research programme as the new orthogonally stiffened model series that will follow the one reported here, identical geometries have been chosen at Surrey. This new work is expected to show the deleterious effect of a dent to be amplified under external pressure loading.

If resources permit it would be desirable to extend the scope of work, and subject dented models to several loading hybrids in order to build up a complete picture of the interaction curve between axial compression and external pressure. However it should be remembered that ship impact will occur close to the water-line.

Value would also come from eccentric loading tests to ascertain the consequences of bending moment on the dented section. Combined axial compression and bending is a very likely loading condition in practice.

All of the tests undertaken for this dissertation are on models representing only a small part of a prototype member. This is a common procedure and is regarded to give a reliable indication of the behaviour of a longer component. This is certainly true in the estimation of compressive strength. Even with the complexities of stress redistribution and additional bending moments, mentioned in Section 6.7, faithful reproduction of the response of a member with many bays is relatively straight forward by means of a computer model that assigns the properties of the dented bay to one or more elements.

Not everything is entirely clear, however. The present research has shown that for lateral loading the

response is dependent on the degree of restraint provided against longitudinal displacements. Artificial end conditions are employed in the tests and it would be interesting to investigate the axial stiffness existing in a longer member. Presumably the stiffness will prove to be dependent on the member length, its support conditions, and the frequency and rigidity of bulkheads. (Of course the equations derived for the lateral load versus deflection response in Section 3.4.3 remain valid for any value of longitudinal restraint.)

These are only the most obvious subjects for consideration. New data will yield a greater and more complete understanding of the problem whilst always suggesting further research.

NOTATION

a_{0j} length of each leg of stringer j at start of longitudinal loading
a_j length of each leg of stringer j during longitudinal loading
a_{tr} length of each leg of trip at stiffener tip
A total cross sectional area of stringer beam = $A_p + A_t$
A_t stiffener web cross sectional area = $h_t t_t$
A_p panel cross sectional area = bt
A_r intermediate ring frame cross sectional area = $h_r t_r$
a total cylinder cross sectional area
a_e effective cross sectional area of dented cylinder
b stringer spacing = αR
B half width of dent

C_0 $(A_p - A_t)/A$

C_1 $\dfrac{\frac{1}{4}\sigma_{YT}/E}{\gamma}$

C_{1*} $\frac{1}{4}\sigma_{YT}/E$

C_2 Lb/A

C_3 $\dfrac{2L/A}{1/t_t + 1/b}$

C_4 $(A_p - A_t)(1/t_t - 1/b)/2L$

C_5 $2Lt_t/A$

C_6 $A_p^2(1/t_t - 1/b)/2LA$

C_7 $(A_t/A_p)^2 C_6$

C_8 $(1-\gamma_*)(1 - \cos\phi)R/L$

C_{13} LA/Z_p

d moment distribution factor
e axial extension or compression
$2e'$ total apparent membrane extension

ecc eccentricity of load application from cylinder centre
E Young's modulus
f $A^2/4bZ_p$
I stringer beam second moment of area
I_e effective second moment of area of dented cylinder
k_D stiffness and strength reduction factor of dented fibres
k_1 elastic support spring stiffness
k_2 elastic foundation unit spring stiffness
ℓ_h plastic hinge length
L bay length between ring frames $= 2a_I$
L_t overall length of three bay cylinder $= L + L_U$
L_U undamaged length
L_D length of dent

m $\dfrac{\text{bending moment in stringer beam}}{\text{plastic moment capacity of stringer beam}} = \dfrac{M}{M_p} = \dfrac{M}{\sigma_Y Z_p}$

$M_{\bar{y}}$ bending moment in cylinder due to eccentricity of longitudinal load

∂m $\dfrac{\partial M}{\partial M_p} = \dfrac{\partial M}{\sigma_Y \partial Z_p} = \dfrac{\partial M.\ 4}{\sigma_Y t_t^2 \partial y}$

n $\dfrac{\text{axial force in stringer beam}}{\text{yield force of stringer beam}} = \dfrac{N}{N_p} = \dfrac{N}{\sigma_Y A}$

n_I initial pretension ratio acting before lateral load applied
n_{Ij} initial pretension ratio acting at $\delta_j/L = 0$

∂n $\dfrac{\partial N}{\partial N_p} = \dfrac{\partial N}{\sigma_Y \partial A} = \dfrac{\partial N}{\sigma_Y t_t \partial y}$

p_{Aj} $\dfrac{\text{longitudinal load on stringer beam } j}{\text{yield force of stringer beam}} = \dfrac{P_{Aj}}{N_p}$

p_{Dj} $\dfrac{\text{lateral load on stringer } j}{\text{plastic collapse load of encastre stringer beam}} = \dfrac{P_{Dj}}{P_p}$

p_A $\dfrac{\text{total longitudinal compression load}}{\text{cylinder squash force}} = \dfrac{P_A}{\Pi_p} = \dfrac{P_A}{\sigma_{YC} A}$

p_D $\dfrac{\text{total applied damage load on cylinder}}{\text{plastic collapse load of encastre stringer beam}} = \dfrac{P_D}{P_p} = \dfrac{P_D L}{8M_p}$

q distributed transverse force
Q elastic foundation stiffness parameter = $k_2 a_{Dj}^3/3\sigma_y Z_p$
r_3 factor comparing experimental and theoretical behaviour = C_3'/C_3
R radius of cylinder
s number of longitudinal stiffeners around circumference = $s_D + s_U$
s_D number of dented longitudinal stiffeners
t_e equivalent uniform plate thickness = A/b
V shear force
w trip deflection out-of-plane at intermediate depth in stiffener
$\hat{w}$ trip amplitude during loading
$\hat{w}_D$ trip amplitude at start of longitudinal loading
W_j energy absorbed by denting stringer beam j
W total energy absorbed by cylinder
y centroidal axis running parallel to stiffener
y_{cen} distance to centroid from stiffener outstand
y_{eqa} distance to equal area axis from stiffener outstand
$\bar{y}$ location of centroidal axis of effective section from cylinder centre
z neutral axis location
z axis running parallel to knife edge
Z_{min} smaller elastic modulus of stringer beam = I/y_{cen}
Z_p plastic modulus of stringer beam
Z elastic modulus of total cylinder

α angle subtended by adjacent stringers = $2\pi/s$

β angle between outer and central trip hinge lines

γ Hodge's support axial stiffness parameter

γ_* Jones's support axial stiffness parameter

$\tilde{\gamma}$ support flexural stiffness parameter

δ_0 central dent depth

δ_j mid-span lateral deflection of stringer $j = \delta_{0j} + \Delta\delta_j$

δ_{0j} mid-span lateral deflection of stringer j at start of longitudinal loading

$\Delta\delta_j$ additional lateral deflection during longitudinal loading

$\bar{\delta}_{00}$ mean depth for arc of dented fibres

Δ end shortening

ϵ axial strain

ϵ_Y yield strain = σ_Y/E

η angle subtended by half of dent

θ_{0j} inclination of leg of stringer beam j at start of longitudinal loading

θ_j inclination of leg of stringer beam j during loading

k length ratio of model to prototype structure

μ elastic support axial stiffness parameter = $k_1 L/2AE$

ν Poisson's ratio

σ axial stress

σ_a axial strength of nominally perfect cylinder

σ_{YT} tensile yield stress

σ_{YC} compressive yield stress

σ_{ULT} ultimate stress

ϕ angle to stringer $j = j\alpha$

Ω Koiter's total curvature parameter

x distance from dent centre along longitudinal centre line

Ψ rotation of cylinder ends

ω lateral deflection at x

$$\Omega \quad 1/\left[1 + \frac{(\bar{y}/R - ecc/R)(\bar{y}/R + \cos\eta)}{I_e/A_e R^2}\right] \cdot \frac{A}{A_e}$$

SUBSCRIPTS

a	elastic bar between hinges
A	longitudinal
c	centre
cen	elastic centroid of section
cr	critical
C	compression
D	dent
e	effective
eqa	equal area axis of section
E	Euler buckling
f	flange of T-bar stiffener
h	plastic hinge
i	integration
I	initial
j	longitudinal stiffener counter
ℓ	web of longitudinal stiffener
m	maximum
min	minimum
N	axial force effect
p	panel
P	plastic
r	intermediate ring frame
s	support
t	total
tr	tripping mechanism
T	tension
U	undamaged
ULT	ultimate
V	transverse force effect
Y	yield
*	alternative

SUPERSCRIPTS

F	fixed
'	modified
^	critical

BIBLIOGRAPHY

1. AGELIDIS N.
'Collapse of stringer-stiffened cylinders'
Ph.D thesis, Imperial College, Univ. of London (1984)

2. AKITA Y. & KITAMURA K.
'A study on collision by an elastic stem to a side structure of ships'
Trans. Soc. Naval Arch. Japan, 131, p.307 (1972)

3. AKITA Y.
'Lessons learned from failure and damage of ships'
8th. Int. Ship Structures Congress, Gdansk (1982)

4. AMDAHL J. & SOREIDE T.H.
'Energy absorption in axially compressed cylindrical shells with special reference to bulbous bows in collision'
Norwegian Maritime Research, 9, No. 4, p.2 (1981)

5. AMDAHL J.
'Experimental and analytical studies on ship/platform impacts'
Dr.ing. thesis, Div. Marine Structures, Norwegian Inst. Technology, Trondheim (1983)

6. AMERICAN PETROLEUM INSTITUTE (API)
'Planning, designing and constructing fixed offshore platforms'
API RP2A, 13th. ed., Washington DC (1982)

7. BOOTH E., COLLIER D. & MILES J.
'Impact scalability of plated steel structures'
JONES N. & WIERZBICKI T. eds., 'Structural Crashworthiness', First Int. Symp. on Structural Crashworthiness, Liverpool, p.136 (1983)

8. BRITISH STANDARDS INSTITUTION (BSI)
'Code of practice for fixed offshore structures'
BS6235, London (1982)

9. BUDJANSKI B.
'A reassessment of deformation theories of plasticity'
Trans. ASME, J. App. Mech., 26, p.259 (1959)

10. CAMPBELL T.I. & CHARLTON T.M.
'Finite deformation of a fully fixed beam comprised of a non-linear material'
Int. J. Mech. Sci. 5, p.415 (1973)

11. CARIDIS P.A. & FRIEZE P.A.
'Torsional buckling of stringers of flat stiffened plating and ring-frames of ring-stiffened cylinders'
Dept. Naval Architecture & Ocean Engineering Report, Univ. of Glasgow (1982)

12. CARIDIS P.A., SANDS G. & FRIEZE P.A.
'Torsional buckling of flatbar stiffeners'
Dept. Naval Architecture & Ocean Engineering Report, Univ. of Glasgow (1983)

13. CARLSEN C.A.
'Collapse of stiffened panels in compression. Report II: Simplified stiffener collapse analysis'
Det norske Veritas, Technical Report No. 77-338 (1977)

14. CARLSEN C.A.
'Torsional buckling of flat-bar stiffeners'
Det norske Veritas, Technical Report No. 80-0562 (1980)

15. CARLSEN C.A., SHAO W.J. & FREDHEIM S.
'Experimental and theoretical analysis of post-buckling strength of flatbar stiffeners subjected to tripping'
Det norske Veritas, Technical Report No. 80-0149 (1980)

16. CARLSEN C.A. et al
'Lessons learned from failure and damage of offshore structures'
8th. Int. Ship Structures Congress, Gdansk (1982)

17. CARNEY J.F. III & VEILLETTE J.R.
'Impact response and energy dissipation characteristics of stiffened metallic tubes'
MORTON J. ed., 'Structural impact and crashworthiness', Elsevier Applied Science, 2, p.564 (1984)

18. CHYRSSANTHOPOULOS M. & SKJERVEN E.
'Progressive collapse analysis of a jack-up platform in intact and damaged condition'
Det norske Veritas, Technical Report No. 83-1026 (1983)

19. COWPER G.R. & SYMONDS P.S.
'Strain hardening and strain rate effects in the impact loading of cantilever beams'
Brown Univ., Technical Report No. 28 (1957)

20. DANAY A.
'A simplified method for analysis of flexural members to resist low velocity head-on collision'
Arup Journal, Ove Arup & Partners (1975)

21. DAVIES I.L. & MAVRIDES A.
'Assessment of the damage arising from collisions between ships and offshore structures'
FAULKNER D. et al eds., 'Integrity of Offshore Structures', Applied Science Publishers, p.363 (1981)

22. DAVIES I.L.
'A method for the determination of the reaction forces and structural damage arising in ship collisions'
J. Petroleum Technology, 33, p.2006 (1981)

23. DE DONATO O. & MAIER G.
'Historical deformation analysis of elastoplastic structures as a parametric linear complementarity problem'
Meccanica, 11, No. 3, p.166 (1976)

24. DE OLIVEIRA J.G. & JONES N.
'Some remarks on the influence of transverse shear on the plastic yielding of structures'
Int. J. Mech. Sci., 20, p.759 (1978)

25. DE OLIVEIRA J.G.
'Simple methods of estimating the energy absorption capability of steel tubular members used in offshore structures'
Report No. SK/R50, Div. Marine Structures, Norwegian Inst. Technology, Trondheim (1979)

26. DE OLIVEIRA J.G.
'The behavior of steel offshore structures under accidental collisions'
Proc. 13th. OTC, Houston, 4136 (1981)

27. DE OLIVEIRA J.G.
'Design of steel offshore structures against impact loads due to dropped objects'
Proc. 3rd. Int. Symp. Offshore Engineering Structures, Rio de Janeiro, p.466 (1981)

28. DE OLIVEIRA J.G. & WIERZBICKI T.
'Crushing analysis of rotationally symmetric plastic shells'
J. Strain Analysis, 17, No. 4, p.229 (1982)

29. DEPARTMENT OF ENERGY (UK)
'Offshore installations: guidance on design and construction'
HMSO, London (1981)

30. DE RUNTZ J.A. & HODGE P.G.
'Crushing of a tube between rigid plates'
Trans. ASME, J. App. Mech., 30, p.391 (1963)

31. DET NORSKE VERITAS
'Rules for classification of mobile offshore units'
Hovik, Norway (1981)

32. DET NORSKE VERITAS
'Rules for the design, construction and inspection of offshore structures'
Hovik, Norway, (1982)

33. DET NORSKE VERITAS
'Classification notes - buckling strength analysis'
Note No. 30.1, Hovik, Norway (1982)

34. DET NORSKE VERITAS
'Classification notes - buckling strength analysis of mobile offshore units'
Note No. 30.1, Hovik, Norway (1984)

35. DEUTSCHER AUSSCHUSS FUR STAHLBAU (DASt)
Beulsicherheitsnachweise fur Schalen, Richtlinie 013, Cologne, Germany (1980)

36. DONEGAN E.M.
'Appraisal of accidental impact loadings on steel piled North Sea structures'
Proc. 14th. OTC, Houston, 4193 (1982)

37. DONEGAN E.M.
'Designing offshore structures to overcome collisions'
Offshore Engineer, p.95 (Aug. 1982)

38. DOW R.S. & SMITH C.S.
'Effects of localized imperfections on compressive strength of long rectangular plates'
J. Constructional Steel Research, 4, p.51 (1984)

39. DOWLING P.J. & HO T.
'Effect of initial deformations on the strength of axially compressed cylindrical panels'
Proc. Conf. Significance of Deviations from Design Shapes, I. Mech. E., London, (1979)

40. DOWLING P.J. & HARDING J.E.
'Strength of steel jacket leg components'
Proc. 11th. OTC, Houston, 3428 (1979)

41. DOWLING P.J. & HARDING J.E.
'Current research into the strength of cylindrical shells used in steel jacket construction'
BOSS '79, London, 2, p.327 (1979)

42. DOWLING P.J., HARDING J.E., FAHY W.G. & AGELIDIS N.
'Report on the testing of large and small scale stiffened shells under axial compression'
Department of Energy Report No. OT-R-8107 (1981)

43. DOWLING P.J. & HARDING J.E.
'Experimental behaviour of ring and stringer stiffened shells'
HARDING J.E. et al eds., 'Buckling of shells in offshore structures', Granada p.73 (1982)

44. DOWLING P.J. & HARDING J.E.
'Research in Great Britain on the stability of circular tubes'
BOSS '82, MIT, p.59 (1982)

45. DUTHIE G., WHITE G.C. & TOOTH A.S.
'An analysis for cylindrical vessels under local loading - application to saddle supported vessel problems'
J. Strain Analysis, 17, No. 3, p.157 (1982)

46. ELLINAS C.P., BATISTA R.C. & CROLL J.G.A.
'Overall buckling of stringer-stiffened cylinders'
Proc. ICE, Part 2, 71, p.479 (1981)

47. ELLINAS C.P. & CROLL J.G.A.
written discussion
Proc. ICE, Part 2, 71, p.563 (1981)

48. ELLINAS C.P. & WALKER A.C.
'Damage on offshore tubular bracing members'
IABSE Colloq. Ship Collision with Bridges & Offshore Structures, Copenhagen, p.253 (1983)

49. ELLINAS C.P.
'Ultimate strength of damaged tubular bracing members'
Proc. ASCE, J. Struct. Engineering, 110, No. ST2, p.245 (1984)

50. ELLINAS C.P. & VALSGARD S.
'Collisions and damage of offshore structures: a state-of-the-art'
Proc. 4th. Int. Symp. Offshore Mechanics & Arctic Engineering, Texas (1985)

51. ERIKSSON C. & VALSGARD S.
'Instability of flatbar ring stiffeners subjected to external pressure'
Det norske Veritas, Technical Report No. 81-0516 (1981)

52. ESTEFEN S.F.
'Collapse of ring stiffened cylinders'
Ph.D thesis, Imperial College, Univ. of London (1984)

53. EUROPEAN CONVENTION FOR CONSTRUCTIONAL STEELWORK (ECCS)
'European recommendations for steel construction'
Construction Press, London (1981)

54. FAHY W.G.
'Collapse of longitudinally stiffened cylinders subject to axial and pressure loading'
Ph.D thesis, Imperial College, Univ. of London (1985)

55. FAULKNER D., CHEN Y.N. & DE OLIVEIRA J.G.
'Limit state design criteria for stiffened cylinders of offshore structures'
ASME 4th. Nat. Congress Pressure Vessels & Piping Technology, Portland, Oregon (1983)

56. FJELD S.
'Offshore oil production and drilling platforms. Design against accidental loads'
BOSS '79, London, 2, p.391 (1979)

57. FOK W.C., WALKER A.C. & RHODES J.
'Buckling of locally imperfect stiffeners in plates'
Proc. ASCE, J. Engineering Mech. Div., 103, No. EM5, p.895 (1977)

58. FOSS G. & EDVARDSEN G.
'Energy absorption during ship impact on offshore steel structures'
Proc. 14th. OTC, Houston, 4217 (1982)

59. FRIEZE P.A. & SAMUELIDES A.
'Collision and other impacts on ships and offshore platforms'
Colloquium on Offshore Collisions, Norway (1982)

60. FRIEZE P.A. & SACHINIS A.
'Compressive strength of stress-relieved ring-stiffened cylinders including local damage'
Proc. Int. Conf. Marine Safety, Univ. of Glasgow (1983)

61. FURNES O. & AMDAHL J.
'Ship collisions with offshore platforms'
Intermaritec '80 Symposium, Hamburg (1980)

62. FURNES O. & AMDAHL J.
'Computer simulation study of offshore collisions and analysis of ship-platform impacts'
Norwegian Maritime Research, 8, No. 1, p.43 (1980)

63. GREEN D.R. & NELSON H.M.
'Compression tests on large-scale, stringer-stiffened tubes'
HARDING J.E. et al eds., 'Buckling of shells in offshore structures', Granada, p.25 (1982)

64. HAGIWARA K. & YUHARA T.
'Study on wave impact load on ship bow'
Mitsubishi Heavy Industries (1975)

65. HARDING J.E. & DOWLING P.J.
'Analytical results for the behaviour of ring and stringer stiffened shells'
HARDING J.E. et al eds., 'Buckling of shells in offshore structures', Granada, p.231 (1982)

66. HARDING J.E., ONOUFRIOU A. & TSANG S.R.
'Collisions - what is the danger to offshore rigs?'
J. Constructional Steel Research, 3, No. 2 (1983)

67. HARDING J.E., DOWLING P.J., VALSGARD S. & WALKER A.C.
'The buckling design of stringer-stiffened shells subject to combined pressure and axial compression'
Proc. 15th. OTC, Houston, 4473 (1983)

68. HAYTHORNTHWAITE R.M.
'Beams with full end fixity'
Engineering, 183, p.110 (1957)

69. HETENYI M.
'Beams on elastic foundation'
Univ. of Michigan Press (1946)

70. HILL R.
'The mathematical theory of plasticity'
Clarendon Press, Oxford (1950)

71. HO T.K.
'Collapse of singly-curved shell structures'
M.Sc thesis, Imperial College, Univ. of London (1976)

72. HODGE P.G.
'Post-yield behaviour of a beam with partial end fixity'
Int. J. Mech. Sci., 16, p.385 (1974)

73. HUTCHINSON J.W.
'Plastic buckling'
Advances in App. Mech., 14, p.67 (1974)

74. JOHNSON W. et al
'The quasi-static piercing of cylindrical tubes of shells'
Int. J. Mech. Sci., 22, p.9 (1980)

75. JONES N.
'A theoretical study of the dynamic plastic behaviour of beams and plates with finite deflections'
Int. J. Solids & Structures, 7, p.1007 (1971)

76. JONES N.
'Slamming damage'
J. Ship Research, 17, No. 2, p.80 (1973)

77. JONES N.
'Influence of in-plane displacements at the boundaries of rigid-plastic beams and plates'
Int. J. Mech. Sci., 15, p.547 (1973)

78. JONES N.
written discussion
Trans. SNAME, New York, 82, p.408 (1974)

79. JONES N.
'Plastic behaviour of ship structures'
Trans. SNAME, New York, 84, p.115 (1976)

80. JONES N.
'Damage estimates for plating of ships and marine vehicles'
PRADS '77, 1st. Int. Symp. Practical Design in Shipbuilding, Tokyo (1977)

81. JONES N. & PAPAGEORGIOU E.A.
'Dynamic axial plastic buckling of stringer stiffened cylindrical shells'
Int. J. Mech. Sci., 24, p.1 (1982)

82. JONES N.
'Structural aspects of ship collisions'
JONES N. & WIERZBICKI T. eds., 'Structural Crashworthiness', First Int. Symp. on Structural Crashworthiness, Liverpool, p.308 (1983)

83. KAVLIE D. & SOREIDE T.
'Progressive collapse of mobile offshore platforms'
PRADS '83, 2nd. Int. Symp. Practical Design in Shipbuilding, Tokyo & Seoul (1983)

84. KENDRICK S.
'The local instability of ring frames'
Naval Construction Research Establishment, Report No. R255 (1957)

85. KENDRICK S.
'The influence of shape imperfections and residual stresses on the collapse of stiffened cylinders'
Proc. Conf. Significance of Deviations from Design Shapes, I. Mech. E., London (1979)

86. KENNY J.P. & PARTNERS
'Buckling of offshore structures'
Granada, London (1984)

87. KINRA R.K.
'Hydrostatic and axial collapse tests of stiffened cylinders'
Proc. 8th. OTC, Houston, 2685 (1976)

88. KJEOY H. & AMDAHL. J.
'Ship impact forces in collision with platform legs'
Det norske Veritas, Technical Report No. 79-0691 (1979)

89. KJEOY H.
'Ship/platform collisions. A summary report on damage assessment and energy absorption'
Det norske Veritas, Technical Report No. 82-0914 (1982)

90. KOITER W.T.
'Buckling and postbuckling behaviour of a cylindrical panel under axial compression'
Nat. Aeronaut. Res. Inst. Amsterdam, Report S476 (1956)

91. LINDSTROM G.
'Column strength of welded I-sections in postbuckling range of component plates'
Bulletin No. 138, Dept. Struct. Mech. & Eng., Royal Inst. Tech., Stockholm, (1982)

92. LOW H.Y.
'Behaviour of rigid-plastic beam loaded to finite deflections by a rigid circular indenter'
Int. J. Mech. Sci., 23, No. 7, p.387 (1981)

93. LOW H.Y.
'Some structural aspects of collisions between ships and offshore concrete platforms'
Ph.D thesis, Univ. of Cambridge (1982)

94. LOW H.Y. & MORLEY C.T.
'Indentation tests on simplified models of ship structures'
IABSE Colloq. Ship Collision with Bridges & Offshore Structures, Copenhagen, p.213 (1983)

95. McDERMOTT J.F. et al
'Tanker structural analysis for minor collisions'
Trans. SNAME, New York, 82, p.382 (1974)

96. MILLER C.D.
'Buckling of axially compressed cylinders'
Proc. ASCE, J. Struct. Div., 103, No. ST3, p.695 (1977)

97. MILLER C.D.
'Summary of buckling tests on fabricated steel cylindrical shells in USA'
HARDING J.E. et al eds., Buckling of shells in offshore structures', Granada, p.429 (1982)

98. MILLER C.D. et al
'Current research related to buckling of shells for offshore structures'
Proc. 15th. OTC, Houston, 4474 (1983)

99. MILLER C.D., FRIEZE P.A., ZIMMER R.A. & JAN H.Y.
'Collapse tests of fabricated stiffeed steel cylinders under combined loads'
ASME 4th. Nat. Congress Pressure Vessels & Piping Technology, Portland, Oregon (1983)

100. MINORSKY V.U.
'An analysis of ship collisions with reference to protection of nuclear power plants'
J. Ship Research, 3, No. 2, p.1 (1959)

101. MOAN T. & HOLAND I.
'Risk assessment of offshore structures. Experience & principles'
MOAN. T & SHINOZUKA M. eds., 'Structural safety and Reliability', Proc. ICOSSAR '81, Elsevier (1981)

102. MORLEY L.S.D.
'The thin-walled circular cylinder subected to concentrated radial loads'
Quart. J. Mech. App. Math. 13, p.27 (1960)

103. MORRIS A.J.
'Experimental investigation into the effects of indenting a cylindrical shell by a load applied through a rigid boss'
J. Mech. Engineering Sci., 13, No. 1, p.36 (1971)

104. MORRIS A.J. & CALLADINE C.R.
'Simple upper-bound calculations for indentation of shells'
Int. J. Mech. Sci., 13, No. 4, p.331 (1971)

105. MURRAY N.W.
'Buckling of stiffened panels loaded axially and in bending'
Structural Engineer, 51, No. 8, p.285 (1973)

106. NATIONAL MARITIME INSTITUTE (NMI)
'The risk of ship/platform encounters in UK waters'
Report of Project No. 402002, England (1977)

107. NORWEGIAN PETROLEUM DIRECTORATE (NPD)
'Regulations for the structural design of fixed structures on the Norwegian continental shelf'
Norway, (1977)

108. ODLAND J.
'Buckling resistance of unstiffened and stiffened circular cylindrical shell structures'
Norwegian Maritime Research, 6, No. 3, p.2 (1978)

109. ODLAND J.
'Response and strength analysis of jack-up platforms'
Norwegian Maritime Research, 10, No. 4 (1982)

110. ONOUFRIOU A. & HARDING J.E.
'Residual strength of damaged ring-stiffened cylinders'
Proc. 4th. Int. Symp. Offshore Mechanics & Arctic Engineering, Texas (1985)

111. PARIS P.C.
'Limit Design of Columns'
J. Aero. Sci., 21, No. 1, p.43 (1954)

112. PETERSEN M.J. & PEDERSEN P.T.
'Collisions between ships and offshore platforms'
Proc. 13th. OTC, Houston, 4134 (1981)

113. PETTERSEN E. & JOHNSEN K.R.
'New non-linear methods for estimation of collision resistance of mobile offshore units'
Proc. 13th. OTC, Houston, 4135 (1981)

114. PETTERSEN E.
'Assessment of impact damage by means of a simplified non-linear approach'
FAULKNER D. et al eds., 'Integrity of Offshore Structures', Applied Science Publishers, p.317 (1981)

115. PETTERSEN E. & VALSGARD S.
'Collision resistance of marine structures'
JONES N. & WIERZBICKI T. eds., 'Structural Crashworthiness', First Int. Symp. on Structural Crashworthiness, Liverpool, p.338 (1983)

116. PUGSLEY A.G.
'The crumpling of tubular structures under impact conditions'
Proc. Symp. Use of Aluminium Railway Structures, Inst. Loco. Engrs., London (1960)

117. PYMAN M.A.F., AUSTIN J.S. & LYON P.R.
'Ship/platform collision risk in the U.K Sector'
IABSE Colloq. Ship Collision with Bridges & Offshore Structures, Copenhagen, p.145 (1983)

118. RASHED S.M.H
'Behaviour to ultimate strength of tubular offshore structures by the idealized structural unit method'
Report No. SK/R51, Div. Marine Structures, Norwegian Inst. Technology, Trondheim (1980)

119. RASHED S.M.H.
'Ultimate strength and post ultimate strength behaviour of damaged tubular structural members'
Report No. SK/R52, Div. Marine Structures, Norwegian Inst. Technology, Trondheim (1980)

120. RASHED S.M.H., TABY J. & MOAN T.
'Theoretical and experimental study of the behaviour of damaged tubular members in offshore structures'
Proc. 1st. Indian Conf. Ocean Engineering, INCOE 81, Madras, (1981)
also Norwegian Maritime Research, 9, No.2 (1981)

121. REDWOOD R.G.
'Crushing of a tube between rigid plates'
Trans. ASME, J. App. Mech. 31, p.357 (1964)

122. REID S.R. & REDDY T.Y.
'Effects of strain hardening on the lateral compression of tubes between rigid plates'
Int. J. Solids & Structures, 14, p.213 (1978)

123. REID S.R.
'Laterally compressed metal tubes as impact energy absorbers'
JONES N. & WIERZBICKI T. eds., 'Structural Crashworthiness', First Int. Symp. on Structural Crashworthiness, Liverpool, p.1 (1983)

124. RHODES J. & HARVEY J.M.
'Plates in uniaxial compression with various support conditions at the unloaded boundaries'
Int. J. Mech. Sci., 13, p.787 (1971)

125. RICHARDS D.M. & ANDRONICOU A.
'Residual strength of dented tubulars: impact energy correlation'
Proc. 4th. Int. Symp. Offshore Mechanics & Arctic Engineering, Texas (1985)

126. ROGERS N.A.
'Local buckling of welded steel outstands'
Ph.D thesis, Univ. of Cambridge (1975)

127. RONALDS B.F. & DOWLING P.J.
'Damage of orthogonally stiffened shells'
BOSS '85, Delft (1985)

128. ROSENBLATT M. & SON INC
'Tanker structural analysis for minor collisions'
US Coast Guard, Report CG-D-72-76 (1975)

129. SAMUELIDES E. & FRIEZE P.A.
'Rigid bow impacts on ship-hull models'
IABSE Colloq. Ship Collision with Bridges & Offshore Structures, Copenhagen, p.263 (1983)

130. SAMUELIDES E. & FRIEZE P.A.
'Analytical and numerical simulation of beams subjected to impact'
MORTON J. ed., 'Structural impact and crashworthiness', Elsevier Applied Science, 2, p.355 (1984)

140. SAMUELSON A. & VESTERGREN P.
'Analysis of axially loaded stringer stiffened circular cylinders'
Aeronautical Research Inst. Sweden, Technical Note HU-2134 (1979)

141. SHANG J.C., MARULIC W.J. & STURM R.G.
'Buckling of longitudinally stiffened cylinders'
Proc. ASCE, J. Struct. Div., 90, No. ST5, p.161 (1964)

142. SHERMAN D.R.
'Inelastic local buckling of circular tubes'
HARDING J.E. et al eds., 'Buckling of shells in offshore structures', Granada p.365 (1982)

143. SINGER J.
'Shell buckling research in Israel and its application to offshore structures'
Technion, Israel Inst. Tech., Haifa, Israel (1982)

144. SMITH C.S. & KIRKWOOD W.C.
'Influence of initial deformation and residual stress on inelastic flexural buckling of stiffened plates and shells'
Proc. Int. Conf. Steel Plated Structures, Imperial College, London, p.838 (1976)

145. SMITH C.S., KIRKWOOD W.C & SWAN J.W.
'Buckling strength and post-collapse behaviour of tubular bracing members including damage effects'
BOSS '79, London, p.303 (1979)

146. SMITH C.S., SOMERVILLE W.L. & SWAN J.W.
'Residual strength and stiffness of damaged steel bracing members'
Proc. 13th. OTC, Houston, 3981 (1981)

147. SMITH C.S. & DOW R.S.
'Residual strength of damaged steel ships and offshore structures'
J. Constructional Steel Research, 1, No. 4, p.2 (1981)

148. SMITH C.S.
'Strength and stiffness of damaged tubular beam columns'
HARDING J.E. et al eds., 'Buckling of shells in offshore structures', Granada p.1 (1982)

149. SMITH C.S.
'Assessment of damage in offshore steel platforms'
Proc. Int. Conf. Marine Safety, Univ. of Glasgow (1983)

150. SOARES C.G. & SOREIDE T.H.
'Plastic analysis of laterally loaded circular tubes'
Proc. ASCE, J. Struct. Engineering, 109, No. ST2, p.451 (1983)

151. SOREIDE T.H.
'Ultimate load analysis of marine structures'
Tapir Publishing Co., Trondheim (1982)

152. SOREIDE T.H. & AMDAHL J.
'Deformation characteristics of tubular members with reference to impact loads from collision and dropped objects'
Norwegian Maritime Research, 10, No. 2, p.3 (1982)

153. SOREIDE T.H., MOAN T., AMDAHL J, & TABY J.
'Analysis of ship/platform impacts'
BOSS '82, MIT, p.257 (1982)

154. SOREIDE T.H. &. AMDAHL J.
'Energy absorption in ship-platform impacts'
IABSE Colloq. Ship Collision with Briges & Offshore Structures, Copenhagen, p. 195 (1983)

155. SORENSEN K.A.
'Behaviour of reinforced and prestressed concrete tubes under static and impact loading'
BOSS '76, Trondheim, 2, p.798 (1976)

156. STEEN E.
private communication
Det norske Veritas (1984)

157. STOLARSKI H.
'Assessment of large displacements of a rigid-plastic shell withholding a localized impact'
Nuclear Engineering & Design, 41, p.327 (1977)

158. SUPPLE W.J. & COLLINS I.
'Post-critical behaviour of tubular struts'
Eng. Struct., 2, p.225 (1980)

159. SYMONDS P.S. & JONES N.
'Impulsive loading of fully clamped beams with finite plastic deflections and strain-rate sensitivity'
Int. J. Mech. Sci., 14, p.49 (1972)

160. SYNGELLAKIS S. & WALKER A.C.
'Elastic local buckling of longitudinally stiffened cylinders'
RICHARDS T.H. & STANLEY P. eds., 'Stability problems in engineering structures and components', Applied Science Publishers, p.159 (1981)

161. THOMAS S.G. et al
'Large deformations of thin-walled circular tubes under transverse loading - I,II,III'
Int. J. Mech. Sci., 18, p.325, p.387, p.501 (1976)

162. TOOTH A.S. & JONES N.
'Plastic collapse loads of cylindrical pressure vessels supported by rigid saddles'
J. Strain Analysis, 17, No. 3, p.187 (1982)

163. TRANSPORT & ROAD RESEARCH LABORATORY
'Recommended standard practices for structural testing of steel models'
Supplementary Report No. 254 (1977)

164. TSANG S.K. & HARDING J.E.
'A literature survey on collisions with particular emphasis on offshore structures'
Dept. Civil Engineering, Imperial College (1982)

165. TSANG S.K. & HARDING J.E.
'A literature review on the behaviour of circular cylindrical shells under external pressure'
Dept. Civil Engineering, Imperial College (1983)

166. TSANG S.K., HARDING J.E., WALKER A.C. & ANDRONICOU A.
'Buckling of ring stiffened cylinders subjected to combined pressure and axial compressive loading'
ASME 4th. Nat. Congress Pressure Vessels & Piping Technology, Portland, Oregon (1983)

167. TSANG S.K. & HARDING J.E.
'A plastic mechanism formulation for the general instability of ring-stiffened cylinders under pressure dominated loadings'
Int. J. Mech. Sci. (accepted for publication)

168. TSANG S.K. & HARDING J.E.
'Collapse of ring stiffened cylindrical shells under combined external pressure and axial compression'
Ph.D thesis, Imperial College, Univ. of London, (1985)

169. UEDA Y. & RASHED S.M.H.
'Behavior of damaged tubular structural members'
Proc. 4th. Int. Symp. Offshore Mechanics & Arctic Engineering, Texas (1985)

170. VALSGARD S., SHAO W.J. & STEEN E.
'Data collection on geometry and design loads for stiffened cylindrical shells in maritime structures'
Det norske Veritas, Technical Report No. 80-0156 (1980)

171. VALSGARD S. & STEEN E.
'Simplified strength analysis of narrow panelled stringer stiffened cylinders under axial compression and lateral load'
Det norske Veritas, Technical Report No. 80-0590 (1980)

172. VALSGARD S. & ERIKSSON C.
'Collapse test on two point loaded rings with internal flatbar stiffeners'
Det norske Veritas, Technical Report No. 81-0515 (1981)

173. VALSGARD S. & FOSS G.
'Buckling research in Det norske Veritas'
HARDING J.E. et al eds., 'Buckling of shells in offshore structures', Granada p.491 (1982)

174. VALSGARD S. & PETTERSEN E.
'Simplified nonlinear analysis of ship/ship collisions'
Norwegian Maritime Research, 10, No. 3, p.2 (1982)

175. VALSGARD S.
'Design against accidental loads on mobile platforms'
Safety Offshore Conf., Stavanger (1982)

176. WAH T.
'A theory for the plastic design of ship plating under uniform pressure'
J. Ship Research, 4, p.17 (1960)

177. WALKER A.C. & DAVIES P.
'The collapse of stiffened cylinders'
DOWLING P.J. et al eds., 'Steel plated structures', Crosby Lockwood Staples, p.791 (1976)

178. WALKER A.C. & SRIDHARAN S.
'Experimental investigation of the buckling behaviour of stringer-stiffened shells'
Department of Energy Report No. OT-R-7835 (1979)

179. WALKER A.C. & SRIDHARAN S.
'Buckling of compressed longitudinally stiffened cylindrical shells'
BOSS '79, London, 2, p.341 (1979)

180. WALKER A.C. & SRIDHARAN S.
'Analysis of the behaviour of axially compressed stringer-stiffened cylindrical shells'
Proc. ICE, Part 2, 69, p.447 (1980)

181. WALKER A.C., ANDRONICOU A. & SRIDHARAN S.
'Experimental investigation of the buckling of stiffened shells using small scale models'
HARDING J.E. et al eds., 'Buckling of shells in offshore structures', Granada p.45 (1982)

182. WALKER A.C., ANDRONICOU A. & SRIDHARAN S.
'Theoretical analysis of stringer and ring stiffened shells'
HARDING J.E. et al eds., 'Buckling of shells in offshore structures', Granada p.183 (1982)

183. WASZCZYSZYN Z.
'Experimental verification of finite, elastic-plastic deflections of beams on immovable supports'
Bull. Acad. Polon. Des. Sci., Ser. Des. Sci. Tech., 14, p.139 (1966)

184. WENGER A. et al
'Design for impact of dropped objects'
Proc. 15th. OTC, Houston, 4471 (1983)

185. YOUNG A.G.
'Ship plating loaded beyond the elastic limit'
Trans. RINA, 101, p.143 (1959)

186. ZAYAS V.A., MAHIN S.A. & POPOV E.P.
'Ultimate strength of steel offshore structures'
BOSS '82, MIT, 2, p.39 (1982)